Baryon properties from chiral QCD

Dissertation
zur
Erlangung des Doktorgrades (Dr. rer. nat.)
der
Mathematisch-Naturwissenschaftlichen Fakultät
der
Rheinischen Friedrich-Wilhelms-Universität Bonn

von
Daniel Severt
aus
Troisdorf, Deutschland

Bonn, April 2023

Angefertigt mit Genehmigung der Mathematisch-Naturwissenschaftlichen Fakultät der Rheinischen Friedrich-Wilhelms-Universität Bonn

1. Gutachter:	Prof. Dr. Dr. h.c. Ulf-G. Meißner
2. Gutachter:	PD. Dr. Akaki Rusetsky
Tag der Promotion:	26.05.2023
Erscheinungsjahr:	2023

Abstract

This thesis contains a collection of studies on the properties of baryons within the context of effective field theory, especially Chiral Perturbation Theory (ChPT). The thesis focuses primarily on the Roper resonance, an excited state of the nucleon with some interesting and puzzling features. With a pole mass of approximately $m_R \approx 1.4\,\text{GeV}$, the Roper mass lies below its quark model prediction. Additionally, the Roper can decay into a nucleon and a pion, as well as into a nucleon and two pions, where both branching ratios are of the same magnitude, causing an almost equal probability of two- and three-particle final states. Investigating the Roper resonance and its properties is key for understanding the excited hadron spectrum of Quantum Chromodynamics (QCD). The second part of this thesis studies electric dipole moments (EDMs) of heavy baryons containing a single bottom quark. EDMs are an important observable in precision measurements, since they violate the discrete symmetries time-reversal (T) and parity (P) at the same time. The inclusion of P- and T-violating sources is done within the framework of Standard Model effective field theory (SMEFT). Dimension-six operators from SMEFT are considered and their induced effect on the EDMs of heavy bottom baryons is calculated. This thesis contains three chapters that have been published in peer-reviewed journals. The publications are

- D. Severt and U.-G. Meißner, "The Roper Resonance in a finite volume", Commun. Theor. Phys. **72**, no.7, 075201 (2020) [arXiv:2003.05745 [hep-lat]],
- D. Severt, M. Mai and U.-G. Meißner, "Particle-dimer approach for the Roper resonance in a finite volume", JHEP **04**, 100 (2023) [arXiv:2212.02171 [hep-lat]],
- Y. Ünal, D. Severt, J. de Vries, C. Hanhart and U.-G. Meißner, "Electric dipole moments of baryons with bottom quarks", Phys. Rev. D **105**, no.5, 055026 (2022) [arXiv:2111.13000 [hep-ph]].

Additionally, as a contribution to the conference *Lattice2022*, the Proceedings of Science (PoS) article

- D. Severt, "Towards the finite-volume spectrum of the Roper resonance", PoS **LATTICE2022**, 085 (2023) [arXiv:2210.09423 [hep-lat]],

has been published during the work on this thesis.

Contents

“Science is not everything, but science is very beautiful.”

J. Robert Oppenheimer

CHAPTER 1

Introduction

What is our world made of? This simple but fundamental question is almost as old as human history. Many philosophers and scientists have asked themselves this question over millennia. The ancient Greeks had the idea that everything in our world is made out of four elements: earth, water, air and fire. This idea was quite successful in the sense that it was a prominent theory for a long time and ancient philosophers used to "explain" various natural phenomena with it. Similar lists of elements were also introduced by early cultures in India and Tibet [1]. Around the fifth century BC the novel idea came up that all four elements might be made of something more fundamental, something so small that it should be invisible to the human eye. Leucippus and his student Democritus called these particles "atomos" (ancient Greek for "uncuttable") and proposed that everything in the universe consists of infinitely different variations ot these fundamental entities [2]. For readers who used to play – or still play – with *LEGO*® bricks, this idea seems rather natural, but for the early time, this new view was revolutionary.

Fast forward approximately 2500 years, the idea of fundamental particles, which build up all the matter around us, still exists and it is now supported by a much more rigorous scientific foundation. The Standard Model (SM) of particle physics is the best description we have of our universe today. It includes all elementary matter particles and characterizes their interactions with each other, except of the gravitational interaction. We call those particles "elementary", because they have – as far as we know today – no substructure and can, therefore, be considered fundamental. However, the *real* fundamental entites are quantum fields, since the SM is a relativistic quantum field theory (QFT). The particles we observe are the quantized excitations of those fields (for a pedagogical introduction, see e.g. Refs. [3–5]). There are two types of fields in the SM: the half-integer spin fields, called "fermions", which build up all the matter around us, and the integer spin "bosons", which mediate the forces between the fermions and also between each other. From a mathematical viewpoint, the SM is defined by a Lagrangian, which is invariant under local $\mathrm{SU}(3)_C \times \mathrm{SU}(2)_L \times \mathrm{U}(1)_Y$ gauge transformations. The $\mathrm{SU}(2)_L \times \mathrm{U}(1)_Y$ part of the gauge symmetry gives rise to the electroweak interaction and the $\mathrm{SU}(3)_C$ part corresponds to the strong interaction, which will be at the center of all investigations in this thesis. The theory of the strong force, Quantum Chromodynamics (QCD), describes the interactions of all particles that possess a so-called color charge C (the "C" in $\mathrm{SU}(3)_C$), these are the spin-$1/2$ quarks (q) and the spin-1 gluons (g), which mediate the force. This works in analogy to the quantum theory of

electrodynamics, QED[1], where the interaction of all electrically charged particles is described by an interchange of a virtual photon. However, there are two major differences, which makes QCD a much more complicated theory: First, the gluons themselves carry color charge, meaning that they do not just interact with quarks but also with each other, leading to a larger amount of possible interactions. Second, the strong coupling constant g_s, which quantifies the interaction strength, is much larger at smaller energies than the electromagnetic coupling (hence the name "strong interaction"). While conventional perturbative calculations in QCD still work at high energies, the method fails in the low-energy regime meaning that different approaches, which will be discussed later, must be used to calculate QCD processes.
The low-energy behaviour of QCD is particulary interesting, because in this region bound states of the strong interaction form. These bound states, called "hadrons", come in a large variety. In fact, in the 1950s experimental physicists discovered a tremendous amount of different particles with different characteristics. A first try to classify all these new particles was given by the quark model [6, 7], which proposed that the hadrons fall into two categories: mesons and baryons. Mesons consist of two quarks, a quark and an anti-quark ($\bar{q}q$), whereas baryons consist of three quarks (qqq). For example, the building blocks of atomic nuclei, protons and neutrons, are baryons. Similar to the atom – a bound state of the electromagnetic interaction – the quarks inside the hadrons can also be excited, leading to multiple excited hadronic states, which are called "resonances" and can be observed in modern experiments. The quark model was successful, since it was able to organize the discovered hadrons into clear schemes and predicted some missing particles in the spectrum, like the Ω^- baryon [8]. However, the model had some issues like, for example, the apparent violation of the Pauli exclusion principle in some baryonic states, which led to the introduction of the color charge [9] and ultimately resulted in the formulation of QCD. Moreover, some states from the rich hadronic spectrum that we know today cannot be explained anymore by the simple quark model, but can only be understood within the context of QCD.

Over the last years a lot of effort has been made to deepen our understanding of the QCD hadron spectrum (for some current reviews see [10, 11]). Especially, the excited baryon spectrum remains one of the least understood features of the strong interaction. One of the most prominent and challenging systems is the Roper resonance. Discovered in 1964 via partial wave analysis of nucleon-pion-scattering data [12], the Roper, or $N(1440)$, posseses some interesting features. The resonance has identical quantum numbers as the nucleon, i.e. $I(J^P) = 1/2(1/2^+)$, where I, J and P denote isospin, spin and parity, respectively, but a larger mass (pole mass: $m_R = 1.365\,\text{GeV}$, see PDG [13]). The most remarkable characteristic of the Roper lies in its decays: It can decay into a nucleon (N) and a pion (π), as well as into a nucleon and two pions, where the branching ratios of these two decay modes are of the same magnitude. This makes two- and three-particle final states equally likely and complicates the Roper system significantly.
There are several options to explore the spectrum of the Roper resonance. One method is Lattice QCD (LQCD), a non-perturbative approach to QCD, where numerical calculations of correlation functions are performed on a discretized Euclidean space-time in a finite volume (see e.g. Ref. [14] for an introduction). There are already some preliminary studies of the Roper system in LQCD (see [15, 16]), which indicate that both two-particle $N\pi$ and three-particle $N\pi\pi$ dynamics might be important to generate the Roper resonance. Another method is an effective field theory (EFT) approach (see Ref. [17] for a very good introduction to EFTs and their applications) for the Roper, which has

[1] QED: Quantum Electrodynamics.

already been established within the framework of baryon chiral perturbation theory (BChPT) [18–22]. Therein, the Roper resonance is included in BChPT as an explicit degree of freedom and one can calculate various observables, like decay widths, within this framework. However, difficulties arise in general when comparing results from EFT with results from LQCD. For example, the fact that LQCD calculations are always performed in a box of finite size, causes a shift in the energy levels of the system. In order to improve the investigation of the Roper resonance and to simplify the comparison between LQCD and infinite volume EFT, one can use an EFT approach in a finite volume (see e.g. [17]). When a narrow resonance is present, the energy levels show a particular behaviour near the resonance's energy: The levels shift when the box size L is changed, but they do not cross each other. This behaviour is known as "avoided level crossing" [23] and it has been already discovered in other resonance systems, such as the delta resonance [24].
For the Roper resonance, the case is complicated due to its two- and three-particle final states. The two-body sector in a finite volume is already well established from Lüscher's method [25, 26], whereas the three-body sector remains challenging. A lot of work has been done and different methods have been introduced to tackle the three-particle dynamics. These methods usually require the formulation of a so-called three-body quantization condition (for some examples, see Refs. [27–36]). A very promising approach to describe three-particle scattering in a finite box is the particle-dimer framework (see [37–42]), which reformulates the three-body problem as a two-body problem and, therefore, significantly simplifies the three-particle dynamics. This particle-dimer picture might also be a suitable approach to investigate the Roper resonance [43].

Despite of the immense success the SM had and still has in predicting experimental results, we know quite well that it cannot be a full discription of nature. For instance, the force of gravity is not included in the SM and there are several observations that cannot be explained by the SM alone[2]. One open problem is the matter-antimatter asymmetry, which comes from the observation that we have mainly matter in our universe, but no antimatter. The SM, however, treats matter and antimatter in a symmetric way for the most part: There are some interactions in the SM, which violate the discrete symmetries parity (P) and time-reversal (T) and, therefore, CP symmetry according to the CPT theorem, see e.g. [4]. The C denotes the symmetry under charge conjugation, i.e. the symmetry by replacing a particle with its antiparticle. The different treatment of matter and antimatter in the early universe is crucial for explaining the matter-antimatter asymmetry [44]. CP-violating sources can be found in the weak (weak Cabibbo-Kobayashi-Maskawa (CKM) phase) and in the strong sector (QCD θ-term). Nevertheless, modern research suggests that the CP-violating interactions in the SM are not sufficient to explain the observed large discrepancy between matter and antimatter.
There are several theories, collected under the name "beyond-the-Standard-Model" (BSM) physics, aiming to explain the matter-antimatter-asymmetry by introducing additional interactions that explicitly violate C or CP. Most of them postulate new heavy particles, which have not been observed yet by experiments due to their large masses. One way to investigate the effects that these new particles have on SM physics in a model-independent and systematic framework is Standard Model effective field theory (SMEFT) [45]. In this EFT, it is assumed that BSM physics shows up at an energy scale Λ, which lies well beyond the electroweak scale $v \simeq 250\,\text{GeV}$. The BSM heavy particles can, therefore, not be resolved in our current experiments, since the necessary energy is not reached. However, the effects of these particles should still influence the behaviour of SM particles at low energies, especially

[2] For example neutrino masses, dark matter, dark energy, and more. See e.g. [5] for further reading.

when these effects violate CP symmetry. One of the observables that can probe CP violation is the electric dipole moment (EDM) of a particle.
The hunt for measuring EDMs is already going on for a longer time. While elementary particles could in principle have an EDM as well, most experiments try to measure EDMs of composite particles, like baryons. Some of the most precise measurements have been performed on the neutron, where its EDM was found to be $|d_n| < 1.8 \times 10^{-26} e\,\text{cm}$ [46]. This result is, however, just an upper bound on the neutron EDM and not a direct detection. Measuring a permanent EDM would imply that P and T symmetry are violated simultaneously (and, hence, also CP symmetry). Apart from the neutron, there are also plans to measure EDMs of baryons containing a single heavy charm (c) or bottom (b) quark in future experiments, see e.g. Refs. [47–50]. One of the main ideas behind these prospects is that the heavy c- and b-quarks might feel a stronger influence from BSM physics due to their large masses than the light-quark sector. In the last part of this thesis, CP-violating interactions from SMEFT, which explicitly include b-quarks, are investigated. Afterwards, the EDMs that these interactions induce into the spin-$1/2$ single-bottom baryons are calculated with the help of BChPT methods.

This thesis is organized in the following way: In chapter 2 some important theoretical concepts are introduced, which are relevant for understanding the studies performed in this work. Readers, who are already experts in the field, might be able to skip these introductory sections. After that, the investigation of the Roper resonance starts in chapter 3 and is continued in chapter 4. Then, the second part of this thesis, the study on EDMs of heavy bottom baryons, is presented in chapter 5. Finally, a summary of the most important results together with an overall conclusion is given in chapter 6. Some additional information, as well as several technicalities, can be found in the appendices.

CHAPTER 2

Theoretical foundations

2.1 The Standard Model of particle physics

The Standard Model (SM) of elementary particle physics is the result of many theoretical and experimental studies conducted in the 20th century, where its final formulation, which is still used today, has been introduced in the 1970s (see e.g. Refs. [51–54] and many more). The particle content in the SM includes the spin-1/2 fermions, which build up all baryonic matter around us, and the spin-1 gauge bosons, which exchange the forces between the fermions and also between each other. Additionally, there is the spin-0 Higgs field responsible for giving mass to the elementary particles. The fermions fall into two categories: There are the leptons, which contain the electron (e), the muon (μ), the tau (τ), and three neutrinos ($\nu_{e,\mu,\tau}$), one for each lepton flavor, and the quarks, which come in six different flavors: up (u), down (d), strange (s), charm (c), bottom (b), and top (t). All fermions come with their respective antimatter partner. The gauge bosons in the SM are the gluons (g), which mediate the strong interaction, the photon (γ), which mediates the electromagnetic interaction and the three heavy bosons Z^0, W^+ and W^-, which mediate the weak interaction[1].
As a quantum field theory (QFT), the SM is described by a Lagrangian, which is invariant under local $\mathrm{SU}(3)_C \times \mathrm{SU}(2)_L \times \mathrm{U}(1)_Y$ (C: color, L: left, Y: hypercharge) gauge transformations. The $\mathrm{SU}(3)_C$ part of the symmetry gives rise to the strong interaction, whereas the $\mathrm{SU}(2)_L \times \mathrm{U}(1)_Y$ part is responsible for the electroweak force. The full Lagrangian is given by[2]

$$\begin{aligned}
\mathcal{L}_{\mathrm{SM}} = {} & \bar{q}_L^\alpha i \not{D} q_L^\alpha + \bar{u}_R^\alpha i \not{D} u_R^\alpha + \bar{d}_R^\alpha i \not{D} d_R^\alpha + \bar{l}_L^\alpha i \not{D} l_L^\alpha + \bar{e}_R^\alpha i \not{D} e_R^\alpha \\
& + (D_\mu \Phi)^\dagger D^\mu \Phi + \mu^2 \Phi^\dagger \Phi - \lambda (\Phi^\dagger \Phi)^2 \\
& - \bar{q}_L^\alpha f_u \tilde{\Phi} u_R^\alpha - \bar{q}_L^\alpha f_d \Phi d_R^\alpha - \bar{l}_L^\alpha f_e \Phi e_R^\alpha + \mathrm{h.c.} \\
& - \frac{1}{4} G^a_{\mu\nu} G^{a,\mu\nu} - \frac{1}{4} W^i_{\mu\nu} W^{i,\mu\nu} - \frac{1}{4} B_{\mu\nu} B^{\mu\nu} \\
& + \theta \frac{g_s^2}{64\pi^2} \epsilon^{\mu\nu\rho\sigma} G^a_{\mu\nu} G^a_{\rho\sigma} \ . \qquad (2.1)
\end{aligned}$$

[1] The full particle content is usually denoted in a very compact table form, see e.g. wikipedia.org/Standard_Model.
[2] The notations and conventions of Ref. [5] are mainly used throughout this section.

Here, the first line on the right-hand side showes the dynamical part of the fermions, which are written in terms of the weak left-handed $\mathrm{SU}(2)_L$ doublets q_L^α (quarks) and l_L^α (leptons) with generation index α, i.e.

$$q_L^\alpha = \left(\begin{pmatrix} u \\ d \end{pmatrix}_L, \begin{pmatrix} c \\ s \end{pmatrix}_L, \begin{pmatrix} t \\ b \end{pmatrix}_L \right), \quad l_L^\alpha = \left(\begin{pmatrix} \nu_e \\ e \end{pmatrix}_L, \begin{pmatrix} \nu_\mu \\ \mu \end{pmatrix}_L, \begin{pmatrix} \nu_\tau \\ \tau \end{pmatrix}_L \right). \tag{2.2}$$

Note that $\bar{q}_L^\alpha = (q_L^\alpha)^\dagger \gamma^0$ and $\bar{l}_L^\alpha = (l_L^\alpha)^\dagger \gamma^0$, where γ^0 is the first Dirac gamma matrix γ^μ ($\mu = 0, 1, 2, 3$). The right-handed singlets for quarks and leptons (also with generation index α) are denoted by

$$u_R^\alpha = (u_R,\, c_R,\, t_R)\,, \quad d_R^\alpha = (d_R,\, s_R,\, b_R)\,, \quad e_R^\alpha = (e_R,\, \mu_R,\, \tau_R)\,, \tag{2.3}$$

where one can observe that the SM does not include right-handed neutrinos. The coupling of the left- and right-handed fermions to the gauge fields is described by the covariant derivative D_μ, which is denoted with the Feynman slash notation $\not{D} = \gamma^\mu D_\mu$. In the left-handed doublet case D_μ is given by

$$D_\mu \psi_L(x) = \left(\partial_\mu + \frac{i}{2} g_s A_\mu^a \lambda^a + \frac{i}{2} g W_\mu^i \tau^i + \frac{i}{2} Y g' B_\mu \right) \psi_L(x)\,, \tag{2.4}$$

where ψ_L denotes an arbitrary right-handed fermion. The first interaction term in (2.4) is from the strong force: A_μ^a denotes the gluon fields, g_s the strong coupling constant and λ^a the Gell-Mann matrices. The second term describes the interaction with the $\mathrm{SU}(2)_L$ gauge field W_μ^i via the coupling g, where τ^i are the Pauli matrices, and the third term indicates the interaction with the $\mathrm{U}(1)_Y$ gauge field B_μ, where g' (times the hypercharge Y) is the corresponding coupling. On the contrary, right-handed fermions, ψ_R, do not interact with the $\mathrm{SU}(2)_L$ gauge field, so that the covariant derivative becomes

$$D_\mu \psi_R(x) = \left(\partial_\mu + \frac{i}{2} g_s A_\mu^a \lambda^a + \frac{i}{2} Y g' B_\mu \right) \psi_R(x)\,. \tag{2.5}$$

The dynamical parts of the gauge fields are given in the fourth line on the right-hand side of Eq. (2.1), where $G_{\mu\nu}^a$, $W_{\mu\nu}^i$ and $B_{\mu\nu}$ denote the field-strength tensors of the $\mathrm{SU}(3)_C$, $\mathrm{SU}(2)_L$ and $\mathrm{U}(1)_Y$ gauge fields, respectively. These are defined by

$$G_{\mu\nu}^a = \partial_\mu A_\nu^a - \partial_\nu A_\mu^a - g_s f^{abc} A_\mu^b A_\nu^c\,, \tag{2.6}$$

$$W_{\mu\nu}^i = \partial_\mu W_\nu^i - \partial_\nu W_\mu^i - g \epsilon^{ijk} W_\mu^j W_\nu^k\,, \tag{2.7}$$

$$B_{\mu\nu} = \partial_\mu B_\nu - \partial_\nu B_\mu\,, \tag{2.8}$$

with the SU(3) structure constants f^{abc} and the SU(2) structure constants ϵ^{ijk}, i.e. the Levi-Civita symbol. The last line in (2.1) shows the so-called QCD θ-term, which is briefly discussed in the next section. The second line in the SM Lagrangian describes the dynamics and the potential of the Higgs field, which is defined by the doublet of spin-0 fields

$$\Phi = \begin{pmatrix} \phi^+ \\ \phi^0 \end{pmatrix}. \tag{2.9}$$

The covariant derivative acts on the Higgs doublet according to Eq. (2.4), however, it does not couple to the guon fields, but only to the W_μ^i and B_μ gauge fields. The constants μ and λ parametrize the Higgs potential and the third line in Eq. (2.1) shows the Yukawa couplings, i.e. how the Higgs couples to the fermions, proportional to the constants $f_{u,d,e}$ and with the definition $\tilde{\Phi} := i\tau_2\Phi^*$. Except the Higgs field, none of the elementary particles in (2.1) has a mass term, which ensures the gauge invariance. This changes after the process of so-called "spontaneous symmetry breaking". In that, the Higgs field acquires a non-trivial vavuum expectation value v, i.e.

$$\langle 0|\, \Phi^\dagger \Phi \,|0\rangle = \frac{v^2}{2}\,, \quad \text{with} \quad v \equiv \sqrt{\frac{\mu^2}{\lambda}}\,. \tag{2.10}$$

The energy scale $v = 246.22\,\text{GeV}$ [13] has to be measured by experiment and is not predicted by the theory. A possible field configuration for Φ that obeys the above relation and conserves electric charge is then given by

$$\langle 0|\, \Phi \,|0\rangle = \begin{pmatrix} 0 \\ v/\sqrt{2} \end{pmatrix}\,. \tag{2.11}$$

With this configuration, the $\mathrm{SU}(2)_L \times \mathrm{U}(1)_Y$ gauge symmetry is (spontaneously) broken[3] down to a $\mathrm{U}(1)_e$ gauge symmetry, where e denotes the electromagnetic charge. This causes the gauge bosons to obtain a mass: The W_μ^i and B_μ fields become mixed up in the process, leading to the definition of the physical $W^\pm$ boson fields

$$W_\mu^\pm = \frac{1}{\sqrt{2}}\left(W_\mu^1 \mp W_\mu^2\right)\,, \tag{2.12}$$

and the neutral Z^0 boson and photon fields

$$\begin{aligned} Z_\mu &= \cos(\theta_w) W_\mu^3 - \sin(\theta_w) B_\mu\,, \\ A_\mu &= \sin(\theta_w) W_\mu^3 + \cos(\theta_w) B_\mu\,, \end{aligned} \tag{2.13}$$

where θ_w is the Weinberg angle, which is defined by

$$\tan(\theta_w) = \frac{g'}{g}\,. \tag{2.14}$$

The mixing of the fundamental gauge bosons ensures that the $W^\pm$ and Z^0 bosons acquire a mass after the symmetry breaking, whereas the photon, γ, stays massless. Their respective masses are

$$M_\gamma = 0\,, \quad M_W = \frac{v}{2} g\,, \quad M_Z = \frac{v}{2}\sqrt{g^2 + g'^2}\,. \tag{2.15}$$

Not just the gauge bosons, but also the fermions become massive via the Yukawa couplings in Eq. (2.1). In general, however, the flavor states and mass eigenstates of the fermions do not have to coincide. There is a mixing between different generations in the quark sector, which influences charged weak

[3] In the literature one can often find the term "hidden symmetry" instead of spontaneously broken symmetry.

currents. To obtain a diagonal quark mass matrix, a unitary transformation can be applied, i.e.

$$q_L^\alpha \rightarrow \left(\begin{pmatrix} u \\ d' \end{pmatrix}_L, \begin{pmatrix} c \\ s' \end{pmatrix}_L, \begin{pmatrix} t \\ b' \end{pmatrix}_L \right), \quad \text{with} \quad \begin{pmatrix} d' \\ s' \\ b' \end{pmatrix} = V \begin{pmatrix} d \\ s \\ b \end{pmatrix}, \tag{2.16}$$

where V is a unitary 3×3 matrix known as the Cabibbo-Kobayashi-Maskawa (CKM) matrix [55, 56]. For more technical details concerning the SM, the Higgs-mechanism and CKM mixing, the reader is adviced to see for example Refs. [4, 5]. We will now concentrate on the fundamental interaction, which is of major importance for this thesis: the strong interaction.

2.2 Quantum Chromodynamics

Quantum Chromodynamics (QCD) is the $SU(3)_C$ part of the Standard Model and it describes the interaction of quarks and gluons that carry the so-called color charge C (see e.g. [57]). As already mentioned, the quarks are spin-$1/2$ matter fields (fermions) and there are six different quark flavors: $q_f = (u, d, s, c, b, t)$. The gluons are the spin-1 gauge bosons of QCD that mediate the strong force. A crucial difference to the electromagnetic interaction, QED, is that the gluons themselves carry color charge, which enables them to interact with each other. In QED, on the other hand, the photon, which communicates the electromagnetic force, is electrically neutral and cannot interact with itself. These self-interactions of the gluons are the defining property of a non-Abelian gauge theory [58].
The coupling strength of the strong interaction is quantified by the QCD coupling constant g_s. Analogously to QED, one can define the parameter α_s, which is given by $\alpha_s = g_s^2/(4\pi)$. The numerical value of the coupling depends on the momentum transfer Q^2 during reactions: The coupling is small for large momentum transfers ($Q^2 \sim M_Z^2$), but grows quickly for decreasing values of Q^2. This phenomenon is called asymptotic freedom [59] and it is a typical feature of non-Abelian gauge theories in four spacetime dimensions. Another characteristic of QCD is the so-called color confinement, which implies that one is not able to observe singly colored particles, e.g. single quarks. The quarks and gluons must always form color neutral bound states, which are called hadrons. A color neutral hadron can, for example, be achieved by a bound state of a quark and an anti-quark ($\bar{q}q$), which is called meson, or a three quark state (qqq), called baryon. In theory, also bound states of more quarks (e.g. tetra- or pentaquarks) are possible, as well as pure gluonic bound states (glueballs). However, in this thesis we will concentrate mainly on baryons and their properties. Both phenomena, the asymptotic freedom and the color confinement, make QCD a very remarkable but complicated theory, which cannot be treated with conventional perturbative methods at low energies.
There are two very promising approaches to describe the low-energy regime of QCD, which have been developed and improved in recent years: Lattice QCD (LQCD) and effective field theories (EFTs). Both approaches offer a framework to study QCD, which can be improved systematically.
In LQCD one attempts to calculate QCD processes directly on a discretized Euclidean space-time lattice of finite volume[4]. The lattice itself is a hyper-cubic structure of usually three space dimensions and one time dimension, where the time component is analytically continued to imaginary times by a Wick-rotation, i.e. $t \rightarrow -it$. The quarks are then defined on the lattice points and the gauge-fields are on the links that connect two lattice points. This setup allows one to numerically calculate observables,

[4] For an introduction to LQCD see e.g. Ref. [14] or the review [10].

like hadron masses. However, there are some issues with this formalism: The fact that LQCD operates on a finite lattice automatically breaks Lorentz invariance. Also, particle momenta can only take on discrete values due to the finite volume and have a natural UV cutoff proportional to $1/a$, where a is the lattice spacing. To obtain real-world physics the so-called continuum limit $a \longrightarrow 0$ has to be performed. These finite-volume effects are an important aspect to relate LQCD results with observables from the physical world, which we will also investigate in chapters 3 and 4.
The second approach, EFT, is the one we will use in this thesis to study low-energy QCD and baryon properties. A brief introduction to EFTs is given in the next section.

The Lagrangian of QCD with quarks and gluons as fundamental degrees of freedom is after the previously discussed spontaneous symmetry breaking given by

$$\mathcal{L}_{\text{QCD}} = \sum_f \bar{q}_f \left(i \not{D} - m_f \right) q_f - \frac{1}{4} G^a_{\mu\nu} G^{a,\mu\nu} \ . \tag{2.17}$$

Here, q_f denotes the quark field of flavor f with its corresponding mass m_f. Each quark field consists of a color triplet

$$q_f = \begin{pmatrix} q_{f,r} \\ q_{f,g} \\ q_{f,b} \end{pmatrix} , \tag{2.18}$$

where the subscripts r (red), g (green), and b (blue) represent the three color charges. The covariant derivative D_μ ensures gauge invariance of the fermionic part and introduces the interaction between quark and gluon fields. It is given by

$$D_\mu \, q_f = \left(\partial_\mu + i \frac{g_s}{2} A^a_\mu \lambda^a \right) q_f \ , \tag{2.19}$$

where A^a_μ represents the eight independent gluon fields ($a = 1, 2, ..., 8$) and λ^a are the Gell-Mann matrices. The second term in (2.17) describes the dynamics of the gluon fields via the field strength tensor $G^a_{\mu\nu}$, which is already defined in Eq. (2.6). The squared field strength tensor in the Lagrangian gives rise to gluon self-interactions proportional to g_s and g_s^2.
From a theoretical perspective, the Lagrangian in (2.17) could also contain the so-called QCD θ-term, which is given by

$$\mathcal{L}_\theta = \theta \frac{g_s^2}{64\pi^2} \epsilon^{\mu\nu\rho\sigma} G^a_{\mu\nu} G^a_{\rho\sigma} \ , \tag{2.20}$$

where $\epsilon^{\mu\nu\rho\sigma}$ is the totally antisymmetric Levi-Civita tensor in four dimensions and θ is a real parameter. This term is gauge invariant and has dimension four, but, due to the antisymmetric Levi-Civita tensor, it violates the discrete CP symmetry (P: parity, C: charge conjugation). Hence, this term could induce a permanent electric dipole moment (EDM) into baryons, like the neutron n. So far, however, measurements of the neutron EDM only find a very small upper bound of $|d_n| < 1.8 \times 10^{-26} e\,\text{cm}$ [46] for a permanent dipole moment. This suggests that the θ parameter must be very close to zero, $|\theta| < 10^{-10}$, which is also validated by Lattice QCD calculations [60]. The fact that θ is almost

vanishing and, therefore, QCD seems to preserve CP is a fine tuning problem known as the "strong CP problem"[5]. For our further studies in this thesis we assume that $\theta = 0$ and omit the QCD θ-term. In later chapters we will discuss other sources of CP violation in the strong sector.
The QCD Lagrangian was constructed to be invariant under local $SU(3)_C$ gauge transformations and under Lorentz transformations. Without the θ-term (2.20) also the discrete symmetries P, C, and T are not violated. Additionally, the QCD Lagrangian possesses a global flavor symmetry, meaning that one can replace any quark flavor in a QCD process and the interaction will look the same (neglecting electromagnetic and weak force effects). The flavor of the quark will also not change during the interaction.
Usually one divides the six different quark flavors into two groups: the light quarks u, d, s, and the heavy quarks c, b, t, where the terms light and heavy refer to the QCD scale $\Lambda_{\text{QCD}} \simeq 210\,\text{MeV}$[6]. Note, however, that the light quark masses can only be determined indirectly at a specific renormalization scale μ, see e.g. Ref. [13] for further details. In the low-energy region of the strong force, a good approximation for the QCD Lagrangian is to include only the light quark flavors. Then, one can consider the so-called "chiral limit", where the quark masses approach zero, i.e. $m_{u,d,s} \to 0$, which is equivalent to the situation before the spontaneous symmetry breaking. The Lagrangian in (2.17) then becomes

$$\mathcal{L}^0_{\text{QCD}} = \sum_{f=u,\,d,\,s} \bar{q}_f i \not{D} q_f - \frac{1}{4} G^a_{\mu\nu} G^{a,\,\mu\nu} \,. \tag{2.21}$$

Now, one can introduce the projection operators P_L and P_R, which are defined by

$$P_L = \frac{1}{2}\left(\mathbb{1} - \gamma_5\right) \,, \quad P_R = \frac{1}{2}\left(\mathbb{1} + \gamma_5\right) \,, \tag{2.22}$$

where γ_5 is given by $\gamma_5 = i\gamma^0\gamma^1\gamma^2\gamma^3$ and obeys the anti-commutation relation $\{\gamma_5, \gamma^\mu\} = 0$, as well as $(\gamma_5)^\dagger = \gamma_5$ and $(\gamma_5)^2 = \mathbb{1}$. As projection operators, P_L and P_R also fulfill the identities

$$P_L + P_R = \mathbb{1} \,, \quad P_L P_R = P_R P_L = 0 \,, \quad \text{and} \quad P^2_{L/R} = P_{L/R} \,. \tag{2.23}$$

With these operators, the quark spinor q_f can be decomposed into left- and right-handed components

$$q_f = \left(P_L + P_R\right) q_f = P_L q_f + P_R q_f \equiv q_{L,f} + q_{R,f} \,. \tag{2.24}$$

Using the above identities, the Lagrangian in the chiral limit (2.21) can be rewritten in terms of left- and right-handed quark fields,

$$\mathcal{L}^0_{\text{QCD}} = \sum_{f=u,\,d,\,s} \left(\bar{q}_{L,f} i \not{D} q_{L,f} + \bar{q}_{R,f} i \not{D} q_{R,f}\right) - \frac{1}{4} G^a_{\mu\nu} G^{a,\,\mu\nu} \,. \tag{2.25}$$

The left- and right-handed quark fields completely decouple and the Lagrangian manifests a global $SU(3)_L \times SU(3)_R$ symmetry, which is called "chiral symmetry". The full symmetry group of massless

[5] For more information on the strong CP problem, check e.g. Refs. [17, 61].
[6] Λ_{QCD} evaluated in $\overline{\text{MS}}$ scheme for five flavors ($N_f = 5$) at the renormalization scale $\mu = 2\,\text{GeV}$, see Ref. [10].

QCD with three flavors is

$$G = \mathrm{SU}(3)_L \times \mathrm{SU}(3)_R \times \mathrm{U}(1)_V \,, \tag{2.26}$$

where the $\mathrm{U}(1)_V$ symmetry, with $V = L + R$, corresponds to baryon number conservation. There is no axial $\mathrm{U}(1)_A$ ($A = L - R$) symmetry due to the axial anomaly (see e.g. [5, 17]). This chiral symmetry, however, is only fulfilled in the limit of vanishing quark masses, since a mass term mixes the left- and right-handed components of the quark fields, i.e.

$$\mathcal{L}_m = \bar{q}_f m_f q_f = \bar{q}_f \left(P_L + P_R\right) m_f \left(P_L + P_R\right) q_f = \bar{q}_{L,f} m_f q_{R,f} + \bar{q}_{R,f} m_f q_{L,f} \,. \tag{2.27}$$

Therefore, a mass term explicitly breaks the symmetry. Today we know that the chiral symmetry of QCD must be spontaneously broken (see e.g. Ref. [62]). Additionally, the small non-vanishing quark masses also break the chiral symmetry explicitly. This observation is the starting point of chiral perturbation theory (ChPT), the low-energy effective field theory of QCD, which we will discuss in an upcoming section.

2.3 Effective field theories

The non-perturbative nature of QCD at low energies makes the study of hadrons significantly non-trivial. We have already mentioned the two most important approaches to investigate the low-energy regime of the strong interaction: Lattice QCD (LQCD) and effective field theories (EFTs), where the latter will be shortly introduced in this section[7].

The basic idea of an EFT is to find a simpler description of a physical process, that would normally have to be described by a highly non-trivial physical theory, e.g. QCD. The most important concept underlying EFTs is the so-called "separation of scales". To construct an EFT for a given physical system one has to find the scales (length scales or energy/momentum scales), which are inherent to the system, and identify the relevant scales and degrees of freedom for the problem at hand. For example, to describe a freely moving ball in a gravitational field one can use classical Newtonian mechanics, whereas the inclusion of molecular or nuclear forces inside the ball are not necessary [17]. Another important building block for EFTs are symmetries. For a given quantum field theory (QFT) that obeys certain continuous and discrete symmetries, a corresponding EFT must obey the same symmetries. This ensures that an S-matrix element calculated from the EFT leads to the same symmetry structure, which the S-matrix element would have when it is calculated from the underlying QFT [63], which ultimately is the reason why EFTs work and that they can make predictions about physical processes. Once the relevant scales and degrees of freedom are known, the EFT is constructed by writing down all possible terms, which include the degrees of freedom and are allowed by the symmetries. This, however, implies that an EFT consists of infinitely many terms of arbitrary dimension, which need to be ordered in some systematic manner to keep EFT calculations feasible. The procedure one uses to order the terms and identify their relevance for a given calculation is the so-called "power counting". To apply power counting, one typically uses a perturbative expansion parameter $(Q/\Lambda)^\kappa$, where Λ is the energy scale where the EFT breaks down, Q is a small energy/momentum ($\Lambda \gg Q$) and κ is a positive exponent. It is then straightforward to see that terms with smaller powers of the

[7] See Ref. [17] for a very good pedagogical and comprehensive introduction.

expansion parameter will give a larger contribution to a matrix element. For any given EFT, such a power counting scheme has to be introduced. Two additional remarks should be added here: First, since an EFT consists of infinitely many terms, the theory is not renormalizable up to arbitrary scales. However, renormalizability can be achieved until the breakdown scale Λ (see e.g. [64]). Second, from the construction procedure of EFTs it is evident that any QFT is, in fact, an EFT itself [17].
To clear up the EFT construction procedure a bit more, we take a look at a concrete example: Standard Model effective field theory (SMEFT) [45]. Let us assume that there is beyond-the-Standard-Model (BSM) physics appearing at an energy scale Λ, which is much larger than the electroweak scale $v \simeq 250\,\text{GeV}$. The BSM physics could for example be new heavy particles, which cannot be produced yet in modern particle accelerators. However, those particles should still influence the behaviour of the SM particles at lower energies. We can, therefore, construct an EFT, which includes the SM as a low-energy approximation: This is known as SMEFT.
For constructing the EFT for the SM, we now have a scale separation, i.e. $\Lambda \gg v$, and as degrees of freedom we can take the whole particle content of the SM. We now have to write down all possible terms that fulfill the symmetries of the SM, i.e. Lorentz symmetry and $\mathrm{SU}(3)_C \times \mathrm{SU}(2)_L \times \mathrm{U}(1)_Y$ gauge symmetry. The resulting Lagrangian takes the following form

$$\mathcal{L}_{\text{SMEFT}} = \mathcal{L}_{\text{SM}} + \frac{1}{\Lambda}\mathcal{L}_5 + \frac{1}{\Lambda^2}\mathcal{L}_6 + \frac{1}{\Lambda^3}\mathcal{L}_7 + \frac{1}{\Lambda^4}\mathcal{L}_8 + \dots\,, \tag{2.28}$$

where $\mathcal{L}_{\text{SM}}$ is the SM Lagrangian from Eq. (2.1) and $\mathcal{L}_D$ are higher order terms in the $1/\Lambda$ expansion. The index D, with $D > 4$, denotes the mass dimension of the operators inside the Lagrangians. It can be clearly observed that for very low energies the SM Lagrangian is the dominating contribution of this expansion, whereas all other terms are suppressed by inverse powers of Λ. This brings up the question how these BSM effects can be resolved by experiments? The first option is, obviously, going to higher energies, but also at low energies their influence can be measured: Many BSM models include violations of the discrete symmetries C and CP, which would then also effect the low-energy regime. Hence, one can construct higher dimensional terms $\mathcal{L}_D$ that explicitly violate C and CP and calculate their consequences on SM particles. Some effects that C and CP violating sources can cause are, for example, inducing a permanent electric dipole moment (EDM) in baryons or enhancing specific particle decays that would be supressed in the SM[8]. In chapter 5 we will analyze the effects of C and CP violating dimension-six operators, i.e. $\mathcal{L}_6$, on the EDMs of baryons that contain one (valence) bottom quark. For this, however, we need an EFT for low-energy QCD, which we introduce in the next section.

2.4 Chiral perturbation theory

Chiral perturbation theory (ChPT) is the effective field theory (EFT) of low-energy QCD. It describes the interactions and behaviour of the lightest asymptotic hadronic states at low energies. Also, external weak or electromagnetic currents, like e.g. photons, can be treated within this EFT. In this following section we briefly recap the basic ideas of ChPT in the mesonic sector. For simplicity, only effects of the strong interaction are considered in this section, neglecting any contributions from weak or electromagnetic interactions.

[8] See e.g. Ref. [65] and the references therein.

We have seen before that the QCD Lagrangian in the chiral limit is invariant under global transformations of the symmetry group G given by Eq. (2.26). However, the ground state of QCD does not seem to obey the full symmetries in G, which can be deduced from certain indications in the the hadronic spectrum. For example, if chiral symmetry would be realized in the ground state, all lowest-lying hadrons must aqcuire a hadronic "partner" state with the same mass but opposite parity quantum number (see e.g. [62]). But these parity doublets are not observed in nature. Instead, the ground state appears to fulfill a $\mathrm{SU}(3)_V$ symmetry in the chiral limit [66], which leads to the conclusion that chiral symmetry must be spontaneously broken. This, explicitly, means that the left- and right-handed part of the group G breaks down to a vectorial subgroup,

$$\mathrm{SU}(3)_L \times \mathrm{SU}(3)_R \times \mathrm{U}(1)_V \rightarrow \mathrm{SU}(3)_V \times \mathrm{U}(1)_V \ . \tag{2.29}$$

This sponteneous symmetry breaking causes the appearence of $3^2 - 1 = 8$ massless, scalar (spin 0) bosons, according to Goldstone's theorem [67, 68]. In the case of spontaneous breakdown of chiral symmetry, these bosons have to be pseudoscalar (i.e. they must have negative parity $J^P = 0^-$), since the ground state is not invariant under axial transformations. However, due to the explicit chiral symmetry breaking caused by the small quark masses, it is expected that the pseudo-Goldstone bosons are not exactly massless but aquire, indeed, a non-vanishing mass.
As it turns out, the perfect candidates for the 8 pseudo-Goldstone bosons are the members of the lowest-lying meson octet consisting of the pions (π^0, π^+, π^-), the kaons (K^+, K^-, K^0, $\bar{K}^0$), and the eta meson (η). These particles have the right quantum numbers ($J^P = 0^-$) and possess masses, which are considerably smaller than the masses of the second lowest-lying meson octet, the $J^P = 1^-$ vector mesons[9]. The goal is now to construct an effective field theory, which contains the pseudo-Goldstone bosons as explicit degrees of freedom and describes their interactions with each other.

We now want to construct the effective Lagrangian for the pseudo-Goldstone bosons meaning that we need to consider all terms which are allowed by the symmetries we impose. Since we aim to find an EFT for low-energy QCD, the necessary symmetries include Lorentz invariance, the discrete symmetries C, P, T and, according to our findings before, the group G (2.26) and $\mathrm{SU}(3)_V \times \mathrm{U}(1)_V$ for the ground state. The Goldstone boson fields are introduced via the unitary matrix U, which is defined by

$$U(x) = \exp\left(i\frac{\phi(x)}{F_\phi}\right) = \mathbb{1} + i\frac{\phi(x)}{F_\phi} - \frac{\phi^2(x)}{2F_\phi^2} + \dots \ . \tag{2.30}$$

Here, F_ϕ is the pseudoscalar decay constant in the chiral limit and $\phi(x)$ is a 3×3 matrix, that includes the pseudoscalar octet meson particles

$$\phi(x) = \sum_{a=1}^{8} \lambda^a \phi^a(x) = \sqrt{2}\begin{pmatrix} \frac{1}{\sqrt{2}}\pi^0 + \frac{1}{\sqrt{6}}\eta & \pi^+ & K^+ \\ \pi^- & -\frac{1}{\sqrt{2}}\pi^0 + \frac{1}{\sqrt{6}}\eta & K^0 \\ K^- & \bar{K}^0 & -\frac{2}{\sqrt{6}}\eta \end{pmatrix}, \tag{2.31}$$

[9] For example, the pions have a mass of around 139 MeV, whereas the ρ meson has a mass of 775 MeV [13].

where the λ^a are the Gell-Mann matrices. Note that it is sometimes better suited to work in a flavor SU(2) approximation, meaning that only the two lightest quarks u and d are considered. In this case the $2^2 - 1 = 3$ pseudo-Goldstone bosons are solely the pions and the $\phi(x)$ matrix reduces to

$$\phi(x) = \sum_{i=1}^{3} \tau^i \phi^i(x) = \begin{pmatrix} \pi^0 & \sqrt{2}\pi^+ \\ \sqrt{2}\pi^- & -\pi^0 \end{pmatrix} , \tag{2.32}$$

with the Pauli matrices τ^i. We, however, continue our explanations in the three-flavor case. The matrix U transforms as $U \to RUL^\dagger$, where R and L are global right- and left-handed symmetry transformations, respectively, i.e. $R, L \in \mathrm{SU}(3)_{R,L}$. Using this transformation behaviour, it is possible to write down the leading-order Lagrangian for the Goldstone boson fields, which fulfills all of the above considerations. It is given by [69, 70]

$$\mathcal{L}_\phi^{(2)} = \frac{F_\phi^2}{4} \mathrm{Tr}\left(D_\mu U (D^\mu U)^\dagger\right) + \frac{F_\phi^2}{4} \mathrm{Tr}\left(\chi U^\dagger + U \chi^\dagger\right) , \tag{2.33}$$

where the traces act in flavor space and the covariant derivative, D_μ, is defined by

$$D_\mu U = \partial_\mu U - i r_\mu U + i U l_\mu . \tag{2.34}$$

Here, the notation $r_\mu = v_\mu + a_\mu$ and $l_\mu = v_\mu - a_\mu$ is used, where v_μ and a_μ denote external vector and axial-vector currents, respectively. Since we do not consider any external sources, we can simply set $v_\mu = a_\mu = 0$. The covariant derivative acting on U ensures the transformation behaviour $D_\mu U \to R(D_\mu U)L^\dagger$. The second term in (2.33) contains the matrix χ, which introduces quark masses and, hence, induces explicit chiral symmetry breaking,

$$\chi = 2B_0 \mathcal{M} , \quad \text{with} \quad \mathcal{M} = \mathrm{diag}(m_u, m_d, m_s) , \tag{2.35}$$

where the constant B_0 is related to the chiral quark condensate. Although the quark mass matrix is, in fact, a constant matrix, one imposes the transformation behaviour $\mathcal{M} \to R\mathcal{M}L^\dagger$ on it, so that invariance under chiral symmetry transformations is warranted.
An important approximation when considering quark masses is the so-called "isospin limit". In it, the masses of the lightest quark flavors, u and d, are set to the same value, i.e. $m_u = m_d = \hat{m}$, leading to the simplified expression $\mathcal{M} = \mathrm{diag}(\hat{m}, \hat{m}, m_s)$ for the quark mass matrix. The isospin limit will be used throughout all our investigations in this thesis. One can, for example, easily obtain the lowest order meson masses using this limit, i.e.

$$M_\pi^2 = 2B_0 \hat{m} , \quad M_K^2 = B_0(\hat{m} + m_s) , \quad M_\eta^2 = \frac{2}{3} B_0(\hat{m} + 2m_s) , \tag{2.36}$$

which are known as the Gell-Mann-Oakes-Renner relations [71]. These expressions also demonstrate that the mesons become massless if the quark masses vanish (chiral limit), which is a required feature in the construction of ChPT.
The Lagrangian in Eq. (2.33) has a superscript (2), which denotes that this Lagrangian is of second order in the power-counting scheme used in ChPT. This scheme uses small four-momenta p divided by the so-called chiral symmetry breaking scale Λ_χ, where $\Lambda_\chi \sim 4\pi F_\pi \sim 1\,\mathrm{GeV}$, with the pion decay

constant F_π. According to our statements from the previous section, the power counting is then performed by analyzing factors of $(p/\Lambda_\chi)^\kappa$, where κ is usually called the "chiral order". For example, the Lagrangian in Eq. (2.33) has chiral order 2, which is commonly denoted as $O(p^2)$. This is due to the two derivatives in the first term of (2.33), which give rise to two small four-momenta of the meson fields when deriving the corresponding Feynman rules in momentum space, i.e. $p^\mu p_\mu = p^2$. The quark masses from the matrix χ in the second term of (2.33) also count as order p^2, since the linear quark masses give rise to the squared Goldstone boson masses (see Eq. (2.36)). In fact, the chiral order $O(p^2)$ Lagrangian from Eq. (2.33) is the lowest-order (and, hence, leading-order) Lagrangian in the power counting that fulfills all necessary symmetries. One can further construct the EFT by writing down all possible combinations of the building blocks U, $D_\mu U$ and χ, which are allowed by the symmetries. The next to leading-order Lagrangian appears at order $O(p^4)$ and is given in Ref. [70]. For more information, we refer to Ref. [17].

2.5 Baryon chiral perturbation theory

In this section, we want to illustrate shortly how the introduced formalism of ChPT can be extended to also include heavier degrees of freedom, like e.g. baryons. This extension of ChPT is known as Baryon chiral perturbation theory (BChPT).
The consistent inclusion of baryons in ChPT turns out to be non-trivial. Not only the appearing Dirac structures, coming from the fact that baryons are fermionic particles, complicate the matter, but also the large masses of the baryons cause issues. The mass of the proton ($m_p \simeq 938\,\text{MeV}$ [13]), for example, is significantly larger than the pseudo-Goldstone boson masses and already around the size of the chiral symmetry breaking scale $\Lambda_\chi \sim 1\,\text{GeV}$. This large mass difference implies that nucleons (protons and neutrons) should remain massive even in the chiral limit $m_{u,d,s} \to 0$. In fact, it can be shown that the nucleon mass does not vanish if the quark masses are zero: In massless QCD, where only the dimensionless constant g_s appears, an energy scale Λ_{QCD} emerges due to the breakdown of scale invariance, i.e. the trace anomaly. As a consequence, bound states of the strong interaction acquire a mass proportional to Λ_{QCD} in the chiral limit. This process is called "dimensional transmutation" and it is responsible for the large masses of the baryons, as well as other mesonic states, like e.g. the ρ meson. Only the pseudo-Goldstone bosons are unaffected by this mass generation (for more information on the subject, see e.g. [17]). The baryon mass in the chiral limit, which we denote by m_0[10], introduces an additional mass scale in ChPT, which has to be treated with special care as we will see later.

In the two-flavor case (flavor SU(2)) the nucleon field is introduced by the doublet

$$\Psi(x) = \begin{pmatrix} p \\ n \end{pmatrix} , \tag{2.37}$$

[10] In the literature, the convention $\mathring{m}$ is also frequently used.

where p and n denote the four-component Dirac fields for the proton and neutron, respectively. For flavor SU(3), the lowest-lying octet baryons must be introduced via a matrix $B(x)$, which is given by

$$B(x) = \frac{1}{\sqrt{2}} \sum_{a=1}^{8} \lambda^a B^a(x) = \begin{pmatrix} \frac{1}{\sqrt{2}}\Sigma^0 + \frac{1}{\sqrt{6}}\Lambda & \Sigma^+ & p \\ \Sigma^- & -\frac{1}{\sqrt{2}}\Sigma^0 + \frac{1}{\sqrt{6}}\Lambda & n \\ \Xi^- & \Xi^0 & -\frac{2}{\sqrt{6}}\Lambda \end{pmatrix}, \tag{2.38}$$

with the Gell-Mann matrices λ^a. Under chiral transformations, the baryon fields transform according to

$$\Psi \to K\Psi\,, \quad \text{and} \quad B \to KBK^\dagger\,, \tag{2.39}$$

where $K = K(L, R, U)$ is the so called compensator field. This function K is an element of the conserved subgroup $SU(3)_V$ after the spontaneous symmetry breaking of the group G (2.26). It depends on the left- and right-handed transformations (L and R) and on the matrix $U(x)$ (2.30), which includes the pseudo-Goldstone boson fields. The fact that U depends on the position x, makes $K(L, R, U)$ a local transformation (see e.g. Refs. [62, 72] for more information). The resulting effective Lagrangians that describe the baryons and their interactions with the pseudoscalar mesons, must be invariant under the corresponding transformations in (2.39).
In the flavor-SU(2) case, the leading-order Lagrangian is given by [73]

$$\mathcal{L}^{(1)}_{\pi\Psi} = \bar{\Psi}\left(i\not{D} - m_0\right)\Psi + \frac{1}{2} g_A \bar{\Psi}\not{u}\gamma_5\Psi\,. \tag{2.40}$$

Here, the covariant derivative obeys the transformation property $D_\mu\Psi \to K(D_\mu\Psi)$ and is defined by

$$D_\mu\Psi = \left(\partial_\mu + \Gamma_\mu\right)\Psi\,, \tag{2.41}$$

with

$$\Gamma_\mu = \frac{1}{2}\left[u^\dagger\left(\partial_\mu - ir_\mu\right)u + u\left(\partial_\mu - il_\mu\right)u^\dagger\right]\,, \tag{2.42}$$

where $u = \sqrt{U} = \exp\left(i\phi/(2F_\phi)\right)$ and l_μ/r_μ are external left- and right-handed fields, respectively. The second term in Eq. (2.40) is the axial-vector interaction with the axial-vector coupling constant g_A and the so-called chiral vielbein

$$u_\mu = i\left\{u^\dagger\left(\partial_\mu - ir_\mu\right)u - u\left(\partial_\mu - il_\mu\right)u^\dagger\right\}\,, \tag{2.43}$$

which transforms according to $u_\mu \to Ku_\mu K^\dagger$. From the above equations, it can be observed that interactions between nucleons and pions emerge from the covariant derivative, as well as from the chiral vielbein.
A leading-order Lagrangian with a very similar structure as in (2.40) is obtained in flavor SU(3). However, there are some differences occurring since the octet baryons are now included inside the

matrix B. The Lagrangian is given by [74]

$$\mathcal{L}^{(1)}_{\phi B} = \mathrm{Tr}\left(\bar{B}\left(i\not{D} - m_0\right)B\right) + \frac{D}{2}\mathrm{Tr}\left(\bar{B}\gamma^\mu\gamma_5\left\{u_\mu, B\right\}\right) + \frac{F}{2}\mathrm{Tr}\left(\bar{B}\gamma^\mu\gamma_5\left[u_\mu, B\right]\right) , \tag{2.44}$$

where the introduced traces operate in flavor space. The covariant derivative is also slightly changed, i.e.

$$D_\mu B = \partial_\mu B + \left[\Gamma_\mu, B\right] , \tag{2.45}$$

and it transforms as $D_\mu B \longrightarrow K(D_\mu B)K^\dagger$. Also, in Eq. (2.44) there are two axial-vector interactions proportional to the constants D and F, which have to fulfill the relation $D + F = g_A$ to translate back to the two-flavor case (matching).
Considering the power counting for the above Lagrangians in the two- and three-flavor case, the chiral vielbein contains derivatives of the pseudo-Goldstone bosons and, hence, has chiral order $O(p)$. The baryon mass in the chiral limit, m_0, has no chiral order, since it is of the same order as the chiral symmetry breaking scale Λ_χ. It can therefore not serve as a "small" expansion parameter and counts as order $O(1)$. The same is also true for the baryon momenta, which are generated by the derivative term $i\not{D}$ in momentum space. However, the difference $(i\not{D} - m_0)$ corresponds to $(\not{p} - m_0)$ in momentum space, which can be considered as a small scale with chiral order $O(p)$. Using these properties, baryon Lagrangians of higher order can be constructed.

Unfortunately, the appearence of the baryon mass m_0 still causes problems in the power counting when loop calculations are performed. This was first pointed out in Ref. [73]. The large mass m_0 also enters the baryon propagator

$$S_B^{ab}(\not{p}) = \frac{i\delta^{ab}(\not{p} + m_0)}{p^2 - m_0^2 + i\epsilon} , \tag{2.46}$$

and leads to terms in the loop function, which explicitly break the power counting. This is a severe issue, because if the power counting does not work, one is not able to identify relevant Feynman diagrams for a calculation. Diagrams that appear to be of higher order could still contribute at lowest order, which makes the EFT inconclusive.
Fortunately, there are some methods, which can be used to restore the power counting. One method is to systematically subtract the polynomial terms, which violate the power counting, within a modified regularization scheme of the loop integrals. This process is called "Extended On-Mass-Shell (EOMS)" scheme [75] and it is one of the widely used approaches today to calculate observables within the fully relativistic formulation of BChPT (see e.g. [76]). A different method, which also uses a modified regularization scheme, is the so-called "Infrared Regularization" [77]. In it, the integration limits of occurring Feynman parameter integrals (see App. B.2) are changed to tame the loop integral parts, which lead to the violation of the power counting. A lucid overview of both methods can also be found in Ref. [17].
Another method to restore the power counting is the heavy-baryon (HB) formulation of BChPT, also called heavy baryon chiral perturbation theory (HBChPT) [78]. In this approach, the inverse baryon mass, $1/m_0$, is used as an additional expansion parameter, which, in turn, eliminates the mass scale from the leading order Lagrangian. To achieve this, the momentum of the very heavy baryon is written

as

$$p_\mu = m_0 v_\mu + l_\mu \,, \tag{2.47}$$

where v_μ is the four-velocity[11], which obeys $v^2 = 1$, and l_μ is a small off-shell momentum satisfying $(v \cdot l) \ll m_0$. Then, the baryon field B can be decomposed into eigenstates of the four-velocity projection operator $P_v = \frac{1}{2}(1 + \not{v})$ according to

$$B = e^{-im_0 v\cdot x} \left(B_v + b_v\right) \,, \quad \text{with} \quad \not{v} B_v = B_v \,, \quad \text{and} \quad \not{v} b_v = -b_v \,, \tag{2.48}$$

where B_v is the large component field and b_v is the small component field. After inserting the above ansatz into Eq. (2.44), one obtains a Lagrangian in terms of B_v and b_v. Then, one can perform a shift of variables to absorb mixing terms of b_v and B_v and integrate out the small component field b_v[12]. The resulting Lagrangian is given by

$$\mathcal{L}^{(1)}_{HB} = \mathrm{Tr}\left(\bar{B}_v \left(iv\cdot D\right) B_v\right) + D\,\mathrm{Tr}\left(\bar{B}_v S^\mu \left\{u_\mu, B_v\right\}\right) + F\,\mathrm{Tr}\left(\bar{B}_v S^\mu \left[u_\mu, B_v\right]\right) + \ldots \,, \tag{2.49}$$

where S^μ is the Pauli-Lubanski spin operator, which is defined by

$$S^\mu = -\frac{1}{2}\gamma_5 \left(\gamma^\mu \not{v} - v^\mu\right) \,, \tag{2.50}$$

and obeys the relations $v \cdot S = 0$ and $S^2 = (1 - D)/4$ in D spacetime dimensions. The ellipses in (2.49) denote terms of order $O(1/m_0)$, which can be neglected assuming that m_0 is very large. The corresponding propagator for the B_v field takes the form

$$S^{ab}_{HB}(\omega) = \frac{i\delta^{ab}}{\omega + i\epsilon} \,, \quad \text{with} \quad \omega = v \cdot l \,. \tag{2.51}$$

One can clearly observe that the mass scale does not appear anymore at lowest order and, hence, the power counting can be carried out without problems. Corrections of order $O(1/m_0)$ can be included systematically within the framework. We will utilize the HB formulation later in chapter 5 when we consider the heavy bottom-quark baryons. In fact, the idea of the four-velocity decomposition in HBChPT is exactly the same, which is used in heavy quark EFTs (see e.g. Ref. [80]). For additional information on BChPT for baryons containing a single heavy quark, see Refs. [81, 82].

2.6 Non-relativistic EFTs and the particle-dimer picture

Although chiral perturbation theory provides a successful description of mesons and baryons and their interactions, it is not the only effective field theory (EFT) approach, which can give meaningful insights to low-energy phenomena of QCD. As we have already seen in the heavy baryon formulation of BChPT, some useful approximations can be made if the mass of an appearing particle is very large. In fact, once the particle's three momentum $\vec{p}$ is significantly smaller than its mass m, the physics

[11] For example, in the baryon rest frame the four-velocity is given by $v_\mu = (1, 0, 0, 0)$.

[12] This procedure can be performed very elegantly in the path integral formalism, see Ref. [79].

of this partice can be described by non-relativistic quantum mechanics. In this limit, the relativistic particle field can be separated into its particle and antiparticle part by using the Foldy-Wouthuysen transformation [83]. Afterwards, the antiparticles can be integrated out resulting in a theory that only contains particles and conserves particle number, which is obviously not the case in the fully relativistic limit.
Such a non-relativistic effective field theory (NREFT) presents a valuable approximation when describing processes in which all appearing particles are low energetic and particle number conservation can be assumed. We now want to give two examples on how to implement non-relativistic kinematics for the particle in NREFT. The first possibility is to use the well-known Schrödinger equation as the equation of motion. For this case, the Lagrangian takes the form (see e.g. [41])

$$\mathcal{L}_{SE} = \psi^\dagger \left(i\partial_0 + \frac{1}{2m}\vec{\nabla}^2 \right) \psi \,, \tag{2.52}$$

where ψ denotes a non-relativistic scalar field[13] with mass m. The corresponding propagator of the particle is given by

$$S_{SE}\left(p_0, \vec{p}\right) = \frac{1}{p_0 - \frac{\vec{p}^2}{2m} + i\epsilon} \,. \tag{2.53}$$

One can clearly observe that the propagator does not contain a quadratic structure in the variable p_0 meaning that there is no pole coming from the antiparticle.
The second possibility is the so-called covariant NREFT, which is especially used to describe particle processes in which some momenta can become larger. This covariant framework is, for example, utilized when pions appear in the physical reaction, like in the calculation of the kaon decay amplitude into three pions ($K \longrightarrow 3\pi$) [84]. The covariant Lagrangian is given by [84, 85]

$$\mathcal{L}_{cov} = \psi^\dagger 2W \left(i\partial_t - W \right) \psi \,, \quad \text{with} \quad W = \sqrt{m^2 - \vec{\nabla}^2} \,, \tag{2.54}$$

where the non-local differential operator W has to be understood as a series expansion in inverse powers of the mass, i.e.

$$\sqrt{m^2 - \vec{\nabla}^2} = m - \frac{\vec{\nabla}^2}{2m} - \frac{\vec{\nabla}^4}{8m^3} + \dots \,. \tag{2.55}$$

The square root structure of the operator ensures that resulting amplitudes are relativistically invariant and leads to the well-known relativistic energy-momentum relation in momentum space, which can be observed in the propagator

$$S_{cov}\left(p_0, \vec{p}\right) = \frac{1}{2\omega(\vec{p})\left[p_0 - \omega(\vec{p}) + i\epsilon\right]} \,, \quad \text{with} \quad \omega(\vec{p}) = \sqrt{m^2 + |\vec{p}|^2} \,. \tag{2.56}$$

Also here, the propagator does not contain a pole from the antiparticle. We suggest Ref. [17] and the references therein for further reading.

[13] We consider only scalar fields in this brief introduction. However, the formalism can also be extended to include particles with spin, see e.g. [17].

Another important concept within the framework of NREFT is the so-called "particle-dimer approach" [38, 39]. This approach was introduced to provide a convenient treatment of three-particle systems and their dynamics, which can become very complex due to the appearence of two- and three-body forces (see e.g. Refs. [41, 42] for a detailed introduction). The particle-dimer picture simplifies the calculation of three-particle scattering processes by introducing an auxiliary field, the so-called "dimer field", into the theory. This dimer field incorporates two-particle scattering information. Then, instead of calculating three-particle scattering, one calculates the scattering of one particle with the dimer field. The obtained particle-dimer scattering amplitude is equivalent to the original three-particle scattering amplitude [38, 40]. We want to utilize this particle-dimer formalism later in chapter 4 to describe the Roper resonance.
To better understand the functionality of the dimer formalism, we want to take a look at a specific example. Consider the Lagrangian [41]

$$\mathcal{L} = \psi^\dagger \left(i\partial_0 + \frac{1}{2m}\vec{\nabla}^2 \right) \psi - \frac{C_0}{2} \left(\psi^\dagger \psi \right)^2 - \frac{D_0}{6} \left(\psi^\dagger \psi \right)^3 + \dots \,, \tag{2.57}$$

where ψ again denotes a non-relativistic field with mass m and C_0 and D_0 are two low-energy constants (LECs) describing a two- and three-body contact interaction, respectively. The ellipses denote terms with more field insertions or derivatives. From the Lagrangian it seems obvious that calculating a three-particle scattering amplitude is still manageable at tree level but becomes much more complex at the loop level due to the large amount of possible Feynman diagrams. Let us instead consider the modified Lagrangian

$$\mathcal{L}' = \psi^\dagger \left(i\partial_0 + \frac{1}{2m}\vec{\nabla}^2 \right) \psi + \Delta T^\dagger T - \frac{g}{\sqrt{2}} \left(T^\dagger \psi\psi + \text{h.c.} \right) + h T^\dagger T \psi^\dagger \psi \,. \tag{2.58}$$

Here, T is a non-dynamical auxiliary field called the "dimer field" and Δ, g and h are three new LECs. Since the field T does not have any derivative terms, one can straightforwardly find the equations of motion for it. These equations can then be used to integrate out the auxiliary field. After this, one arrives at

$$\mathcal{L}' = \psi^\dagger \left(i\partial_0 + \frac{1}{2m}\vec{\nabla}^2 \right) \psi - \frac{g^2 (\psi^\dagger \psi)^2}{2(\Delta + h\psi^\dagger \psi)} \,.$$

where the denominator in the second term has to be expanded in terms of the fields, so that

$$\mathcal{L}' = \psi^\dagger \left(i\partial_0 + \frac{1}{2m}\vec{\nabla}^2 \right) \psi - \frac{g^2}{2\Delta} (\psi^\dagger \psi)^2 + \frac{g^2 h}{2\Delta^2} (\psi^\dagger \psi)^3 + \dots \,.$$

This Lagrangian does now look very similar to the one in Eq. (2.57) and, in fact, they are equivalent ($\mathcal{L}' = \mathcal{L}$) if the matching conditions

$$C_0 = \frac{g^2}{\Delta} \,, \quad \text{and} \quad D_0 = -\frac{3g^2 h}{\Delta^2} \,, \tag{2.59}$$

hold. Therefore, instead of calculating the three-particle scattering amplitude from Eq. (2.57), one can use the mathematically equivalent Lagrangian in (2.58) and calculate the scattering amplitude between one particle and the particle-dimer field. This means the three-body problem is reformulated as a two-body problem, which can be investigated with much more ease. The particle-dimer Lagrangian can also be modified to include derivative terms for the dimer field, so that it becomes a dynamical field. Further information about the dimer approach and its applicability can be found in Ref. [17].

CHAPTER 3

The Roper resonance in a finite volume

3.1 Prologue

The content of this chapter including appendix B is based on the publication

- D. Severt and U.-G. Meißner, "The Roper Resonance in a finite volume", Commun. Theor. Phys. **72**, no.7, 075201 (2020) [arXiv:2003.05745 [hep-lat]].

In this chapter, we calculate the finite-volume energy levels corresponding to the Roper resonance based on a two-flavor chiral effective Lagrangian for pions, nucleons, deltas and the Roper resonance at leading one-loop order. We show that the Roper mass can be extracted from these levels for not too large lattice volumes (Ref. [86]).
The project started with the idea to find the finite-volume (FV) energy spectrum of the Roper resonance. This spectrum has not been determined before with EFT methods. For the baryon resonance lying below the Roper, the delta (Δ) resonance, such a calculation has been performed some years prior in Ref. [24]. An analogous calculation for the Roper resonance was the goal at the start of the investigation.
The author of this thesis used the chiral effective Lagrangian for the Roper resonance that was already introduced in Ref. [22] to calculate the Roper mass up to third chiral order in the infinite volume. To calculate the mass, one has to find the pole positions of the particle propagator, in this case the Roper resonance propagator, and evaluate the self-energy contributions of the particle. The self-energy of a particle is caused by interactions of the particle field with itself or with other fields. Once these self-energy contributions are calculated, one can deduce the physical mass of the particle. Since the Roper is a resonance, its pole position is typically parametrized by $Z = m_R - i\Gamma_R/2$, where m_R is the mass and Γ_R is the decay width of the Roper. The calculation of the mass and width was also performed in Ref. [22] and the author of this thesis reproduced the result from the reference. It turned out that the self-energy of the Roper depends on interactions of the Roper field with nucleons (N), delta resonances (Δ) and pions (π). After this step, the author performed the transition to the finite volume. In that, the Roper resonance is placed into a cubic box of side length L, which means that the particle is confined in a fixed volume. This naturally influences the energy of the particle, since its spatial momentum $\vec{k}$ is now quantized and can only take on values of $\vec{k} = 2\pi\vec{n}/L$, where the components of $\vec{n}$ are integers. The loop functions in the self-energy must then be calculated by summing over

the spatial momenta, instead of integrating over them[1]. The author introduced the Roper resonance to the finite-volume formalism and obtained the FV self-energy contributions. The evaluation of the three-dimensional sums is in general non-trivial. In some cases, sums can be simplified using modified Bessel functions of the second kind. In other cases, sums can lead to pole structures, which have to be treated with care. These poles arise, when intermediate particles inside the loop go on-shell. For example, the Roper resonance can decay into a nucleon and a pion, which produces a pole in the self-energy. The author simplified the sums as far as possible, analogously to the procedures given in Refs. [24, 87]. After that, an equation for the finite-volume energy levels was obtained, which yields the FV spectrum of the Roper. To obtain this spectrum, the equation for the energy levels must be solved numerically for a specific box length L. The procedure is repeated for different values of L to investigate how the energy levels change, when the volume is changed. The author obtained the said FV spectrum for three different cases: Considering first only nucleon and pion as intermediate states in the self-energy and, second, only delta resonance and pion. Then, both cases are combined to one coupled channel system.
One problem in the theoretical description is the delta resonance, which is not a stable final state, but decays further into a nucleon and a pion. In the beginning, the author of this thesis was not aware, how the unstable nature of the delta can be implemented into the calculation. U.-G. Meißner and the author then decided to keep the delta stable to obtain a first approximation for the Roper resonance FV spectrum. The inclusion of an unstable delta resonance should be achieved in an upcoming work. This work is discussed later in chapter 4.

3.2 Introduction

In the last years a lot of work has been done to understand the hadron spectrum as it emerges from Quantum Chromodynamics (QCD). However, the excited baryon spectrum of QCD is still not very well understood and requires further theoretical investigations. At low energies chiral perturbation theory (ChPT) has proven to be an important tool to describe hadrons and their interactions, especially in the Goldstone boson sector. The inclusion of baryon states in ChPT is also possible and baryon chiral perturbation theory (BChPT) is widely and successfully used today. BChPT requires a more sophisticated approach because of the breakdown of the power counting due to the inclusion of these heavy degrees of freedom and their large masses. This issue can, however, be resolved either by using the so-called heavy-baryon approach or a suitably chosen renormalization scheme within an explicitly Lorentz-invariant formalism, like the infrared regularization (IR) or extended-on-mass shell (EOMS) approaches, see e.g. the review [88]. This allows to investigate the properties of a few low-lying excited states. Unitarization methods allow to address more meson and baryon resonances, however, at the cost of introducing some model-dependence as various unitarization schemes can be employed. To access a larger part of the spectrum, a different approach is required. Lattice QCD is a first principles method that allows to calculate the hadron spectrum from the underlying fundamental quark and gluon fields. Calculations do an outstanding job in describing the lowest-lying hadron states. With ever increasing computational power, improved algorithms and refined finite volume methods, especially hadron ground states are simulated more and more precisely on the lattice. Excited states are more difficult to access, though there has been some visible progress in the last years. The present state of the art is reviewed in Ref. [89].

[1] The three-dimensional spatial integral is replaced by a three-dimensional sum.

One excited state that is of perticular interest is the Roper resonance, which was found in 1964 using a partial wave analysis of pion-nucleon scattering data [12]. It is a spin-$1/2$ state with positive parity (like the nucleon) and with a mass of around $m_R = 1.44\,\text{GeV}$[2] it lies slighty above the delta resonance. The most remarkable feature of this low-lying baryon resonance are its decays. Besides the decay into a pion and a nucleon, it also decays into a nucleon and two pions (via the $\Delta\pi$ and $N\sigma$ intermediate states) with a branching fraction comparable to the $N\pi$ mode. This three particle final state becomes important in lattice simulations involving three or more hadrons, see Ref. [91] for a recent review. It is also worth noting that there are going experimental programs to map out the electromagnetic structure of the Roper resonance, in particular through electro-excitatation and related theoretical studies, see e.g. Refs. [92–95].
A dedicated lattice QCD study of the Roper using both quark and hadron interpolators was performed in Ref. [15], see also Ref. [16]. In Ref. [15] a number of three-quark interpolating fields was supplemented by operators for $N\pi$ in P-wave and $N\sigma$ in S-wave. In the center-of-momentum frame three eigenstates below 1.65 GeV were found. No eigenstate corresponding to the Roper at $m_R = 1.44\,\text{GeV}$ is found, which indicates that $N\pi$ elastic scattering alone does not render a low-lying Roper. Coupling with other channels, most notably with $N\pi\pi$, seems to be important for generating the Roper resonance. The study of the coupled-channel scattering including a three-particle decay $N\pi\pi$ remains a challenge. Here, we follow another path. An effective field theory treatment of the Roper resonance has already been established. In order to improve the investigation of the Roper on the lattice, a finite volume calculation of the system is performed. The Roper is placed in a finite cubic box of size L and we study the difference between its energy spectrum in the infinite volume and finite volume case, i.e. the finite volume corrections of the Roper resonance. Due to the presence of a narrow resonance, the energy levels in the box show a very characteristic behaviour near the resonance energy. The energy levels get shifted when the box size L is changed, but they do not cross each other. This is the so-called "avoided level crossing" [23].

In this work we want to find out if this behavior can also be seen in the energy levels of the Roper system. To do so, we study the finite volume corrections of the self-energy of the Roper up to third chiral order $O(p^3)$ and perform a fit of the energy levels. A similar study has already been done for the delta resonance in [24] and we treat the Roper resonance accordingly.
Our manuscript is organized as follows: In Sec. 3.3, we display the effective chiral two-flavour Lagrangian of pions and baryons (nucleon, delta, Roper resonance) underlying our calculations. In Sec. 3.4, we calculate the self-energy of the Roper resonance in the continuum volume. The calculation of Roper self-energy in the finite volume is given in Sec. 3.5. The results for the energy levels of the Roper and the pertinent discussion are given in Sec. 3.6. We end with a short summary and outlook in Sec. 3.7. Some technicalities are relegated to the appendices.

[2] This is the less reliable Breit-Wigner mass [90].

3.3 Effective Lagrangian

First, we discuss the chiral effective Lagrangian that we need for our calculations. It is taken from Ref. [22] (for earlier related work, see e.g. Refs. [18–21]) and is given by

$$\mathcal{L}_{\text{eff.}} = \mathcal{L}_{\pi\pi} + \mathcal{L}_{\pi N} + \mathcal{L}_{\pi R} + \mathcal{L}_{\pi\Delta} + \mathcal{L}_{\pi N\Delta} + \mathcal{L}_{\pi NR} + \mathcal{L}_{\pi\Delta R} \,. \tag{3.1}$$

The dynamical degrees of freedom are pions (π), nucleons (N), the delta (Δ) and the Roper resonance (R). We restrict ourselves to flavor SU(2) and work in the isospin limit ($m_u = m_d \equiv \hat{m}$). In what follows, we work to leading one-loop order, $O(p^3)$, where p denotes a small momentum or mass. We count the pion mass as well as the mass differences $m_R - m_N$, $m_\Delta - m_N$ and $m_R - m_\Delta$ as of order p. When going to higher orders, this naive counting requires modification as detailed in Ref. [22]. Now let us enumerate the contributions required for the $O(p^3)$ calculation of the Roper self-energy. The relevant terms from the mesonic Lagrangian are

$$\mathcal{L}^{(2)}_{\pi\pi} = \frac{F^2}{4}\text{Tr}\left(\partial_\mu U \partial^\mu U^\dagger\right) + \frac{F^2}{4}\text{Tr}\left(U\chi^\dagger + \chi U^\dagger\right) \,, \tag{3.2}$$

where U is a 2×2-matrix that contains the pion fields, F is the pion decay constant in the chiral limit, which will later be identfied with the physical pion decay constant F_π. Further, χ is the external scalar source which is given by the diagonal matrix

$$\chi = \begin{pmatrix} M_\pi^2 & 0 \\ 0 & M_\pi^2 \end{pmatrix} \,, \tag{3.3}$$

with the pion mass M_π (we have already identified the leading term in the quark mass expansion of the pion mass with its physical value). The leading order (LO) terms of chiral dimension one and one required next-to-leading order (NLO) term of chiral dimension two containing pion fields and the spin-$1/2$ baryons read

$$\begin{aligned}
\mathcal{L}^{(1)}_{\pi N} &= \bar{\Psi}_N \left(i\not{D} - m_{N0} + \frac{1}{2} g_A \not{u}\gamma_5 \right) \Psi_N \,, \\
\mathcal{L}^{(1)}_{\pi R} &= \bar{\Psi}_R \left(i\not{D} - m_{R0} + \frac{1}{2} g_R \not{u}\gamma_5 \right) \Psi_R \,, \\
\mathcal{L}^{(2)}_{\pi R} &= c_1^R \bar{\Psi}_R \text{Tr}\left(\chi_+\right) \Psi_R \,.
\end{aligned} \tag{3.4}$$

Here, Ψ_N and Ψ_R are the isospin doublet fields with chiral limit masses m_{N0} and m_{R0} of the nucleon and the Roper resonance, respectively. The interaction of these fields with the pion field is characterised by the axial couplings g_A and g_R and the chiral vielbein

$$u_\mu = i\left(u^\dagger \partial_\mu u - u \partial_\mu u^\dagger\right) \,, \tag{3.5}$$

where $u = \sqrt{U}$. The last equation in (3.4) denotes a term of the second order pion-Roper Lagrangian with the low-energy constant (LEC) c_1^R and $\chi_+ = u^\dagger \chi u^\dagger + u \chi^\dagger u$. This term is required in the calculation of the Roper self-energy to be discussed below. Since we are only interested in strong

interaction processes we leave out all other external sources. The covariant derivative is then given by

$$D_\mu \Psi_{N/R} = \left(\partial_\mu + \Gamma_\mu\right) \Psi_{N/R} \,, \tag{3.6}$$

with

$$\Gamma_\mu = \frac{1}{2}\left\{u^\dagger \partial_\mu u + u \partial_\mu u^\dagger\right\} \,. \tag{3.7}$$

The spin-3/2 delta resonances are introduced as usual in terms of Rarita-Schwinger fields Ψ^i_μ, $i \in \{1,2,3\}$ [96]. The LO Lagrangian reads

$$\begin{aligned}\mathcal{L}^{(1)}_{\pi\Delta} = -\bar{\Psi}^i_\mu \xi^{3/2}_{ij} \Big\{ &\left(i \not{D}^{jk} - m_{\Delta 0}\delta^{jk}\right) g^{\mu\nu} - i\left(\gamma^\mu D^{\nu,\,jk} + \gamma^\nu D^{\mu,\,jk}\right) + i\gamma^\mu \not{D}^{jk}\gamma^\nu \\ &+ m_{\Delta 0}\delta^{jk}\gamma^\mu\gamma^\nu + \frac{g_1}{2}\not{u}^{jk}\gamma_5 g^{\mu\nu} + \frac{g_2}{2}\left(\gamma^\mu u^{\nu,\,jk} + u^{\mu,\,jk}\gamma^\nu\right)\gamma_5 \\ &+ \frac{g_3}{2}\gamma^\mu \not{u}^{jk}\gamma_5\gamma^\nu \Big\} \xi^{3/2}_{kl} \Psi^l_\nu \,,\end{aligned} \tag{3.8}$$

where $m_{\Delta 0}$ is the chiral limit mass of the delta, g_1, g_2, and g_3 are coupling constants, that are, however, not independent [97]. Further, $\xi^{3/2}_{ij}$ is the isospin-3/2 projector

$$\xi^{3/2}_{ij} = \delta_{ij} - \frac{1}{3}\tau_i\tau_j \,, \tag{3.9}$$

in terms of the Pauli-matrices τ_i, which are defined as

$$\tau_1 = \begin{pmatrix} 0 & 1 \\ 1 & 0 \end{pmatrix} \,, \quad \tau_1 = \begin{pmatrix} 0 & -i \\ i & 0 \end{pmatrix} \,, \quad \tau_1 = \begin{pmatrix} 1 & 0 \\ 0 & -1 \end{pmatrix} \,. \tag{3.10}$$

The propagator $G^{\rho\mu}(k)$ of the spin-3/2 Rarita-Schwinger propagator in D space-time dimensions is given by

$$G^{\rho\mu}(k) = \frac{-i(\not{k} + m_\Delta)}{k^2 - m^2_\Delta + i\epsilon}\left(g^{\rho\mu} - \frac{1}{D-1}\gamma^\rho\gamma^\mu + \frac{k^\rho\gamma^\mu - \gamma^\rho k^\mu}{(D-1)m_\Delta} - \frac{D-2}{(D-1)m^2_\Delta}k^\rho k^\mu\right) \,, \tag{3.11}$$

where we use the physical delta mass m_Δ, which is legitimate in our calculation. The LO interactions between pions, nucleons, deltas and Roper resonances are completed by

$$\begin{aligned}\mathcal{L}^{(1)}_{\pi NR} &= \bar{\Psi}_R\left(\frac{g_{\pi NR}}{2}\not{u}\gamma_5\right)\Psi_N + \text{h.c.} \,, \\ \mathcal{L}^{(1)}_{\pi N\Delta} &= h\bar{\Psi}^i_\mu \xi^{3/2}_{ij}\Theta^{\mu\alpha}\left(z_1\right)\omega^j_\alpha \Psi_N + \text{h.c.} \,, \\ \mathcal{L}^{(1)}_{\pi\Delta R} &= h_R\bar{\Psi}^i_\mu \xi^{3/2}_{ij}\Theta^{\mu\alpha}\left(z_2\right)\omega^j_\alpha \Psi_R + \text{h.c.} \,.\end{aligned} \tag{3.12}$$

Here, $g_{\pi NR}$, h, and h_R are coupling constants and

$$\omega^j_\nu = \frac{1}{2}\text{Tr}\left(\tau^j u_\nu\right) \,, \quad \Theta^{\mu\nu}(z) = g^{\mu\nu} + z\gamma^\mu\gamma^\nu \,, \tag{3.13}$$

Figure 3.1: One-loop diagrams contributing to the Roper mass at third chiral order. Thick solid, dashed, solid, and solid double lines refer to the Roper resonance, pions, nucleons, and delta baryon states, respectively. The vertices denoted by a filled dot refer to insertions from the first order chiral Lagrangian.

where z_1 and z_2 are off-shell parameters. Throughout this text we follow Ref. [22] and set $g_1 = -g_2 = -g_3$ and $z_1 = z_2 = 0$, see also Refs. [98, 99]. More terms have to be taken into account if one is interested in performing calculations of higher chiral order.

3.4 Self-energy of the Roper resonance

To calculate the mass of the Roper resonance in the infinite (and also finite) volume we have to determine the poles of the dressed propagator

$$iS_R(p) = \frac{i}{\not{p} - m_{R0} - \Sigma_R(\not{p})} \,. \tag{3.14}$$

Here, Σ_R denotes the self-energy of the Roper, which can be calculated from all one-particle-irreducible contributions to the two-point function of the Roper resonance field Ψ_R. The poles are obtained by solving the equation

$$\left[\not{p} - m_{R0} - \Sigma_R(\not{p})\right]\Big|_{\not{p}=Z} \stackrel{!}{=} 0 \,, \tag{3.15}$$

where in the infinite volume Z is parametrized by

$$Z = m_R - i\frac{\Gamma_R}{2} \,, \tag{3.16}$$

in terms of the physical Roper mass m_R and its width Γ_R. This implies that the real part of the self-energy corresponds to corrections of m_R, whereas the imaginary part corresponds to corrections of Γ_R.

At third chiral order there are three one-loop diagrams contributing to the self-energy of the Roper resonance, which are depicted in Fig. 3.1. The diagrams differ by the internal baryon state, which can be a Roper, a nucleon or a delta baryon. Additionally, there is a contact interaction coming from the second order Lagrangian of the Roper in Eq. (3.4). The self-energy up to order $O\left(p^3\right)$ then reads

$$\Sigma_R(\not{p}) = \underbrace{\Sigma_R^{(2)}(\not{p})}_{\text{contact int.}} + \underbrace{\Sigma_{\pi R}^{(3)}(\not{p}) + \Sigma_{\pi N}^{(3)}(\not{p}) + \Sigma_{\pi\Delta}^{(3)}(\not{p})}_{\text{loops}} + O\left(p^4\right) \,. \tag{3.17}$$

Using the effective Lagrangians from Sec. 3.3, we can straightforwardly write down the expressions for the self-energy. For the second order contact interaction we find

$$\Sigma_R^{(2)} = -4c_1^R M_\pi^2 \,, \tag{3.18}$$

and the three loop contributions are given by

$$\Sigma_{\pi R}^{(3)}\left(\not{p}\right) = \frac{3g_R^2}{4F_\pi^2}\int \frac{d^4k}{(2\pi)^4}\frac{i\not{k}\gamma_5\left(\not{p}-\not{k}+m_R\right)\not{k}\gamma_5}{[(p-k)^2-m_R^2+i\epsilon][k^2-M_\pi^2+i\epsilon]}\,, \tag{3.19}$$

$$\Sigma_{\pi N}^{(3)}\left(\not{p}\right) = \frac{3g_{\pi NR}^2}{4F_\pi^2}\int \frac{d^4k}{(2\pi)^4}\frac{i\not{k}\gamma_5\left(\not{p}-\not{k}+m_N\right)\not{k}\gamma_5}{[(p-k)^2-m_N^2+i\epsilon][k^2-M_\pi^2+i\epsilon]}\,, \tag{3.20}$$

$$\Sigma_{\pi\Delta}^{(3)}\left(\not{p}\right) = \frac{2h_R^2}{F_\pi^2}\int \frac{d^4k}{(2\pi)^4}\frac{(p-k)_\mu\, G^{\mu\nu}(k)\,(p-k)_\nu}{(p-k)^2-M_\pi^2+i\epsilon}\,, \tag{3.21}$$

where $G^{\rho\mu}(k)$ is given in Eq. (3.11). The three one-loop contributions to the Roper mass can be expanded in terms of the scalar Passarino-Veltman integrals (PV integrals). This expansion is done using the Mathematica package FeynCalc [100, 101]. The definitions and solutions of the PV integrals

can be found in App. B.1. This results in

$$\begin{aligned}\Sigma_{\pi R}^{(3)}\left(\not{p}=m_R\right) &= \frac{3g_R^2}{4F_\pi^2}\int\frac{d^4k}{(2\pi)^4}\frac{i\not{k}\gamma_5\left(\not{p}-\not{k}+m_R\right)\not{k}\gamma_5}{[(p-k)^2-m_R^2+i\epsilon][k^2-M_\pi^2+i\epsilon]}\Bigg|_{\not{p}=m_R}\\ &= \frac{3g_R^2 m_R}{32F_\pi^2}\left\{M_\pi^2 B_0\left(m_R^2,m_R^2,M_\pi^2\right)+A_0\left(m_R^2\right)\right\}, \end{aligned} \tag{3.22}$$

$$\begin{aligned}\Sigma_{\pi\Delta}^{(3)}\left(\not{p}=m_R\right) &= \frac{2h_R^2}{F_\pi^2}\int\frac{d^4k}{(2\pi)^4}\frac{(p-k)_\mu G^{\mu\nu}(k)(p-k)_\nu}{(p-k)^2-M_\pi^2+i\epsilon}\Bigg|_{\not{p}=m_R}\\ &= \frac{h_R^2}{96\pi^2F_\pi^2m_\Delta^2m_R}\Bigg\{\\ &\quad -\left[\left(m_\Delta+m_R\right)^2-M_\pi^2\right]\lambda\left(m_R^2,m_\Delta^2,M_\pi^2\right)B_0\left(m_R^2,m_\Delta^2,M_\pi^2\right)\\ &\quad +\Bigg[m_\Delta^4+2m_\Delta^3m_R+\left(M_\pi^2-m_R^2\right)^2-m_\Delta^2\left(m_R^2+2M_\pi^2\right)\\ &\quad +2m_\Delta m_R\left(m_R^2-M_\pi^2\right)\Bigg]A_0\left(m_\Delta^2\right)+\Bigg[m_\Delta^4+2m_\Delta^3m_R-2m_\Delta m_R^3\\ &\quad -m_R^4-2m_\Delta^2M_\pi^2+6m_\Delta m_RM_\pi^2+5m_R^2M_\pi^2+M_\pi^4\Bigg]A_0\left(M_\pi^2\right)\Bigg\}\\ &\quad +\frac{h_R^2}{576\pi^2F_\pi^2m_\Delta^2}\Bigg\{3m_\Delta^4m_R-12m_\Delta^3m_R^2-4m_\Delta^2m_R^3+2m_R^5\\ &\quad -8m_R^3M_\pi^2+13m_RM_\pi^4+4m_\Delta\left(m_R^4-3m_R^2M_\pi^2+4M_\pi^4\right)\Bigg\}, \end{aligned} \tag{3.23}$$

$$\begin{aligned}\Sigma_{\pi N}^{(3)}\left(\not{p}=m_R\right) &= \frac{3g_{\pi NR}^2}{4F_\pi^2}\int\frac{d^4k}{(2\pi)^4}\frac{i\not{k}\gamma_5\left(\not{p}-\not{k}+m_N\right)\not{k}\gamma_5}{[(p-k)^2-m_N^2+i\epsilon][k^2-M_\pi^2+i\epsilon]}\Bigg|_{\not{p}=m_R}\\ &= \frac{-3g_{\pi NR}^2}{128\pi^2F_\pi^2m_R}\Bigg\{\left(m_R+m_N\right)^2\Bigg[\left(\left(m_R-m_N\right)^2-M_\pi^2\right)B_0\left(m_R^2,m_N^2,M_\pi^2\right)\\ &\quad -A_0\left(m_N^2\right)\Bigg]-\left(m_R^2-m_N^2\right)A_0\left(M_\pi^2\right)\Bigg\}. \end{aligned} \tag{3.24}$$

We used Källén's triangle function $\lambda(x,y,z)=(x-y-z)^2-4yz$ to simplify the lengthy expression of $\Sigma_{\pi\Delta}^{(3)}$.
Evaluating these scalar integrals in the infinite volume leads to the well-known infinities that one has to tame within the framework of renormalization. Procedures like the $\widetilde{\text{MS}}$ scheme use redefinitions of the bare parameters in the Lagrangian to subtract the infinities. Additionally in baryonic ChPT one will encounter terms in the expansion of the loop diagrams that break the power counting. These so-called power counting violating terms can be handeld with different techniques, like the heavy

baryon approach, IR or the EOMS scheme. Within this EOMS scheme one performs additionally finite subtractions to cancel the power counting violating terms. In the end one obtains a finite result that is consistent with the power counting. Further details relevant for our calculations can be found, e.g., in Refs. [75, 76].

3.5 Finite volume formalism

Next, we consider the Roper resonance in a finite volume. We place our system in a cubic box of length L and calculate the difference between the finite and infinite volume case [26]. In the finite volume the (Euclidean) loop integral is replaced by an infinite sum of the spatial momenta while the integration over the time component remains unchanged (in actual lattice QCD calculations, the time direction is also discrete, but we keep it continuous for simplicity)

$$\int \frac{d^4k_E}{(2\pi)^4}(\ldots) \mapsto \int_{-\infty}^{\infty} \frac{dk_4}{2\pi} \frac{1}{L^3} \sum_{\vec{k}} (\ldots) \ . \tag{3.25}$$

In a finite volume the spatial momenta are discretized and can only take values that are integer multiples of $2\pi/L$, i.e. (for a general discussion of theories with spontaneous symmetry breaking in a finite volume, see e.g. Ref. [102])

$$\vec{k} = \frac{2\pi}{L}\vec{n} \,, \quad \vec{n} \in \mathbb{Z}^3 \ . \tag{3.26}$$

This change obviously influences the self-energy of the Roper resonance. The poles of the propagator are now given by

$$\not{p} - m_{R0} - \Sigma_R^L\left(\not{p}\right) = 0 \,, \tag{3.27}$$

where $\Sigma_R^L\left(\not{p}\right)$ denotes the self-energy of the Roper in the finite box. The difference beetween the self-energy in the box and in the infinite volume is defined as the finite volume correction (FV correction) of the system [103, 104]

$$\tilde{\Sigma}_R^L\left(\not{p}\right) := \Sigma_R^L\left(\not{p}\right) - \mathrm{Re}\left\{\Sigma_R\left(\not{p}\right)\right\} \ . \tag{3.28}$$

Note that in the finite volume the self-energy can only yield real values due to the summation over real momenta $\vec{k}$. Therefore we have to restrict the infinite volume self-energy to its real part to ensure a non-imaginary FV correction.
Using Eq. (3.28) we can reformulate Eq. (3.27). We choose the center-of-mass frame $p_\mu = (E, \vec{0})$ and use the on-shell condition $\not{p} = E$ to obtain

$$\begin{aligned} 0 &\stackrel{!}{=} E - m_{R0} - \left[\tilde{\Sigma}_R^L(E) + \mathrm{Re}\left\{\Sigma_R(E)\right\}\right] \\ &= E - \underbrace{\left[m_{R0} + \mathrm{Re}\left\{\Sigma_R(E)\right\}\right]}_{m_R} - \tilde{\Sigma}_R^L(E) \quad \Leftrightarrow \quad m_R - E = -\tilde{\Sigma}_R^L(E) \ , \end{aligned}$$

where we used the definition of the physical Roper mass m_R, i.e. the real part of the pole, in the last step. At third chiral order, the contributions to the self-energy are the ones from Fig. 3.1. We get

$$m_R - E = -\left\{\tilde{\Sigma}_{\pi R}^{L,(3)}(E) + \tilde{\Sigma}_{\pi N}^{L,(3)}(E) + \tilde{\Sigma}_{\pi\Delta}^{L,(3)}(E)\right\}, \tag{3.29}$$

and our goal will be the numerical evaluation of this equation. The three one-loop contributions to the Roper mass have been expanded in terms of the PV integrals in the last section. Now we have to replace the infinite volume quantities with their finite volume expressions. We obtain

$$\begin{aligned}\tilde{\Sigma}_{\pi R}^{L,(3)}(E) = -\frac{3g_R^2}{128\pi^2 F_\pi^2 E}(E+m_R)\Big\{(E+m_R)\Big[\Big((E-m_R)^2 - M_\pi^2\Big)\tilde{B}_0^L\left(E^2, m_R^2, M_\pi^2\right) \\ - \tilde{A}_0^L\left(m_R^2\right)\Big] + (m_R - E)\,\tilde{A}_0^L\left(M_\pi^2\right)\Big\},\end{aligned} \tag{3.30}$$

$$\begin{aligned}\tilde{\Sigma}_{\pi N}^{L,(3)}(E) = -\frac{3g_{\pi NR}^2}{128\pi^2 F_\pi^2 E}(E+m_N)\Big\{(E+m_N)\Big[\Big((E-m_N)^2 - M_\pi^2\Big)\tilde{B}_0^L\left(E^2, m_N^2, M_\pi^2\right) \\ - \tilde{A}_0^L\left(m_N^2\right)\Big] + (m_N - E)\,\tilde{A}_0^L\left(M_\pi^2\right)\Big\},\end{aligned} \tag{3.31}$$

$$\begin{aligned}\tilde{\Sigma}_{\pi\Delta}^{L,(3)}(E) = \frac{h_R^2}{96\pi^2 F_\pi^2 m_\Delta^2 E}\Big\{-\Big[(m_\Delta+E)^2 - M_\pi^2\Big]\lambda\left(E^2, m_\Delta^2, M_\pi^2\right)\tilde{B}_0^L\left(E^2, m_\Delta^2, M_\pi^2\right) \\ + \Big[m_\Delta^4 + 2m_\Delta^3 E + \left(M_\pi^2 - E^2\right)^2 - m_\Delta^2\left(E^2 + 2M_\pi^2\right) \\ + 2m_\Delta E\left(E^2 - M_\pi^2\right)\Big]\tilde{A}_0^L\left(m_\Delta^2\right) + \Big[m_\Delta^4 + 2m_\Delta^3 E - 2m_\Delta E^3 \\ - E^4 - 2m_\Delta^2 M_\pi^2 + 6m_\Delta E M_\pi^2 + 5E^2 M_\pi^2 + M_\pi^4\Big]\tilde{A}_0^L\left(M_\pi^2\right)\Big\},\end{aligned} \tag{3.32}$$

where $\tilde{A}_0^L$ and $\tilde{B}_0^L$ are the finite volume corrections of the PV integrals which will be determined next.

3.5.1 Calculation of loop integrals in the finite volume

Let us consider as an example

$$A_0(m^2) = -16\pi^2 \int \frac{d^4k}{(2\pi)^4}\frac{i}{k^2 - m^2} \tag{3.33}$$

in four-dimensional Minkowski space. We will follow the procedure described in Ref. [24] here. First of all we perform the Wick rotation $k_0 \to ik_4$ to Euclidean space, so that the integral can be rewritten

as

$$A_0\left(m^2\right) = -16\pi^2 \int \frac{d^4k_E}{(2\pi)^4} \frac{1}{k_E^2 + m^2} \,. \tag{3.34}$$

Now we can define the finite volume PV integral by replacing the Euclidean spatial integral with a discrete sum

$$A_0^L\left(m^2\right) = -16\pi^2 \int_{-\infty}^{\infty} \frac{dk_4}{2\pi} \frac{1}{L^3} \sum_{\vec{k}} \frac{1}{k_4^2 + |\vec{k}|^2 + m^2} \,, \tag{3.35}$$

where the momenta $\vec{k}$ are restricted according to Eq. (3.26). The evaluation of this sum is the next task. First, we note that the function inside the sum is regular, i.e. it does not possess a pole on the real axis for all values of k_4 and $\vec{k}$. Therefore we can use the so called Poisson trick to simplify the calculation. We insert the Dirac delta into the equation

$$A_0^L\left(m^2\right) = -16\pi^2 \int_{-\infty}^{\infty} \frac{dk_4}{2\pi} \frac{1}{L^3} \int d^3k \frac{1}{k_4^2 + |\vec{k}|^2 + m^2} \sum_{\vec{n}} \delta^{(3)}\left(\vec{k} - \frac{2\pi}{L}\vec{n}\right) \,, \tag{3.36}$$

and then we use the Poisson formula in three dimensions

$$\sum_{\vec{n}} \delta^{(3)}\left(\vec{k} - \frac{2\pi}{L}\vec{n}\right) = \left(\frac{L}{2\pi}\right)^3 \sum_{\vec{n}} \exp\left(iL\vec{n}\cdot\vec{k}\right) \,. \tag{3.37}$$

Plugging this result in our finite volume PV integral we obtain

$$A_0^L\left(m^2\right) = -16\pi^2 \int \frac{d^4k_E}{(2\pi)^4} \frac{1}{k_4^2 + |\vec{k}|^2 + m^2} \sum_{\vec{n}} e^{iL\vec{k}\cdot\vec{n}} \,, \tag{3.38}$$

where we have regained a four-dimensional integral over momenta times a sum of exponential functions. We observe that the term in the sum with $\vec{n} = \vec{0}$ reproduces the infinite volume PV integral from Eq. (3.34)

$$\begin{aligned} A_0^L\left(m^2\right) &= -16\pi^2 \left\{ \int \frac{d^4k_E}{(2\pi)^4} \frac{1}{k_4^2 + |\vec{k}|^2 + m^2} + \sum_{\vec{n}\neq 0} \int \frac{d^4k_E}{(2\pi)^4} \frac{e^{iL\vec{k}\cdot\vec{n}}}{k_4^2 + |\vec{k}|^2 + m^2} \right\} \\ &= A_0\left(m^2\right) - 16\pi^2 \sum_{\vec{n}\neq 0} \int \frac{d^4k_E}{(2\pi)^4} \frac{e^{iL\vec{k}\cdot\vec{n}}}{k_4^2 + |\vec{k}|^2 + m^2} \,. \end{aligned} \tag{3.39}$$

Thus, the finite volume correction is given by

$$\tilde{A}_0^L\left(m^2\right) := A_0^L\left(m^2\right) - A_0\left(m^2\right) = -16\pi^2 \sum_{\vec{n}\neq 0} \int \frac{d^4k_E}{(2\pi)^4} \frac{e^{iL\vec{k}\cdot\vec{n}}}{k_4^2 + |\vec{k}|^2 + m^2} \,. \tag{3.40}$$

The remaining integral is finite and can be solved with standard methods. After integrating the spatial part we are left with

$$\tilde{A}_0^L\left(m^2\right) = -4\sum_{j\neq 0}\frac{1}{Lj}\int_0^\infty dk_4 e^{-Lj\sqrt{k_4^2+m^2}} = -4m^2\sum_{j\neq 0}\frac{K_1\left(mLj\right)}{mLj}\,, \tag{3.41}$$

where $j = |\vec{n}| = \sqrt{n_1^2+n_2^2+n_3^2}$ and $K_\nu(z)$ is the modified Bessel function of the second kind. For large values of the box length L and the summation index j the finite volume correction decreases exponentially so that it becomes negligible for large volumes (usually this is expected for $M_\pi L > 4$). A similar calculation can be done for $\tilde{B}_0^L$. After performing the Wick rotation in the infinite volume, the integral has the form

$$B_0\left(E^2, m_X^2, M_\pi^2\right) = 16\pi^2\int\frac{d^4k_E}{(2\pi)^4}\frac{1}{[k_E^2+M_\pi^2][(\hat{P}-k_E)^2+m_X^2]}\,, \quad \hat{P}_\mu = (iE,\vec{0})\,, \tag{3.42}$$

and the finite volume expression is given by

$$B_0^L\left(E^2, m_X^2, M_\pi^2\right) = 16\pi^2\int_{-\infty}^{\infty}\frac{dk_4}{2\pi}\frac{1}{L^3}\sum_{\vec{k}}\frac{1}{[k_4^2+|\vec{k}|^2+M_\pi^2][(iE-k_4)^2+|\vec{k}|^2+m_X^2]}\,. \tag{3.43}$$

The next step is to use Feynman parameterization, see App. B.2 for further details, to combine the two denominators and then perform a shift in the non-discret momentum component k_4. The resulting expression reads

$$B_0^L\left(E^2, m_X^2, M_\pi^2\right) = 16\pi^2\int_0^1 dy\int_{-\infty}^{\infty}\frac{dk_4}{2\pi}\frac{1}{L^3}\sum_{\vec{k}}\frac{1}{\left[k_4^2+|\vec{k}|^2+g_X\left(y,E^2\right)\right]^2}\,, \tag{3.44}$$

with

$$g_X\left(y,E^2\right) = y\left(y-1\right)E^2 + ym_X^2 + \left(1-y\right)M_\pi^2\,. \tag{3.45}$$

Depending on the values for E, m_X and M_π, the function $g_X\left(y,E^2\right)$ can be positive, negative or zero for some values of y. If $g_X\left(y,E^2\right) > 0$ for all $y\in[0,1]$, the function inside the sum is regular and we can again use the Poisson formula analogously to A_0^L. The finite volume correction then is

$$\tilde{B}_0^L\left(E^2, m_X^2, M_\pi^2\right) = 2\int_0^1 dy\sum_{j\neq 0}K_0\left(Lj\sqrt{g_X\left(y,E^2\right)}\right)\,. \tag{3.46}$$

Also here the correction drops exponentially for large L and j. Note that the parameter integral over y has to be evaluated numerically. However, if the function g_X is negative or equal to zero for some values of y, the Poisson formula is no longer applicable. In our calculation for example, if $m_X = m_R$ the difference between the pole position E and m_R is small and g_X stays positive. If $m_X = m_N$, m_Δ the function can become negative and we have to find another way to evaluate the finite volume

contribution. To do so we follow again Ref. [24] and introduce a scale μ, which will be used to subtract ultraviolet divergences from the infinite sum. Also the scale can be choosen in such a way that the function $g_X\left(y,\mu^2\right)$ stays positive. We expand the finite volume correction as

$$\begin{aligned}
\tilde{B}_0^L\left(E^2,m_X^2,M_\pi^2\right) &= B_0^L\left(E^2,m_X^2,M_\pi^2\right) - \mathrm{Re}\left\{B_0\left(E^2,m_X^2,M_\pi^2\right)\right\} \\
&= B_0^L\left(E^2,m_X^2,M_\pi^2\right) - \mathrm{Re}\left\{B_0\left(E^2,m_X^2,M_\pi^2\right)\right\} \\
&\quad + \tilde{B}_0^L\left(\mu^2,m_X^2,M_\pi^2\right) - B_0^L\left(\mu^2,m_X^2,M_\pi^2\right) + B_0\left(\mu^2,m_X^2,M_\pi^2\right) \\
&\quad + \left(E^2-\mu^2\right)\frac{d}{dE^2}\Big\{\tilde{B}_0^L\left(E^2,m_X^2,M_\pi^2\right) \\
&\quad - B_0^L\left(E^2,m_X^2,M_\pi^2\right) + B_0\left(E^2,m_X^2,M_\pi^2\right)\Big\}\Big|_{E^2=\mu^2} \\
&\equiv 16\pi^2\left\{H_1^X\left(E^2\right) + H_2^X\left(E^2\right) + H_3^X\left(E^2\right)\right\}\,,
\end{aligned} \tag{3.47}$$

and separate it into three terms, which are given by

$$\begin{aligned}
16\pi^2\,H_1^X\left(E^2\right) &= \Big\{B_0^L\left(E^2,m_X^2,M_\pi^2\right) - B_0^L\left(\mu^2,m_X^2,M_\pi^2\right) \\
&\qquad - \left(E^2-\mu^2\right)\frac{d}{dE^2}B_0^L\left(E^2,m_X^2,M_\pi^2\right)\Big|_{E^2=\mu^2}\Big\}\,,
\end{aligned} \tag{3.48}$$

$$16\pi^2\,H_2^X\left(E^2\right) = \left\{\tilde{B}_0^L\left(\mu^2,m_X^2,M_\pi^2\right) + \left(E^2-\mu^2\right)\frac{d}{dE^2}\tilde{B}_0^L\left(E^2,m_X^2,M_\pi^2\right)\right\}\,, \tag{3.49}$$

$$\begin{aligned}
16\pi^2\,H_3^X\left(E^2\right) &= -\Big\{\mathrm{Re}\left\{B_0\left(E^2,m_X^2,M_\pi^2\right)\right\} - B_0\left(\mu^2,m_X^2,M_\pi^2\right) \\
&\qquad - \left(E^2-\mu^2\right)\frac{d}{dE^2}B_0\left(E^2,m_X^2,M_\pi^2\right)\Big|_{E^2=\mu^2}\Big\}\,.
\end{aligned} \tag{3.50}$$

The first subtraction term with the newly introduced scale μ ensures that the correction converges, while the derivative terms lead to a faster convergence. The first term, H_1^X, contains only terms with momentum sums. After the integration over k_4, one obtains

$$H_1^X\left(E^2\right) = \left(E^2-\mu^2\right)^2\frac{1}{L^3}\sum_{\vec{n}}\frac{E_X+E_\pi}{2E_XE_\pi}\frac{1}{(E_X+E_\pi)^2-E^2}\frac{1}{((E_X+E_\pi)^2-\mu^2)^2}\,, \tag{3.51}$$

with $E_X = \sqrt{m_X^2+\left(\frac{2\pi}{L}\right)^2|\vec{n}|^2}$ and $E_\pi = \sqrt{M_\pi^2+\left(\frac{2\pi}{L}\right)^2|\vec{n}|^2}$. In the second term one finds finite volume corrections that can be calculated with the Poisson summation formula, since the functions

are regular. We get

$$H_2^X\left(E^2\right) = \frac{1}{8\pi^2}\int_0^1 dy \sum_{j\neq 0}\left\{K_0\left(Lj\sqrt{g_X\left(y,\mu^2\right)}\right)\right.$$
$$\left. -\left(E^2-\mu^2\right)\frac{y(y-1)Lj}{2\sqrt{g_X\left(y,\mu^2\right)}}K_1\left(Lj\sqrt{g_X\left(y,\mu^2\right)}\right)\right\}. \tag{3.52}$$

The last term only contains infinite volume quantities which can be calculated with standard methods

$$\begin{aligned}
H_3^X\left(E^2\right) = &-\frac{B_E}{32\pi^2E^2}\left\{\ln\left(\frac{E^2+m_X^2-M_\pi^2+B_E}{E^2+m_X^2-M_\pi^2-B_E}\right)+\ln\left(\frac{E^2-m_X^2+M_\pi^2+B_E}{E^2-m_X^2+M_\pi^2-B_E}\right)\right\}\\
&+\frac{B_\mu}{16\pi^2\mu^2}\left\{\arctan\left(\frac{\mu^2+m_X^2-M_\pi^2}{B_\mu}\right)+\arctan\left(\frac{\mu^2-m_X^2+M_\pi^2}{B_\mu}\right)\right\}\\
&-\frac{E^2-\mu^2}{16\pi^2\mu^2}\left\{1+\frac{\left(E^2-\mu^2\right)\left(m_X^2-M_\pi^2\right)}{2E^2\mu^2}\ln\left(\frac{M_\pi^2}{m_X^2}\right)\right.\\
&\qquad+\frac{\left(m_X^2-M_\pi^2\right)^2-\mu^2\left(m_X^2+M_\pi^2\right)}{\mu^2B_\mu}\\
&\qquad\left.\times\left[\arctan\left(\frac{\mu^2+m_X^2-M_\pi^2}{B_\mu}\right)+\arctan\left(\frac{\mu^2-m_X^2+M_\pi^2}{B_\mu}\right)\right]\right\},
\end{aligned} \tag{3.53}$$

where we used again the triangle function to define

$$B_E = \lambda^{1/2}\left(E^2,m_X^2,M_\pi^2\right) := \sqrt{\left(E^2-m_X^2-M_\pi^2\right)^2-4m_X^2M_\pi^2}\,, \tag{3.54}$$

$$B_\mu = i\lambda^{1/2}\left(\mu^2,m_X^2,M_\pi^2\right) := \sqrt{-\left(\mu^2-m_X^2-M_\pi^2\right)^2+4m_X^2M_\pi^2}\,. \tag{3.55}$$

We now have evaluated all PV integrals in the finite volume that we need. We note that the issue of using the PV reduction in the finite volume was already discussed in Ref. [24] and we refer to that paper for details. Thus we return to the main task, the numerical calculation of Eq. (3.29).

3.6 Results

3.6.1 Calculation of the energy levels

We now want to determine the energy spectrum of the Roper resonance system. To obtain this we take a look at Eq. (3.29) and try to find numerical solutions for the energy E for different box sizes L. Due to the presence of the Roper we expect to see the so-called avoided level crossing of the energy levels.

Before we start to solve Eq. (3.29) by numerical methods, let us again consider the results of the finite volume PV integrals. We have seen that all regular functions in the self-energy of the Roper decrease exponentially for large L. This includes all tadpoles, i.e. all $\tilde{A}_0^L$ functions, as well as $\tilde{B}_0^L\left(E^2, m_R^2, M_\pi^2\right)$ from the πR loop in Fig. 3.1. Choosing L to be large we can neglect the contributions from these functions, leaving just the FV correction from the πN and the $\pi\Delta$ loop (see also Refs. [24, 87]). This facilitates the numerical computation of the energy levels significantly. The simplified equation reads

$$\begin{aligned} m_R - E = &\frac{3g_{\pi NR}^2}{128\pi^2 F_\pi^2 E}\left(E+m_N\right)^2\left[\left(E-m_N\right)^2 - M_\pi^2\right]\tilde{B}_0^L\left(E^2, m_N^2, M_\pi^2\right) \\ &+ \frac{h_R^2}{96\pi^2 F_\pi^2 m_\Delta^2 E}\left[\left(m_\Delta+E\right)^2 - M_\pi^2\right]\lambda\left(E^2, m_\Delta^2, M_\pi^2\right)\tilde{B}_0^L\left(E^2, m_\Delta^2, M_\pi^2\right), \end{aligned} \tag{3.56}$$

where only the non-regular functions and two LECs ($g_{\pi NR}$ and h_R) are left. Leaving out these contributions also simplifies the treatment of power counting breaking terms that would normally appear in such a calculation. The remaining expression, however, does not contain any power counting violating terms, so that an additional renormalization scheme, like EOMS, is redundant. Additional remarks on this issue are given in Ref. [24]. The further numerical studies of the energy levels are performed by using this equation. Values of the used parameters are given in the next subsection.

3.6.2 Numerical results

For the hadron masses and constants we use the numerical values from Ref. [22]. The baryon masses are $m_N = 939\,\text{MeV}$, $m_R = 1\,365\,\text{MeV}$ [3], and $m_\Delta = 1\,210\,\text{MeV}$. For the pion mass we use $M_\pi = 139\,\text{MeV}$ and for the pion decay constant $F_\pi = 92.2\,\text{MeV}$. The two coupling constants are also taken from Ref. [22] and are $g_{\pi NR} = \pm 0.47$, and $h_R = h = 1.42$, with the assumption that the coupling h_R is equal to the pion-nucleon-delta-coupling h (the so-called maximal mixing [18]). Note that the sign of $g_{\pi NR}$ does not matter as this coupling appears squared in our analysis. We also have to choose the scale μ for the calculation and set $\mu = m_N$ for the nucleon, and $\mu = m_\Delta$ for the delta case.

Now we have everything we need to find the numerical values of E. We evaluate the sums in the finite volume corrections from $|\vec{n}|^2 = 1$ up-to-and-including $|\vec{n}|^2 = 4$. Then we solve Eq. (3.56) for the respective energy levels for different box sizes. To make things easier we first look at the Roper resonance without the delta, i.e. we set $h_R = 0$ and take only the interaction between Roper, nucleon and pion into account. The results are displayed in Fig. 3.2. The energy is depicted in units of the

[3] This is the more reliable pole mass [90].

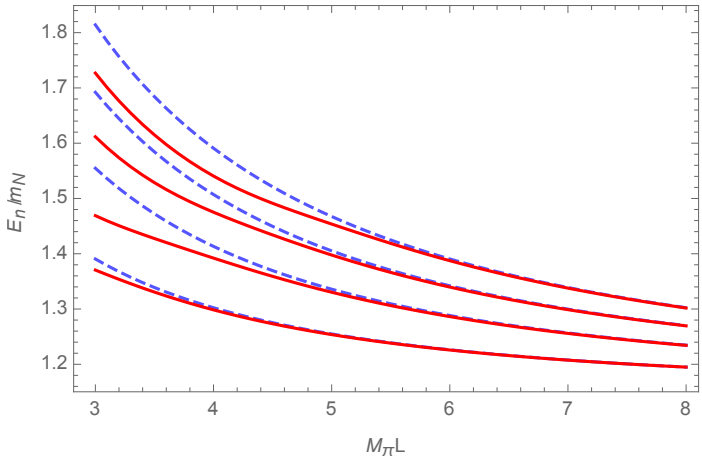

Figure 3.2: Energy levels for different box sizes L considering only pion and nucleon as intermediate states. Red solid lines display the numerical results and blue dashed lines the free energy levels of the pion and nucleon for $|\vec{n}|^2 = 1, 2, 3, 4$ (lowest to highest curve).

nucleon mass m_N and the box size L is multiplied by the pion mass M_π. The red solid lines denote the numerical results of E for the respective energy levels while the blue dashed lines denote the free energy levels of the pion-nucleon final states, i.e.

$$E_{\pi N}^{\text{free}}(\vec{n}) = \sqrt{m_N^2 + \left(\frac{2\pi}{L}\right)^2 |\vec{n}|^2} + \sqrt{M_\pi^2 + \left(\frac{2\pi}{L}\right)^2 |\vec{n}|^2}\,, \tag{3.57}$$

for $|\vec{n}|^2 = 1, 2, 3, 4$. We can clearly see signs of avoided level crossing at small box sizes, whereas the curves asymptotally approach the free energy levels at larger box sizes. Also the curves seem to switch between different free energy levels which is also a typical behaviour for a resonance (see Ref. [24]). It can be especially observed in the upmost curve between the $|\vec{n}|^2 = 3$ and $|\vec{n}|^2 = 4$ levels. This is exactly the energy region where the Roper resonance is found, i.e. $1\,365\,\text{MeV}/m_N \approx 1.45$ (which is called the "critical value" from here on) and the curves approximate more and more the free energy levels at energies below the critical value.
Now we will do the opposite and set $g_{\pi NR} = 0$. The calculation is performed like before and is displayed in Fig. 3.3. The free energy levels of the pion and delta in the final state, i.e.

$$E_{\pi\Delta}^{\text{free}}(\vec{n}) = \sqrt{m_\Delta^2 + \left(\frac{2\pi}{L}\right)^2 |\vec{n}|^2} + \sqrt{M_\pi^2 + \left(\frac{2\pi}{L}\right)^2 |\vec{n}|^2}\,, \tag{3.58}$$

are denoted by the grey dashed lines. This time we see no clear evidence for an avoided level crossing. One reason for this is the fact that we are now in an energy region which is mostly above the critical value. Only the two lowest lying energy levels come close to this energy. Another reason is the relatively large coupling h_R, which tends to "wash out" the typical signature of avoided level crossing. This effect has been also observed in the energy levels of the delta resonance in a box [24]. It is important to note that although the delta baryon is a resonance itself we treat it here as a stable particle.

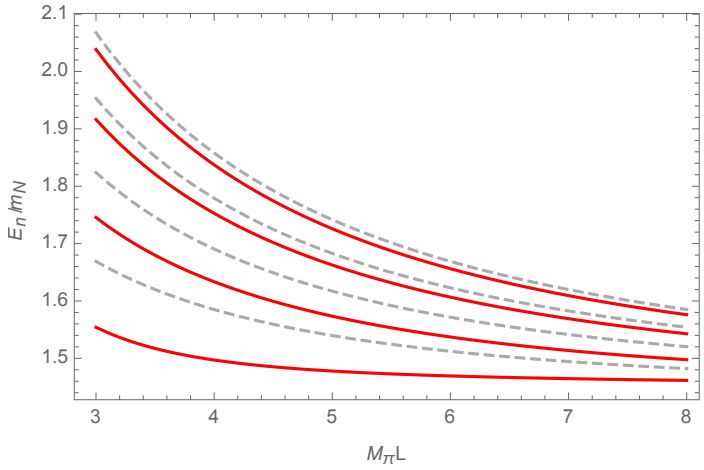

Figure 3.3: Energy levels for different box sizes L considering only pion and delta baryon as intermediate states. Red solid lines display the numerical results and grey dashed lines the free energy levels of the pion and delta for $|\vec{n}|^2 = 1, 2, 3, 4$ (lowest to highest curve).

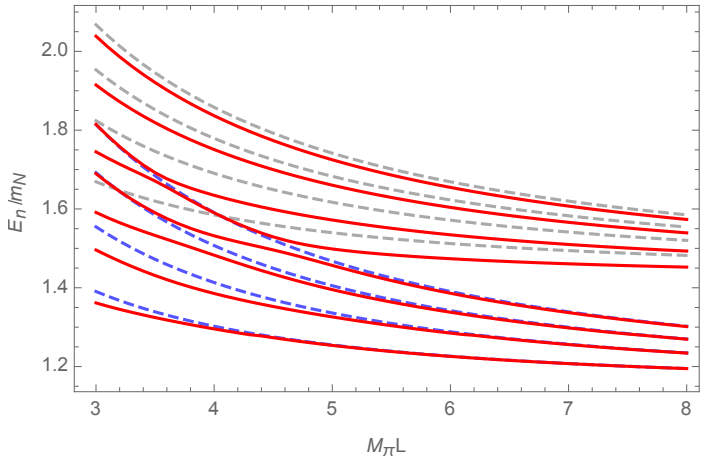

Figure 3.4: Energy levels for the full system for different box sizes L. Red solid lines display the numerical results and blue dashed lines, grey dashed lines display the free energy levels of the pion and nucleon, pion and delta, respectively.

This holds as a first approximation with the argument that the Roper first decays in a pion and a delta baryon (or pion and nucleon) and then later the delta can decay further. For future investigations we should take the unstable nature of the delta into account. One example to achieve this can be the replacement of the delta propagator in our calculations with a modified propagator including the decay width of the delta. This will be done in a forthcoming work.
Now we take a look at the full system with pions, nucleons and deltas. Our results are given in Fig. 3.4, which now include both possible interactions. The avoided level crossing is again visible at small box sizes and most pronounced between the free $|\vec{n}|^2 = 3$ level of the pion and the nucleon

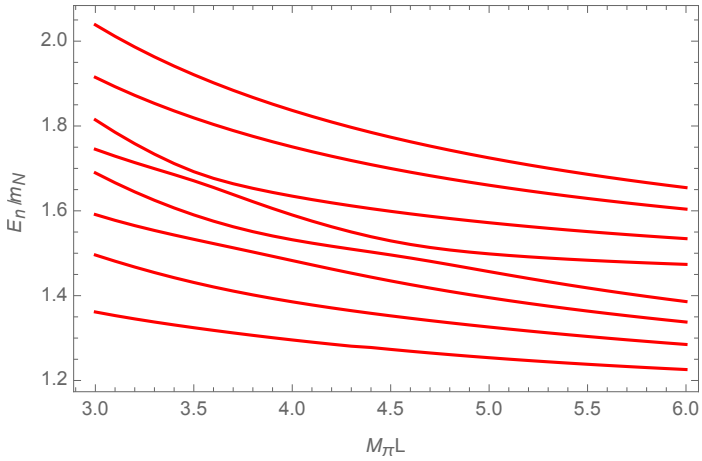

Figure 3.5: Energy levels for the full system for different box sizes L without displaying the free energy levels.

and the free $|\vec{n}|^2 = 2$ level of the pion and the delta. The switching of the energy levels between different free energy levels is clearly seen in the vicinity of the critical value. We also depict the results without the free energy levels in Fig. 3.5 to better display the shape of the curves in this energy region. Further away from the critical value and for larger box sizes the energy levels behave like the free ones. Looking at the part of the fit with small box sizes, one may ask the question what happens at $M_\pi L$ values smaller than the ones depicted. Going to smaller box sizes is problematic because of two things. One is the fact that for small box sizes around $M_\pi L \simeq 3$ the numerical calculation is already quite unstable due to the overlapping energy levels. At smaller $M_\pi L$ it will be extremely difficult to distinguish between the different levels. The other reason is that at smaller box sizes the exponentially suppressed contributions from the tadpoles and the πR loop can not be neglected any more and have to be considered explicitly.
All in all the energy levels behave according to our expectations and we see the typical signature of avoided level crossing due to a resonance. A next possible step would be the investigation of the energy levels with the inclusion of an unstable delta resonance propagator. Also a calculation beyond chiral order $O(p^3)$ should be considered.

3.7 Summary and conclusions

In this paper, we have analyzed the Roper resonance in a finite volume. The calculation of the Roper self-energy up to third chiral order in the infinite volume has been repeated and the extension to the finite volume case has been achieved to find the finite volume corrections of the system. We have seen that the FV correction of the self-energy contains exponentially suppressed contributions for large L, which we neglected, and contributions with poles that have to be regularized. The calculation of the energy levels has been performed using physical baryon and pion masses and only two LECs had to be taken into account, which had been determined earlier [22]. The main results are:

- In the delta-free case ($h_R = 0$) the avoided level crossing can be clearly seen in the vicinity of the Roper resonance energy. For large box sizes, the energy levels approach the free energy levels.

- In the nucleon-free case ($g_{\pi NR} = 0$) there are no clear signs for avoided level crossing. This is caused by the large value of h_R and by the fact that the energy region lies mostly above the Roper. The approach to the free energy levels for large L is not as explicit as in the delta free case.
- Looking at the full system with nucleons and deltas, the avoided level crossing is observed again. Also in this case the approach to the free energy levels for large L can be seen.

Note that all the discussed calculations here can also be performed at non-physical pion masses. The remaining question is the treatment of the delta resonance in the finite volume. Assuming the delta to be a stable particle is a reasonable first approximation, but in further calculations its resonance characteristic must be included. Further, a calculation to fourth order (or higher) in the chiral expansion can be considered. However, this will increase the number of LECs that have to be taken into account.

Acknowledgemets

We are grateful to Akaki Rusetsky for many useful discussions and Jambul Gegelia for collaboration in the initial stage of this project and a careful reading of the manuscript. This work was supported in part by DFG and NSFC through funds provided to the Sino-German CRC 110 “Symmetries and the Emergence of Structure in QCD" (NSFC Grant No. 11621131001, DFG Grant No. TRR110), by VolkswagenStiftung (Grant no. 93562) and by the CAS President’s International Fellowship Initiative (PIFI) (Grant No. 2018DM0034).

CHAPTER 4

Particle-dimer approach for the Roper resonance in a finite volume

4.1 Prologue

The content of this chapter is based on the publication

- D. Severt, M. Mai and U.-G. Meißner,
  "Particle-dimer approach for the Roper resonance in a finite volume",
  JHEP **04**, 100 (2023) [arXiv:2212.02171 [hep-lat]].

This chapter is a continuation of the research on the Roper resonance and can be seen as a follow-up work to chapter 3. We propose a new finite-volume approach which implements two- and three-body dynamics in a transparent way based on an effective field theory Lagrangian. The formalism utilizes a particle-dimer picture and formulates the quantization conditions based on the self-energy of the decaying particle. The formalism is studied for the case of the Roper resonance, using input from lattice QCD and phenomenology. Finally, finite-volume energy eigenvalues are predicted and compared to existing results of lattice QCD calculations. This crucially provides initial guidance on the necessary level of precision for the finite-volume spectrum (Ref. [105]).
One of the main questions at the end of chapter 3 (i.e. Ref. [86]) was how to implement the unstable nature of the delta resonance into the energy spectrum of the Roper resonance, so that the delta is able to decay into a nucleon and a pion. This should then result in the $N\pi\pi$ final state the Roper is known for. A first idea was to modify the delta resonance propagator by including the delta decay width explicitly. However, this straightforward guess produced some issues in the finite-volume formalism, i.e. complex numbers appeared in the self-energy sums, which complicated their evaluation and interpretation. A more promising ansatz seemed to be the so-called particle-dimer approach (see e.g. [37–42]). This approach was developed to describe three-particle scattering in a convenient and straightforward way. It reformulates the three-body problem as a two-body problem by introducing a so-called particle-dimer field, which incorporates two-particle scattering. Then, instead of calculating a three-particle scattering amplitude, one can calculate the scattering amplitude of one particle with the dimer field. The calculation yields the same result in both ways, which was proven in the literature several times (see e.g. [40]), but the particle-dimer approach simplifies the computational effort significantly.

The three-particle $N\pi\pi$ final state of the Roper resonance is one of its most intriguing features and the dimer formalism should help to investigate it. The author of this thesis started by formulating a Lagrangian for the Roper in a non-relativistic covariant framework (see e.g. [85]) with the help of A. Rusetsky. The degrees of freedom included in the Lagrangian are nucleons and pions, as well as three dimer fields: the σ (sigma) meson, the Δ (delta) baryon and the Roper resonance. With such a Lagrangian, the usual procedure to find the finite-volume (FV) energy spectrum is by calculating scattering amplitudes of dimer fields with the other asymptotic states (see e.g. [36]). In the case of the Roper system, these would be nucleons and pions, but calculating all possible scattering reactions causes several difficulties. One of the problems is that a lot of unknown low-energy constants (LECS) are involved, which are hard to determine, since there are not enough experimental or lattice data. Due to this reason and other issues, the author of this thesis decided to calculate the FV energy spectrum by using the Roper resonance self-energy, analogously to the calculation in chapter 3, but this time within the covariant particle-dimer picture. A first test for the framework was the recreation of the Roper energy spectrum including only nucleons and pions (see Fig. 3.2 in chapter 3). The new approach produced a very similar result, which was a striking argument to continue this method. The next step was the inclusion of the self-energy contributions from the dimer fields, which turned out to be quite challenging. At around this time M. Mai joined the project, who shared a lot of his valuable insights about three-particle dynamics with U.-G. Meißner and the first author. One of M. Mai's suggestions was to analyze the σ-dimer field by using data from Lattice QCD [106]. This helped to fix some of the dimer LECs. After that, the author was able to find a first FV energy spectrum for the Roper resonance with the σ-dimer. An analogous calculation for the Δ-dimer was also performed by the author. As a final step, the results for the FV energy levels were compared with lattice QCD results from Ref. [15]. The author found an overall good agreement between the two very different approaches to determine the Roper resonance FV energy levels.

4.2 Introduction

Our understanding of the strong interaction is tested by our ability to unravel the pattern and production mechanism behind its bound states and resonances. The exploration of this non-trivial and very rich spectrum is the main motivation behind the large international experimental programs at, e.g., MAMI (Germany), ELSA (Germany), Jefferson Laboratory (USA), Spring-8 (Japan) or CERN (Switzerland), see [107–113] for some recent reviews. Unraveling the pattern of the resonance spectrum and the mechanism behind its generation has also prompted the develop-ment of many theoretical tools such as quark models [114–116], or Dyson-Schwinger approaches [117–119]. While some features of the resonance spectrum seem to be captured by such approaches, they also include some uncontrolled approximations and do not allow for a first-principle connection to Quantum Chromodynamics (QCD). Lattice QCD provides such an approach, which already reshaped the field of hadron spectroscopy leading to many valuable insights on, e.g., the ground state spectrum of baryons [120] and many excited states, see e.g. Refs. [106, 121–129] as recently reviewed in Ref. [10].

Two paramount examples of the puzzles in the baryon spectrum are the negative strangeness $\Lambda(1405)1/2^-$-resonance with its double pole structure (see for example the recent reviews [130–132]) and the first excited state of the nucleon, the Roper resonance $N(1440)1/2^+$. The latter is considerably lighter than the parity partner of the nucleon, the $N(1535)1/2^-$. This is at odds with the quark model

expectation [133, 134], associated there with the second radial excitation of the nucleon. More recent phenomenological analyses revealed the complex analytic structure of the Roper [135–138] including the strong coupling to the three-body ($\pi\pi N$) channels distorting its shape from the usual Breit-Wigner form. Ab-initio access to such three-body systems from lattice QCD has been obscured for a long time due to computational complexity and, equally importantly, by the lack of theoretical tools relating lattice results to real-world quantities. The need for such tools is simply necessitated by the fact that in lattice methodology QCD Green's functions are determined numerically in a finite volume. Ultimately, this leads to a discretization of obtained real-valued spectrum to be related to the infinite-volume (real-world) in general complex-valued interaction spectrum. This cannot be overcome in an adiabatic enlargement of the considered volume and mathematical mapping is required, usually referred to as the *quantization condition*, for dedicated reviews see Refs. [27, 91, 139]. Lattice results for such systems are becoming available, see Refs. [15, 16, 140–151]. This is also partially fostered by the recent progress deriving three-body quantization conditions [28–30, 32, 34–36, 41, 42, 152–171].

In the present work we propose and test a new approach to the three-body quantization conditions which can serve as a transparent approach to access resonant systems in a finite-volume. Our formalism builds on the previous work [86] and is based on the particle-dimer framework [37–40, 42], which conveniently allows us to express the self-energy diagram of a resonant field in terms of either ordinary (asymptotically stable) meson and baryon fields or, alternatively, one of these fields can also be replaced by an unstable field from the particle-dimer Lagrangian. The latter in turn acquires a complex-valued self-energy due to the coupling to stable fields going on-shell. Obviously, the interplay of these two effects leads to an on-shell configuration of three stable intermediate particles. Indeed, these are precisely the configurations which lead to power-law finite-volume effects. Some of these finite-volume effects are proportional to $\exp(-M_\pi L)$, where M_π denotes the mass of the pion, i.e. the lightest asymptotic particle in QCD, and L is the length of the cubic volume with periodic boundary conditions in which our calculations are performed. Thus, neglecting these exponentially suppressed contributions, one can separate off the volume-dependent from the volume-independent quantities which ultimately allows one to map finite- to infinite-volume quantities. To demonstrate the advantages and limitations of the present work, we concentrate specifically on the complicated Roper resonance including the πN and $\pi\pi N$ dynamics using Δ and σ auxiliary dimer-fields. Given the presently still scarce lattice results in this sector [15, 16, 140] we estimate the volume-independent quantities from phenomenology. The predicted finite-volume spectrum is then compared to lattice results both in the two- and three-body sector [15, 172].

The manuscript is organized in the following way: First, we introduce the theoretical framework in section 4.3. Then, we determine the self-energy of the Roper resonance within our theory in section 4.4. The sections 4.5 and 4.6 discuss the particle-dimer fields and their contributions to the Roper self-energy, respectively. After that, the finite-volume formalism is introduced in section 4.7. Our numerical calculations are discussed in section 4.8 and the results are given in 4.9. Finally, we conclude with a brief summary and outlook in section 4.10.

4.3 Covariant non-relativistic framework

We begin with an introduction of the covariant non-relativistic effective field theory, following the general formalism of Refs. [40–42, 84, 85], see also Ref. [17] for a pedagogical introduction. To describe a few-particle system containing pions (π) and nucleons (N), such as the three-particle $N\pi\pi$-system, we introduce the following Lagrangian

$$\mathcal{L}_{\pi\pi N} = \mathcal{L}_{\text{dyn}} + c_1 \phi^\dagger \phi^\dagger \phi\phi + c_2 \psi^\dagger \phi^\dagger \phi\psi + c_3 \psi^\dagger \phi^\dagger (\phi + \phi^\dagger)\phi\psi + c_4 \psi^\dagger \phi^\dagger \phi^\dagger \phi\phi\psi + \dots \,. \tag{4.1}$$

Here, ϕ is the non-relativistic pion field and ψ the non-relativistic nucleon field. The interaction between these particles is parameterized by the low-energy constants (LECs) $c_{1,2,3,4}$. The ellipses denote terms with higher numbers of (pion) field insertions not required for the purpose of this work and terms with derivatives, which are not taken into account for now. Containing short-range physics, the LECs are in general not known, but can be determined from experimental data or lattice QCD results. The LEC c_1, for example, can be related to the $\pi\pi$ scattering length. The dynamical part of the covariant Lagrangian for the pions and nucleons is given by [85]

$$\mathcal{L}_{\text{dyn}} = \mathcal{L}_\phi + \mathcal{L}_\psi = \phi^\dagger 2W_\pi \left(i\partial_t - W_\pi\right) \phi + \psi^\dagger 2W_N \left(i\partial_t - W_N\right) \psi \,, \tag{4.2}$$

where

$$W_\pi = \left[M_\pi^2 - \vec{\nabla}^2\right]^{1/2} , \quad W_N = \left[m_N^2 - \vec{\nabla}^2\right]^{1/2} . \tag{4.3}$$

The differential operators W_π and W_N contain the pion mass M_π and the nucleon mass m_N, respectively. The square root structure of these operators leads to the relativistic energy-momentum relation in momentum space and ensures that the resulting amplitudes (e.g. two-particle scattering amplitudes) are relativistically invariant. This is not the case in the convenient non-relativistic treatment, which uses the Schrödinger equation to describe the dynamics of the free particles, see e.g. Ref. [40].
The Lagrangian (4.1) defines the pattern of the interactions driving the construction of various n-particle scattering amplitudes. However, already the case of three particles would result in a tremendous amount of Feynman diagrams. This is where the particle-dimer formalism becomes particularly handy, which we, therefore, utilize to address the Roper resonance. In the particle-dimer formalism one introduces an auxiliary field, called *dimer field* (sometimes also referred to *isobar*, see e.g. Ref. [173]), that incorporates two-particle dynamics and scattering. This means one effectively reduces a three-body problem to a two-body problem, which can be solved with much more ease. A common example to show the strength of the dimer formalism is the calculation of the scattering amplitude of three identical bosons, see e.g. Ref. [40]. In this case one introduces a dimer field, which describes the two-particle scattering of these bosons. Then, to obtain the three-particle scattering amplitude, one calculates the scattering of one boson with the dimer field, which is equivalent to three-particle scattering. The validity of this formalism has been discussed already several times in the literature, see e.g. Refs. [36, 40–42, 174]. However, the situation becomes more complex if one has three non-identical particles, like in our case with nucleons and pions. To investigate the Roper resonance in the $N\pi\pi$-system, we need to introduce three different dimer fields. The first dimer field is the $\Delta(1232)$ resonance (from here on called the Δ) with quantum numbers $J^P = 3/2^+$. This dimer field takes into account intermediate P-wave nucleon-pion interactions and its quantum numbers together with a pion overlap with the Roper resonance. The second dimer field is the σ with

the quantum numbers $J^P = 0^+$, i.e. the scalar-isoscalar resonance $f_0(500)$, formerly known as the σ-meson. It accounts for intermediate S-wave pion-pion interactions. Also here the quantum numbers of the $f_0(500)$ with a nucleon can have an overlap with the Roper. Finally, the third dimer field R is for the Roper resonance itself, which has the quantum numbers of the nucleon ($J^P = 1/2^+$) but a larger mass[1]. Considering all above dimer-fields, the particle-dimer Lagrangian takes the form

$$\mathcal{L}_{\text{Dimer}} = \mathcal{L}_{\text{dyn}} + \mathcal{L}_T \,, \tag{4.4}$$

where the dimer fields and their interactions are contained in $\mathcal{L}_T$, which reads

$$\begin{aligned}\mathcal{L}_T = {} & R^\dagger 2W_R \left(i\partial_t - W_R\right) R + \alpha_\Delta m_\Delta^2 \Delta^\dagger \Delta + \alpha_\sigma M_\sigma^2 \sigma^\dagger \sigma \\ & + f_1 R^\dagger \phi^\dagger \phi R - f_2[R^\dagger \phi \psi + R\phi^\dagger \psi^\dagger] - f_3[R^\dagger \phi \Delta + \Delta^\dagger \phi^\dagger R] - f_4[R^\dagger \sigma \psi + \psi^\dagger \sigma^\dagger R] \\ & + g_1 \Delta^\dagger \phi^\dagger \phi \Delta - g_2[\Delta^\dagger \phi \psi + \Delta \phi^\dagger \psi^\dagger] + h_1 \psi^\dagger \sigma^\dagger \sigma \psi - h_2[\sigma^\dagger \phi \phi + \sigma \phi^\dagger \phi^\dagger] \\ & - G_{R\sigma}[R^\dagger \phi^\dagger \sigma \psi + \psi^\dagger \sigma^\dagger \phi R] - G_{R\Delta}[R^\dagger \phi^\dagger \phi \Delta + \Delta^\dagger \phi^\dagger \phi R] - G_{\Delta\sigma}[\Delta^\dagger \phi^\dagger \sigma \psi + \psi^\dagger \sigma^\dagger \phi \Delta] \,.\end{aligned} \tag{4.5}$$

An important detail to note is that the dimer fields Δ and σ are not dynamical, i.e. the Lagrangian does not contain time or spatial derivatives of these fields. For the Roper resonance, on the other hand, the same dynamical Lagrangian as for the nucleon and pion is introduced with $W_R = [m_{R0}^2 - \vec{\nabla}^2\,]^{1/2}$ for the bare mass of the Roper m_{R0}. Making the Roper resonance dynamical should give a more accurate treatment of its properties. Overall, the dimer fields are auxiliary fields and the choice of their kinetic energy term should depend on the overall goal of the calculation. Naturally, the introduction of derivative terms for the dimer fields results in more complex calculations, since these terms will enter the dimer propagators. Therefore, to simplify our analysis, we keep the Δ- and σ-dimer static. Additionally, it should be stressed that the Lagrangian in Eq. (4.5) does not posess any spin- or isospin-structure. Also here the Lagrangian can be modified to include these effects, but we do not consider them for now in this pioneering work.

There are several coupling constants in Eq. (4.5) accompanying the terms describing the interactions between the particles and dimer fields. The LECs $f_{1,2,3,4}$, $g_{1,2}$, $h_{1,2}$ and $G_{R\sigma,R\Delta,\Delta\sigma}$ can be related to the LECs in Eq. (4.1) after integrating out the dimer fields. We also have two real mass scales m_Δ and M_σ for the Δ- and σ-dimer, respectively. Very often in the literature these mass scales are absorbed inside the definition of the auxiliary dimer fields. We, on the other hand, want to make sure that all appearing fields have the same dimension and later use the physical masses for our numerical calculations. Both of these mass scales come with prefactors

$$\alpha_\Delta = \pm 1 \,, \quad \alpha_\sigma = \pm 1 \,, \tag{4.6}$$

[1] Note that there is in principle also a nucleon pole appearing in the Roper system, due to the identical quantum numbers. This pole has to be taken into account in a lattice QCD calculations, for a recent example of a lattice calculation of a 3-point function see Ref. [175]. However, in our work we look at energies larger than the nucleon mass so that an explicit inclusion is not necessary.

which depend on the signs of the corresponding LECs in Eq. (4.1). For example, integrating out the σ-field yields

$$c_1 = -\frac{h_2^2}{\alpha_\sigma M_\sigma^2} \,. \tag{4.7}$$

It can be seen that the sign of c_1 dictates the value of α_σ, since h_2^2/M_σ^2 is a positive number. Later in the manuscript, we will see how $\pi\pi$ scattering information (e.g. the S-wave scattering length or the corresponding phase shifts) determine this LEC.
Another notable difference between Eq. (4.5) and most other Lagrangians in the particle-dimer picture are the interactions among the dimer fields. The Roper dimer R is allowed to decay in one of the other dimer fields, i.e. R can decay into σN, or $\Delta\pi$ pairs through the interactions proportional to f_3 and f_4, respectively. An example for a particle-dimer theory with two dimer fields that can interact with each other can be found in Ref. [176]. After integrating out the dimer fields, interactions with an odd number of pion fields can be obtained, e.g. the term proportional to c_3 in Eq. (4.1) can change the number of particles. This yields the feature that a two-particle $N\pi$ initial state could result in a three-particle $N\pi\pi$ final state and vice versa. Obviously, this then also means that there can in principle be a four-particle $N\pi\pi\pi$ final state when starting with an initial three-particle $N\pi\pi$ state, etc.. However, in practice we avoid such a four-particle (and higher) final state by a suitable energy/momentum cutoff.

The particle-dimer Lagrangian Eq. (4.5) yields the following Feynman rules for the propagators:

$$-iS_N\left(p_0,\vec{p}\right) = \frac{i}{2\omega_N(\vec{p})\left[p_0-\omega_N(\vec{p})+i\epsilon\right]} \,, \quad \omega_N(\vec{p}) = \sqrt{|\vec{p}|^2+m_N^2} \,, \tag{4.8}$$

and

$$-iS_\pi\left(p_0,\vec{p}\right) = \frac{i}{2\omega_\pi(\vec{p})\left[p_0-\omega_\pi(\vec{p})+i\epsilon\right]} \,, \quad \omega_\pi(\vec{p}) = \sqrt{|\vec{p}|^2+M_\pi^2} \,. \tag{4.9}$$

Looking at ω_N and ω_π, one notes that the square root differential operator in the dynamical part of the Lagrangian leads to the well-known energy-momentum relation. Our notation for the propagators follows the common sign convention used in the literature, see e.g. [85]. For the dimer fields, we have the bare propagator of the Roper resonance

$$-iS_R\left(p_0,\vec{p}\right) = \frac{i}{2\omega_R(\vec{p})\left[p_0-\omega_R(\vec{p})+i\epsilon\right]} \,, \quad \omega_R(\vec{p}) = \sqrt{|\vec{p}|^2+m_{R0}^2} \,, \tag{4.10}$$

and the bare Δ and σ propagators

$$-iD_\Delta^0\left(p_0,\vec{p}\right) = \frac{i}{\alpha_\Delta m_\Delta^2} \,, \quad -iD_\sigma^0\left(p_0,\vec{p}\right) = \frac{i}{\alpha_\sigma M_\sigma^2} \,, \tag{4.11}$$

where the latter are constant with respect to the particle energy. An explicit momentum dependence can be given to D_Δ^0 and D_σ^0 by either adding higher order terms in the particle-dimer Lagrangian Eq. (4.5) or by "dressing" the propagators with the respective dimer self-energies. The latter is

discussed in detail in section 4.5.

4.4 Self-energy of the Roper resonance

The dressed propagator of the Roper resonance is given by

$$S_R^d\left(p_0,\vec{p}\right) = \frac{1}{2\omega_R(\vec{p})\left[\omega_R(\vec{p}) - p_0 - i\epsilon\right] - \Sigma_R(p_0,\vec{p})}\,, \tag{4.12}$$

where $\Sigma_R(p_0,\vec{p})$ is Roper self-energy. The pole of the propagator is obtained by finding the zeros of the denominator, i.e.

$$2\omega_R(\vec{p})\left[\omega_R(\vec{p}) - p_0\right] - \Sigma_R(p_0,\vec{p}) = 0\,. \tag{4.13}$$

In the infinite volume, one possibility to parameterize the pole is to choose the rest-frame, $\vec{p} = 0$, and set $p_0 = Z$ for $Z = m_R - i\Gamma_R/2$, with m_R the physical mass of the Roper resonance and Γ_R its width. The equation for the pole then reads

$$2m_{R0}\left[m_{R0} - Z\right] - \Sigma_R(Z,\vec{0}) = 0\,, \tag{4.14}$$

which can be reordered to give

$$Z = m_{R0} - \frac{1}{2m_{R0}}\Sigma_R(Z) = m_{R0} - \frac{1}{2m_{R0}}\Big(\mathrm{Re}\left\{\Sigma_R(Z)\right\} + i\mathrm{Im}\left\{\Sigma_R(Z)\right\}\Big)\,, \tag{4.15}$$

where the self-energy has been separated into its real and imaginary part. It is then straightforward to identify the physical mass and width

$$m_R = m_{R0} - \frac{1}{2m_{R0}}\mathrm{Re}\left\{\Sigma_R(Z)\right\}\,, \quad \text{and} \quad \Gamma_R = \frac{1}{m_{R0}}\mathrm{Im}\left\{\Sigma_R(Z)\right\}\,. \tag{4.16}$$

These two relations can, of course, only be solved iteratively, since the self-energy depends on Z itself. If the imaginary part of the self-energy vanishes, the width Γ_R is zero. A vanishing real part, on the other hand, allows to set the bare mass equal to the physical mass, i.e. $m_R = m_{R0}$.
Looking at the full particle-dimer Lagrangian in Eq. (4.5), we see that there are several interactions which lead to different contributions to the self-energy, as depicted in Fig. 4.1. At one-loop order, the first option is a pion and a nucleon inside the loop. Since both are stable particles and we know that the Roper R can decay into a $N\pi$ final-state, we expect this diagram to be of great importance. The next option is N and the σ-dimer inside the loop. This diagram is interesting, because the dimer itself is an unstable particle. We know that the Roper can decay into the $N\sigma$ pair, but we expect that the σ decays further into two pions, which would leave us with the three particle ($N\pi\pi$) final-state. This is similar to the third option, a π and Δ-dimer inside the loop. Also here, the Δ can decay further into a $N\pi$ state, which again results in a three-particle $N\pi\pi$-system. Note, further that one-loop tadpole diagrams do not appear in the non-relativistic theory. We can summarize these statements, see Fig. 4.1, into the following equation

$$\Sigma_R(p_0,\vec{p}) = \Sigma_{N\pi}(p_0,\vec{p}) + \Sigma_{N\sigma}(p_0,\vec{p}) + \Sigma_{\Delta\pi}(p_0,\vec{p})\,, \tag{4.17}$$

Figure 4.1: Feynman diagrams contributing to the Roper resonance mass at one-loop order. The thick solid line with an arrow, the solid line with an arrow and the double solid line with an arrow refer to the Roper resonance, the nucleon, and the Δ-dimer field, respectively. The dotted line represents pions and the double solid line the σ-dimer fields.

and our goal is to calculate the different self-energy contributions.
We start by evaluating the self-energy $\Sigma_{N\pi}(p_0, \vec{p})$. Applying the Feynman rules, we obtain

$$i\Sigma_{N\pi}(p) = \int \frac{d^4k}{(2\pi)^4}(-if_2)^2 \left[-iS_N(p-k)\right]\left[-iS_\pi(k)\right] = f_2^2 \int \frac{d^4k}{(2\pi)^4} S_N(p-k)S_\pi(k)\,. \tag{4.18}$$

From here on, we use the four-vector p as a shorthand notation for $(p_0, \vec{p})$. After dividing by i on both sides we find

$$\Sigma_{N\pi}(p) = f_2^2 J_{N\pi}(p)\,, \tag{4.19}$$

with

$$J_{N\pi}(p) = \int \frac{d^4k}{(2\pi)^4 i} \frac{1}{2\omega_N(\vec{p}-\vec{k})\left[\omega_N(\vec{p}-\vec{k}) - (p_0 - k_0) - i\epsilon\right]} \frac{1}{2\omega_\pi(\vec{k})\left[\omega_\pi(\vec{k}) - k_0 - i\epsilon\right]}\,. \tag{4.20}$$

This is the main one-loop scalar integral appearing in the covariant non-relativistic frame-work. The evaluation of this integral is non-trivial, due to the square root structures appearing in the denominator, see e.g. Ref. [177]. However, the first step is straightforward, integrating over the time component of the loop momentum k_0, i.e.

$$\begin{aligned} J_{N\pi}(p) = \int_{-\infty}^{+\infty} \frac{dk_0}{2\pi i} \int \frac{d^3k}{(2\pi)^3} \frac{1}{4\omega_N(\vec{p}-\vec{k})\omega_\pi(\vec{k})} \\ \times \left\{ \frac{1}{\left[\omega_N(\vec{p}-\vec{k}) - (p_0 - k_0) - i\epsilon\right]\left[\omega_\pi(\vec{k}) - k_0 - i\epsilon\right]} \right\}\,. \end{aligned} \tag{4.21}$$

Looking at the denominator inside the brackets, we see that it has two poles in the complex k_0-plane, namely one in the upper half (positive imaginary part) and one in the lower half (negative imaginary part). Using Cauchy's theorem, we can solve the integral by calculating a contour integral around one of the poles. Choosing a contour around the upper pole[2], we obtain

$$J_{N\pi}(p) = \int \frac{d^3k}{(2\pi)^3} \frac{1}{4\omega_N(\vec{p}-\vec{k})\omega_\pi(\vec{k})\left[\omega_N(\vec{p}-\vec{k}) + \omega_\pi(\vec{k}) - p_0 - i\epsilon\right]}\,. \tag{4.22}$$

[2] The result of the integral does not change, if one would choose the pole in the lower half.

We are left with a three-dimensional integral over the spatial momentum components, which will also be our starting point when we consider the finite-volume case later in section 4.7. One observes that the integral has a pole for $p_0 > 0$ (taking $\epsilon \to 0$) and that the integral is logarithmically divergent. It is therefore practical to use dimensional regularization for the further evaluation. In D dimensions Eq. (4.22) takes the form

$$J_{N\pi}(p) = \int \frac{d^D k}{(2\pi)^D} \frac{1}{4\omega_N(\vec{p}-\vec{k})\omega_\pi(\vec{k})\big[\omega_N(\vec{p}-\vec{k}) + \omega_\pi(\vec{k}) - p_0 - i\epsilon\big]} \,. \tag{4.23}$$

The main complexity still comes from the square root terms in the denominator. To simplify matters, let us consider the same integral in the rest frame, i.e. $p = (E, \vec{0})$,

$$J_{N\pi}(E) = \int \frac{d^D k}{(2\pi)^D} \frac{1}{4\omega_N(\vec{k})\omega_\pi(\vec{k})\big[\omega_N(\vec{k}) + \omega_\pi(\vec{k}) - E - i\epsilon\big]} \,, \tag{4.24}$$

such that we can rewrite the integrand as

$$\begin{aligned} \frac{1}{4\omega_N(\vec{k})\omega_\pi(\vec{k})\big[\omega_N(\vec{k}) + \omega_\pi(\vec{k}) - E - i\epsilon\big]} = \frac{1}{2E} \frac{1}{|\vec{k}|^2 - q^2(E) - i\epsilon'} \\ + \frac{1}{4\omega_N(\vec{k})\omega_\pi(\vec{k})\big[\omega_N(\vec{k}) + \omega_\pi(\vec{k}) + E + i\epsilon\big]} \\ + \frac{1}{4\omega_N(\vec{k})\omega_\pi(\vec{k})\big[\omega_N(\vec{k}) - \omega_\pi(\vec{k}) - E + i\epsilon\big]} \\ + \frac{1}{4\omega_N(\vec{k})\omega_\pi(\vec{k})\big[-\omega_N(\vec{k}) + \omega_\pi(\vec{k}) - E + i\epsilon\big]} \,, \end{aligned} \tag{4.25}$$

with

$$q^2(E) = \frac{\lambda\left(E^2, m_N^2, M_\pi^2\right)}{4E^2} \,, \tag{4.26}$$

where we used the Källén triangle function $\lambda(x,y,z) = x^2 + y^2 + z^2 - 2xy - 2xz - 2yz$. The rearrangement of the integrand allows us to isolate the pole of the quotient, $q^2(E)$, which can be seen in the first term on the right-hand side of Eq. (4.25). The remaining three terms on the right-hand side are regular, which means that they do not contain a pole anymore for physical values of E. Note that in this work we consider energies above the nucleon mass. Therefore, these terms can be expanded in powers of the integration momentum $\vec{k}$ leading to polynomials in $|\vec{k}|$ which vanish in dimensional regularization. We are left with

$$J_{N\pi}(E) = \frac{1}{2E} \int \frac{d^D k}{(2\pi)^D} \frac{1}{|\vec{k}|^2 - q^2(E) - i\epsilon'} \,, \tag{4.27}$$

which is evaluated with standard methods. After taking the limit $D \to 3$ we obtain

$$J_{N\pi}(E) = -\frac{1}{8\pi E}\sqrt{-q^2(E) - i\epsilon'} = \frac{i\lambda^{1/2}\left(E^2, m_N^2, M_\pi^2\right)}{16\pi E^2}\,, \tag{4.28}$$

where we used that $\lim_{\epsilon'\to 0}\sqrt{-q^2(E) \pm i\epsilon'} = \pm iq(E)$. The result of Eq. (4.28) in an arbitrary reference frame reads [177]

$$J_{N\pi}(p) = \frac{i\lambda^{1/2}\left(p^2, m_N^2, M_\pi^2\right)}{16\pi p^2} = \frac{i\lambda^{1/2}\left(s, m_N^2, M_\pi^2\right)}{16\pi s}\,, \tag{4.29}$$

with $s = p^2 = p_0^2 - |\vec{p}|^2$ the usual Mandelstam variable. Thus, the self-energy of the Roper resonance becomes

$$\Sigma_{N\pi}(p) = \frac{if_2^2}{16\pi p^2}\lambda^{1/2}\left(p^2, m_N^2, M_\pi^2\right)\,, \tag{4.30}$$

which is a notable result. Specifically, the function $J_{N\pi}$ and with it the Roper self-energy is purely imaginary at the energies of interest, i.e. $p^2 \approx m_R^2$.
Next, we consider the self-energy contributions with dimer fields, i.e. σN and $\Delta\pi$ loop-diagram contributions. Taking $\Sigma_{\Delta\pi}$ as an example, we obtain

$$i\Sigma_{\Delta\pi}(p) = f_3^2\int\frac{d^4k}{(2\pi)^4}D_\Delta^0(p-k)S_\pi(k) = -\frac{f_3^2}{\alpha_\Delta m_\Delta^2}\int\frac{d^4k}{(2\pi)^4}\frac{1}{2\omega_\pi(\vec{k})\left[\omega_\pi(\vec{k}) - k_0 - i\epsilon\right]}\,, \tag{4.31}$$

which is basically a tadpole integral, i.e. an integral over a single propagator, due to the constant D_Δ^0 propagator. These tadpole diagrams usually do not exist in non-relativistic EFTs, since they vanish within time-ordered perturbation theory. However, if such a diagram shows up, a common way to treat the k_0-integral is to rewrite it as a contour integral according to Cauchy's theorem. For example, one can evaluate the k_0-integral by choosing the contour in the upper k_0-plane excluding the pole. Then, $\Sigma_{\Delta\pi}(p)$ vanishes like the other tadpole contributions, which is the usual procedure, see Ref. [17] and the references therein for more information. On the other hand, if one would decide to include the pole (lower plane), the following would happen: The k_0-integral is replaced by $2\pi i$ and a spatial $\vec{k}$-integral over $1/\omega_\pi(\vec{k})$ remains. But this expression does not posses a pole and, thus, one can expand the denominator in powers of the momentum $|\vec{k}|$, like before, to obtain a polynomial. Dimensional regularization is then used to make the polynomial terms disappear, so that again $\Sigma_{\Delta\pi}(p) = 0$. This illustrates that the loop integral vanishes no matter how the k_0-integral is performed. An analogous calculation for the $N\sigma$-case shows that also $\Sigma_{N\sigma}(p) = 0$.
This of course cannot be the final answer, which roots in the fact that the dimer propagators are not dynamical, see Eq. (4.5). Interestingly, and as we will discuss below, improving this by dressing dimer propagators actually introduces three-particle dynamics in the intermediate states.

4.5 Dressed dimer fields

We have seen that a constant dimer propagator leads to a vanishing particle-dimer self-energy. Obviously, the constant propagator is just a first approximation and higher correc-tions have to be taken into account. To do this, we consider the self-energies of the dimer fields and *dress* the propagators as

$$D_\Delta(p) = -\frac{1}{\alpha_\Delta m_\Delta^2 + \Sigma_\Delta(p)}\,, \tag{4.32}$$

for the Δ-dimer propagator and

$$D_\sigma(p) = -\frac{1}{\alpha_\sigma M_\sigma^2 + \Sigma_\sigma(p)}\,, \tag{4.33}$$

for the σ-dimer. The self-energies Σ_Δ and Σ_σ are given by

$$\Sigma_\Delta(p) = g_2^2 \int \frac{d^4k}{(2\pi)^4 i} S_N(p-k) S_\pi(k) = \frac{i g_2^2}{16\pi p^2} \lambda^{1/2}\left(p^2, m_N^2, M_\pi^2\right)\,, \tag{4.34}$$

and

$$\Sigma_\sigma(p) = \frac{1}{2}(2h_2)^2 \int \frac{d^4k}{(2\pi)^4 i} S_\pi(p-k) S_\pi(k) = \frac{i h_2^2}{8\pi p^2} \lambda^{1/2}\left(p^2, M_\pi^2, M_\pi^2\right)\,, \tag{4.35}$$

respectively. Note the additional symmetry factor of $1/2$ in front of the σ self-energy. The evaluation of these self-energies is analogous to the proof of Eq. (4.30) in the last section. Due to the simpler structure of the Källén function in the case of two equal masses, i.e.

$$\lambda\left(p^2, M_\pi^2, M_\pi^2\right) = p^2\left(p^2 - 4M_\pi^2\right)\,, \tag{4.36}$$

we proceed with the σ-dimer propagator. We start by reformulating the dressed propagator as

$$D_\sigma(p) = -\frac{1}{\alpha_\sigma M_\sigma^2 + i c \lambda^{1/2}\left(p^2, M_\pi^2, M_\pi^2\right)/p^2}\,, \qquad c = \frac{h_2^2}{8\pi}\,. \tag{4.37}$$

Subsequently, we simplify the denominator by expanding the above expression so that

$$D_\sigma(p) = -\frac{\alpha_\sigma M_\sigma^2 p^4 - i c p^2 \lambda^{1/2}\left(p^2, M_\pi^2, M_\pi^2\right)}{\alpha_\sigma^2 M_\sigma^4 p^4 + c^2\left(p^4 - 4M_\pi^2 p^2\right)}\,. \tag{4.38}$$

From our initial definitions we know that $\alpha_\sigma^2 = 1$ and we can rewrite the denominator as

$$\alpha_\sigma^2 M_\sigma^4 p^4 + c^2\left(p^4 - 4M_\pi^2 p^2\right) = \left(M_\sigma^4 + c^2\right)\left(p^2 - \mu_\sigma^2\right) p^2\,, \tag{4.39}$$

where we have introduced a new mass parameter

$$\mu_\sigma^2 = \frac{4M_\pi^2 c^2}{M_\sigma^4 + c^2} \,. \tag{4.40}$$

From Eq. (4.39) it is evident that μ_σ is, indeed, one of the poles of the σ-dimer. Coming back to Eq. (4.38), we can split up the expression into a real and an imaginary part

$$D_\sigma(p) = -\frac{\alpha_\sigma M_\sigma^2}{M_\sigma^4 + c^2} \frac{p^2}{p^2 - \mu_\sigma^2} + \frac{ic}{M_\sigma^4 + c^2} \frac{\lambda^{1/2}\left(p^2, M_\pi^2, M_\pi^2\right)}{p^2 - \mu_\sigma^2} \,. \tag{4.41}$$

In this form, we observe that $D_\sigma(p)$ possesses an imaginary part above the two-particle threshold, i.e. for $p^2 = s > 4M_\pi^2$. Below threshold, $D_\sigma(p)$ is a real-valued function. This is in perfect agreement with the general properties of scattering amplitudes, which in this case ($\pi\pi \to \pi\pi$ scattering) is simply proportional to the dimer propagator

$$T_{\pi\pi\to\pi\pi}(s) \propto D_\sigma(s) \,, \tag{4.42}$$

see, e.g., Ref. [10, 38]. This relation allows us to connect the coefficients appearing in $D_\sigma(s)$ with observables from $\pi\pi$-scattering. The first quantity one can look at is the scattering length a defined via an effective range expansion[3]

$$|\vec{q}|\cot\delta(s) = +\frac{1}{a} + O\left(|\vec{q}|^2\right) , \tag{4.43}$$

where

$$\cot\delta(s) = \frac{\mathrm{Re}\left\{T_{\pi\pi\to\pi\pi}(s)\right\}}{\mathrm{Im}\left\{T_{\pi\pi\to\pi\pi}(s)\right\}} \,. \tag{4.44}$$

Here, $\delta(s)$ is the phase shift and $\vec{q}$ is the center-of-mass (CMS) three-momentum above threshold. It can be deduced that $|\vec{q}| = \sqrt{s - 4M_\pi^2}/2$. To calculate the cotangent of the phase shift, we use the proportionality between the $\pi\pi$-scattering amplitude and the σ-dimer propagator. We find

$$\frac{\mathrm{Re}\left\{T_{\pi\pi\to\pi\pi}(s)\right\}}{\mathrm{Im}\left\{T_{\pi\pi\to\pi\pi}(s)\right\}} = \frac{\mathrm{Re}\left\{D_\sigma(s)\right\}}{\mathrm{Im}\left\{D_\sigma(s)\right\}} = -\frac{\alpha_\sigma M_\sigma^2}{c} \frac{s}{\lambda^{1/2}\left(s, M_\pi^2, M_\pi^2\right)} \,, \tag{4.45}$$

and we can simplify the triangle function to $\lambda^{1/2}\left(s, M_\pi^2, M_\pi^2\right) = 2\sqrt{s}|\vec{q}|$. Utilizing these identities, we obtain

$$|\vec{q}|\cot\delta(s) = -\frac{\alpha_\sigma M_\sigma^2}{c}\frac{\sqrt{s}}{2} = -\frac{\alpha_\sigma M_\sigma^2}{c}\sqrt{|\vec{q}|^2 + M_\pi^2} = -\frac{\alpha_\sigma M_\sigma^2 M_\pi}{c} + O\left(|\vec{q}|^2\right) . \tag{4.46}$$

[3] Note that the sign in front of the $1/a$ term varies in the literature depending on the definition of the effective range expansion.

A comparison with Eq. (4.43) shows that the scattering length a is given by

$$a = -\frac{c}{\alpha_\sigma M_\sigma^2 M_\pi} \;\Leftrightarrow\; aM_\pi = -\frac{c}{\alpha_\sigma M_\sigma^2} = -\frac{h_2^2}{8\pi\alpha_\sigma M_\sigma^2} \,. \tag{4.47}$$

This is a very useful result, because it fixes the ratio h_2^2/M_σ^2 and the value for α_σ. If the scattering length is positive (attractive interaction) then we must set $\alpha_\sigma = -1$, since all other constants in Eq. (4.47) are positive. Analogously, we set $\alpha_\sigma = +1$ for $a < 0$ (repulsive interaction). The $\pi\pi$-scattering length in the isospin $I = 0$ channel, where the σ resonance appears, is measured to be $a^{I=0}M_\pi = 0.2220 \pm 0.0128(\text{stat.}) \pm 0.0050(\text{syst.}) \pm 0.0037(\text{th.})$, see Ref. [178]. Therefore, we conclude that α_σ must be -1, leading to an attractive interaction that produces the σ resonance.
Instead of using the scattering length to fix the LECs of the particle-dimer Lagrangian, one can also fit them directly to the phase shifts $\delta(s)$. It is convenient to use the tangent of $\delta(s)$ for this

$$\tan\delta(s) = \frac{\text{Im}\left\{D_\sigma(s)\right\}}{\text{Re}\left\{D_\sigma(s)\right\}} = -\frac{c}{\alpha_\sigma M_\sigma^2}\frac{\lambda^{1/2}\left(s, M_\pi^2, M_\pi^2\right)}{s} = aM_\pi\sqrt{1-\frac{4M_\pi^2}{s}} \,. \tag{4.48}$$

We can see that the function $\tan\delta(s)$ is zero at the threshold ($s = 4M_\pi^2$) and reaches aM_π for $s \to \infty$. Therefore, we expect that the above function is only able to describe the phase shift in the low-energy region. However, this does not come as a surprise, since the σ-dimer field is a constant at leading order, constructed specifically to approximate the low-energy regime. Another method to calculate the parameters of the σ-dimer is to use mass and decay width of the σ-resonance. Here, one assumes that the σ-dimer has the same dynamic properties as the Roper dimer and fulfills an equation analogous to Eq. (4.16). Then, one can approximate the width of the σ resonance Γ_σ as

$$\Gamma_\sigma \approx \frac{1}{M_\sigma}\text{Im}\left\{\Sigma_\sigma(p)\right\}\Big|_{p=M_\sigma} = \frac{h_2^2}{8\pi M_\sigma^3}\lambda^{1/2}\left(M_\sigma^2, M_\pi^2, M_\pi^2\right) \,. \tag{4.49}$$

Using phenomenological values for the mass and width of the σ-resonance, one can then fix the coupling h_2. This method is more speculative, because we introduced the dimer as a constant field and not as a dynamical one. Nonetheless, we do not abandon this method yet, using it as an additional cross-check.

Our analysis of the σ-dimer can be repeated analogously for the Δ-dimer. First, we take the dressed propagator in Eq. (4.32) and expand it like before to obtain

$$D_\Delta(p) = -\frac{\alpha_\Delta m_\Delta^2 p^4 - ibp^2\lambda^{1/2}\left(p^2, m_N^2, M_\pi^2\right)}{m_\Delta^4 p^4 + b^2\lambda\left(p^2, m_N^2, M_\pi^2\right)} \,, \quad b = \frac{g_2^2}{16\pi} \,, \tag{4.50}$$

where we again used that $\alpha_\Delta^2 = 1$. The two different masses inside the Källén function give the propagator a more complex structure. After some algebra the denominator can be rewritten as

$$\begin{aligned} m_\Delta^4 p^4 + b^2 \lambda\left(p^2, m_N^2, M_\pi^2\right) &= m_\Delta^4 p^4 + b^2\left(p^4 - 2p^2(m_N^2 + M_\pi^2) + (m_N^2 - M_\pi^2)^2\right) \\ &= \left(m_\Delta^4 + b^2\right)\left(p^2 - \mu_\Delta^2 + i\nu\right)\left(p^2 - \mu_\Delta^2 - i\nu\right) , \end{aligned} \tag{4.51}$$

with

$$\mu_\Delta^2 = \frac{b^2(m_N^2 + M_\pi^2)}{m_\Delta^4 + b^2} , \quad \text{and} \quad \nu = \frac{b}{m_\Delta^4 + b^2}\sqrt{m_\Delta^4\left(m_N^2 - M_\pi^2\right)^2 - 4b^2 m_N^2 M_\pi^2} . \tag{4.52}$$

In the case of two equal masses in the Källén function, the result from the σ-dimer can be restored. All together, we have

$$D_\Delta(p) = -\frac{\alpha_\Delta m_\Delta^2}{m_\Delta^4 + b^2}\frac{p^4}{\left(p^2 - \mu_\Delta^2\right)^2 + \nu^2} + \frac{ib}{m_\Delta^4 + b^2}\frac{p^2\lambda^{1/2}\left(p^2, m_N^2, M_\pi^2\right)}{\left(p^2 - \mu_\Delta^2\right)^2 + \nu^2} . \tag{4.53}$$

One observes that the propagator does not have poles on the real axis, in contrast to the σ case. An imaginary part emerges above the pion-nucleon threshold, $p^2 = s > (m_N + M_\pi)^2$, and the relation to the πN-scattering length $a_{\pi N}$ reads

$$|\vec{q}|\cot\delta_{\pi N}(s) = |\vec{q}|\frac{\mathrm{Re}\left\{T_{\pi N\to\pi N}(s)\right\}}{\mathrm{Im}\left\{T_{\pi N\to\pi N}(s)\right\}} = |\vec{q}|\frac{\mathrm{Re}\left\{D_\Delta(s)\right\}}{\mathrm{Im}\left\{D_\Delta(s)\right\}} = +\frac{1}{a_{\pi N}} + O\left(|\vec{q}|^2\right) . \tag{4.54}$$

The pion-nucleon phase shift is denoted by $\delta_{\pi N}(s)$ and $T_{\pi N\to\pi N}(s) \propto D_\Delta(s)$ is the pion-nucleon scattering amplitude. With $\lambda^{1/2}\left(s, m_N^2, M_\pi^2\right) = 2\sqrt{s}\,|\vec{q}|$ and $\sqrt{s} = \sqrt{m_N^2 + |\vec{q}|^2} + \sqrt{M_\pi^2 + |\vec{q}|^2}$, we find

$$a_{\pi N} M_\pi = -\frac{2bM_\pi}{\alpha_\Delta m_\Delta^2(m_N + M_\pi)} = -\frac{g_2^2 M_\pi}{8\pi\alpha_\Delta m_\Delta^2(m_N + M_\pi)} . \tag{4.55}$$

The experimental value of the scattering length in the isospin $I = 3/2$ channel from the Roy-Steiner analysis is $a_{N\pi}^{I=3/2} M_\pi = (-86.3 \pm 1.8)\times 10^{-3}$ [179], which fixes the value of α_Δ to be $+1$. Analogously to the σ-case, one can also use the decay width to deduce the coupling g_2. We then have

$$\Gamma_\Delta \approx \frac{1}{m_\Delta}\mathrm{Im}\left\{\Sigma_\Delta(p)\right\}\Big|_{p=m_\Delta} = \frac{g_2^2}{16\pi m_\Delta^3}\lambda^{1/2}\left(m_\Delta^2, m_N^2, M_\pi^2\right) , \tag{4.56}$$

where we again stress that the above method of determining the coupling might be more speculative than using the scattering length. The insights from this section will help us to determine the dimer contributions to the Roper resonance self-energy. The numerical calculation of the dimer LECs will be discussed later in section 4.8.

4.6 Roper self-energy with dynamical dimer fields

Let us now come back to the self-energy contributions of the Roper resonance. From the $N\sigma$ channel, we obtain the loop-integral

$$\Sigma_{N\sigma}(p) = f_4^2 \int \frac{d^4k}{(2\pi)^4 i} S_N(p-k)\, D_\sigma(k) \ . \tag{4.57}$$

In section 4.4 we already discussed that a constant dimer propagator D_σ^0 leads to a vanishing integral. Therefore, we now consider the dressed propagator $D_\sigma(k)$ from Eq. (4.33) and obtain

$$\begin{aligned}\Sigma_{N\sigma}(p) &= -f_4^2 \int \frac{d^4k}{(2\pi)^4 i} \frac{1}{2\omega_N(\vec{p}-\vec{k})\big[\omega_N(\vec{p}-\vec{k}) - (p_0-k_0) - i\epsilon\big]} \frac{1}{\alpha_\sigma M_\sigma^2 + \Sigma_\sigma(k)} \\ &= -f_4^2 \int \frac{d^4k}{(2\pi)^4 i} \frac{1}{2\omega_N(\vec{p}-\vec{k})\big[\omega_N(\vec{p}-\vec{k}) - (p_0-k_0) - i\epsilon\big]} \Bigg\{ \alpha_\sigma M_\sigma^2 + 2h_2^2 \\ &\quad \times \int \frac{d^4l}{(2\pi)^4 i} \frac{1}{4\omega_\pi(\vec{k}-\vec{l})\omega_\pi(\vec{l})\big[\omega_\pi(\vec{k}-\vec{l}) - (k_0-l_0) - i\epsilon\big]\big[\omega_\pi(\vec{l}) - l_0 - i\epsilon\big]} \Bigg\}^{-1} ,\end{aligned} \tag{4.58}$$

where we have used the σ-dimer self-energy from Eq. (4.35). We can see that the l_0 integration inside the σ self-energy can be carried out right away according to our findings in section 4.4. We then arrive at

$$\begin{aligned}\Sigma_{N\sigma}(p) &= -\frac{f_4^2}{\alpha_\sigma M_\sigma^2} \int \frac{d^4k}{(2\pi)^4 i} \frac{1}{2\omega_N(\vec{p}-\vec{k})\big[\omega_N(\vec{p}-\vec{k}) - (p_0-k_0) - i\epsilon\big]} \\ &\quad \times \Bigg\{ 1 + \frac{2h_2^2}{\alpha_\sigma M_\sigma^2} \int \frac{d^3l}{(2\pi)^3} \frac{1}{4\omega_\pi(\vec{k}-\vec{l})\omega_\pi(\vec{l})\big[\omega_\pi(\vec{k}-\vec{l}) + \omega_\pi(\vec{l}) - k_0 - i\epsilon\big]} \Bigg\}^{-1} .\end{aligned} \tag{4.59}$$

The next step is to integrate out the remaining time component k_0, which is a bit more challenging. For this, we use again Cauchy's theorem, going first to the rest-frame of the $N\sigma$-system, i.e. $p = (E, \vec{0})$.

We expand then the propagator of the σ-dimer into a geometric series

$$\begin{aligned}
\Sigma_{N\sigma}(E) &= -\frac{f_4^2}{\alpha_\sigma M_\sigma^2}\int\frac{d^4k}{(2\pi)^4 i}\frac{1}{2\omega_N(\vec{k})\left[k_0-(E-\omega_N(\vec{k})+i\epsilon)\right]} \\
&\quad\times\left\{1-\frac{2h_2^2}{\alpha_\sigma M_\sigma^2}\int\frac{d^3l}{(2\pi)^3}\frac{1}{4\omega_\pi(\vec{k}-\vec{l})\omega_\pi(\vec{l})\left[k_0-(\omega_\pi(\vec{k}-\vec{l})+\omega_\pi(\vec{l})-i\epsilon)\right]}\right\}^{-1} \\
&= -\frac{f_4^2}{\alpha_\sigma M_\sigma^2}\int\frac{d^4k}{(2\pi)^4 i}\frac{1}{2\omega_N(\vec{k})\left[k_0-(E-\omega_N(\vec{k})+i\epsilon)\right]} \\
&\quad\times\left\{1+\frac{2h_2^2}{\alpha_\sigma M_\sigma^2}\int\frac{d^3l}{(2\pi)^3}\frac{1}{4\omega_\pi(\vec{k}-\vec{l})\omega_\pi(\vec{l})\left[k_0-(\omega_\pi(\vec{k}-\vec{l})+\omega_\pi(\vec{l})-i\epsilon)\right]}\right. \\
&\qquad+\left(\frac{2h_2^2}{\alpha_\sigma M_\sigma^2}\right)^2\left[\int\frac{d^3l}{(2\pi)^3}\frac{1}{4\omega_\pi(\vec{k}-\vec{l})\omega_\pi(\vec{l})\left[k_0-(\omega_\pi(\vec{k}-\vec{l})+\omega_\pi(\vec{l})-i\epsilon)\right]}\right]^2 \\
&\qquad+\left(\frac{2h_2^2}{\alpha_\sigma M_\sigma^2}\right)^3\left[\int\frac{d^3l}{(2\pi)^3}\frac{1}{4\omega_\pi(\vec{k}-\vec{l})\omega_\pi(\vec{l})\left[k_0-(\omega_\pi(\vec{k}-\vec{l})+\omega_\pi(\vec{l})-i\epsilon)\right]}\right]^3 \\
&\qquad\left.+\ldots\right\}.
\end{aligned} \tag{4.60}$$

Note that we rewrote the denominators containing the k_0 integration variable to better exhibit the pole structure of the expression. The nucleon propagator has a pole in the upper complex plane ($k_0 \in \mathbb{C}$), whereas all propagators appearing in the geometric series have their pole in the lower plane. We choose the pole of the nucleon propagator and close the contour around the upper half of the complex plane. The first appearing k_0-integral is the already discussed tadpole diagram

$$\mathcal{I}_0 = \int_{-\infty}^{+\infty}\frac{dk_0}{2\pi i}\frac{1}{\left[k_0-(E-\omega_N(\vec{k})+i\epsilon)\right]}\,, \tag{4.61}$$

which we replace with its residue in the upper complex plane, i.e. $\mathcal{I}_0 = 1$, according to our arguments from section 4.4. The next integrals can be summarized by the following expression

$$\begin{aligned}
\mathcal{I}_n = \int_{-\infty}^{+\infty}\frac{dk_0}{2\pi i}&\frac{1}{\left[k_0-(E-\omega_N(\vec{k})+i\epsilon)\right]} \\
&\times\left[\int\frac{d^3l}{(2\pi)^3}\frac{1}{4\omega_\pi(\vec{k}-\vec{l})\omega_\pi(\vec{l})\left[k_0-(\omega_\pi(\vec{k}-\vec{l})+\omega_\pi(\vec{l})-i\epsilon)\right]}\right]^n,
\end{aligned} \tag{4.62}$$

where n is a positive integer fulfilling $n \geq 1$. For $n = 1$ we obtain a similar k_0-integral as in $J_{N\pi}$ from Eq. (4.20), which can be evaluated analogously. Choosing the contour around the upper pole we

obtain

$$\mathcal{I}_1 = \int \frac{d^3l}{(2\pi)^3} \frac{1}{4\omega_\pi(\vec{k}-\vec{l})\omega_\pi(\vec{l})\big[E-\omega_N(\vec{k})-\omega_\pi(\vec{k}-\vec{l})-\omega_\pi(\vec{l})+i\epsilon\big]} \,. \tag{4.63}$$

If $n > 1$, the integral looks more complicated, however, there is still just one pole in the upper complex plane resulting in a single residue. We can therefore deduce that

$$\mathcal{I}_n = \left[\int \frac{d^3l}{(2\pi)^3} \frac{1}{4\omega_\pi(\vec{k}-\vec{l})\omega_\pi(\vec{l})\big[E-\omega_N(\vec{k})-\omega_\pi(\vec{k}-\vec{l})-\omega_\pi(\vec{l})+i\epsilon\big]}\right]^n \,. \tag{4.64}$$

Using these results, the self-energy is given by

$$\begin{aligned}\Sigma_{N\sigma}(E) = &-\frac{f_4^2}{\alpha_\sigma M_\sigma^2}\int \frac{d^3k}{(2\pi)^3}\frac{1}{2\omega_N(\vec{k})} \\ &\times\left\{1+\frac{2h_2^2}{\alpha_\sigma M_\sigma^2}\int\frac{d^3l}{(2\pi)^3}\frac{1}{4\omega_\pi(\vec{k}-\vec{l})\omega_\pi(\vec{l})\big[E-\omega_N(\vec{k})-\omega_\pi(\vec{k}-\vec{l})-\omega_\pi(\vec{l})+i\epsilon\big]}\right. \\ &+\left(\frac{2h_2^2}{\alpha_\sigma M_\sigma^2}\right)^2\left[\int\frac{d^3l}{(2\pi)^3}\frac{1}{4\omega_\pi(\vec{k}-\vec{l})\omega_\pi(\vec{l})\big[E-\omega_N(\vec{k})-\omega_\pi(\vec{k}-\vec{l})-\omega_\pi(\vec{l})+i\epsilon\big]}\right]^2 \\ &\left.+\ldots\right\},\end{aligned} \tag{4.65}$$

which is again a geometric series that can be summed up to

$$\begin{aligned}\Sigma_{N\sigma}(E) = -f_4^2\int\frac{d^3k}{(2\pi)^3}\frac{1}{2\omega_N(\vec{k})}\Bigg\{&\alpha_\sigma M_\sigma^2 \\ &+2h_2^2\int\frac{d^3l}{(2\pi)^3}\frac{1}{4\omega_\pi(\vec{k}-\vec{l})\omega_\pi(\vec{l})\big[\omega_N(\vec{k})+\omega_\pi(\vec{k}-\vec{l})+\omega_\pi(\vec{l})-E-i\epsilon\big]}\Bigg\}^{-1}.\end{aligned} \tag{4.66}$$

This remaining expression for the $N\sigma$ self-energy now contains only the spatial integration over an internal loop momentum $\vec{l}$ and an external momentum $\vec{k}$, which is a useful starting point for a numerical evaluation. The integral in the denominator of the latter equation produces poles, when the rest-frame energy E equals the energy of a free nucleon and two pions

$$E = \omega_N(\vec{k})+\omega_\pi(\vec{k}-\vec{l})+\omega_\pi(\vec{l}) \,. \tag{4.67}$$

In other words, we encounter exactly the three particle on-shell configuration $N\pi\pi$ that is crucial to describe the dynamics of the Roper system. We can analyze the result in Eq. (4.66) a little further and see what happens, when the σ-dimer becomes stable. In this case, we assume that $h_2 \to 0$, which leads to a vanishing integral over the internal momentum $\vec{l}$, so that the dimer propagator becomes

constant, i.e.

$$\Sigma_{N\sigma}(E) = -\frac{f_4^2}{\alpha_\sigma M_\sigma^2}\int \frac{d^3k}{(2\pi)^3}\frac{1}{2\omega_N(\vec{k})} = -\frac{f_4^2}{2\alpha_\sigma M_\sigma^2}\int \frac{d^3k}{(2\pi)^3}\frac{1}{\sqrt{|\vec{k}|^2+m_N^2}}\,, \tag{4.68}$$

which is a regular integral and vanishes in dimensional regularization. This we have already observed in section 4.4 and, hence, agrees with our expectation.
A similar calculation can also be performed for the Δ-dimer case. Its self-energy contribution to the Roper with the dressed dimer propagator is given by

$$\begin{aligned}\Sigma_{\Delta\pi}(p) &= f_3^2\int \frac{d^4k}{(2\pi)^4 i} S_\pi(p-k)\, D_\Delta(k) \\ &= -f_3^2\int \frac{d^4k}{(2\pi)^4 i}\frac{1}{2\omega_\pi(\vec{p}-\vec{k})\big[\omega_\pi(\vec{p}-\vec{k})-(p_0-k_0)-i\epsilon\big]}\,\frac{1}{\alpha_\Delta m_\Delta^2+\Sigma_\Delta(k)}\,,\end{aligned} \tag{4.69}$$

and after integrating out the k_0 component we arrive at

$$\begin{aligned}\Sigma_{\Delta\pi}(E) = -f_3^2\int \frac{d^3k}{(2\pi)^3}\frac{1}{2\omega_\pi(\vec{k})}\Bigg\{&\alpha_\Delta m_\Delta^2 \\ &+ g_2^2\int \frac{d^3l}{(2\pi)^3}\frac{1}{4\omega_\pi(\vec{k}-\vec{l})\omega_N(\vec{l})\big[\omega_\pi(\vec{k})+\omega_\pi(\vec{k}-\vec{l})+\omega_N(\vec{l})-E-i\epsilon\big]}\Bigg\}^{-1}.\end{aligned} \tag{4.70}$$

This result looks similar to Eq. (4.66), only the LECs differ. Both dimer field self-energy contributions to the Roper resonance mass will be investigated next. From here on, however, we will work in a finite volume, which is explored in the next section.

4.7 Finite-volume formalism

In this section, we consider the Roper resonance in a finite volume (FV) and introduce the corresponding formalism. Since lattice QCD calculations are performed on a space-time lattice of finite size, the system under investigation is always confined in a finite volume, which limits its spacial (and time) extent. The finite volume influences the particle system and leads to so-called finite-volume effects. We now place the Roper resonance system in a cubic box of length L and calculate the finite-volume energy eigenvalues (in the following referred to as 'energy levels'). This allows us to compare the energy levels from our effective approach with lattice QCD spectra of the Roper. Note that for simplicity we keep the time direction continuous.
In a finite volume the loop integral of the spatial momenta is replaced by an infinite, three-dimensional sum while the integration over the time component remains unchanged

$$\int \frac{d^3k}{(2\pi)^3}(\ldots) \mapsto \frac{1}{L^3}\sum_{\vec{k}}(\ldots) \qquad \text{for} \quad \vec{k} = \frac{2\pi}{L}\vec{n}\,, \quad \vec{n}\in\mathbb{Z}^3\,. \tag{4.71}$$

These changes naturally influence the self-energy of the Roper resonance as well. In particular, the poles of the FV Roper-propagator arise when

$$2\omega_R(\vec{p})\left[\omega_R(\vec{p}) - p_0\right] - \Sigma_R^L(p_0, \vec{p}) = 0\,, \tag{4.72}$$

where $\Sigma_R^L(p_0, \vec{p})$ denotes the self-energy of the Roper in the finite box. Choosing again the rest-frame, $p_0 = E$ and $\vec{p} = 0$, we can reformulate Eq. (4.72) so that we obtain an equation for the energy levels in the finite volume. We find

$$2m_{R0}\left(m_{R0} - E\right) = \Sigma_R^L(E) \quad \Leftrightarrow \quad m_{R0} - E = \frac{1}{2m_{R0}}\Sigma_R^L(E)\,, \tag{4.73}$$

which is the master equation for the finite-volume energy levels of the Roper resonance in this framework. A remaining problem is the appearance of the bare mass m_{R0} in the equation. However, for the numerical calculation of the energy levels we set the bare mass equal to the physical mass m_R. After this, one arrives at

$$m_R - E - \frac{1}{2m_R}\Sigma_R^L(E) = 0\,, \tag{4.74}$$

which is the equation we will work with. Note that this self-energy equation shares similarities with the usual three-body quantization conditions [28, 42, 154], e.g. by accounting for three-particle on-shell configurations, see Eq. (4.67).

Next, we have to determine the exact form of $\Sigma_R^L(E)$. As we have seen in Eq. (4.17), the Roper self-energy consists of three contributions, which is also true in the finite volume,

$$\Sigma_R^L(E) = \Sigma_{N\pi}^L(E) + \Sigma_{N\sigma}^L(E) + \Sigma_{\Delta\pi}^L(E)\,. \tag{4.75}$$

Let us start with $\Sigma_{N\pi}^L(E)$, which is given by

$$\Sigma_{N\pi}^L(E) = f_2^2 J_{N\pi}^L(E)\,, \tag{4.76}$$

where $J_{N\pi}^L$ is the finite-volume version of integral $J_{N\pi}$ from Eq. (4.20). We have seen in the discussion of Eq. (4.20), that the first step is integrating over the time component of the momentum. One then arrives at Eq. (4.22) and the spatial integral is now replaced by a sum leading to

$$J_{N\pi}^L(E) = \frac{1}{L^3}\sum_{\vec{k}} \frac{1}{4\omega_N(\vec{k})\omega_\pi(\vec{k})\left[\omega_N(\vec{k}) + \omega_\pi(\vec{k}) - E\right]}\,, \tag{4.77}$$

in the rest-frame. We expand the integrand again according to Eq. (4.25) and get

$$J_{N\pi}^L(E) = \frac{1}{L^3}\sum_{\vec{k}} \frac{1}{2E}\frac{1}{|\vec{k}|^2 - q^2(E)} + \dots\,, \tag{4.78}$$

where the ellipses denote the remaining regular terms. These terms, as we have observed, vanish in the infinite volume and lead to contributions proportional to $\exp(-M_\pi L)$ in the finite volume. The

latter effects are sub-leading to the other effects discussed here and are neglected in what follows. Thus, analogous to the infinite-volume case, also in the finite volume only the term containing the pole survives. Using Eq. (4.71), we can write

$$J^L_{N\pi}(E) = \frac{1}{8\pi EL}\sum_{\vec{n}}\frac{1}{|\vec{n}|^2 - \tilde{q}^2(E)} = \frac{1}{4\pi^{3/2}EL}\mathcal{Z}_{00}\left(1,\tilde{q}^2(E)\right)\,, \tag{4.79}$$

where we rescaled the variable $q(E)$ as $\tilde{q}^2(E) = L^2q^2(E)/(2\pi)^2$ and used the standard Lüscher Zeta-function [26]. The finite-volume expression for the $N\pi$ contribution is then given by

$$\Sigma^L_{N\pi}(E) = \frac{f_2^2}{4\pi^{3/2}EL}\mathcal{Z}_{00}\left(1,\tilde{q}^2(E)\right)\,. \tag{4.80}$$

Now, we turn to the self-energy contribution with the nucleon and σ-dimer field, $\Sigma^L_{N\sigma}$. For this, we take the result from Eq. (4.66) and replace the integrals by sums

$$\begin{aligned}\Sigma^L_{N\sigma}(E) = -\frac{f_4^2}{L^3}\sum_{\vec{k}}\frac{1}{2\omega_N(\vec{k})}\Bigg\{&\alpha_\sigma M_\sigma^2\\ &+\frac{2h_2^2}{L^3}\sum_{\vec{l}}\frac{1}{4\omega_\pi(\vec{k}-\vec{l})\omega_\pi(\vec{l})\left[\omega_N(\vec{k})+\omega_\pi(\vec{k}-\vec{l})+\omega_\pi(\vec{l})-E-i\epsilon\right]}\Bigg\}^{-1}\,.\end{aligned} \tag{4.81}$$

Analogously, the finite-volume contribution with pion and Δ-dimer field has the form

$$\begin{aligned}\Sigma^L_{\Delta\pi}(E) = -\frac{f_3^2}{L^3}\sum_{\vec{k}}\frac{1}{2\omega_\pi(\vec{k})}\Bigg\{&\alpha_\Delta m_\Delta^2\\ &+\frac{g_2^2}{L^3}\sum_{\vec{l}}\frac{1}{4\omega_\pi(\vec{k}-\vec{l})\omega_N(\vec{l})\left[\omega_\pi(\vec{k})+\omega_\pi(\vec{k}-\vec{l})+\omega_N(\vec{l})-E-i\epsilon\right]}\Bigg\}^{-1}\,.\end{aligned} \tag{4.82}$$

These two expressions can readily be worked out numerically, however, a cutoff is naturally required to tame the otherwise infinite sums. In our calculations, the outer sum runs to $L|\vec{k}|/(2\pi) \approx 3$ to ensure a similar energy coverage as in Ref. [86]. The inner momentum is carried out until $L|\vec{l}|/(2\pi) \approx 10$, so that $|\vec{l}| > |\vec{k}|$ is fulfilled. With these results we can now calculate the energy levels of the Roper resonance numerically.

4.8 Numerical calculation

The energy spectrum of the Roper resonance system is determined by numerically finding solutions of

$$m_R - E = \frac{1}{2m_R}\left(\Sigma^L_{N\pi}(E) + \Sigma^L_{N\sigma}(E) + \Sigma^L_{\Delta\pi}(E)\right)\,, \tag{4.83}$$

with respect to $E \in \mathbb{R}$. Here $\Sigma^L_{N\pi}$, $\Sigma^L_{N\sigma}$ and $\Sigma^L_{\Delta\pi}(E)$ are given in Eqs. (4.80), (4.81) and (4.82), respectively. Note that during the derivation of Eq. (4.83), we have seen that certain contributions decrease exponentially for large L, which we already neglected. We therefore have to choose L large enough to justify these approximations. An avoided level crossing in the energy spectrum is expected around the Roper resonance mass.

For the hadron masses we use the numerical values from Ref. [22] and the PDG [13]. Specifically, the Roper resonance mass is $m_R = 1365\,\text{MeV}$, the pion mass in the isospin-limit is set to $M_\pi = 139\,\text{MeV}$ and the nucleon mass is $m_N = 939\,\text{MeV}$. To fix the LECs $\{f_2, f_3, f_4, g_2, h_2\}$, we need further observables. The self-energy $\Sigma_{N\pi}$, for example, is proportional to the LEC f_2, see Eq. (4.30). This constant is connected to the decay of the Roper resonance into a nucleon and a pion. According to the PDG [13] the width of the Roper is $\Gamma_R = 190\,\text{MeV}$, where the decay into a nucleon and a pion contributes to (approximately) 65%, i.e. $\Gamma_{R\to N\pi} = 123.5\,\text{MeV}$. The other 35% contribute to the decay with two pions in the final state, $\Gamma_{R\to N\pi\pi} = 66.5\,\text{MeV}$. However, this final state can be reached by the different intermediate $N\sigma$ or $\Delta\pi$ states. The decay widths into these unstable intermediate states are approximately $\Gamma_{R\to N\sigma} = 38\,\text{MeV}$ and $\Gamma_{R\to\Delta\pi} = 28.5\,\text{MeV}$ [13]. We can use these decay widths to fit some of the LECs, like f_2. From Eq. (4.16), we know that the width is connected to the imaginary part of the self-energy. We find

$$\Gamma_{R\to N\pi} \approx \frac{1}{m_R}\text{Im}\left\{\Sigma_{N\pi}(E)\right\}\Big|_{E=m_R} = \frac{1}{m_R}\text{Im}\left\{\Sigma_{N\pi}(m_R)\right\}\,, \tag{4.84}$$

where $\Sigma_{N\pi}(m_R)$ consists solely of known parameters, except f_2. Using the PDG estimate for $\Gamma_{R\to N\pi}$, we find

$$\Gamma_{R\to N\pi} = 7.24\times 10^{-3} f_2^2\,\text{GeV}^{-1} \;\Leftrightarrow\; f_2 = \pm 4.13\,\text{GeV}\,. \tag{4.85}$$

The sign of f_2 cannot be determined through this procedure, but this does not matter for our further analysis. The matter becomes more complicated when looking at the self-energy contributions including dimer fields. The self-energy $\Sigma_{N\sigma}$, for example, contains three parameters h_2, M_σ and f_4 that have to be determined. We set M_σ to the physical mass of the $f_0(500)$, since this scale appears in the σ-dimer propagator. The PDG [13] estimates for the $f_0(500)$ are $M_\sigma = (400-550)\,\text{MeV}$ and $\Gamma_\sigma = (400-700)\,\text{MeV}$. For simplicity we take the lower values, assuming $M_\sigma = 400\,\text{MeV}$, which also fulfills $(M_\sigma + m_N) < m_R$, and $\Gamma_\sigma = 400\,\text{MeV}$. For the self-energy contribution from the Δ-dimer, $\Sigma_{\Delta\pi}$, the unknown LECs are g_2 and f_3, and we also set m_Δ to the physical delta mass. The mass and width of the delta resonance have been more accurately determined, and we set them here to $m_\Delta = 1210\,\text{MeV}$ and $\Gamma_\Delta = 100\,\text{MeV}$.

Using these phenomenological values we determine the unknown constants as follows. We begin with an estimate for the constants f_3 and f_4. Assuming that σ and Δ are stable final states with the same kinematic behaviour as the nucleons and pions, their self-energy contributions to the Roper resonance mass are given by

$$\Sigma^{\text{stable}}_{N\sigma}(E) = \frac{i f_4^2}{16\pi E^2}\lambda^{1/2}\left(E^2, m_N^2, M_\sigma^2\right)\,, \quad \text{and} \quad \Sigma^{\text{stable}}_{\Delta\pi}(E) = \frac{i f_3^2}{16\pi E^2}\lambda^{1/2}\left(E^2, m_\Delta^2, M_\pi^2\right)\,. \tag{4.86}$$

Taking $\Sigma_{N\sigma}^{\text{stable}}$, for example, we can approximate the decay width of Roper going to a $N\sigma$ final state by

$$\Gamma_{R\to N\sigma} \approx \frac{1}{m_R}\text{Im}\left\{\Sigma_{N\sigma}^{\text{stable}}(E)\right\}\Big|_{E=m_R} = \frac{f_4^2}{16\pi m_R^3}\lambda^{1/2}\left(m_R^2, m_N^2, M_\sigma^2\right) . \tag{4.87}$$

Using our values for the decay width and masses, one arrives at $f_4 = \pm 3.82\,\text{GeV}$. An analogous calculation with $\Sigma_{\Delta\pi}^{\text{stable}}$ leads to $f_3 = \pm 4.55\,\text{GeV}$, meaning that within this approximation f_3 and f_4 are of the same magnitude. In the future, one might also consider lattice QCD data to determine the numerical values for these constants, but, for now, we use the above estimations.
Next, we consider the LECs h_2 and g_2. As already stated in section 4.5, these constants can be related to the two-particle scattering lengths. For h_2, we found the relation given in Eq. (4.47). Using the σ mass, $\alpha_\sigma = -1$ for an attractive interaction and the value $a^{I=0}M_\pi = 0.222$ for the $\pi\pi$-scattering length, we obtain

$$h_2^2 = 8\pi M_\sigma^2 (a^{I=0}M_\pi) \quad \Rightarrow \quad h_2 = \pm 0.95\,\text{GeV} . \tag{4.88}$$

Now, we take a look what happens if we use the decay width to fix h_2. With Eq. (4.49) and the PDG [13] data above, we find

$$h_2^2 = \frac{8\pi M_\sigma^3 \Gamma_\sigma}{\lambda^{1/2}\left(M_\sigma^2, M_\pi^2, M_\pi^2\right)} \quad \Rightarrow \quad h_2 = \pm 2.36\,\text{GeV} , \tag{4.89}$$

which is interestingly of the same order of magnitude albeit around two times larger than the prediction from the scattering length. As of the coupling g_2, we use the πN-scattering length, $a_{\pi N}^{I=3/2}M_\pi = -0.086$ with the delta resonance mass, $\alpha_\Delta = +1$ and the help of Eq. (4.55). This yields

$$g_2^2 = -8\pi\alpha_\Delta m_\Delta^2 (m_N^2 + M_\pi^2) a_{N\pi}^{I=3/2} \quad \Rightarrow \quad g_2 = \pm 4.96\,\text{GeV} , \tag{4.90}$$

whereas using Eq. (4.56) and the above value for Γ_Δ leads to

$$g_2^2 = \frac{16\pi m_\Delta^3 \Gamma_\Delta}{\lambda^{1/2}\left(m_\Delta^2, m_N^2, M_\pi^2\right)} \quad \Rightarrow \quad g_2 = \pm 4.22\,\text{GeV} . \tag{4.91}$$

We see that in the Δ case both ways to fix the LEC g_2 lead to approximately the same value. This might be related to the fact that the delta resonance has a Breit-Wigner shape to very good accuracy. It is good to see that the particle-dimer approach is consistent with this by giving g_2 almost equally from the scattering length and the decay width.

Before turning to the prediction of the Roper finite-volume spectrum, we try to test the quality of the dimer LECs determination presented above. For this we turn to the σ-dimer, and concentrate solely on the two-particle $\pi\pi$ final state. In the finite volume, the σ-dimer propagator is given by

$$D_\sigma(E) = -\frac{1}{\alpha_\sigma M_\sigma^2 + \Sigma_\sigma^L(E)} , \quad \text{with} \quad \Sigma_\sigma^L(E) = \frac{2h_2^2}{L^3}\sum_{\vec{k}} \frac{1}{4\omega_\pi(\vec{k})\omega_\pi(\vec{k})\left[2\omega_\pi(\vec{k}) - E\right]} , \tag{4.92}$$

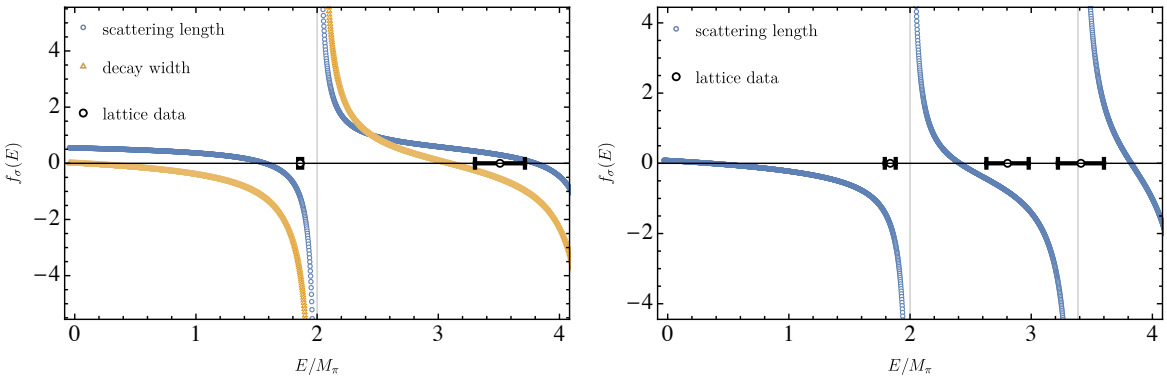

Figure 4.2: Predicted energy levels (zeroes of $f_\sigma(E)$) of the $\pi\pi$-system within the σ-dimer approach using Set 1 (4.94) (left panel) and 2 (4.95) (right panel). The blue curves show the function $f_\sigma(E)$ with h_2 determined from the two scattering lengths $a^{I=0}M_\pi$ in each data set and the orange curve shows $f_\sigma(E)$ with h_2 determined from the decay width Γ_σ (only for Set 1). Black circles display the lattice results with errors from Ref. [106] and the grey vertical lines the non-interacting $\pi\pi$ energy eigenvalues.

where we again restricted ourselves to the rest-frame ($p_0 = E, \vec{p} = 0$). The poles of the propagator in Eq. (4.92) correspond to the interacting finite-volume energy levels of the $\pi\pi$ system, i.e.

$$f_\sigma(E) := 1 + \frac{1}{\alpha_\sigma M_\sigma^2}\Sigma_\sigma^L(E) \stackrel{!}{=} 0 \,. \tag{4.93}$$

Using this formula we can compare the energy levels from the particle-dimer picture with lattice QCD results. Before going to this we wish to remark that the latter condition is related to the well established Lüscher's method [25, 26]. This can be seen by using a similar decomposition as shown in Eq. (4.25) of the integrand in (4.92). In this pilot study of the proposed formalism, we stay with the condition (4.93) leaving a more quantitative discussion to future studies. Lattice studies on the σ resonance have already been performed, see e.g. Refs. [172, 180–183]. Here we consider results of the combined $I = 0, 1, 2$ finite-volume analysis [106] of GWQCD lattice results [172, 184, 185] obtained at two values of pion mass. For both cases the $\pi\pi$ scattering length $a^{I=0}$, the σ mass M_σ and the width Γ_σ have been determined

$$\begin{aligned} \text{Set 1}: \; & M_\pi = 0.224\,\text{GeV}\,, \;\; M_\pi L = 3.3\,, \\ & M_\sigma = 0.502\,\text{GeV}\,, \;\; \Gamma_\sigma = 0.350\,\text{GeV}\,, \;\; a^{I=0}M_\pi = 0.699\,, \end{aligned} \tag{4.94}$$

$$\begin{aligned} \text{Set 2}: \; & M_\pi = 0.315\,\text{GeV}\,, \;\; M_\pi L = 4.6\,, \\ & M_\sigma = 0.591\,\text{GeV}\,, \;\; \Gamma_\sigma = 0.218\,\text{GeV}\,, \;\; a^{I=0}M_\pi = 1.901\,. \end{aligned} \tag{4.95}$$

We now take each data set and calculate the LEC h_2 from the scattering length $a^{I=0}M_\pi$ and width Γ_σ. For Set 1, we obtain $h_2 = 2.10\,\text{GeV}$ using the scattering length and Eq. (4.47), and $h_2 = 3.13\,\text{GeV}$ using the width and Eq. (4.49). For Set 2, the scattering length leads to $h_2 = 4.08\,\text{GeV}$, while Eq. (4.49) cannot be used. This is because of the large pion mass $M_\pi = 0.315\,\text{GeV}$ preventing the decay of the σ meson into two pions. In principal, one could test the above procedure even further by using more

lattice QCD data on the σ meson for various pion masses from different working groups. However, this would go beyond the scope of this work and especially well beyond this qualitative check-up of the numerical estimation of the dimer LECs. A comparison of those data within our framework could be dedicated to future works. The predicted two-body finite-volume spectrum for both data sets is depicted in Fig. 4.2. Therein, the left panel of Fig. 4.2 shows the function $f_\sigma(E)$ for data set 1 with h_2 fixed by the scattering length (blue pionts) and by the decay width (orange pionts). The zeros of this function show the energy levels for this two-pion system. The black circles are the lattice QCD results from Ref. [106]. We observe that the levels from the blue curve lie very close to the lattice results. The orange curve, on the other hand, still reproduces the first excited level above the two-pion threshold at $\approx 1\sigma$, but the ground-state level is at odds with the lattice result. The zero for the ground state lies very close to $E/M_\pi \approx 0$. Since the driving term includes only momentum-independent structures we do not expect any predictive power from this formalism so far below threshold. Therefore, the constant h_2 fixed by the scattering length leads to a better reproduction of the lattice results. The right panel of Fig. 4.2 shows $f_\sigma(E)$ obtained with data set 2. Here, as stated before, we only have the result from the scattering length estimation. The lattice results are again depicted by the black circles. Overall, there is less agreement between the predicted levels and those from the lattice. The ground-state level lies again well below $E/M_\pi = 1$ and merely, the excited levels are somewhat close to the lattice QCD results. We emphasize again that the data from set 2 are determined by a pion mass much larger than set 1 and that the σ-meson mass is smaller than two pion masses, which forbids the decay of σ into two pions. This is a condition that we did not take into account in our theoretical framework and it might explain the large deviations between the dimer and lattice results.

There are two take-away messages from this analysis of the σ-dimer propagator and the corresponding $\pi\pi$ finite-volume spectrum: First, we have seen that the particle-dimer approach works better for smaller pion masses. This does not come as a surprise, since the dimer propagator is by construction a constant at leading order. Second, we have seen that for lower pion mass the $\pi\pi$ scattering length ensures a better description of the lattice QCD spectrum than the decay width of the σ meson. Hence, we will use the scattering length to fix the dimer LECs h_2 and g_2 for our calculation of the Roper resonance energy levels. Finally, we note that no fit to the lattice data and, also, no similar study for the two-particle $N\pi$ scattering in the Δ channel (some lattice studies of Δ-resonance can be found in Refs. [186–191]) are performed in this pioneering study.

4.9 Results

Now that numerical values of constants are determined, we proceed with the determination of energy levels of the Roper system for the three different channels $N\pi$, $N\sigma$ and $\Delta\pi$. After this, we also take a look at the coupled channel $N\pi/N\sigma$ and compare our obtained energy values with lattice QCD calculations. We note again that Δ and σ fields are allowed to decay to $N\pi$ and $\pi\pi$ channels, respectively. Thus, these states can simply be seen as auxiliary degrees of freedom accounting for different configurations of the $N\pi\pi$ system.

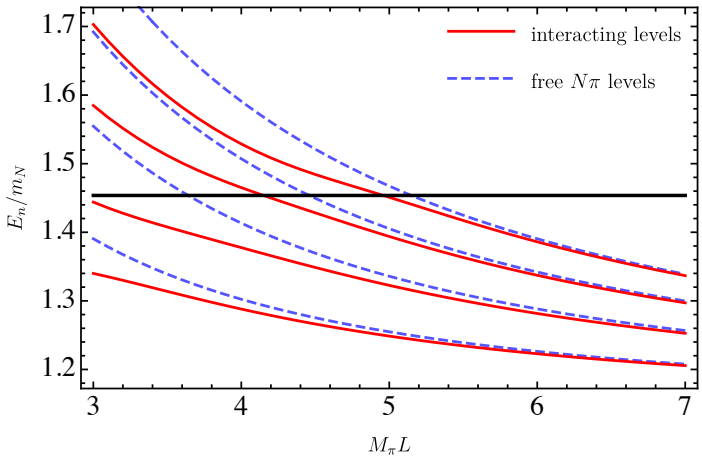

Figure 4.3: Energy levels for different box sizes L considering only pion and nucleon as intermediate states. The red solid lines display the numerical results for the interacting energy levels and the blue dashed lines the free (non-interacting) energy levels of the pion and nucleon for $|\vec{n}_{1,2}|^2 = 1, 2, 3, 4$ (lowest to highest curve). The thick solid black line marks the mass of the Roper resonance.

4.9.1 $N\pi$ channel

First of all, we perform a numerical calculation including only the $\Sigma_{N\pi}$ contribution. That means only pion and nucleon intermediate states are considered and we neglect the self-energy with the σ-dimer and Δ-dimer, i.e. we set $f_3 = f_4 = 0$ for now. The obtained levels can be compared with the results from Ref. [86], which serves as a test for the theoretical framework. The results are displayed in Fig. 4.3, where the energy is given in units of the nucleon mass m_N and the box length L is multiplied by the pion mass M_π to obtain a dimensionless quantity for the box size. The red solid lines denote the numerical results of E for the respective energy levels while the blue dashed lines denote the free energy levels of the pion-nucleon final states (also in units of m_N), i.e.

$$E_{\pi N}^{\text{free}}\left(\vec{n}_1, \vec{n}_2\right) = \sqrt{m_N^2 + \left(\frac{2\pi}{L}\right)^2 |\vec{n}_1|^2} + \sqrt{M_\pi^2 + \left(\frac{2\pi}{L}\right)^2 |\vec{n}_2|^2} \,. \tag{4.96}$$

Here, $\vec{n}_1$ and $\vec{n}_2$ are the discretized momenta of the nucleon and pion with $\vec{n}_1 + \vec{n}_2 = 0$. We restrict ourselves to the first four levels for simplicity. The thick solid black line corresponds to the real part of the Roper resonance mass, i.e. $m_R/m_N \approx 1.45$, which is from here on called the "critical value". We can see clear signs of avoided level crossing at small box sizes around the critical value, i.e. the energy levels switch from one free energy level to another, most notably between the free levels $|\vec{n}_{1,2}| = 3$ and $|\vec{n}_{1,2}| = 4$ in Fig. 4.3. Overall, Fig. 4.3 is in very good agreement with the result obtained in Ref. [86] (for more comparisons, see Ref. [43]). This is a noteworthy result considering that the present formalism is much simpler. In Ref. [86] the full Lagrangian from baryon chiral perturbation theory has been used including Lorentz-, spin- and isospin-structure. Slight deviations in the numerical results can be observed mostly for small values of $M_\pi L$ which is expected. However, the general similarity between the numerical results is striking, making us optimistic to proceed with this approach.

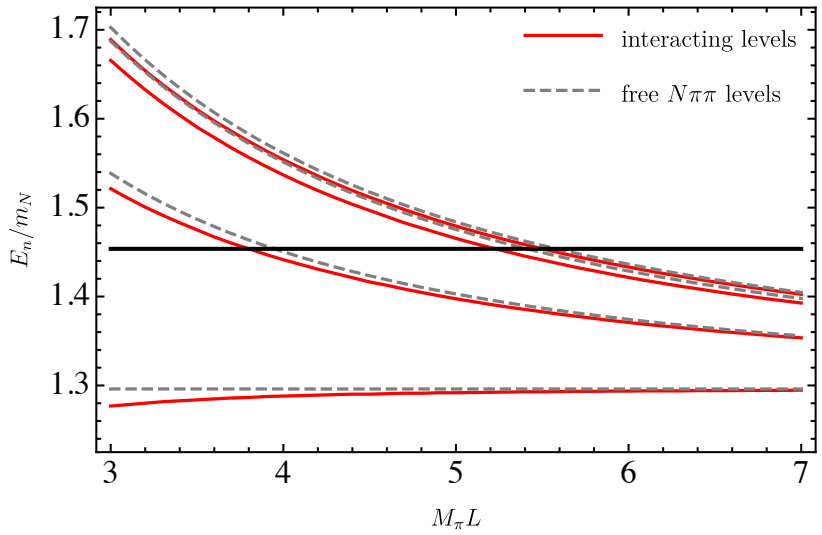

Figure 4.4: Roper energy levels for different box sizes L considering only nucleon and σ-dimer as intermediate states. Red solid lines display the numerical results for the interacting energy levels and grey dashed lines the free (non-interacting) lowest-lying three-particle $N\pi\pi$ energy levels. The thick solid black line marks the mass of the Roper resonance.

4.9.2 $N\sigma$ channel

Next, we include the dimer fields starting with the σ-dimer, which we studied in detail throughout this work. We set f_2 and f_3 to zero, leaving us with the self-energy $\Sigma_{N\sigma}$ only. The numerical results for the $N\sigma$ contribution are displayed in Fig. 4.4. In this system, the free, non-interacting three-particle $N\pi\pi$ energies are determined as

$$E^{\text{free}}_{\pi\pi N}\left(\vec{n}_1,\vec{n}_2,\vec{n}_3\right) = \sqrt{m_N^2+\left(\frac{2\pi}{L}\right)^2|\vec{n}_1|^2}+\sqrt{M_\pi^2+\left(\frac{2\pi}{L}\right)^2|\vec{n}_2|^2}+\sqrt{M_\pi^2+\left(\frac{2\pi}{L}\right)^2|\vec{n}_3|^2}\,. \tag{4.97}$$

There are, naturally, more free energy levels in this three-particle system, but some of them overlap with each other. Also, it should be noted that not all possible combinations of the free $N\pi\pi$ system have the quantum numbers of the Roper resonance $L_{2J2I} = P_{11}$. Since we did not include isospin, spin and angular momentum structures in our fundamental Lagrangian, we simply show all interacting energy levels that appear in our calculation. In Fig. 4.4 the lowest lying free $N\pi\pi$ levels $N(0)\pi(0)\pi(0)$ (the $N\pi\pi$ threshold), $N(1)\pi(1)\pi(0)$, $N(0)\pi(1)\pi(1)$, and $N(2)\pi(2)\pi(0)$ are shown. We observe that all our obtained energy levels lie very close to the non-interacting three-particle levels and converge to them for large box sizes, similar to the two-particle case from Fig. 4.3. The energy shift is negative caused by setting $\alpha_\sigma = -1$ for the σ-dimer field. We tested what happens in the case that $\alpha_\sigma = +1$ and, indeed, the interacting levels then approach the free levels from above. There are no clear signs of avoided level crossing near the critical value. Solely the behaviour of the energy level between the free levels $N(0)\pi(1)\pi(1)$ and $N(2)\pi(2)\pi(0)$ may be affected by avoided level crossing, being first closer to $N(0)\pi(1)\pi(1)$, but then approaching $N(2)\pi(2)\pi(0)$ for $M_\pi L > 5$. A possible explanation why no other signs of avoided level crossing are visible might be the fact that the interacting energy

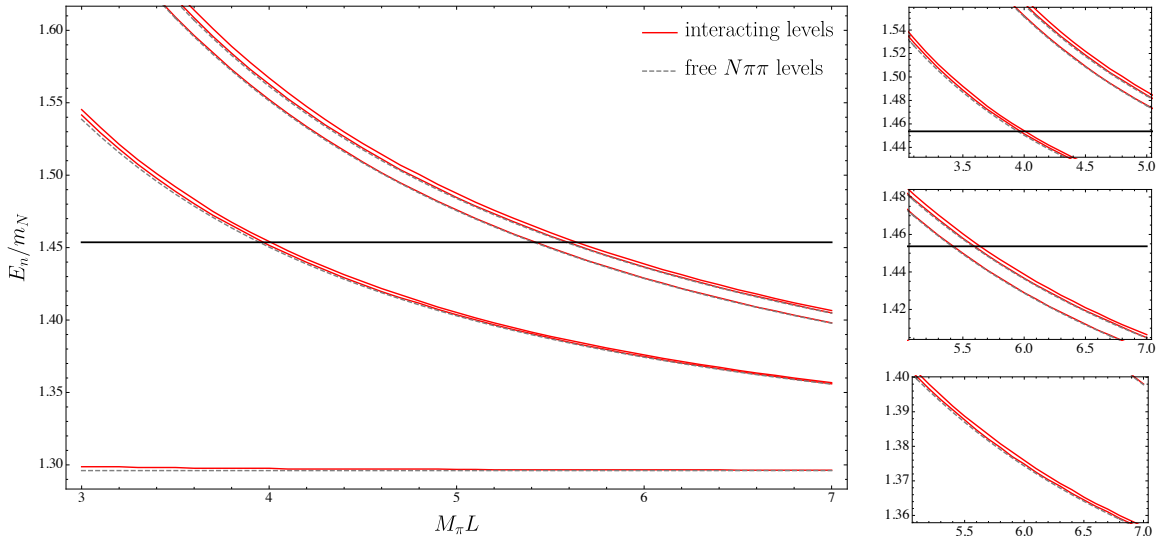

Figure 4.5: Energy levels for different box sizes L considering only pion and Δ-dimer as intermediate states. Red solid lines display the numerical results for the interacting energy levels and grey dashed lines the free (non-interacting) lowest-lying three-particle $N\pi\pi$ energy levels. The thick solid black line marks the mass of the Roper resonance. The small pictures on the right-hand side show more precisely the behaviour of the close lying energy levels.

levels lie too close to the free levels, which can mitigate the typical signature of avoided level crossing. We tested that an increase of the constants h_2 and f_4 within reasonable limits does not change this picture significantly. In future studies, one should reconsider the numerical estimates of all involved LECs, perhaps with the help of newly acquired lattice data.

4.9.3 $\Delta\pi$ channel

Now, we take a look at the second dimer-field, the Δ-dimer. Analogously to the cases before, we set the LECs f_2 and f_4 to zero, leaving us with the self-energy contribution $\Sigma_{\Delta\pi}$ only. The results are shown in Fig. 4.5. Like in the σ-dimer spectrum, the obtained energy levels lie very close to the non-interacting levels and asymptotically approach them for larger box sizes. This time the free levels are approached from above due to $\alpha_\Delta = +1$ and the distance between the interacting and non-interacting levels is overall much smaller than in the $N\sigma$ case. Also, in Fig. 4.5 there are no visible signs of avoided level crossing. Instead, another interesting effect appears in this spectrum: Above the free levels $N(1)\pi(1)\pi(0)$ and $N(2)\pi(2)\pi(0)$ there are two interacting energy levels visible, which lie very close, but do not cross each other when increasing $M_\pi L$, see the zoom-in in Fig. 4.5. Indeed, these energy levels belong to the same free energy eigenvalue, i.e. the lower energy double line belongs to $N(1)\pi(1)\pi(0)$ and the upper one to $N(2)\pi(2)\pi(0)$. We tested this by reducing the coupling g_2, which causes both double lines to move closer to their respective free energy levels and also decreases the splitting between the levels. The splitting of these interacting energy levels comes from the fact that in the $\Delta\pi$ system either a spectator pion or a pion within the Δ-dimer propagator ($\Delta \to \pi N \to \Delta$) can carry momentum away. Since both possibilities come with a different LEC, f_3

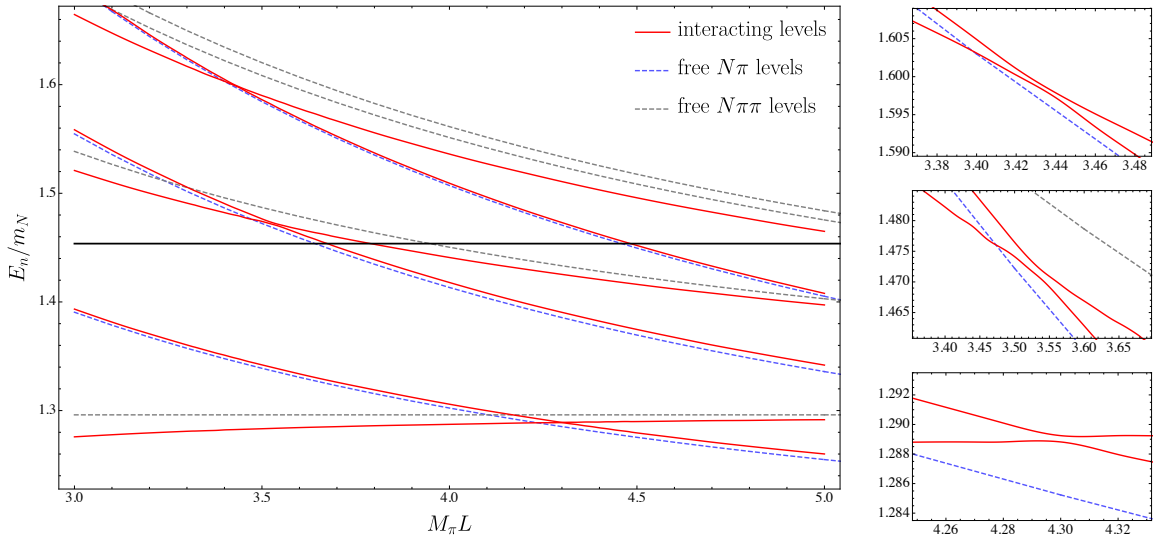

Figure 4.6: Energy levels for different box sizes L considering the coupled channel with $N\pi$ and $N\sigma$ self-energy contributions. Red lines display the numerical results for the interacting energy levels. Blue dashed and grey dashed lines show the non-interacting $N\pi$ and $N\pi\pi$ energy levels, respectively. The thick solid black line marks the mass of the Roper resonance. The small pictures on the right-hand side show the three critical points where the interacting energy levels come very close to each other.

or g_2, respectively, there is a small splitting between the levels. This also explains why we did not see such a splitting of the interacting levels in the $N\sigma$ spectrum. There, the nucleon is the spectator particle and the two pions interact with each other in the σ-dimer propagator, so that it does not matter which pion carries away the momentum. The question whether this splitting should be observed in a full coupled-channel ($\pi N/\Delta\pi/\sigma N$) calculation brings us to an interesting point. In particular, a coupled $\Delta\pi/\sigma N$ system allows for the appearance of a (pion) exchange diagram. These exchange diagrams enable transitions between Δ- and σ-dimer fields, which are important to fulfill unitarity. Such contributions, however, cannot be included at leading one-loop order in the self-energy, but enter at two-loop order. This issue is left out for a future work.

4.9.4 $N\pi/N\sigma$ coupled-channel

For our final analysis we take a look at a coupled $N\pi/N\sigma$ system. This means that we include both self-energy contributions at once in Eq. (4.83), neglecting only the $\pi\Delta$ ($f_3 = 0$) part for the reasons discussed before. The results of the coupled-channel energy levels are depicted in Fig. 4.6. We restricted ourselves to $M_\pi L \leq 5$, since many energy levels appear in this case, many of which lie too close to the non-interacting ones. Furthermore, we note that the free levels can naturally cross as a function of $M_\pi L$, see the grey lines in Fig. 4.6. However, a crossing of interacting levels would be in conflict with the hermiticity of the perturbation theory Hamiltonian [192]. Indeed, this does not occur as shown in the close-ups on the right-hand side of Fig. 4.6. Furthermore, we observe that the avoided level crossing signature of the two-particle $N\pi$ spectrum seen in Fig. 4.3 is now washed out in the coupled channel case, i.e. the interacting levels now lie much closer to the free energy levels

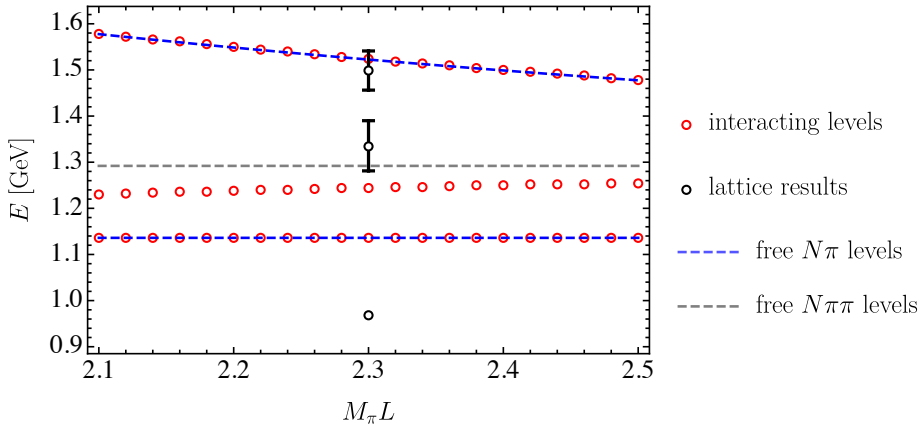

Figure 4.7: Comparison of the Roper resonance energy levels with lattice results using the $N\pi$ and $N\sigma$ self-energy contributions. Red circles display the numerical results for the interacting energy levels and black circles the lattice results with errors from Ref. [15]. Blue dashed and grey dashed lines show the non-interacting $N\pi$ and $N\pi\pi$ energy levels, respectively.

for small $M_\pi L$. This is probably caused by the large contribution from the double sum in the $N\sigma$ self-energy contribution, which gives the whole self-energy function an offset, that pushes the zeros of the function (interacting energy levels) closer to its poles (non-interacting energy levels).

4.9.5 Comparison to lattice QCD results

Lastly, we can test how our results compare to previously obtained lattice QCD results from Ref. [15]. Therein, the energy eigenvalues in the G_1^+ irreducible representation have been obtained in a box of length $M_\pi L = 2.3$ with a pion mass close to the physical point, i.e. $M_\pi = 156\,\text{MeV}$, and a nucleon mass of $m_N \approx 980\,\text{MeV}$, also slightly larger than the physical value. To ensure a better comparison with the lattice results, we use these values for M_π and m_N. The other masses and LECs in our calculation are not changed, i.e. we use the same estimates as described before in section 4.8. The comparison of our $N\pi/N\sigma$ coupled channel and the lattice results is shown in Fig. 4.7. We observe that the lattice QCD study found an energy level located at the nucleon mass, since the nucleon has the same quantum numbers as the Roper resonance. In our calculation, this nucleon energy level does not exist, because there is no self-energy contribution that produces a nucleon pole. Instead, our ground-state level is located at the $N\pi$ threshold which, however, does not have the correct quantum numbers. The $N\pi$ threshold has negative parity meaning that it cannot show up in the Roper channel. Still, since no projection to definite parity is done here, this state appears as the lowest level in the $N\pi$ self-energy contribution from Eq. (4.80). Note that in the baryon chiral perturbation theory framework of Ref. [86] the $N\pi$ threshold does not appear since the chiral effective Lagrangian with all the proper symmetries forbids this state. Hence, the appearance of this threshold can be seen as an artifact of our non-relativistic EFT approximation. Once our formalism here is extended to include more symmetries and structures from chiral effective Lagrangians, we expect that the $N\pi$ threshold does not enter the spectrum anymore. The next higher energy level is the $N\pi\pi$ threshold. Our prediction for the corresponding interacting energy level lies slightly below the threshold, whereas the lattice prediction lies just above it. The error of the

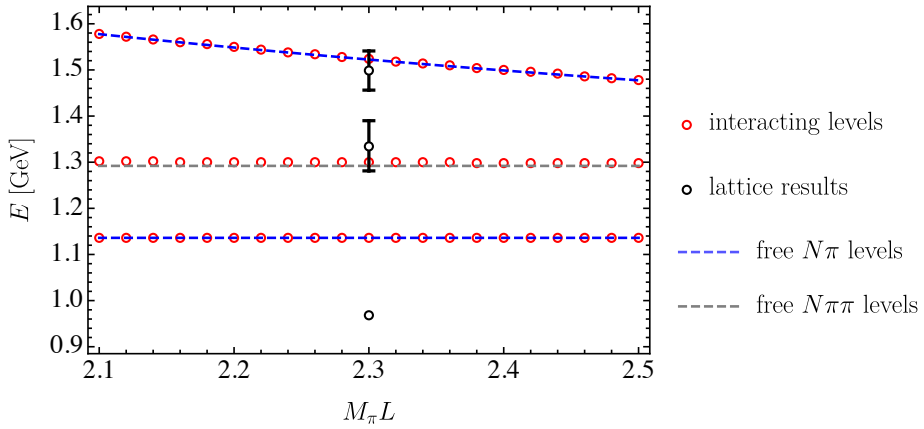

Figure 4.8: Comparison of the Roper resonance energy levels with lattice results using the $N\pi$ and $\Delta\pi$ self-energy contributions. Red circles display the numerical results for the interacting energy levels and black circles the lattice results with errors from Ref. [15]. Blue dashed and grey dashed lines show the non-interacting $N\pi$ and $N\pi\pi$ energy levels, respectively.

lattice result, however, is large enough to also allow a level below the threshold. The next observed level corresponds to the first momentum including free level, i.e. $N(1)\pi(1)$. Here, our prediction lies barely above the free level, but agrees with the lattice results within the 1σ uncertainty quoted there [15].

For completeness, we also consider the $N\pi/\Delta\pi$ coupled-channel for the comparison with the lattice results. Setting $f_4 = 0$ and turning on the Δ-dimer contribution, the finite-volume spectrum is obtained and depicted in Fig. 4.8. The spectra look almost identical to Fig. 4.7. We again include the $N\pi$ threshold in the figure according to our explanation from before. The only difference is that the prediction related to the $N\pi\pi$ threshold lies now slightly above the free level, which actually creates a better overlap with the lattice result but also makes our prediction more consistent with a non-interacting theory. However, more work is needed here to find a suitable way to include both Δ-dimer and σ-dimer fields in one coupled channel. Also, for both plots, Figs. 4.7 and 4.8, we emphasize that the box length is relatively small with $M_\pi L = 2.3$ meaning that exponentially suppressed contributions can still give sizeable corrections at this point. Some of these contributions have been neglected in our finite-volume approach, which can lead to further systematic uncertainties. Nevertheless, we see that even without fitting to the lattice energy eigenvalues and assuming that the other parameters (masses and LECs) do not change by increasing the pion and nucleon mass, our predictions agree well with the lowest-lying states of the lattice spectrum. More specifically, we observe that our highest energy-eigenvalue ($\sim$ 1.6 GeV) is barely shifted from the corresponding free-energy irrespectively to the inclusion of $N\sigma$ or $\Delta\pi$ fields. The next lower energy-eigenvalue is shifted down/up from the $N\pi\pi$ free-energy, respectively to the $\{N\pi, N\sigma\}$ or $\{N\pi, \Delta\pi\}$ cases. Neither of these cases can be preferred statistically from the currently available lattice QCD results. Still, the fact that the energy shift from the free energy has different signs when including $N\sigma$ or $\Delta\pi$ cases tells one that when higher precision lattice results are available we indeed have the chance to resolve interaction patterns of the Roper.

4.10 Summary and conclusions

In this paper, we have analyzed the finite-volume spectrum of the Roper resonance using a particle-dimer approach. We introduced a non-relativistic covariant Lagrangian with nucleons, pions and three dimer fields as degrees of freedom. These dimer fields are the Roper resonance itself, the σ-meson and the Δ-resonance. We then calculated the Roper self-energy within our framework to one-loop order. Furthermore, we analyzed the σ- and Δ-dimer fields and dressed their corresponding propagators to explicitly include three-particle dynamics. From then on, we restricted ourselves to a finite volume. We showed how the self-energy of the Roper resonance can be calculated in a finite volume and how to extract the interacting energy levels of the Roper system. Afterwards, we discussed methods to determine the appearing LECs that contribute to the self-energy corrections. Then, we calculated the finite-volume spectra of the Roper resonance for various cases. Our main findings are the following:

- In the $N\pi$ channel, avoided level crossing can clearly be observed around the Roper resonance mass. For large box sizes, the energy levels approach the free $N\pi$ energies. The spectrum agrees very well with our previous result in Ref. [86], using baryon chiral perturbation theory.
- Including the $N\sigma$ channel, with the σ dressed by the pertinent $\pi\pi$ loops, we were able to implement three-body ($N\pi\pi$) dynamics. While we checked that the two-body sub-system can reproduce the finite-volume spectrum for not too large pion masses, no clear signs of avoided level crossing could be observed in the three-body ($N\pi\pi$) spectrum. We observed similar behaviour for the $\Delta\pi$ channel.
- Uniting the $N\pi$ and $N\sigma$ contributions in a coupled-channel system, we observed that the interacting energy levels lie very close to their respective free $N\pi$ or $N\pi\pi$ levels. Strikingly, the obtained spectrum in our formalism showed an overall good agreement to the lattice QCD results [15] even without a fit to their energy eigenvalues.

In conclusion, we think that albeit very simple, the proposed alternative finite-volume formalism defines a new, systematically improvable pathway of extracting resonance proper-ties from finite-volume spectra. Moreover, already now the formalism shows that effects due to $N\sigma$ and $\Delta\pi$ channels can be decomposed once more precise lattice results are available. With that, the formalism provides already at this stage a valuable guidance on the required precision of the lattice QCD input. Systematical updates to the formalism include spin and isospin projections as well as inter-couplings between different particle-dimer channels via pion exchange diagrams, so that a full $N\pi/N\sigma/\Delta\pi$ coupled-channel system can be achieved. Work in this direction is planed.

Acknowledgemets

We thank A. Rusetsky and F. Müller for many useful discussions. This work is supported by the Deutsche Forschungsgemeinschaft (DFG, German Research Foundation), the NSFC through the funds provided to the Sino-German Collaborative Research Center CRC 110 “Symmetries and the Emergence of Structure in QCD” (DFG Project-ID 196253076 - TRR 110, NSFC Grant No. 12070131001). The work of UGM was further supported by VolkswagenStiftung (grant No. 93562) and by the Chinese Academy of Sciences (PIFI grant 2018DM0034). MM was further supported by the National Science Foundation under Grant No. PHY-2012289.

CHAPTER 5

Electric dipole moments of baryons with bottom quarks

5.1 Prologue

The content of this chapter including appendix C is based on the publication

- Y. Ünal, D. Severt, J. de Vries, C. Hanhart and U.-G. Meißner,
  "Electric dipole moments of baryons with bottom quarks",
  Phys. Rev. D **105**, no.5, 055026 (2022) [arXiv:2111.13000 [hep-ph]].

In this chapter, we move away from the Roper resonance and consider the second topic of this thesis: The electric dipole moments of heavy bottom baryons.
Triggered by experimental prospects to measure electromagnetic dipole moments of baryons containing a bottom quark, we calculate the CP-odd electric dipole moments (EDMs) of spin-$1/2$ single-bottom baryons in this chapter. We consider CP-violating dimension-six operators in the Standard Model effective field theory that involve bottom quarks, and apply heavy-baryon chiral perturbation theory to compute the EDMs of several baryons. We discuss the expected size of the EDMs for beyond-the-Standard Model physics appearing at the TeV scale (Ref. [193]).
The project started with an e-mail by J. de Vries to Y. Ünal and U.-G. Meißner, who had just finished a work on strong CP violation in spin-$1/2$ single-charm baryons [194]. In that, the QCD θ-term and its CP-violating consequences on c-baryons was considered. J. de Vries had the idea to consider dimension-six operators from Standard Model effective field theory (SMEFT) as the source of CP violation. He asked if one could construct a chiral effective Lagrangian for heavy b-baryons that includes the dimension-six SMEFT operators and calculate the induced electric dipole moment (EDM) of the Λ_b-baryon from it. Y. Ünal and U.-G. Meißner decided to take up this idea and started working on this project. After a few weeks, Y. Ünal asked the author of this thesis, who was her office colleague at the time, if he wants to join the project as well. The author agreed and the two began to look for the relevant SMEFT operators that needed to be considered to calculate the baryon EDMs.
The SMEFT operators in flavor $SU(2)$ were already discussed in [195]. However, when including the heavy b quark, also an extension to flavor $SU(3)$ should be considered. Together with Y. Ünal and J. de Vries the author helped to find the relevant dimension-six operators, which then should be used to construct a chiral effective Lagrangian for the bottom baryons. To create the chiral Lagrangian

that includes bottom baryons and octet mesons as degrees of freedom from a given Lagrangian at quark/gluon level is not a straightforward task. At this point C. Hanhart was invited to join the collaboration for helping to formulate the effective theory. Together with his collaborators the author of this thesis constructed the Lagrangian for the four different SMEFT operators. For this, the chiral transformation behaviour of the dimension-six terms had to be determined. Depending on the transformation properties, different chiral building blocks containing bottom baryons and meson fields were introduced and combined together in a way that all necessary symmetries are fulfilled (see e.g. [196]). This procedure was one of the major tasks of the project. After obtaining the newly constructed Lagrangian, the author of this thesis expressed the Lagrangian in the so-called heavy-baryon formulation (see e.g. [78, 79]), which simplified many of the appearing structures. Then, the EDMs of the bottom baryons were calculated. Since the Lagrangian includes all bottom baryons, i.e. the anti-symmetric triplet and the symmetric sextet, the idea came up to calculate the EDMs of all baryons and not just the Λ_b. Y. Ünal calculated the EDMs and the author of this thesis checked the results. J. de Vries analyzed the results further by looking at patterns inside the equations, which could be used to estimate relative sizes between the different EDMs. The main problem is that the equations for the baryon EDMs include a significant amount of low-energy constants (LECs), which are unkown. One way to estimate the order of magnitude of these LECs is naive dimensional analysis (NDA) [197, 198]. Together with Y. Ünal and J. de Vries, the author used the rules of NDA to connect the unknown LECs with physical constants and energy scales. Additionally, the author performed a Monte Carlo (MC) sampling to estimate the absolute sizes of the baryon EDMs numerically. All members of the collaboration hope that these findings can help to motivate future experiments aiming to measure the EDMs of heavy baryons.

5.2 Introduction

Experiments aiming to detect permanent electric dipole moments (EDMs) set strong bounds on flavor-diagonal mechanisms that simultaneously violate time-reversal (T) and parity (P) (and thus CP symmetry if we take CPT to be a good symmetry of nature). For instance, the strongest constraints on the QCD $\bar{\theta}$-term arise from measurements of the EDMs of the neutron and the ^{199}Hg atom [46, 199]. In addition, EDM experiments strongly constrain possible sources of CP violation from beyond-the-Standard-Model (BSM) physics. While EDMs have been calculated in a plethora of different BSM models, BSM CP violation can be described more systematically in the framework of the Standard Model Effective Field Theory (SMEFT) [45] under the reasonable assumption that the scale of BSM physics, Λ, lies well beyond the electroweak scale, $v \simeq 250\,\text{GeV}$.
A lot of effort has gone into more and more accurate calculations of EDMs of systems containing first-generation valence quarks such as nucleons, nuclei, atoms, and molecules [195, 200–203]. The associated experiments are mainly sensitive to CP-odd SMEFT operators containing light quarks (and leptons, but we will not pursue leptonic CP violation in this work). For instance, the non-observation of a neutron EDM sets stringent limits on the electric and chromo-electric dipole moments of up and down quarks and various four-quark interactions [204]. The experimental limits are so stringent, that the same experiments also indirectly constrain CP violation in interactions involving heavier quarks. For instance, a chromo-electric dipole moment of a bottom or top quark, induced at the scale Λ in some BSM theory, will in turn induce chromo-electric dipole moments of light quarks and gluons due to renormalization-group evolution to lower energies and threshold effects when the heavier quarks

are integrated out. Systematic studies of the resulting indirect limits have appeared in several places in the literature see e.g. [205–208].
Although those indirect limits are already valuable, more direct information on CP-violating interactions involving heavy quarks would be welcome. First of all, additional observables would help in setting global constraints leaving less room for possible cancellations among various sources. Second, as soon as a non-zero EDM will be found, hopefully in the near future, additional information is needed to pin down the underlying source of CP violation. Third, while operators with heavy quarks contribute to first-generation EDMs, the contributions are loop suppressed and sometimes involve small dimensionless numbers such as Cabibbo-Kobayashi-Maskawa (CKM) matrix elements or light-quark Yukawa couplings. Finally, and arguably most importantly, plans are being discussed to measure EDMs of baryons with a heavy valence quarks directly. For instance, Refs. [47–49] discuss the prospects of measuring EDMs of charm and bottom baryons. Further discussions on the mechanism of CP violation resulting from the QCD θ-term in the charm baryon sector can be found in [194]. In this work, we calculate the EDMs of spin-$1/2$ bottom baryons in the framework of the SMEFT. In this way, we can determine what is the sensitivity of potential future measurements on the scale of BSM physics, and whether different baryons have a different sensitivity to various CP-violating SMEFT operators.
This paper is organized as follows. In Sect. 5.3 we discuss dimension-six SMEFT CP-violating operators involving bottom quarks. In Sect. 5.4 we discuss how to match these operators to the hadronic level using chiral perturbation theory focusing on the operators most relevant for our EDM calculations. In Sect. 5.5 we perform the calculation of the EDMs of bottom-quark baryons at leading order for each source of CP violation. We discuss the expected sizes of EDMs in Sect. 5.7 and conclude in Sect. 5.8. Several appendices are devoted to technical issues.

5.3 CP-violating operators involving bottom quarks

We start with listing CP-violating operators involving b quarks at the quark level. We focus on operators with at least one $\bar{b}\Gamma b$ bilinear, where Γ is a general Lorentz-structure, while the remaining fields are light quarks or gauge or scalar bosons. Operators with more b quark fields lead to suppressed EDMs of systems containing a single b valence quark in the same way as b quark effects are suppressed in light states. We do not consider operators with just light quarks even though they would contribute to b-quark containing baryons. The reason being that the limits on these CP-odd operators from traditional EDM experiments, such as those for the neutron EDM, are very stringent.
At low energies, right above the b-quark threshold, the effective P- and T-violating dimension-six

operators of relevance here reads [45, 196, 201]

$$
\begin{aligned}
\mathcal{L}^{(6)}_{b,\mathrm{qEDM}} &= d_b \bar{b}\, \sigma^{\mu\nu}\gamma_5 b\, F_{\mu\nu}\,, \\
\mathcal{L}^{(6)}_{b,\mathrm{qCEDM}} &= \tilde{d}_b \bar{b}\, \sigma^{\mu\nu}\gamma_5 \lambda^a b\, G^a_{\mu\nu}\,, \\
\mathcal{L}^{(6)}_{b,4\mathrm{q}} &= i\mu_1^{ub}(\bar{u}u\bar{b}\gamma_5 b + \bar{u}\gamma_5 u\bar{b}b - \bar{b}\gamma_5 u\bar{u}b - \bar{b}u\bar{u}\gamma_5 b) + i\mu_1^{db}(\bar{d}d\bar{b}\gamma_5 b + \bar{d}\gamma_5 d\bar{b}b \\
&\quad - \bar{b}\gamma_5 d\bar{d}b - \bar{b}d\bar{d}\gamma_5 b) + i\mu_1^{sb}(\bar{s}s\bar{b}\gamma_5 b + \bar{s}\gamma_5 s\bar{b}b - \bar{b}\gamma_5 s\bar{s}b - \bar{b}s\bar{s}\gamma_5 b) \\
&\quad + i\mu_8^{ub}(\bar{u}\lambda^a u\bar{b}\gamma_5\lambda^a b + \bar{u}\gamma_5\lambda^a u\bar{b}\lambda^a b - \bar{b}\gamma_5\lambda^a u\bar{u}\lambda^a b - \bar{b}\lambda^a u\bar{u}\gamma_5\lambda^a b) \\
&\quad + i\mu_8^{db}(\bar{d}\lambda^a d\bar{b}\gamma_5\lambda^a b + \bar{d}\gamma_5\lambda^a d\bar{b}\lambda^a b - \bar{b}\gamma_5\lambda^a d\bar{d}\lambda^a b - \bar{b}\lambda^a d\bar{d}\gamma_5\lambda^a b) \\
&\quad + i\mu_8^{sb}(\bar{s}\lambda^a s\bar{b}\gamma_5\lambda^a b + \bar{s}\gamma_5\lambda^a s\bar{b}\lambda^a b - \bar{b}\gamma_5\lambda^a s\bar{s}\lambda^a b - \bar{b}\lambda^a s\bar{s}\gamma_5\lambda^a b)\,, \\
\mathcal{L}^{(6)}_{b,4\mathrm{qLR}} &= i\nu_1^{ub}V_{ub}(\bar{b}_L\gamma_\mu u_L\bar{u}_R\gamma^\mu b_R) - i\nu_1^{ub}V^*_{ub}(\bar{b}_R\gamma_\mu u_R\bar{u}_L\gamma^\mu b_L) \\
&\quad + i\nu_8^{ub}V_{ub}(\bar{b}_L\gamma_\mu\lambda^a u_L\bar{u}_R\gamma^\mu\lambda^a b_R) - i\nu_8^{ub}V^*_{ub}(\bar{b}_R\gamma_\mu\lambda^a u_R\bar{u}_L\gamma^\mu\lambda^a b_L)\,,
\end{aligned}
\tag{5.1}
$$

where V_{ub} is an element of the CKM matrix, $F_{\mu\nu}$ and $G^a_{\mu\nu}$ are the electromagnetic and the gluon field-strength tensors, respectively.

The bottom-quark EDM (qEDM) and bottom-quark chromo-EDM (qCEDM) operators arise from the following dimension-six operators in the SMEFT Lagrangian

$$
\begin{aligned}
\mathcal{L}_{4\mathrm{q}} &= C^{bB}\,(\bar{Q}_3\sigma^{\mu\nu}b_{R_b})HB_{\mu\nu} + C^{bW}\,(\bar{Q}_3\sigma^{\mu\nu}\tau^a b_{R_b})HW^a_{\mu\nu} + C^{bG}\,(\bar{Q}_3\sigma^{\mu\nu}\lambda^a b_{R_b})HG^a_{\mu\nu} \\
&\quad + \mathrm{h.c.}\,,
\end{aligned}
\tag{5.2}
$$

where Q_3 denotes a left-doublet of third-generation quarks, H is the Higgs doublet, and $B_{\mu\nu}$ and $W^a_{\mu\nu}$ denote, respectively, the $U(1)_Y$ and $SU(2)_L$ field strengths. To preserve gauge invariance, the SMEFT dipole operators involve a Higgs field in the SMEFT Lagrangian. Eq. (5.1) is subsequent to electroweak symmetry breaking where we have replaced the Higgs field by its vacuum expectation value. The bottom qEDM arises from a linear combination of $U(1)_Y$ and $SU(2)_L$ dimension-six dipole operators (there is in principle an associated dipole operator coupled to Z and $W^\pm$ bosons that play no role in our analysis). In most models of BSM physics, the dipoles scale with the bottom quark Yukawa and we expect $d_b, \tilde{d}_b \sim m_b/\Lambda^2$. These dipole operators are generated in various classes of BSM physics ranging from supersymmetric scenarios [209], to two-Higgs doublet models [210], to leptoquarks [211].

The four-quark (4q) operators in $\mathcal{L}^{(6)}_{b,4\mathrm{q}}$ are induced from gauge invariant operators of the form

$$
\mathcal{L}_{4\mathrm{q}} = C^{abcd}_{4\mathrm{q}}\,(\bar{Q}^I_a u_{R_b})\epsilon_{IJ}(\bar{Q}^J_c d_{R_d}) + \mathrm{h.c.} + \ldots\,,
\tag{5.3}
$$

where the ellipses denote terms with additional color structure, and $abcd$ are generation indices. These operators induce $\mathcal{L}^{(6)}_{b,4\mathrm{q}}$ for the generation indices $a = b = \{1,2\}$ and $c = d = 3$ or $a = d = 3$ and $b = c = \{1,2\}$ (the operator in Eq. (5.1) are associated to the former generation configuration. The second configuration leads to very similar low-energy operators and the analysis presented here will be the same) and additional operators involving top quarks that play no role at low energies. We expect $\mu^{ub,db,sb}_{1,8} \sim 1/\Lambda^2$. For instance, the CP-odd four-quark operators are induced in models of

leptoquarks in which case Λ is related to the mass of the exchange leptoquark [211].

The four-quark operators in $\mathcal{L}^{(6)}_{b,4qLR}$ are induced from the gauge-invariant operator

$$\mathcal{L}_{\rm 4qLR} = C^{ab}_{\rm 4qLR}\left(\tilde{H}^\dagger D_\mu H\right)\bar{u}^a_R\gamma^\mu b^b_R + \text{h.c.}\,. \tag{5.4}$$

After electroweak symmetry breaking this operator leads to a right-handed charged current. This operator is usually called four-quark left-right (4qLR) operator. The interactions in $\mathcal{L}^{(6)}_{b,4qLR}$ are generated when the W boson is integrated out at tree level between quarks giving rise to the additional factor of V_{ub}. By power counting $\nu^{ub}_{1,8} \sim v^2/(m_W^2\Lambda^2) \sim 1/\Lambda^2$. An example where this operator is generated is the minimal left-right symmetric model [204].

5.4 Chiral perturbation theory for bottom baryons

The way to include heavy bottom quarks into standard Chiral Perturbation Theory (ChPT) is known for some time [81, 82]. In the SU(3) flavor representation the spin-1/2 anti-symmetric triplet and symmetric sextet bottom baryon states are denoted by the following matrices, respectively,

$$B_{\bar{3}} = \begin{pmatrix} 0 & \Lambda_b^0 & \Xi_b^0 \\ -\Lambda_b^0 & 0 & \Xi_b^- \\ -\Xi_b^0 & -\Xi_b^- & 0 \end{pmatrix}, \quad B_6 = \begin{pmatrix} \Sigma_b^+ & \frac{\Sigma_b^0}{\sqrt{2}} & \frac{\Xi_b^{\prime 0}}{\sqrt{2}} \\ \frac{\Sigma_b^0}{\sqrt{2}} & \Sigma_b^- & \frac{\Xi_b^{\prime -}}{\sqrt{2}} \\ \frac{\Xi_b^{\prime 0}}{\sqrt{2}} & \frac{\Xi_b^{\prime -}}{\sqrt{2}} & \Omega_b^- \end{pmatrix}. \tag{5.5}$$

The Goldstone boson octet is given by

$$\phi = \begin{pmatrix} \frac{1}{\sqrt{2}}\pi^0 + \frac{1}{\sqrt{6}}\eta & \pi^+ & K^+ \\ \pi^- & -\frac{1}{\sqrt{2}}\pi^0 + \frac{1}{\sqrt{6}}\eta & K^0 \\ K^- & \bar{K}^0 & -\frac{2}{\sqrt{6}}\eta \end{pmatrix}, \tag{5.6}$$

and we define

$$U = u^2 = \exp\left(i\frac{\phi}{F_\pi}\right), \tag{5.7}$$

where F_π is the pion decay constant. The relevant P- and T-conserving free and interaction Lagrangians up to the second chiral order in a covariant formalism are given by [82, 212–214]

$$\begin{aligned} \mathcal{L}^{(1)}_{\rm free} &= \frac{1}{2}\langle\bar{B}_{\bar{3}}(i\not{D} - m_{\bar{3}})B_{\bar{3}}\rangle + \langle\bar{B}_6(i\not{D} - m_6)B_6\rangle\,, \\ \mathcal{L}_{\rm int} &= \frac{g_1}{2}\langle\bar{B}_6\not{u}\gamma_5 B_6\rangle + \frac{g_2}{2}\langle\bar{B}_6\not{u}\gamma_5 B_{\bar{3}} + h.c.\rangle + \frac{g_3}{2}\langle\bar{B}_{\bar{3}}\not{u}\gamma_5 B_{\bar{3}}\rangle\,, \\ \mathcal{L}^{(2)}_{B\gamma} &= w_1\langle\bar{B}_{\bar{3}}\sigma^{\mu\nu}F^+_{\mu\nu}B_{\bar{3}}\rangle + w_2\langle\bar{B}_6\sigma^{\mu\nu}F^+_{\mu\nu}B_6\rangle + w_3\langle\bar{B}_6\sigma^{\mu\nu}F^+_{\mu\nu}B_3 + h.c.\rangle \\ &\quad + w_4\langle\bar{B}_{\bar{3}}\sigma^{\mu\nu}B_{\bar{3}}\rangle\langle F^+_{\mu\nu}\rangle + w_5\langle\bar{B}_6\sigma^{\mu\nu}B_6\rangle\langle F^+_{\mu\nu}\rangle\,. \end{aligned} \tag{5.8}$$

Here, D_μ is the covariant derivative defined as

$$D_\mu B = \partial_\mu B + \Gamma_\mu B + B\Gamma_\mu^T, \quad \Gamma_\mu = \frac{1}{2}\left[u^\dagger(\partial_\mu - ir_\mu)u + u(\partial_\mu - il_\mu)u^\dagger\right], \tag{5.9}$$

and u_μ is the standard chiral Vielbein

$$u_\mu = i\left[u^\dagger(\partial_\mu - ir_\mu)u - u(\partial_\mu - il_\mu)u^\dagger\right], \tag{5.10}$$

where r_μ and l_μ denote external right- and left-handed sources. Also, we have

$$F_{\mu\nu}^+ = u^\dagger Q_B F_{\mu\nu} u + u Q_B F_{\mu\nu} u^\dagger, \tag{5.11}$$

with the bottom baryon charge matrix [215]

$$Q_B = \frac{e}{2}\text{diag}\,(1, -1, -1). \tag{5.12}$$

The prefactors g_{1-3} and w_{1-5} are low-energy constants (LECs). g_2 is calculated using the widths of the heavy baryons. g_1 and g_3 are related to g_2 with the help of the quark model and heavy quark spin flavor symmetry [82, 213, 215, 216]. Due to heavy quark spin symmetry, the vertex $B_{\bar{3}}B_{\bar{3}}\phi$ is forbidden and the term has to vanish, i.e. $g_3 = 0$. This result can be deduced from angular momentum and parity conservation arguments (see e.g. [82]). The conventional magnetic moment couplings, w_{1-5} are determined from fits to calculations to baryon magnetic moments in [217, 218]. However, in the present calculation, they do not contribute to the EDMs at the order we work. The numerical values of the contributing couplings are given in Section 5.7.

5.4.1 Construction of the effective CP-violating Lagrangian

We now turn to the construction of the effective Lagrangian on the hadron level arising from the dimension-six terms in Eq. (5.1). The first operator we want to look at is the bottom-quark EDM (qEDM) which does not contain any light quarks but only the heavy b-quark. As it already contains the electromagnetic field strength tensor $F_{\mu\nu}$, it directly induces EDMs of baryons containing bottom quarks. We find only two terms in the leading chiral Lagrangian corresponding to EDMs of the anti-triplet and sextet of bottom-quark baryons.
Next, we discuss the bottom-quark CEDM (qCEDM). Similarly to the qEDM, there is no light quark content in the Lagrangian and, instead of $F_{\mu\nu}$, we have the gluon field strength tensor $G^a_{\mu\nu}$. The fact that this term contains only heavy quarks and $G^a_{\mu\nu}$ makes this term (like the qEDM) a chiral singlet, i.e. it is invariant under chiral SU(3) transformations. In standard ChPT, there is no fundamental building block that transforms as a chiral singlet. Therefore, we have to introduce a new fundamental block β^+, which gives the proper transformation behaviour, and a partner building block β^-, which transforms accordingly and explicitly violates P and T. This procedure works analogously to the definition of the building blocks χ_+ and χ_- in ChPT. However, in contrast to the building blocks $\chi_\pm$, the chiral singlet β^+ cannot introduce any further structure containing Goldstone boson fields. In fact, it can be shown that β^+ can only enter the effective Lagrangian as an overall constant. In a similar fashion, one can also deduce that a P- and T-violating chiral singlet term β^- will always vanish. There is simply no constant that can violate P and T. Despite β^+ being a constant, we still have to treat it like a

building block. To construct the effective Lagrangian on the hadron level, we need to combine β^+ with other ChPT building blocks that violate CP. This procedure leads to the terms given below. For more information see e.g. Refs. [195, 196].
The next contributions we investigate are the four quark interaction terms (4q-operators). These terms need a little extra treatment, since they not just include the heavy bottom quark, but also the light quarks u, d and s. Due to the presence of the light quarks, we have to study how the 4q-terms transform under chiral transformations. To obtain the transformation properties of $\mathcal{L}^{(6)}_{b,4q}$ under chiral SU(3) transformations, we first express the non-mixing μ_1 terms of the operator as follows

$$i\mu_1^{ub}(\bar{u}u\bar{b}\gamma_5 b + \bar{u}\gamma_5 u\bar{b}b) + i\mu_1^{db}(\bar{d}d\bar{b}\gamma_5 b + \bar{d}\gamma_5 d\bar{b}b) + i\mu_1^{sb}(\bar{s}s\bar{b}\gamma_5 b + \bar{s}\gamma_5 s\bar{b}b). \tag{5.13}$$

These terms have the structure

$$i\bar{q}\mathcal{M}_1 q\,(\bar{b}\gamma_5 b) + i\bar{q}\mathcal{M}_1\gamma_5 q\,(\bar{b}b), \tag{5.14}$$

in terms of the quark column vector $q = (u,\ d,\ s)^T$ and

$$\mathcal{M}_1 = \begin{pmatrix} \mu_1^{ub} & 0 & 0 \\ 0 & \mu_1^{db} & 0 \\ 0 & 0 & \mu_1^{sb} \end{pmatrix}. \tag{5.15}$$

For the light quarks, Eq. (5.14) has the structure of a mass term in ordinary ChPT, because the term containing the b quarks is a SU(3) singlet and does not transform at all. The $\mathcal{M}_1$ matrix will therefore act as a new scalar source, similar to the quark mass matrix in standard ChPT, while the explicit insertions of the b-quark field allow for the appearance of the heavy bottom baryon matrices $B_{\bar{3}}$ and B_6 in the effective Lagrangian. The mixing terms in the 4q Lagrangian,

$$-i\mu_1^{ub}(\bar{b}\gamma_5 u\bar{u}b + \bar{b}u\bar{u}\gamma_5 b) - i\mu_1^{db}(\bar{b}\gamma_5 d\bar{d}b + \bar{b}d\bar{d}\gamma_5 b) - i\mu_1^{sb}(\bar{b}\gamma_5 s\bar{s}b + \bar{b}s\bar{s}\gamma_5 b), \tag{5.16}$$

can be treated in an analogous way. If we use the identities

$$\begin{aligned} \bar{q}q &= \bar{u}u + \bar{d}d + \bar{s}s, \\ q\bar{q} &= \begin{pmatrix} u\bar{u} & u\bar{d} & u\bar{s} \\ d\bar{u} & d\bar{d} & d\bar{s} \\ s\bar{u} & s\bar{d} & s\bar{s} \end{pmatrix}, \\ \langle q\bar{q}\rangle &= u\bar{u} + d\bar{d} + s\bar{s}\,, \end{aligned} \tag{5.17}$$

we can express Eq. (5.16) together with Eqs. (5.15, 5.17) as

$$-i\bar{b}\gamma_5\langle(\mathcal{M}_1 q)\bar{q}\rangle b - i\bar{b}\langle(\mathcal{M}_1 q)\bar{q}\rangle\gamma_5 b. \tag{5.18}$$

Using the cyclic property of the trace one observes that these mixing terms transform again like a mass term. Thus, we can use the same procedure like in the non-mixing case to obtain the effective Lagrangian. For the 4q-operators, the μ_1- and μ_8-terms have identical chiral symmetry properties. While these terms are distinguishable on the quark-level, at low energies the resulting chiral Lagrangians are identical. We are not able to distinguish them without nonperturbative information

about the associated low-energy constants. The effective Lagrangian from the $4q$-operator will therefore combine the effects of the μ_1 and μ_8 terms.
The last terms we have to discuss are the 4qLR-terms. Similarly to the 4q-operator one can reproduce the transformation rules for the 4qLR-operator. First we take the ν_1^{ub}-terms and use Fierz identities to rewrite the left- and right-handed components of the quark fields. Then, we arrange the resulting terms, like before, in structures involving the quark vector q and a new scalar source

$$\mathcal{N}_1 = \begin{pmatrix} \nu_1^{ub} & 0 & 0 \\ 0 & 0 & 0 \\ 0 & 0 & 0 \end{pmatrix}. \tag{5.19}$$

We find the same transformation behaviour as for the 4q case. This leads to an identical EFT Lagrangian construction procedure. Also here the 4qLR-terms involving the constant ν_8^{ub} are not distinguishable from the ν_1^{ub}-terms at the level of chiral EFT. Finally, we mention that after rewriting the terms with Fierz identities, we obtain both P- and T-violating and P- and T-conserving interactions. The latter lead to modifications of P- and T-even observables that are swamped by Standard Model contributions, and we neglect them below.

We are now in the position to write down the hadronic Lagrangians accounting for the various P- and T-violating dimension six operators. For the quark EDM we obtain the two operators

$$\mathcal{L}^{\text{eff.}}_{qEDM} = c_1\langle \bar{B}_{\bar{3}}\sigma^{\mu\nu}\gamma_5 F_{\mu\nu}B_{\bar{3}}\rangle + c_2\langle \bar{B}_6\sigma^{\mu\nu}\gamma_5 F_{\mu\nu}B_6\rangle + \dots . \tag{5.20}$$

A much longer list of operators appears for the qCEDM. Here, we give all operators that appear at the same chiral order. As discussed below not all operators are relevant for the EDM calculations we perform. We list them here for completeness. These read

$$\begin{aligned}
\mathcal{L}^{\text{eff.}}_{\text{qCEDM}} = i\beta^+\Big[& b_1\langle \bar{B}_{\bar{3}}\chi_+\gamma_5 B_{\bar{3}}\rangle + b_2\langle \bar{B}_6\chi_+\gamma_5 B_6\rangle + b_3\langle \bar{B}_6\chi_+\gamma_5 B_{\bar{3}} + h.c.\rangle + b_4\langle \bar{B}_{\bar{3}}\gamma_5 B_{\bar{3}}\rangle\langle\chi_+\rangle \\
& + b_5\langle \bar{B}_6\gamma_5 B_6\rangle\langle\chi_+\rangle + b_6\langle \bar{B}_{\bar{3}}\chi_- B_{\bar{3}}\rangle + b_7\langle \bar{B}_6\chi_- B_6\rangle + b_8\langle \bar{B}_6\chi_- B_{\bar{3}} + h.c.\rangle \\
& + b_9\langle \bar{B}_{\bar{3}}B_{\bar{3}}\rangle\langle\chi_-\rangle + b_{10}\langle \bar{B}_6 B_6\rangle\langle\chi_-\rangle\Big] + i\beta^+\Big[b_{11}\langle \bar{B}_{\bar{3}}u^\mu\gamma_5 u_\mu B_{\bar{3}}\rangle + b_{12}\langle \bar{B}_6 u^\mu\gamma_5 u_\mu B_6\rangle \\
& + b_{13}\langle \bar{B}_6 u^\mu\gamma_5 u_\mu B_{\bar{3}} + h.c.\rangle + b_{14}\langle \bar{B}_{\bar{3}}\gamma_5 B_{\bar{3}}\rangle\langle u^\mu u_\mu\rangle + b_{15}\langle \bar{B}_6\gamma_5 B_6\rangle\langle u^\mu u_\mu\rangle\Big] \\
& + \beta^+\Big[b_{16}\langle \bar{B}_{\bar{3}}\sigma^{\mu\nu}\gamma_5 F^+_{\mu\nu}B_{\bar{3}}\rangle + b_{17}\langle \bar{B}_6\sigma^{\mu\nu}\gamma_5 F^+_{\mu\nu}B_6\rangle + b_{18}\langle \bar{B}_6\sigma^{\mu\nu}\gamma_5 F^+_{\mu\nu}B_{\bar{3}} + h.c.\rangle \\
& + b_{19}\langle \bar{B}_{\bar{3}}\sigma^{\mu\nu}\gamma_5 B_{\bar{3}}\rangle\langle F^+_{\mu\nu}\rangle + b_{20}\langle \bar{B}_6\sigma^{\mu\nu}\gamma_5 B_6\rangle\langle F^+_{\mu\nu}\rangle\Big] \\
& + \beta^+\Big[b_{21}\langle \bar{B}_{\bar{3}}\sigma^{\mu\nu}\gamma_5[u_\mu,u_\nu]B_{\bar{3}}\rangle + b_{22}\langle \bar{B}_6\sigma^{\mu\nu}\gamma_5[u_\mu,u_\nu]B_6\rangle \\
& + b_{23}\langle \bar{B}_6\sigma^{\mu\nu}\gamma_5[u_\mu,u_\nu]B_{\bar{3}} + h.c.\rangle\Big]
\end{aligned}$$

$$
\begin{aligned}
&+\beta^+\Big[b_{24}\langle\bar{B}_{\bar{3}}u^\mu\rangle\langle u^\nu\sigma_{\mu\nu}\gamma_5 B_{\bar{3}}\rangle + b_{25}\langle\bar{B}_6u^\mu\rangle\langle u^\nu\sigma_{\mu\nu}\gamma_5 B_6\rangle \\
&+ b_{26}\langle\bar{B}_6u^\mu\rangle\langle u^\nu\sigma_{\mu\nu}\gamma_5 B_{\bar{3}}\rangle + h.c.\Big] \\
&+i\beta^+\Big[b_{27}\langle\bar{B}_{\bar{3}}u^\mu u^\nu\gamma_\mu\gamma_5 D_\nu B_{\bar{3}}\rangle - b_{28}\langle\bar{B}_{\bar{3}}\overleftarrow{D}_\nu u^\mu u^\nu\gamma_\mu\gamma_5 B_{\bar{3}}\rangle + b_{29}\langle\bar{B}_6u^\mu u^\nu\gamma_\mu\gamma_5 D_\nu B_6\rangle \\
&- b_{30}\langle\bar{B}_6\overleftarrow{D}_\nu u^\mu u^\nu\gamma_\mu\gamma_5 B_6\rangle + b_{31}\langle\bar{B}_6u^\mu u^\nu\gamma_\mu\gamma_5 D_\nu B_{\bar{3}} + h.c.\rangle \\
&- b_{32}\langle\bar{B}_6\overleftarrow{D}_\nu u^\mu u^\nu\gamma_\mu\gamma_5 B_{\bar{3}} + h.c.\rangle\Big] \\
&+i\beta^+\Big[\Big(b_{33}\langle\bar{B}_{\bar{3}}\gamma^\mu\gamma_5 D^\nu B_{\bar{3}}\rangle - b_{34}\langle\bar{B}_{\bar{3}}\overleftarrow{D}^\nu\gamma^\mu\gamma_5 B_{\bar{3}}\rangle\Big)\langle u_\mu u_\nu\rangle \\
&+\Big(b_{35}\langle\bar{B}_6\gamma^\mu\gamma_5 D^\nu B_6\rangle - b_{36}\langle\bar{B}_6\overleftarrow{D}^\nu\gamma^\mu\gamma_5 B_6\rangle\Big)\langle u_\mu u_\nu\rangle \\
&+\Big(b_{37}\langle\bar{B}_6\gamma^\mu\gamma_5 D^\nu B_{\bar{3}} + h.c.\rangle - b_{38}\langle\bar{B}_6\overleftarrow{D}^\nu\gamma^\mu\gamma_5 B_{\bar{3}} + h.c.\rangle\Big)\langle u_\mu u_\nu\rangle\Big] \\
&+\dots\,.
\end{aligned}
\tag{5.21}
$$

For the four-quark operators we obtain

$$
\begin{aligned}
\mathcal{L}_{4q}^{\text{eff.}} &= i\mu_1\langle\bar{B}_{\bar{3}}\tilde{\chi}_+\gamma_5 B_{\bar{3}}\rangle + i\mu_2\langle\bar{B}_6\tilde{\chi}_+\gamma_5 B_6\rangle + i\mu_3\langle\bar{B}_6\tilde{\chi}_+\gamma_5 B_{\bar{3}} + h.c.\rangle + i\mu_4\langle\bar{B}_{\bar{3}}\gamma_5 B_{\bar{3}}\rangle\langle\tilde{\chi}_+\rangle \\
&+ i\mu_5\langle\bar{B}_6\gamma_5 B_6\rangle\langle\tilde{\chi}_+\rangle + i\mu_6\langle\bar{B}_{\bar{3}}\tilde{\chi}_-B_{\bar{3}}\rangle + i\mu_7\langle\bar{B}_6\tilde{\chi}_-B_6\rangle + i\mu_8\langle\bar{B}_6\tilde{\chi}_-B_{\bar{3}} + h.c.\rangle \\
&+ i\mu_9\langle\bar{B}_{\bar{3}}B_{\bar{3}}\rangle\langle\tilde{\chi}_-\rangle + i\mu_{10}\langle\bar{B}_6B_6\rangle\langle\tilde{\chi}_-\rangle + \mu_{11}\langle\bar{B}_{\bar{3}}\tilde{\chi}_+\sigma^{\mu\nu}\gamma_5 F^+_{\mu\nu}B_{\bar{3}}\rangle + \mu_{12}\langle\bar{B}_6\tilde{\chi}_+\sigma^{\mu\nu}\gamma_5 F^+_{\mu\nu}B_6\rangle \\
&+ \mu_{13}\langle\bar{B}_6\tilde{\chi}_+\sigma^{\mu\nu}\gamma_5 F^+_{\mu\nu}B_{\bar{3}} + h.c.\rangle + \mu_{14}\langle\bar{B}_{\bar{3}}\tilde{\chi}_+\sigma^{\mu\nu}\gamma_5 B_{\bar{3}}\rangle\langle F^+_{\mu\nu}\rangle + \mu_{15}\langle\bar{B}_6\tilde{\chi}_+\sigma^{\mu\nu}\gamma_5 B_6\rangle\langle F^+_{\mu\nu}\rangle \\
&+ \mu_{16}\langle\bar{B}_6\tilde{\chi}_+\sigma^{\mu\nu}\gamma_5 B_{\bar{3}} + h.c.\rangle\langle F^+_{\mu\nu}\rangle + \mu_{17}\langle\bar{B}_{\bar{3}}\sigma^{\mu\nu}\gamma_5 F^+_{\mu\nu}B_{\bar{3}}\rangle\langle\tilde{\chi}_+\rangle + \mu_{18}\langle\bar{B}_6\sigma^{\mu\nu}\gamma_5 F^+_{\mu\nu}B_6\rangle\langle\tilde{\chi}_+\rangle \\
&+ \mu_{19}\langle\bar{B}_6\sigma^{\mu\nu}\gamma_5 F^+_{\mu\nu}B_{\bar{3}} + h.c.\rangle\langle\tilde{\chi}_+\rangle + \mu_{20}\langle\bar{B}_{\bar{3}}\sigma^{\mu\nu}\gamma_5 B_{\bar{3}}\rangle\langle\tilde{\chi}_+F^+_{\mu\nu}\rangle + \mu_{21}\langle\bar{B}_6\sigma^{\mu\nu}\gamma_5 B_6\rangle\langle\tilde{\chi}_+F^+_{\mu\nu}\rangle \\
&+ \mu_{22}\langle\bar{B}_{\bar{3}}\tilde{\chi}_-\sigma^{\mu\nu}F^+_{\mu\nu}B_{\bar{3}}\rangle + \mu_{23}\langle\bar{B}_6\tilde{\chi}_-\sigma^{\mu\nu}F^+_{\mu\nu}B_6\rangle + \mu_{24}\langle\bar{B}_6\tilde{\chi}_-\sigma^{\mu\nu}F^+_{\mu\nu}B_{\bar{3}} + h.c.\rangle \\
&+ \mu_{25}\langle\bar{B}_{\bar{3}}\tilde{\chi}_-\sigma^{\mu\nu}B_{\bar{3}}\rangle\langle F^+_{\mu\nu}\rangle + \mu_{26}\langle\bar{B}_6\tilde{\chi}_-\sigma^{\mu\nu}B_6\rangle\langle F^+_{\mu\nu}\rangle + \mu_{27}\langle\bar{B}_6\tilde{\chi}_-\sigma^{\mu\nu}B_{\bar{3}} + h.c.\rangle\langle F^+_{\mu\nu}\rangle \\
&+ \mu_{28}\langle\bar{B}_{\bar{3}}\sigma^{\mu\nu}F^+_{\mu\nu}B_{\bar{3}}\rangle\langle\tilde{\chi}_-\rangle + \mu_{29}\langle\bar{B}_6\sigma^{\mu\nu}F^+_{\mu\nu}B_6\rangle\langle\tilde{\chi}_-\rangle + \mu_{30}\langle\bar{B}_6\sigma^{\mu\nu}F^+_{\mu\nu}B_{\bar{3}} + h.c.\rangle\langle\tilde{\chi}_-\rangle \\
&+ \mu_{31}\langle\bar{B}_{\bar{3}}\sigma^{\mu\nu}B_{\bar{3}}\rangle\langle\tilde{\chi}_-F^+_{\mu\nu}\rangle + \mu_{32}\langle\bar{B}_6\sigma^{\mu\nu}B_6\rangle\langle\tilde{\chi}_-F^+_{\mu\nu}\rangle + \dots\,,
\end{aligned}
\tag{5.22}
$$

and

$$\begin{aligned}
\mathcal{L}^{\text{eff.}}_{\text{4qLR}} = i\text{Re}(V_{ub})\Big[&\nu_1\langle\bar{B}_{\bar{3}}\hat{\tilde{\chi}}_-B_{\bar{3}}\rangle + \nu_2\langle\bar{B}_6\hat{\tilde{\chi}}_-B_6\rangle + \nu_3\langle\bar{B}_6\hat{\tilde{\chi}}_-B_{\bar{3}} + h.c.\rangle + \nu_4\langle\bar{B}_{\bar{3}}B_{\bar{3}}\rangle\langle\hat{\tilde{\chi}}_-\rangle \\
&+ \nu_5\langle\bar{B}_6B_6\rangle\langle\hat{\tilde{\chi}}_-\rangle + \nu_6\langle\bar{B}_{\bar{3}}\hat{\tilde{\chi}}_+\gamma_5B_{\bar{3}}\rangle + \nu_7\langle\bar{B}_6\hat{\tilde{\chi}}_+\gamma_5B_6\rangle + \nu_8\langle\bar{B}_6\hat{\tilde{\chi}}_+\gamma_5B_{\bar{3}} + h.c.\rangle \\
&+ \nu_9\langle\bar{B}_{\bar{3}}\gamma_5B_{\bar{3}}\rangle\langle\hat{\tilde{\chi}}_+\rangle + \nu_{10}\langle\bar{B}_6\gamma_5B_6\rangle\langle\hat{\tilde{\chi}}_+\rangle\Big] + \text{Re}(V_{ub})\Big[\nu_{11}\langle\bar{B}_{\bar{3}}\hat{\tilde{\chi}}_+\sigma^{\mu\nu}\gamma_5F^+_{\mu\nu}B_{\bar{3}}\rangle \\
&+ \nu_{12}\langle\bar{B}_6\hat{\tilde{\chi}}_+\sigma^{\mu\nu}\gamma_5F^+_{\mu\nu}B_6\rangle + \nu_{13}\langle\bar{B}_6\hat{\tilde{\chi}}_+\sigma^{\mu\nu}\gamma_5F^+_{\mu\nu}B_{\bar{3}} + h.c.\rangle + \nu_{14}\langle\bar{B}_{\bar{3}}\hat{\tilde{\chi}}_+\sigma^{\mu\nu}\gamma_5B_{\bar{3}}\rangle\langle F^+_{\mu\nu}\rangle \\
&+ \nu_{15}\langle\bar{B}_6\hat{\tilde{\chi}}_+\sigma^{\mu\nu}\gamma_5B_6\rangle\langle F^+_{\mu\nu}\rangle + \nu_{16}\langle\bar{B}_6\hat{\tilde{\chi}}_+\sigma^{\mu\nu}\gamma_5B_{\bar{3}} + h.c.\rangle\langle F^+_{\mu\nu}\rangle + \nu_{17}\langle\bar{B}_{\bar{3}}\sigma^{\mu\nu}\gamma_5F^+_{\mu\nu}B_{\bar{3}}\rangle\langle\hat{\tilde{\chi}}_+\rangle \\
&+ \nu_{18}\langle\bar{B}_6\sigma^{\mu\nu}\gamma_5F^+_{\mu\nu}B_6\rangle\langle\hat{\tilde{\chi}}_+\rangle + \nu_{19}\langle\bar{B}_6\sigma^{\mu\nu}\gamma_5F^+_{\mu\nu}B_{\bar{3}} + h.c.\rangle\langle\hat{\tilde{\chi}}_+\rangle + \nu_{20}\langle\bar{B}_{\bar{3}}\sigma^{\mu\nu}\gamma_5B_{\bar{3}}\rangle\langle\hat{\tilde{\chi}}_+F^+_{\mu\nu}\rangle \\
&+ \nu_{21}\langle\bar{B}_6\sigma^{\mu\nu}\gamma_5B_6\rangle\langle\hat{\tilde{\chi}}_+F^+_{\mu\nu}\rangle + \nu_{22}\langle\bar{B}_{\bar{3}}\hat{\tilde{\chi}}_-\sigma^{\mu\nu}F^+_{\mu\nu}B_{\bar{3}}\rangle + \nu_{23}\langle\bar{B}_6\hat{\tilde{\chi}}_-\sigma^{\mu\nu}F^+_{\mu\nu}B_6\rangle \\
&+ \nu_{24}\langle\bar{B}_6\hat{\tilde{\chi}}_-\sigma^{\mu\nu}F^+_{\mu\nu}B_{\bar{3}} + h.c.\rangle + \nu_{25}\langle\bar{B}_{\bar{3}}\hat{\tilde{\chi}}_-\sigma^{\mu\nu}B_{\bar{3}}\rangle\langle F^+_{\mu\nu}\rangle + \nu_{26}\langle\bar{B}_6\hat{\tilde{\chi}}_-\sigma^{\mu\nu}B_6\rangle\langle F^+_{\mu\nu}\rangle \\
&+ \nu_{27}\langle\bar{B}_6\hat{\tilde{\chi}}_-\sigma^{\mu\nu}B_{\bar{3}} + h.c.\rangle\langle F^+_{\mu\nu}\rangle + \nu_{28}\langle\bar{B}_{\bar{3}}\sigma^{\mu\nu}F^+_{\mu\nu}B_{\bar{3}}\rangle\langle\hat{\tilde{\chi}}_-\rangle + \nu_{29}\langle\bar{B}_6\sigma^{\mu\nu}F^+_{\mu\nu}B_6\rangle\langle\hat{\tilde{\chi}}_-\rangle \\
&+ \nu_{30}\langle\bar{B}_6\sigma^{\mu\nu}F^+_{\mu\nu}B_{\bar{3}} + h.c.\rangle\langle\hat{\tilde{\chi}}_-\rangle + \nu_{31}\langle\bar{B}_{\bar{3}}\sigma^{\mu\nu}B_{\bar{3}}\rangle\langle\hat{\tilde{\chi}}_-F^+_{\mu\nu}\rangle + \nu_{32}\langle\bar{B}_6\sigma^{\mu\nu}B_6\rangle\langle\hat{\tilde{\chi}}_-F^+_{\mu\nu}\rangle\Big] \\
&+ \dots\,.
\end{aligned} \tag{5.23}$$

The ellipses indicate further terms of higher chiral order, which we will not display. We have defined

$$\begin{aligned}
\chi_\pm &= u^\dagger\chi u^\dagger \pm u\chi^\dagger u, \qquad &\chi &= 2B_0\,\text{diag}(m_u, m_d, m_s), \\
\tilde{\chi}_\pm &= u^\dagger\tilde{\chi}u^\dagger \pm u\tilde{\chi}^\dagger u, \qquad &\tilde{\chi} &\equiv \text{diag}\,(\mu^{ub}, \mu^{db}, \mu^{sb}), \\
\hat{\tilde{\chi}}_\pm &= u^\dagger\hat{\tilde{\chi}}u^\dagger \pm u\hat{\tilde{\chi}}^\dagger u, \qquad &\hat{\tilde{\chi}} &\equiv \text{diag}\,(\nu^{ub}, 0, 0),
\end{aligned} \tag{5.24}$$

with the light quark masses m_q and the LEC B_0 related to the quark condensate. Note that the constants μ^{ub}, μ^{db}, μ^{sb} and ν^{ub} capture both the color-singlet and -octet terms whose chiral Lagrangians are identical.

It is convenient to use heavy-baryon chiral perturbation theory (HBChPT) while working with objects that contain a single heavy quark [78, 79]. In the heavy-baryon formulation, several terms in the relativistic form cancel or appear at higher orders, and loop calculations are simplified. Furthermore, the chiral power counting is manifest. The heavy-baryon Lagrangians are given by

$$\begin{aligned}
\mathcal{L}^{(1)}_{\text{free}} &= \frac{1}{2}\langle\bar{B}_{\bar{3},v}(iv\cdot D)B_{\bar{3},v}\rangle + \langle\bar{B}_{6,v}(iv\cdot D - \Delta)B_{6,v}\rangle, \\
\mathcal{L}_{\text{int}} &= g_1\langle\bar{B}_{6,v}u_\mu S^\mu B_{6,v}\rangle + g_2\langle\bar{B}_{6,v}u_\mu S^\mu B_{\bar{3},v} + h.c.\rangle, \\
\mathcal{L}^{(2)}_{B\gamma} &= 2\varepsilon^{\mu\nu\rho\sigma}\Big[w_1\langle\bar{B}_{\bar{3},v}v_\rho S_\sigma F^+_{\mu\nu}B_{\bar{3},v}\rangle + w_2\langle\bar{B}_{6,v}v_\rho S_\sigma F^+_{\mu\nu}B_{6,v}\rangle + w_3\langle\bar{B}_{6,v}v_\rho S_\sigma F^+_{\mu\nu}B_{\bar{3},v} + h.c.\rangle \\
&\quad + w_4\langle\bar{B}_{\bar{3},v}v_\rho S_\sigma B_{\bar{3},v}\rangle\langle F^+_{\mu\nu}\rangle + w_5\langle\bar{B}_{6,v}v_\rho S_\sigma B_{6,v}\rangle\langle F^+_{\mu\nu}\rangle\Big],
\end{aligned} \tag{5.25}$$

with the four velocity v^μ, the Pauli-Lubanski spin operator $S^\mu = -\gamma_5(\gamma^\mu\not{v} - v^\mu)/2$ and the mass difference between sextet and anti-triplet baryons $\Delta = m_6 - m_{\bar{3}}$. The effective Lagrangians for the P-

and T-odd interactions in the heavy baryon formulation are

$$
\begin{aligned}
\mathcal{L}^{\text{eff.}}_{\text{qEDM}} &= 4i\Big[c_1\langle\bar{B}_{\bar{3},v}v^\mu S^\nu F_{\mu\nu}B_{\bar{3},v}\rangle + c_2\langle\bar{B}_{6,v}v^\mu S^\nu F_{\mu\nu}B_{6,v}\rangle\Big],\\
\mathcal{L}^{\text{eff.}}_{\text{qCEDM}} &= 4i\beta^+\Big[b_{16}\langle\bar{B}_{\bar{3},v}v^\mu S^\nu F^+_{\mu\nu}B_{\bar{3},v}\rangle + b_{17}\langle\bar{B}_{6,v}v^\mu S^\nu F^+_{\mu\nu}B_{6,v}\rangle + b_{18}\langle\bar{B}_{6,v}v^\mu S^\nu F^+_{\mu\nu}B_{\bar{3},v} + h.c.\rangle\\
&\quad + b_{19}\langle\bar{B}_{\bar{3},v}v^\mu S^\nu B_{\bar{3},v}\rangle\langle F^+_{\mu\nu}\rangle + b_{20}\langle\bar{B}_{6,v}v^\mu S^\nu B_{6,v}\rangle\langle F^+_{\mu\nu}\rangle\Big] + \dots,\\
\mathcal{L}^{\text{eff.}}_{\text{4q}} &= i\mu_6\langle\bar{B}_{\bar{3},v}\tilde{\chi}_-B_{\bar{3},v}\rangle + i\mu_7\langle\bar{B}_{6,v}\tilde{\chi}_-B_{6,v}\rangle + i\mu_8\langle\bar{B}_{6,v}\tilde{\chi}_-B_{\bar{3},v} + h.c.\rangle + i\mu_9\langle\bar{B}_{\bar{3},v}B_{\bar{3},v}\rangle\langle\tilde{\chi}_-\rangle\\
&\quad + i\mu_{10}\langle\bar{B}_{6,v}B_{6,v}\rangle\langle\tilde{\chi}_-\rangle + 4i\Big[\mu_{11}\langle\bar{B}_{\bar{3},v}\tilde{\chi}_+v^\mu S^\nu F^+_{\mu\nu}B_{\bar{3},v}\rangle + \mu_{12}\langle\bar{B}_{6,v}\tilde{\chi}_+v^\mu S^\nu F^+_{\mu\nu}B_{6,v}\rangle\\
&\quad + \mu_{13}\langle\bar{B}_{6,v}\tilde{\chi}_+v^\mu S^\nu F^+_{\mu\nu}B_{\bar{3},v} + h.c.\rangle + \mu_{14}\langle\bar{B}_{\bar{3},v}\tilde{\chi}_+v^\mu S^\nu B_{\bar{3},v}\rangle\langle F^+_{\mu\nu}\rangle\\
&\quad + \mu_{15}\langle\bar{B}_{6,v}\tilde{\chi}_+v^\mu S^\nu B_{6,v}\rangle\langle F^+_{\mu\nu}\rangle + \mu_{16}\langle\bar{B}_{6,v}\tilde{\chi}_+v^\mu S^\nu B_{\bar{3},v} + h.c.\rangle\langle F^+_{\mu\nu}\rangle\\
&\quad + \mu_{17}\langle\bar{B}_{\bar{3},v}v^\mu S^\nu F^+_{\mu\nu}B_{\bar{3},v}\rangle\langle\tilde{\chi}_+\rangle + \mu_{18}\langle\bar{B}_{6,v}v^\mu S^\nu F^+_{\mu\nu}B_{6,v}\rangle\langle\tilde{\chi}_+\rangle\\
&\quad + \mu_{19}\langle\bar{B}_{6,v}v^\mu S^\nu F^+_{\mu\nu}B_{\bar{3},v} + h.c.\rangle\langle\tilde{\chi}_+\rangle + \mu_{20}\langle\bar{B}_{\bar{3},v}v^\mu S^\nu B_{\bar{3},v}\rangle\langle\tilde{\chi}_+F^+_{\mu\nu}\rangle\\
&\quad + \mu_{21}\langle\bar{B}_{6,v}v^\mu S^\nu B_{6,v}\rangle\langle\tilde{\chi}_+F^+_{\mu\nu}\rangle\Big] + \dots,\\
\mathcal{L}^{\text{eff.}}_{\text{4qLR}} &= i\text{Re}(V_{ub})\Big[\nu_1\langle\bar{B}_{\bar{3},v}\hat{\tilde{\chi}}_-B_{\bar{3},v}\rangle + \nu_2\langle\bar{B}_{6,v}\hat{\tilde{\chi}}_-B_{6,v}\rangle + \nu_3\langle\bar{B}_{6,v}\hat{\tilde{\chi}}_-B_{\bar{3},v} + h.c.\rangle + \nu_4\langle\bar{B}_{\bar{3},v}B_{\bar{3},v}\rangle\langle\hat{\tilde{\chi}}_-\rangle\\
&\quad + \nu_5\langle\bar{B}_{6,v}B_{6,v}\rangle\langle\hat{\tilde{\chi}}_-\rangle\Big] + 4i\text{Re}(V_{ub})\Big[\nu_{11}\langle\bar{B}_{\bar{3},v}\hat{\tilde{\chi}}_+v^\mu S^\nu F^+_{\mu\nu}B_{\bar{3},v}\rangle + \nu_{12}\langle\bar{B}_{6,v}\hat{\tilde{\chi}}_+v^\mu S^\nu F^+_{\mu\nu}B_{6,v}\rangle\\
&\quad + \nu_{13}\langle\bar{B}_{6,v}\hat{\tilde{\chi}}_+v^\mu S^\nu F^+_{\mu\nu}B_{\bar{3},v} + h.c.\rangle + \nu_{14}\langle\bar{B}_{\bar{3},v}\hat{\tilde{\chi}}_+v^\mu S^\nu B_{\bar{3},v}\rangle\langle F^+_{\mu\nu}\rangle\\
&\quad + \nu_{15}\langle\bar{B}_{6,v}\hat{\tilde{\chi}}_+v^\mu S^\nu B_{6,v}\rangle\langle F^+_{\mu\nu}\rangle + \nu_{16}\langle\bar{B}_{6,v}\hat{\tilde{\chi}}_+v^\mu S^\nu B_{\bar{3},v} + h.c.\rangle\langle F^+_{\mu\nu}\rangle\\
&\quad + \nu_{17}\langle\bar{B}_{\bar{3},v}v^\mu S^\nu F^+_{\mu\nu}B_{\bar{3},v}\rangle\langle\hat{\tilde{\chi}}_+\rangle + \nu_{18}\langle\bar{B}_{6,v}v^\mu S^\nu F^+_{\mu\nu}B_{6,v}\rangle\langle\hat{\tilde{\chi}}_+\rangle\\
&\quad + \nu_{19}\langle\bar{B}_{6,v}v^\mu S^\nu F^+_{\mu\nu}B_{\bar{3},v} + h.c.\rangle\langle\hat{\tilde{\chi}}_+\rangle + \nu_{20}\langle\bar{B}_{\bar{3},v}v^\mu S^\nu B_{\bar{3},v}\rangle\langle\hat{\tilde{\chi}}_+F^+_{\mu\nu}\rangle\\
&\quad + \nu_{21}\langle\bar{B}_{6,v}v^\mu S^\nu B_{6,v}\rangle\langle\hat{\tilde{\chi}}_+F^+_{\mu\nu}\rangle\Big] + \dots\,.
\end{aligned}
\tag{5.26}
$$

We only display the terms which are relevent for the EDM calculation. Additionally, to the order we are working only terms linear in the Goldstone bosons are needed. Terms that begin with more than a single Goldstone boson are hidden in the ellipses. Since the chiral singlet β^+ in the qCEDM Lagrangian can only enter as an overall constant, it is convenient to absorb β^+ into the LECs b_i.

Concerning the power counting rules of the CP-odd vertices, the chiral order of the sources is counted as $O(\delta^0)$, where δ is a generic small mass or momentum, since they do not contain any light scales and in addition will be common to all contributions considered in this work. For the remaining pieces, we employ standard chiral counting. Fig. 5.1 depicts the tree-level and one-loop Feynman diagrams that generate a non-vanishing contribution to the P- and T-violating form factor of the B_b baryons up to the order $O(\delta^2)$. We evaluate the loop diagrams in the framework of dimensional regularization at the renormalization scale $\lambda = 1$ GeV. We apply the modified minimal subtraction scheme ($\widetilde{\text{MS}}$) in HBChPT [69, 219–221] by absorbing the infinite parts in terms of

$$
L = \frac{\lambda^{n-4}}{16\pi^2}\left[\frac{1}{n-4} + \frac{1}{2}\Big(\gamma_E - 1 - \ln(4\pi)\Big)\right]. \tag{5.27}
$$

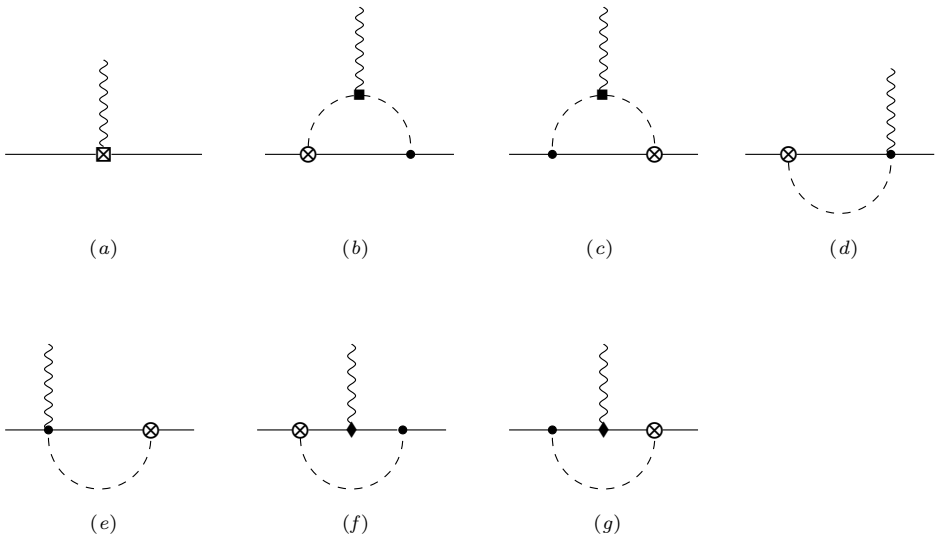

Figure 5.1: Diagrams contributing to the EDMs of the spin-1/2 neutral anti-triplet and sextet b-baryons. Solid lines correspond to contribution from either spin-1/2 anti-triplet or sextet multiplets of bottom baryons. Filled circles and squares are first-order meson-baryon and second order mesonic vertices, respectively. While diamonds represent vertices generated by the first order meson-baryon Lagrangian, CP-violating vertices at $O(\delta^0)$ and $O(\delta^2)$ are represented by $\otimes$ and $\boxtimes$, in order.

into the counterterms, with n the number of space-time dimensions and γ_E the Euler-Mascheroni constant. The tree-level CP-odd diagrams at order $O(\delta^2)$ displayed in diagram (a) receive contributions from all the CP-violating operators. The one-loop diagrams at leading $O(\delta^2)$ are given by diagrams (b)-(g) in Fig. 5.1.

5.5 The P- and T-violating form factor

The EDM of the neutral and charged b-baryons can be extracted from the P- and T-violating form factor $D^{\gamma}_{B_b}(q^2)$. It is defined through

$$\left\langle B_b(p_f)\left|\, J_{\mathrm{EDM},\nu}\,\right|B_b(p_i)\right\rangle = D^{\gamma}_{B_b}(q^2)\,\bar{u}(p_f)\sigma_{\mu\nu}\gamma_5 q^{\mu}u(p_i)\,, \tag{5.28}$$

in the covariant formulation with momentum transfer $q = p_f - p_i$, see e.g. Ref. [214]. The EDM is then given by

$$d^{\gamma}_{B_b} = D^{\gamma}_{B_b}(q^2 = 0). \tag{5.29}$$

One can reformulate the form factor in the heavy baryon approach using the Breit frame. In this frame, we have $v\cdot p_i = v\cdot p_f$ and we set the four-velocity to $v_\mu = (1,\mathbf{0})$. The form factor is then obtained as

$$\left\langle B_b(p_f)\left|\, J_{\mathrm{EDM},\nu}\,\right|B_b(p_i)\right\rangle = -2iD^{\gamma}_{B_b}(q^2)\bar{B}_v v_\nu (S\cdot q)B_v. \tag{5.30}$$

We first consider the contributions from the tree-level diagrams in Fig. 5.1-(a). The expressions of the electric dipole moment of the anti-triplet and sextet b-baryons from the dimension six operators are collected in Tables 5.1-5.3. In addition to the tree-level contributions, we find the one-loop diagrams in Fig. 5.1. In analogy to the neutron EDM, the EDMs of bottom baryons get contributions from the cloud of Goldstone bosons dressing the baryons. For the qEDM and qCEDM operators the meson-loops appear at higher order and only the tree-level diagrams are necessary. But for the 4q and 4qLR operators the loops appear at the same order and the LECs of the tree-level contributions absorb the associated loop divergences.
We calculated the diagrams in Fig. 5.1 explicitly in heavy-baryon ChPT. We find that only diagrams (b) and (c) contribute at the order we work. The other diagrams are proportional to $S \cdot v = 0$, or $v \cdot q = 0$, or mutually cancel. The contributions from the non-vanishing diagrams can be written as

$$\begin{aligned} D_b^\gamma(q^2) &= \frac{A_{b_i}}{2} \int_0^1 dx \, \frac{x}{\tilde{M}_i} \frac{\partial}{\partial \tilde{M}_i} J_1(\tilde{w}, \tilde{M}_i), \\ D_c^\gamma(q^2) &= \frac{A_{c_i}}{2} \int_0^1 dx \, \frac{x-1}{\tilde{M}_i} \frac{\partial}{\partial \tilde{M}_i} J_1(\tilde{w}, \tilde{M}_i), \quad i = 1, 2, 3, 4. \end{aligned} \tag{5.31}$$

where J_1 is the loop function defined in App. C.3, $\tilde{w} = -\Delta$ for a sextet particle inside the loop, or $\tilde{w} = 0$ for an anti-triplet particle. Furthermore, $\tilde{M}_i(x) = \sqrt{x(x-1)q^2 + M_i^2}$, with M_i being $M_{K^\pm}$ or $M_{\pi^\pm}$. The coefficients A_{b_i} and A_{c_i} have to be determined from the vertices of the appearing interacting Lagrangians. A lot of these coefficients are similar to each other with some only differing by their sign. Considering isospin symmetry this leads to additional cancellations when summing up the loop contributions. We refrain from showing the full list of coefficients A_{b_i} and A_{c_i} with their respective M_i here. The surviving terms together with their coefficients can be read off from the full form factor results listed in App. C.1. The expressions for the complete form factors are given in App. C.1. Here,

Table 5.1: Tree-level contributions from the qEDM and qCEDM operators of the b-baryons. Loop diagrams only appear at higher order.

Baryons	qEDM	qCEDM
Λ_b^0	$4c_1$	$-4eb_{19}$
Ξ_b^0	$4c_1$	$-4eb_{19}$
Ξ_b^-	$4c_1$	$-4e(b_{16}+b_{19})$
Σ_b^+	$2c_2$	$2e(b_{17}-b_{20})$
Σ_b^0	$2c_2$	$-2eb_{20}$
Σ_b^-	$2c_2$	$-2e(b_{17}+b_{20})$
$\Xi_b^{\prime 0}$	$2c_2$	$-2eb_{20}$
$\Xi_b^{\prime -}$	$2c_2$	$-2e(b_{17}+b_{20})$
Ω_b^-	$2c_2$	$-2e(b_{17}+b_{20})$

Table 5.2: Tree-level contribution from the 4q operators of the b-baryons. Loop diagrams appear at the same order.

Baryons	4q
Λ_b^0	$4e[\mu_{11}(\mu^{ub}-\mu^{db})-\mu_{14}(\mu^{ub}+\mu^{db})+2\mu_{20}(\mu^{ub}-\mu^{db}-\mu^{sb})]$
Ξ_b^0	$4e[\mu_{11}(\mu^{ub}-\mu^{sb})-\mu_{14}(\mu^{ub}+\mu^{sb})+2\mu_{20}(\mu^{ub}-\mu^{db}-\mu^{sb})]$
Ξ_b^-	$-4e[(\mu_{11}+\mu_{14})(\mu^{db}+\mu^{sb})+2\mu_{17}(\mu^{ub}+\mu^{db}+\mu^{sb})-2\mu_{20}(\mu^{ub}-\mu^{db}-\mu^{sb})]$
Σ_b^+	$4e[(\mu_{12}-\mu_{15})\mu^{ub}+\mu_{18}(\mu^{ub}+\mu^{db}+\mu^{sb})+\mu_{21}(\mu^{ub}-\mu^{db}-\mu^{sb})]$
Σ_b^0	$2e[\mu_{12}(\mu^{ub}-\mu^{db})-\mu_{15}(\mu^{ub}+\mu^{db})+2\mu_{21}(\mu^{ub}-\mu^{db}-\mu^{sb})]$
Σ_b^-	$-4e[(\mu_{12}+\mu_{15})\mu^{db}+\mu_{18}(\mu^{ub}+\mu^{db}+\mu^{sb})-\mu_{21}(\mu^{ub}-\mu^{db}-\mu^{sb})]$
$\Xi_b^{'0}$	$2e[\mu_{12}(\mu^{ub}-\mu^{sb})-\mu_{15}(\mu^{ub}+\mu^{sb})+2\mu_{21}(\mu^{ub}-\mu^{db}-\mu^{sb})]$
$\Xi_b^{'-}$	$-2e[(\mu_{12}+\mu_{15})(\mu^{db}+\mu^{sb})+2\mu_{18}(\mu^{ub}+\mu^{db}+\mu^{sb})-2\mu_{21}(\mu^{ub}-\mu^{db}-\mu^{sb})]$
Ω_b^-	$-4e[(\mu_{12}+\mu_{15})\mu^{sb}+\mu_{18}(\mu^{ub}+\mu^{db}+\mu^{sb})-\mu_{21}(\mu^{ub}-\mu^{db}-\mu^{sb})]$

Table 5.3: Tree-level contribution from 4qLR operators of the b-baryons. Loop diagrams appear at the same order.

Baryons	4qLR
Λ_b^0	$4e\mathrm{Re}(V_{ub})(\nu_{11}-\nu_{14}+2\nu_{20})\nu^{ub}$
Ξ_b^0	$4e\mathrm{Re}(V_{ub})(\nu_{11}-\nu_{14}+2\nu_{20})\nu^{ub}$
Ξ_b^-	$-8e\mathrm{Re}(V_{ub})(\nu_{17}-\nu_{20})\nu^{ub}$
Σ_b^+	$4e\mathrm{Re}(V_{ub})(\nu_{12}-\nu_{15}+\nu_{18}+\nu_{21})\nu^{ub}$
Σ_b^0	$2e\mathrm{Re}(V_{ub})(\nu_{12}-\nu_{15}+2\nu_{21})\nu^{ub}$
Σ_b^-	$-4e\mathrm{Re}(V_{ub})(\nu_{18}-\nu_{21})\nu^{ub}$
$\Xi_b^{'0}$	$2e\mathrm{Re}(V_{ub})(\nu_{12}-\nu_{15}+2\nu_{21})\nu^{ub}$
$\Xi_b^{'-}$	$-4e\mathrm{Re}(V_{ub})(\nu_{18}-\nu_{21})\nu^{ub}$
Ω_b^-	$-4e\mathrm{Re}(V_{ub})(\nu_{18}-\nu_{21})\nu^{ub}$

we present the results for the EDMs. For the 4q operator we obtain

$$d^{\gamma}_{\Lambda_b^0,4q} = 4e\Big[\mu_{11}(\mu^{ub}-\mu^{db})-\mu_{14}(\mu^{ub}+\mu^{db})+2\mu_{20}(\mu^{ub}-\mu^{db}-\mu^{sb})\Big]+\frac{eg_2\mu_8(\mu^{ub}+\mu^{sb})}{32\pi^2F_\pi^2}F^{(2)}_{M_K},$$

$$d^{\gamma}_{\Xi_b^0,4q} = 4e\Big[\mu_{11}(\mu^{ub}-\mu^{sb})-\mu_{14}(\mu^{ub}+\mu^{sb})+2\mu_{20}(\mu^{ub}-\mu^{db}-\mu^{sb})\Big]+\frac{eg_2\mu_8(\mu^{ub}+\mu^{db})}{32\pi^2F_\pi^2}F^{(2)}_{M_\pi},$$

$$\begin{aligned} d^{\gamma}_{\Xi_b^-,4q} = &-4e\Big[(\mu_{11}+\mu_{14})(\mu^{db}+\mu^{sb})+2\mu_{17}(\mu^{ub}+\mu^{db}+\mu^{sb})-2\mu_{20}(\mu^{ub}-\mu^{db}-\mu^{sb})\Big] \\ &-\frac{eg_2\mu_8}{32\pi^2F_\pi^2}\left((\mu^{ub}+\mu^{sb})F^{(2)}_{M_K}+(\mu^{ub}+\mu^{db})F^{(2)}_{M_\pi}\right), \end{aligned}$$

$$
\begin{aligned}
d^{\gamma}_{\Sigma_b^+,4\mathrm{q}} &= 4e\Big[(\mu_{12}-\mu_{15})\mu^{ub}+\mu_{18}(\mu^{ub}+\mu^{db}+\mu^{sb})+\mu_{21}(\mu^{ub}-\mu^{db}-\mu^{sb})\Big]\\
&\quad+\frac{eg_1\mu_7}{32\pi^2F_\pi^2}\left((\mu^{ub}+\mu^{sb})F^{(2)}_{M_K}+(\mu^{ub}+\mu^{db})F^{(2)}_{M_\pi}\right)\\
&\quad+\frac{eg_2\mu_8}{16\pi^2F_\pi^2}\left((\mu^{ub}+\mu^{sb})F^{(1)}_{M_K}+(\mu^{ub}+\mu^{db})F^{(1)}_{M_\pi}\right),\\
d^{\gamma}_{\Sigma_b^0,4\mathrm{q}} &= 2e\Big[\mu_{12}(\mu^{ub}-\mu^{db})-\mu_{15}(\mu^{ub}+\mu^{db})+2\mu_{21}(\mu^{ub}-\mu^{db}-\mu^{sb})\Big]\\
&\quad+\frac{eg_1\mu_7(\mu^{ub}+\mu^{sb})}{64\pi^2F_\pi^2}F^{(2)}_{M_K}+\frac{eg_2\mu_8(\mu^{ub}+\mu^{sb})}{32\pi^2F_\pi^2}F^{(1)}_{M_K},\\
d^{\gamma}_{\Sigma_b^-,4\mathrm{q}} &= -4e\Big[(\mu_{12}+\mu_{15})\mu^{db}+\mu_{18}(\mu^{ub}+\mu^{db}+\mu^{sb})-\mu_{21}(\mu^{ub}-\mu^{db}-\mu^{sb})\Big]\\
&\quad-\frac{eg_1\mu_7(\mu^{ub}+\mu^{db})}{32\pi^2F_\pi^2}F^{(2)}_{M_\pi}-\frac{eg_2\mu_8(\mu^{ub}+\mu^{db})}{16\pi^2F_\pi^2}F^{(1)}_{M_\pi},\\
d^{\gamma}_{\Xi_b^{\prime 0},4\mathrm{q}} &= 2e\Big[\mu_{12}(\mu^{ub}-\mu^{sb})-\mu_{15}(\mu^{ub}+\mu^{sb})+2\mu_{21}(\mu^{ub}-\mu^{db}-\mu^{sb})\Big]\\
&\quad+\frac{eg_1\mu_7(\mu^{ub}+\mu^{db})}{64\pi^2F_\pi^2}F^{(2)}_{M_\pi}+\frac{eg_2\mu_8(\mu^{ub}+\mu^{db})}{32\pi^2F_\pi^2}F^{(1)}_{M_\pi},\\
d^{\gamma}_{\Xi_b^{\prime -},4\mathrm{q}} &= -2e\Big[(\mu_{12}+\mu_{15})(\mu^{db}+\mu^{sb})+2\mu_{18}(\mu^{ub}+\mu^{db}+\mu^{sb})-2\mu_{21}(\mu^{ub}-\mu^{db}-\mu^{sb})\Big]\\
&\quad-\frac{eg_1\mu_7}{64\pi^2F_\pi^2}\left((\mu^{ub}+\mu^{sb})F^{(2)}_{M_K}+(\mu^{ub}+\mu^{db})F^{(2)}_{M_\pi}\right)\\
&\quad-\frac{eg_2\mu_8}{32\pi^2F_\pi^2}\left((\mu^{ub}+\mu^{sb})F^{(1)}_{M_K}+(\mu^{ub}+\mu^{db})F^{(1)}_{M_\pi}\right),\\
d^{\gamma}_{\Omega_b^-,4\mathrm{q}} &= -4e\Big[(\mu_{12}+\mu_{15})\mu^{sb}+\mu_{18}(\mu^{ub}+\mu^{db}+\mu^{sb})-\mu_{21}(\mu^{ub}-\mu^{db}-\mu^{sb})\Big]\\
&\quad-\frac{eg_1\mu_7(\mu^{ub}+\mu^{sb})}{32\pi^2F_\pi^2}F^{(2)}_{M_K}-\frac{eg_2\mu_8(\mu^{ub}+\mu^{sb})}{16\pi^2F_\pi^2}F^{(1)}_{M_K}\,.
\end{aligned}
\tag{5.32}
$$

For the 4qLR operator we obtain

$$
\begin{aligned}
d^{\gamma}_{\Lambda_b^0,4qLR} &= 4e\mathrm{Re}(V_{ub})(\nu_{11}-\nu_{14}+2\nu_{20})\nu^{ub}+\frac{e\mathrm{Re}(V_{ub})g_2\nu_3\nu^{ub}}{32\pi^2F_\pi^2}F^{(2)}_{M_K},\\
d^{\gamma}_{\Xi_b^0,4\mathrm{qLR}} &= 4e\mathrm{Re}(V_{ub})(\nu_{11}-\nu_{14}+2\nu_{20})\nu^{ub}+\frac{e\mathrm{Re}(V_{ub})g_2\nu_3\nu^{ub}}{32\pi^2F_\pi^2}F^{(2)}_{M_\pi},\\
d^{\gamma}_{\Xi_b^-,4\mathrm{qLR}} &= -8e\mathrm{Re}(V_{ub})(\nu_{17}-\nu_{20})\nu^{ub}-\frac{e\mathrm{Re}(V_{ub})g_2\nu_3\nu^{ub}}{32\pi^2F_\pi^2}\left(F^{(2)}_{M_K}+F^{(2)}_{M_\pi}\right),\\
d^{\gamma}_{\Sigma_b^+,4\mathrm{qLR}} &= 4e\mathrm{Re}(V_{ub})(\nu_{12}-\nu_{15}+\nu_{18}+\nu_{21})\nu^{ub}\\
&\quad+\frac{e\mathrm{Re}(V_{ub})g_1\nu_2\nu^{ub}}{32\pi^2F_\pi^2}\left(F^{(2)}_{M_K}+F^{(2)}_{M_\pi}\right)+\frac{e\mathrm{Re}(V_{ub})g_2\nu_3\nu^{ub}}{16\pi^2F_\pi^2}\left(F^{(1)}_{M_K}+F^{(1)}_{M_\pi}\right),\\
d^{\gamma}_{\Sigma_b^0,4\mathrm{qLR}} &= 2e\mathrm{Re}(V_{ub})(\nu_{12}-\nu_{15}+2\nu_{21})\nu^{ub}+\frac{e\mathrm{Re}(V_{ub})g_1\nu_2\nu^{ub}}{64\pi^2F_\pi^2}F^{(2)}_{M_K}+\frac{e\mathrm{Re}(V_{ub})g_2\nu_3\nu^{ub}}{32\pi^2F_\pi^2}F^{(1)}_{M_K},\\
d^{\gamma}_{\Sigma_b^-,4\mathrm{qLR}} &= -4e\mathrm{Re}(V_{ub})(\nu_{18}-\nu_{21})\nu^{ub}-\frac{e\mathrm{Re}(V_{ub})g_1\nu_2\nu^{ub}}{32\pi^2F_\pi^2}F^{(2)}_{M_\pi}-\frac{e\mathrm{Re}(V_{ub})g_2\nu_3\nu^{ub}}{16\pi^2F_\pi^2}F^{(1)}_{M_\pi},\\
d^{\gamma}_{\Xi_b^{\prime 0},4\mathrm{qLR}} &= 2e\mathrm{Re}(V_{ub})(\nu_{12}-\nu_{15}+2\nu_{21})\nu^{ub}+\frac{e\mathrm{Re}(V_{ub})g_1\nu_2\nu^{ub}}{64\pi^2F_\pi^2}F^{(2)}_{M_\pi}+\frac{e\mathrm{Re}(V_{ub})g_2\nu_3\nu^{ub}}{32\pi^2F_\pi^2}F^{(1)}_{M_\pi},\\
d^{\gamma}_{\Xi_b^{\prime -},4\mathrm{qLR}} &= -4e\mathrm{Re}(V_{ub})(\nu_{18}-\nu_{21})\nu^{ub}-\frac{e\mathrm{Re}(V_{ub})g_1\nu_2\nu^{ub}}{64\pi^2F_\pi^2}\left(F^{(2)}_{M_K}+F^{(2)}_{M_\pi}\right)\\
&\quad-\frac{e\mathrm{Re}(V_{ub})g_2\nu_3\nu^{ub}}{32\pi^2F_\pi^2}\left(F^{(1)}_{M_K}+F^{(1)}_{M_\pi}\right),\\
d^{\gamma}_{\Omega_b^-,4\mathrm{qLR}} &= -4e\mathrm{Re}(V_{ub})(\nu_{18}-\nu_{21})\nu^{ub}-\frac{e\mathrm{Re}(V_{ub})g_1\nu_2\nu^{ub}}{32\pi^2F_\pi^2}F^{(2)}_{M_K}-\frac{e\mathrm{Re}(V_{ub})g_2\nu_3\nu^{ub}}{16\pi^2F_\pi^2}F^{(1)}_{M_K},
\end{aligned}
\tag{5.33}
$$

where the loop functions are defined as

$$
\begin{aligned}
F^{(1)}_{M_\pi} &= 1+32\pi^2L+2\ln\left[\frac{M_\pi}{\lambda}\right],\\
F^{(2)}_{M_\pi} &= 1+32\pi^2L+2\ln\left[\frac{M_\pi}{\lambda}\right]+\frac{2\Delta}{\sqrt{\Delta^2-M_\pi^2}}\ln\left[\frac{\Delta}{M_\pi}+\sqrt{\frac{\Delta^2}{M_\pi^2}-1}\right],\\
F^{(1)}_{M_K} &= 1+32\pi^2L+2\ln\left[\frac{M_K}{\lambda}\right],\\
F^{(2)}_{M_K} &= 1+32\pi^2L+2\ln\left[\frac{M_K}{\lambda}\right]+\frac{2\Delta\arccos\left[\frac{\Delta}{M_K}\right]}{\sqrt{M_K^2-\Delta^2}}.
\end{aligned}
\tag{5.34}
$$

5.6 Patterns of EDMs

Before discussing the absolute sizes of the EDMs in the next section, we investigate the relative sizes of the various EDMs. The relative sizes are essentially determined by the chiral symmetry properties and field content of the underlying sources of CP violation. For instance, for the bottom qEDM at the order at which we work, the EDMs of all baryons in the triplet or the sextet are determined by a single LEC, c_1 and c_2, in order. This pattern is different for the qCEDM where in the triplet $d_{\Xi_b^-}$ is expected to be different from $d^\gamma_{\Lambda_b^0} = d^\gamma_{\Xi_b^0}$. Similarly, in the sextet we obtain the relations for the qCEDM $d^\gamma_{\Sigma_b^-} + d^\gamma_{\Sigma_b^+} = 2d^\gamma_{\Sigma_b^0}$, which are also true for the qEDM, but $d^\gamma_{\Sigma_b^-} \neq d^\gamma_{\Sigma_b^+}$. These differences arise because in order for the qCEDM to generate an EDM of a baryon, an insertion of the quark charge is required. As such, EDMs of baryons with a single b quark but different charges differ for the qCEDM. This is not true for the bottom qEDM as the operator already contains a photon.
A richer pattern emerges for the four-quark operators as here loop diagrams provide leading contributions. For instance, for the 4qLR we observe that the tree-level contributions to the triplet and sextet EDMs have an identical pattern as that of the qCEDM. However, the loop contributions induce differences. In the triplet, loop contributions lead to a splitting in the EDMs of the neutral baryons and $d^\gamma_{\Lambda_b^0} \neq d^\gamma_{\Xi_b^0}$, because of the different Goldstone bosons participating in the loops. We find

$$d^\gamma_{\Lambda_b^0,\text{4qLR}} - d^\gamma_{\Xi_b^0,\text{4qLR}} = \frac{e\text{Re}(V_{ub})g_2\nu_3\nu^{ub}}{16\pi^2F_\pi^2}\left(2\ln\left[\frac{M_K}{M_\pi}\right] + \frac{2\Delta\arccos\left[\frac{\Delta}{M_K}\right]}{\sqrt{M_K^2-\Delta^2}} - \frac{2\Delta}{\sqrt{\Delta^2-M_\pi^2}}\ln\left[\frac{\Delta}{M_\pi} + \sqrt{\frac{\Delta^2}{M_\pi^2}-1}\right]\right) \tag{5.35}$$

which is nonzero and finite, whereas for the qCEDM this combination vanishes. In the same way, the degeneracy that is present for the qCEDM for the negatively charged sextet baryons is broken by the 4qLR operator. To illustrate this, while for both the qCEDM and the 4qLF we have $d^\gamma_{\Xi_b'^-} - (d^\gamma_{\Sigma_b^-} + d^\gamma_{\Omega_b^-})/2 = 0$, only for the 4qLF $d^\gamma_{\Sigma_b^-} - d^\gamma_{\Omega_b^-} \neq 0$ (and finite).
Finally, for the 4q operators an even different pattern of EDMs arises depending on the flavor configuration of the underlying operator. From Eqs. (5.15) and (5.19) it is clear that the chiral symmetry properties of μ^{ub} is identical to the 4qLR operator $\sim \nu^{ub}$. As such, for μ^{ub} the same pattern of EDMs emerges as for the 4qLR and these sources cannot be separated from symmetry arguments alone. Different patterns do emerge for μ^{db} and μ^{sb}. For example, the splitting in the triplet is different for μ^{db} with respect to the 4qLR but this can probably only be used with additional information on the LECs.
The above considerations indicate that the pattern of EDMs of bottom baryons provide information about the source of CP violation. If experiments, for instance those proposed in Refs. [47–49], were to see nonzero signals, this information could be used to pinpoint the underlying mechanism. Much more could be said with nonperturbative information about the LECs appearing in the Lagrangians.

5.7 How large are the EDMs?

To determine the sizes of the EDMs of bottom baryons as function of the various dimension-six Wilson coefficients appearing in Eq. (5.1), estimates of the various LECs appearing in EDM expressions are necessary. This requires non-perturbative QCD calculations of the associated matrix elements. While a lot of progress has been made in this direction for EDMs of systems containing first-generation quarks, see e.g. Ref. [222] for a recent review, as far as we know no calculations have been performed for baryons containing heavier valence quarks. In this work, we estimate the contributions using naive dimensional analysis (NDA), a technique discussed in detail in Refs. [197, 198] and used for nucleon EDMs in Ref. [200]. While NDA does not give accurate predictions, it provides a reasonable order-of-magnitude estimate for meson and single-baryon matrix elements and is the guiding principle for a systematic power counting in effective field theories.
The EDMs of the bottom baryons under consideration depend, for each source of CP violation, on several LECs. The easiest estimate are for the bottom EDM. NDA predicts

$$c_{1,2} = O(d_b) = O\left(\frac{m_b}{\Lambda^2}\right), \tag{5.36}$$

which is a rather intuitive result. The bottom quark EDM operator directly induces a bottom baryon EDM up to order-one factors. The factors could be calculated with non-perturbative methods such as lattice QCD or estimated using a quark model. For light quarks, for instance, lattice QCD predicts the neutron EDM to be $d_n = 0.82 d_d - 0.21 d_u$ [223] in agreement with NDA estimates.
Next, we consider the quark CEDM. In this case we need to estimate the LECs b_{16}-b_{20}. NDA predicts

$$b_{16\text{–}20} = O\left(\tilde{d}_b \frac{F_\pi}{\Lambda_\chi} e\right) = O\left(e \frac{F_\pi m_b}{\Lambda_\chi \Lambda^2}\right), \tag{5.37}$$

where we used $4\pi F_\pi \sim \Lambda_\chi$. The loop diagrams only contribute at next-to-next-to-leading order. It would be interesting to compare these predictions with other estimates, for instance through QCD sum rules.
For the four-quark operators we need to estimate both the tree-level LECs as well as the CP-odd Goldstone boson-baryon interactions. For the $4q$ terms we obtain

$$\begin{aligned} \mu_{6\text{–}10}\, \mu^{qb} &= O\left(\mu^{qb} \Lambda_\chi F_\pi^2\right) = O\left(\frac{\Lambda_\chi F_\pi^2}{\Lambda^2}\right), \\ \mu_{11\text{–}21}\, \mu^{qb} &= O\left(e \mu^{qb} \frac{F_\pi^2}{\Lambda_\chi}\right) = O\left(e \frac{F_\pi^2}{\Lambda_\chi \Lambda^2}\right), \end{aligned} \tag{5.38}$$

where $q = \{u, d, s\}$. While the Goldstone boson-baryon terms scale as $\sim \Lambda_\chi^1$, and are thus of lower order than the EDM vertices $\sim \Lambda_\chi^{-1}$, they only contribute to the EDMs at the one-loop level bringing in a loop factor $e/(4\pi F_\pi)^2 \sim e\Lambda_\chi^{-2}$ so that both type of vertices contribute at the same order.

Similarly for the 4qLR operator we obtain

$$\begin{aligned} \nu_{1-5}\,\nu^{ub} &= O\left(\nu^{ub}\Lambda_\chi F_\pi^2\right) = O\left(\frac{\Lambda_\chi F_\pi^2}{\Lambda^2}\right), \\ \nu_{11-21}\,\nu^{ub} &= O\left(e\nu^{ub}\frac{F_\pi^2}{\Lambda_\chi}\right) = O\left(e\frac{F_\pi^2}{\Lambda_\chi\Lambda^2}\right). \end{aligned} \tag{5.39}$$

While the NDA estimates are rough they give a reasonable idea of the scale of BSM physics that can be probed by measuring EDMs of bottom baryons with a given sensitivity. For instance, for a BSM physics scale[1] $\Lambda = 1$ TeV, and considering only the tree-level expressions we estimate

$$d_{B_b}^{\gamma} = \{10^{-19}, 10^{-20}, 10^{-21}, 10^{-24}\}\, e\,\mathrm{cm}, \tag{5.40}$$

for the qEDM, qCEDM, 4q, and 4qLR operator, respectively. The smallness of the last term is explained by the factor of $\mathrm{Re}(V_{ub})$. These estimates involve a sizeable uncertainty. Nevertheless, they can be used to determine the reach of a potential program to measure the EDMs of bottom-quark baryons. To get an idea of the uncertainty we used a Monte Carlo (MC) sampling of the LECs that appear in the EDM expressions. For instance, for the qEDM operator we rescaled the LECs

$$c_{1,2} \to \left(\frac{m_b}{\Lambda^2}\right)\tilde{c}_{1,2}, \tag{5.41}$$

and vary the dimensionless constants $\tilde{c}_{1,2}$ between $[-3, +3]$. After the MC sampling we obtain a list of different values for the qEDM contribution from which we compute the mean value and the standard deviation. We use this procedure for all LECs appearing in the EDM expression and obtain the mean values and standard deviations for the various EDMs for each CP-odd source in Tables 5.4 and 5.5. The MC method is just a tool to determine roughly in what range we can expect an EDM for the various sources at a given scale Λ. The expressions for the EDMs, where the LECs are rescaled with their respective NDA estimates for the MC sampling, are given in App. C.2. In Table 5.4 we collect the different contributions to the EDMs of the anti-triplet states. For each source, we get, unsurprisingly, results that vary around zero with a spread given by the NDA estimates. There is roughly an order-of-magnitude uncertainty. As expected, the qEDM dominates, whereas the 4qLR-term gives the smallest contribution. The standard deviations for all contributions are relatively large, which is explained by the wide range of the dimensionless constants which was used in the MC sampling. The same observations can also be drawn from Table 5.5. In the case that all four dimension-six operators contribute at the same BSM scale Λ, we can take a look at the resulting size of the EDM by adding up the single contributions. Taking the Ω_b^- baryon as an example, the total

[1] This scale is comparable to indirect limits obtained from traditional EDM experiments. For example, a b-quark EDM mixes with a b-quark CEDM under the one-loop QED renormalization group. At the b-quark threshold, the latter induces a Weinberg three-gluon operator [205] which, in turn, induces a neutron EDM. Based on this procedure Ref. [207] quotes an indirect limit $d_b < 1.2 \cdot 10^{-2}$ e cm. Using our parametrization $d_b = m_b/\Lambda^2$ we get $\Lambda > 2$ TeV. However, this indirect limit suffers from a large theoretical uncertainty due to the poorly known neutron EDM matrix element of the Weinberg operator [206, 208]. Furthermore, the neutron EDM can get contributions from other sources. We therefore consider $\Lambda = 1$ TeV as a reasonable and pragmatic choice.

Table 5.4: Numerical contributions to the EDMs of the anti-triplet baryons for $\Lambda = 1\,\text{TeV}$. The results are given in $10^{-19}\,e\,\text{cm}$, $10^{-20}\,e\,\text{cm}$, $10^{-21}\,e\,\text{cm}$, and $10^{-24}\,e\,\text{cm}$ for the qEDM-, qCEDM-, 4q-, and 4qLR-operator, respectively.

Contribution	Λ_b^0	Ξ_b^0	Ξ_b^-
qEDM	-0.24 ± 5.7	-0.24 ± 5.7	-0.24 ± 5.7
qCEDM	$+0.18 \pm 4.6$	$+0.18 \pm 4.6$	$+0.40 \pm 6.5$
4q	-0.070 ± 2.4	-0.020 ± 2.5	$+0.040 \pm 3.2$
4qLR	$+0.15 \pm 9.4$	$+0.58 \pm 9.6$	-0.11 ± 10.8

Table 5.5: Numerical contributions to the EDMs of the sextet baryons for $\Lambda = 1\,\text{TeV}$. The results are given in $10^{-19}\,e\,\text{cm}$, $10^{-20}\,e\,\text{cm}$, $10^{-21}\,e\,\text{cm}$, and $10^{-24}\,e\,\text{cm}$ for the qEDM-, qCEDM-, 4q-, and 4qLR-operator, respectively.

Contribution	Σ_b^+	Σ_b^0	Σ_b^-
qEDM	-0.16 ± 2.8	-0.16 ± 2.8	-0.16 ± 2.8
qCEDM	$+0.10 \pm 3.3$	$+0.04 \pm 2.2$	$+0.070 \pm 3.3$
4q	-0.050 ± 2.1	$+0.070 \pm 1.2$	$+0.040 \pm 2.1$
4qLR	-0.23 ± 7.9	-0.010 ± 4.9	$+0.21 \pm 5.7$
Contribution	$\Xi_b^{\prime 0}$	$\Xi_b^{\prime -}$	Ω_b^-
qEDM	-0.16 ± 2.8	-0.16 ± 2.8	-0.16 ± 2.8
qCEDM	$+0.040 \pm 2.2$	$+0.070 \pm 3.3$	$+0.070 \pm 3.3$
4q	$+0.020 \pm 1.3$	$+0.050 \pm 1.6$	-0.060 ± 2.0
4qLR	$+0.050 \pm 4.8$	$+0.21 \pm 5.6$	$+0.35 \pm 5.3$

EDM would be

$$d^{\gamma}_{\Omega_b^-} = (-0.15 \pm 3.2) \times 10^{-19}\,(\text{TeV}/\Lambda)^2\ e\,\text{cm}\,. \tag{5.42}$$

This value is of course not to be understood as a clear prediction, but as an estimate for the range where the EDM of the Ω_b^- baryon can be found. The experiment would involve the positively charged anti-baryons (e.g. Ω_b^+) whose EDMs are the same as the corresponding baryons by CPT. The errors here reflect the uncertainty on the hadronic theory and, while the error band includes zero, nothing would indicate a vanishing matrix element. For the qEDM and qCEDM operators, indirect limits have been set from the EDM of the neutron and diamagnetic atoms [205–208]. We do not compare these limits here in detail as the indirect limits are plagued by sizeable uncertainties as well (mainly from matrix elements connecting the three-gluon Weinberg operator to the neutron EDM) and assume that there are not other contributions to the neutron EDM (for instance from EDMs or CEDMs of light quarks). Our main goal here is to assess the reach of a potential experimental program to measure the EDMs of bottom-quark baryons.

5.8 Conclusion

Electric dipole moment experiments provide one of the most sensitive searches for BSM physics. Most focus has been on EDMs of stable systems consisting of first-generation quarks, but it has been proposed to look for EDMs of baryons containing heavier quarks as well [47–49]. Such systems are sensitive to CP-odd operators involving second- and third-generation quarks and complement existing searches. However, essentially no theoretical calculations have been performed to guide this developing experimental program.
In this paper, we have analyzed the EDMs of spin-$1/2$ baryons containing a single bottom quark. Our starting point has been operators of dimension-six in the SMEFT Lagrangian that violate CP and contain a $\bar{b}\Gamma b$ bilinear (where Γ denotes a Lorentz structure). We considered a hypothetical bottom quark EDM and chromo-EDM, and several four-quark operators mixing bottom quarks with lighter quarks. We used chiral perturbation theory to construct the resulting CP-violating hadronic interactions between spin-$1/2$ single-bottom baryons, Goldstone bosons, and photons, and calculated the EDMs up to the first non-vanishing order for each source of CP violation.
Our results indicate that different sources of CP violation lead to a different pattern of EDMs due to the chiral- and isospin-symmetry properties of the underlying sources. In principle, this would allow for the identification of the dominant source of CP violation based on the relative sizes of EDMs of triplet and sextet bottom-quark baryons. The absolute sizes of the EDMs, however, are very uncertain as very little is known about the magnitudes of the low-energy constants appearing in the CP-odd chiral Lagrangian. We made estimates using naive dimensional analysis and found that for BSM scales of 1 TeV, we can expect EDMs in the range of $10^{-19} - 10^{-24}$ e cm depending strongly on the dimension-six operators under consideration. All EDMs scale as Λ^{-2} so the sizes of the EDMs can easily be obtained for other BSM scales. If the experimental program picks up steam and EDMs of these systems are targeted it would be good to calculate the LECs with non-perturbative techniques to get more reliable estimates. The techniques developed in this work can be readily extended to calculate EDMs of charmed baryons and work along these lines is in progress.

Acknowledgements

Partial financial support from the DFG (Project number 196253076 - TRR 110) and the NSFC (Grant No. 11621131001) through the funds provided to the Sino-German CRC 110 “Symmetries and the Emergence of Structure in QCD", by the Chinese Academy of Sciences (CAS) through a President’s International Fellowship Initiative (PIFI) (Grant No. 2018DM0034), by the VolkswagenStiftung (Grant No. 93562), and by the EU Horizon 2020 research and innovation programme, STRONG-2020 project (Grant No. 824093) is acknowledged.

CHAPTER 6

Summary and conclusion

In this last chapter we want to summarize the most important results of the thesis and give some remarks towards future research projects. We emphasize, however, that each chapter in this work, which has been published in a scientific journal, contains its separate summary and conclusion. The following text is mostly a repitition of these sections.

The main part of this thesis was dedicated to study the Roper resonance in a finite volume. In chapter 3 we analyzed the resonance in a finite volume within the framework of baryon chiral perturbation theory (BChPT). We repeated the calculation of the Roper self-energy up to third chiral order in the infinite volume and saw that the result agreed with the literature. Then, we made the transition to the finite-volume formalism in order to find the corrections to the energy levels of the system in a finite box with length L. We saw that the finite-volume corrections of the self-energy contain exponentially suppressed contributions, as well as contributions with poles. The exponentially decaying contributions could be neglected for large L, but the terms containing poles had to be regularized. For the numerical evaluation of the finite-volume energy levels, we found that only two low-energy constants (LECs) enter the equation, which were already determined in Ref. [22]. The other parameters in the equation included baryon and pion masses, as well as other known LECs from BChPT. The main results, which we observed in the spectra are the following: In the delta-free case ($h_R = 0$), i.e. considering only nucleon and pion as intermediate states, the avoided level crossing is clearly seen in the vicinity of the Roper resonance energy. For large box sizes, the energy levels approach the free energy levels asymptotically. In the nucleon-free case ($g_{\pi NR} = 0$), i.e. considering only a stable delta resonance and pion as intermediate states, there are no clear signs for avoided level crossing. This is most likely caused by two effects: First, the large value of the coupling h_R can wash out the typical avoided level signature. Second, the energy region, where the non-interacting $\Delta\pi$ levels lie, is mostly above the Roper resonance mass. Therefore, the Roper cannot influence the shape of the energy levels significantly. We also observed that the approach of the interacting levels to the free ones for large L is not as explicit as in the delta free case. Lastly, we considered the full coupled-channel system including nucleons and deltas. Avoided level crossing was again visible near the Roper resonance mass and also the free energy levels are approached asymptotically for large box sizes. All calculations described here can also be performed at larger, non-physical pion masses.
One of the biggest issues in this first consideration of the Roper resonance spectrum is the treatment of the delta resonance in the finite volume. Assuming that the delta is a stable particle is a reasonable first

approximation, but in further calculations its resonance characteristic has to be included. A possible decay of the delta into a nucleon and a pion would result in the three-particle $N\pi\pi$ final state the Roper is known for. Note, that the delta is also not the only possible intermediate resonance state, since there can also be contributions from the $f_0(500)$ resonance (also known as σ meson). A future study on the Roper resonance within the framework of BChPT can include the σ as an additional degree of freedom. Also, a calculation to fourth (or higher) order in the chiral expansion can be considered. However, both of these extensions would come with the cost of increasing the number of LECs and some of them might not be fixed easily with the current available (experimental or lattice) data.

In chapter 4, we have analyzed the finite-volume spectrum of the Roper resonance using a particle-dimer approach. This approached offered a practical framework to implement the unstable nature of resonances into the finite-volume spectrum of the Roper. A non-relativistic covariant Lagrangian was introduced with nucleons, pions and three dimer fields as degrees of freedom. These three dimer fields include the Roper resonance itself, the σ-meson and the Δ-resonance. We added a dynamical term in the Lagrangian for the Roper, but kept the σ- and Δ-dimer static. Then, the Roper resonance self-energy was calculated within our framework to one-loop order. Additionally, we investigated the σ- and Δ-dimer fields even further and dressed their corresponding propagators, which is a crucial step in order to include three-particle dynamics explicitly. From then on, we restricted ourselves to a finite volume like in chapter 3. We derived an equation, which enabled us to calculate the self-energy of the Roper resonance in the finite volume and we showed how the interacting energy levels of the Roper system can be extracted from it. Afterwards, several methods were discussed to determine the appearing LECs that contribute to the self-energy corrections. This also included a comparison between our introduced formalism and existing lattice data on $\pi\pi$ scattering, which helped us to fix LECs coming from the σ-dimer field. Then, the finite-volume spectrum of the Roper resonance was calculated for various cases. The most important findings are the following: The energy spectrum involving only nucleons and pions as intermediate states showed a very good agreement to the delta-free case from chapter 3. Avoided level crossing can clearly be observed around the Roper resonance mass and the energy levels approach the non-interacting $N\pi$ energies for large box sizes. The striking similarity to the result from BChPT, which includes full Lorentz invariance, spin and isospin structure, was one of the main arguments to continue with the non-relativistic covariant approach. Then, the particle-dimer fields were included in the calculation. The implementation of the $N\sigma$ channel into the Roper resonance spectrum, where the σ-dimer is dressed by the corresponding $\pi\pi$ loops, was able to generate three-body ($N\pi\pi$) dynamics. The interacting energy levels approached the free $N\pi\pi$ levels for large box sizes L. However, no clear signs of avoided level crossing were visible. A similar behaviour was also observed for the channel containing the Δ-dimer field. Next, the $N\pi$ and $N\sigma$ contributions were combined in one coupled-channel system. The obtained interacting energy levels lie very close to their respective free $N\pi$ and $N\pi\pi$ levels. This is most likely caused by the very large contribution of the double sum in the $N\sigma$ self-energy term. Also here, no avoided level crossing is observed. Lastly, our results were compared to the Roper energy levels obtained from lattice QCD in Ref. [15]. We observed an overall very good agreement. Overall, the newly proposed approach to investigate the finite-volume spectrum of the Roper resonance seems to offer a fairly simple, but systematically improvable alternative to already existing methods. This first implementation of our formalism shows that effects coming from $N\sigma$ or $\Delta\pi$ channels can be distinguished in the spectrum once more precise lattice results are available. Thus, the approach already serves as a valuable guide for the precision that future lattice QCD studies need to provide. However, it is necessary to include

some improvements in the formalism, like spin and isospin projections. In addition, couplings between the dimer fields, which allow for pion exchange inside the Roper self-energy diagrams, should be included. This, however, implies that two-loop diagrams need to be evaluated. Nevertheless, only in this scenario a full $N\pi/N\sigma/\Delta\pi$ coupled-channel system can be considered.

Then, in the last part of this work, chapter 5, we moved away from the Roper resonance and considered the electric dipole moments (EDMs) of heavy bottom baryons. We have seen that the investigation of EDMs is not only important for testing Standard Model parameters, but also for the hunt of beyond-the-Standard-Model (BSM) physics. In fact, EDM experiments provide one of the most sensitive methods to look for BSM physics. While the main focus of EDM searches lies, so far, on stable systems containing first-generation quarks (e.g. measuring the neutron EDM), it has also been proposed to look for EDMs of baryons containing heavier quarks. These systems should be much more sensitive to higher-dimensional CP-odd operators involving second- and third-generation quarks. However, no theoretical calculations have been performed yet to guide the developement of experimental programs searching for EDMs in those systems. This changed with the work presented in this thesis. We analyzed the EDMs of spin-$1/2$ baryons containing a single bottom quark. The starting point was the consideration of dimension-six operators from the Standard Model effective field theory (SMEFT) Lagrangian, which violate CP and contain a bilinear of bottom quarks. These operators include a bottom quark EDM and chromo-EDM, as well as several four-quark operators mixing bottom quarks with lighter quarks. Then, we used methods from chiral perturbation theory to construct the resulting CP-violating Lagrangian at the baryon level. This Lagrangian includes interactions between spin-$1/2$ single-bottom baryons, Goldstone bosons and photons. After that, the EDMs of the bottom baryons were calculated up to the first non-vanishing order for each of the CP-violating sources. The results indicated that the different dimension-six terms lead to specific patterns in the EDMs due to the symmetry properties of the underlying operators. This could in principle allow to identify the dominant source of CP violation based on the relative sizes of the triplet and sextet bottom baryon EDMs. However, the question arises weather future experiments can achieve the required precision to resolve those patterns. In fact, also the absolute sizes of the EDMs are quite uncertain as not a lot is known about the magnitudes of the LECs appearing in the CP-odd chiral Lagrangian. We, therefore, assumed that BSM physics emerges at a scale of $\Lambda \sim 1\,\text{TeV}$ and estimated the LECs using naive dimensional analysis (NDA). From this, we found that the EDMs can range from $10^{-19}\,e\,\text{cm}$ to $10^{-24}\,e\,\text{cm}$ depending on the considered dimension-six SMEFT operator. Since all EDMs scale as Λ^{-2}, the sizes of the EDM estimates can be adjusted easily for other BSM scales as well. Once experimental projects become concrete, other methods to determine the LECs, like e.g. lattice QCD, might be needed to obtain more accurate estimates.
The calculation techniques described here can also be used to obtain the EDMs of single-charm baryons. Additionally, one could investigate the effects of CP-violating SMEFT operators on the lowest-lying hyperons (baryons with strangeness). Work in both of these directions should be considered.

Overall, we have seen that this thesis includes relevant progress in two very interesting and challenging segments of hadron (baryon) physics, which are also highly active research areas today. However, more work is still needed. Especially the Roper resonance with its specific properties remains a challenging and puzzling baryon system, which can only be demystified by a combination of finite-volume EFT methods and lattice QCD. The author of this thesis hopes that the studies performed here can help to guide and motivate future theoretical and experimental investigations in these two fields.

APPENDIX A

Notation and useful information

A.1 General conventions and identities

The following section contains some general conventions and identities relevant for various calculations in this work[1]. Throughout, natural units, i.e.

$$\hbar = c = 1 \,,$$

are used.

We start with the definition of the Minkowski metric. It is given by

$$g_{\mu\nu} = g^{\mu\nu} = \mathrm{diag}\,(1, -1, -1, -1) \,,$$

with μ and ν running over $0, 1, 2, 3$. With this, one can define the Lorentz scalar product of two four-vectors $a^\mu = \left(a^0, \vec{a}\right)$ and $b^\mu = \left(b^0, \vec{b}\right)$,

$$a \cdot b = g_{\mu\nu} a^\mu b^\nu = a_\mu b^\mu = a^0 b^0 - \vec{a} \cdot \vec{b} \,.$$

We will also use a lot of identities for the Dirac gamma matrices γ^μ. They are 4×4-matrices and defined to obey the Clifford algebra

$$\left\{\gamma^\mu, \gamma^\nu\right\} = \gamma^\mu \gamma^\nu + \gamma^\nu \gamma^\mu = 2 g^{\mu\nu} \,.$$

An explicit expression for the matrices is given by the so-called chiral representation

$$\gamma^\mu = \begin{pmatrix} 0 & \sigma^\mu \\ \bar{\sigma}^\mu & 0 \end{pmatrix} \,,$$

[1] The appendices A.1 and A.2 are partly taken from Ref. [224] due to the similarities in notation.

with $\sigma^\mu = (\mathbb{1}, \tau^1, \tau^2, \tau^3)$, and $\bar{\sigma}^\mu = (\mathbb{1}, -\tau^1, -\tau^2, -\tau^3)$, where τ^i are the Pauli matrices,

$$\tau^1 = \begin{pmatrix} 0 & 1 \\ 1 & 0 \end{pmatrix}, \quad \tau^2 = \begin{pmatrix} 0 & -i \\ i & 0 \end{pmatrix}, \quad \tau^3 = \begin{pmatrix} 1 & 0 \\ 0 & -1 \end{pmatrix}.$$

Note that in the literature the Pauli matrices are also very commonly denoted by σ_i. For a more detailed description of gamma matrices, we suggest the appendix of Ref. [4].

Another common mathematical structure appearing in this thesis is the Levi-Civita symbol, or Levi-Civita tensor. In three dimensions it is defined as

$$\epsilon_{ijk} = \epsilon^{ijk} = \begin{cases} +1, & \text{for } i,j,k \text{ even permutation of } 1,2,3 \\ -1, & \text{for } i,j,k \text{ odd permutation of } 1,2,3 \\ 0, & \text{else} \end{cases}.$$

The product of two Levi-Civita tensors can be written as a determinant of Kronecker deltas,

$$\epsilon_{ijk}\epsilon_{lmn} = \det\begin{pmatrix} \delta_{il} & \delta_{im} & \delta_{in} \\ \delta_{jl} & \delta_{jm} & \delta_{jn} \\ \delta_{kl} & \delta_{km} & \delta_{kn} \end{pmatrix},$$

where δ_{ij} is 1, if $i = j$, and 0, if $i \neq j$. If two or four indices are identical, the above relation simplifies to

$$\epsilon_{ijk}\epsilon_{imn} = \delta_{jm}\delta_{kn} - \delta_{jn}\delta_{km}, \quad \text{or} \quad \epsilon_{ijk}\epsilon_{ijn} = 2\delta_{kn}.$$

Physics that involves the strong interaction very often uses the Gell-Mann matrices. An explicit representation of these matrices is given by

$$\lambda^1 = \begin{pmatrix} 0 & 1 & 0 \\ 1 & 0 & 0 \\ 0 & 0 & 0 \end{pmatrix}, \quad \lambda^2 = \begin{pmatrix} 0 & -i & 0 \\ i & 0 & 0 \\ 0 & 0 & 0 \end{pmatrix}, \quad \lambda^3 = \begin{pmatrix} 1 & 0 & 0 \\ 0 & -1 & 0 \\ 0 & 0 & 0 \end{pmatrix}$$
$$\lambda^4 = \begin{pmatrix} 0 & 0 & 1 \\ 0 & 0 & 0 \\ 1 & 0 & 0 \end{pmatrix}, \quad \lambda^5 = \begin{pmatrix} 0 & 0 & -i \\ 0 & 0 & 0 \\ i & 0 & 0 \end{pmatrix}, \quad \lambda^6 = \begin{pmatrix} 0 & 0 & 0 \\ 0 & 0 & 1 \\ 0 & 1 & 0 \end{pmatrix}$$
$$\lambda^7 = \begin{pmatrix} 0 & 0 & 0 \\ 0 & 0 & -i \\ 0 & i & 0 \end{pmatrix}, \quad \lambda^8 = \sqrt{\frac{1}{3}}\begin{pmatrix} 1 & 0 & 0 \\ 0 & 1 & 0 \\ 0 & 0 & -2 \end{pmatrix}.$$

As generators of the SU(3) Lie group, these matrices fulfill the commutation relations

$$\left[\lambda^a, \lambda^b\right] = 2if^{abc}\lambda^c, \quad (\lambda^a)^\dagger = \lambda^a, \quad \mathrm{Tr}(\lambda^a) = 0, \quad \mathrm{Tr}(\lambda^a\lambda^b) = 2\delta^{ab},$$

where $a, b, c = 1, 2, \ldots, 8$ and f^{abc} being the structure constants of SU(3).

A.2 Loop integrals and dimensional regularization

Evaluating loop diagrams is an essential part of theoretical physics. We use the method of dimensional regularization to calculate the loop diagrams and want to illustrate the procedure with an example. For more information, see e.g. Refs [4, 64]. This appendix is partly taken from Ref. [224].

Consider the loop integral of a scalar propagator

$$I_M = \int \frac{d^4k}{(2\pi)^4} \frac{i}{k^2 - M^2 + i\epsilon} \,.$$

This diagram diverges in 4 space-time dimensions (to be exact, it is *quadratically* divergent). In dimensional regularization, the integral is first solved in D dimensions and afterwards the limit $D \to 4$ is taken. The integral obtains the form

$$I_M = \mu^{4-D} \int \frac{d^Dk}{(2\pi)^D} \frac{i}{k^2 - M^2 + i\epsilon} \,,$$

where μ is the renormalization scale. It is an energy scale, which is introduced to maintain the physical dimension of the integral.
To evaluate the integral, a Wick-rotation to Euclidean space is performed by transforming the time component of the four-vector k

$$k^0 \to ik^0 \,,$$

so that

$$k^2 := \left(k^0\right)^2 - \left(k^1\right)^2 - \left(k^2\right)^2 - \left(k^3\right)^2 \Rightarrow -\left(k^0\right)^2 - \left(k^1\right)^2 - \left(k^2\right)^2 - \left(k^3\right)^2 = -k_E^2 \,,$$

with the Euclidean scalar produkt k_E^2. In Euclidean space, the integral is calculated by using spherical coordinates in D dimensions and the result is given by (see e.g. [4])

$$I_M = \frac{\mu^{4-D}}{(4\pi)^{D/2}} \Gamma\left(1 - \frac{D}{2}\right) \left(\frac{1}{M^2}\right)^{(1-D/2)} \,,$$

where $\Gamma(z)$ denotes the gamma function. One can define the parameter $\epsilon := (4 - D)$ and rewrite I_M as

$$I_M = \frac{M^2}{(4\pi)^2} \Gamma\left(-1 + \frac{\epsilon}{2}\right) \left(\frac{4\pi\mu^2}{M^2}\right)^{\epsilon/2} = \frac{M^2}{(4\pi)^2} \left(-\frac{2}{\epsilon}\right) \frac{\Gamma\left(1 + \frac{\epsilon}{2}\right)}{1 - \frac{\epsilon}{2}} \left(\frac{4\pi\mu^2}{M^2}\right)^{\epsilon/2} \,,$$

where the gamma function identities $\Gamma(z + 1) = z\Gamma(z)$ and $\Gamma(1) = 1$ were used. Since the limit $D \to 4$ will be performed, the parameter ϵ is considered to be very small and a Taylor-expansion around $\epsilon = 0$

can be performed

$$I_M = \frac{M^2}{(4\pi)^2}\left[-\frac{2}{\epsilon} - 1 - \Gamma'(1) - \log\left(\frac{4\pi\mu^2}{M^2}\right)\right] + O(\epsilon)$$
$$= \frac{M^2}{(4\pi)^2}\underbrace{\left[-\frac{2}{\epsilon} - \left(\log(4\pi) + \Gamma'(1) + 1\right)\right]}_{=:R} + \frac{M^2}{(4\pi)^2}\log\left(\frac{M^2}{\mu^2}\right) + O(\epsilon)\,,$$

with $\Gamma'(1)$ the derivative of the gamma function evaluated at $z = 1$. Cutting off contributions of $O(\epsilon)$, the result for I_M is given by

$$I_M = \frac{M^2}{16\pi^2}\left[R + \log\left(\frac{M^2}{\mu^2}\right)\right]\,, \tag{A.1}$$

where R contains the divergent piece $2/(D-4)$.
To cancel these divergencies, we will make use of the minimal subtraction scheme of ChPT called $\widetilde{\text{MS}}$. Within this renormalization scheme the bare parameters of the Lagrangian are redefined in such a way that they cancel all terms, which are proportional to R. This ensures that the physical observables stay finite, while the parameters in the Lagrangian are *not* considered to be the physical values. The renormalized version of I_M is

$$I_M^r = \frac{M^2}{16\pi^2}\log\left(\frac{M^2}{\mu^2}\right)\,.$$

In some references the modified minimal subtraction $\overline{\text{MS}}$ scheme is used instead. In this case, the divergent part is given by

$$\lambda_\epsilon = \frac{2}{D-4} - \left[\log(4\pi) + \Gamma'(1)\right]\,,$$

which is the same as $\lambda_\epsilon = R + 1$. It is important to note that the physical observables should *not* depend on the used renormalization scheme.
Another loop integral that appears in our calculation is the following,

$$I_\Delta^{\mu\nu} = \int \frac{d^4k}{(2\pi)^4}\frac{ik^\mu k^\nu}{\left[k^2 - \Delta^2 + i\epsilon\right]^2}\,.$$

For this case the loop integration yields (see also e.g. [4])

$$\mu^{4-D}\int \frac{d^Dk}{(2\pi)^D}\frac{ik^\mu k^\nu}{\left[k^2 - \Delta^2 + i\epsilon\right]^2} = \frac{\mu^{4-D}}{(4\pi)^{D/2}}\frac{g^{\mu\nu}}{2}\Gamma\left(1 - \frac{D}{2}\right)\left(\frac{1}{\Delta^2}\right)^{(1-D/2)}\,.$$

We should also remark that loop integrals with an odd number of loop momenta, like for example

$$I_\Delta^\mu = \int \frac{d^4k}{(2\pi)^4} \frac{ik^\mu}{k^2 - \Delta^2 + i\epsilon} ,$$

will vanish. The reason for this is that the loop function is odd under the transformation $k \mapsto (-k)$, but the integration is symmetric. This allows us to cancel integrals of this form in our calculations.

A.3 Naive dimensional analysis

In the following we want to briefly introduce the concept of naive dimensional analysis (NDA). It was introduced in Refs. [197, 198] and provides a tool to estimate the order of magnitude of low-energy constants (LECs) appearing in an effective field theory (EFT). NDA is prominently applied in the context of chiral perturbation theory (ChPT), because it was developed for this EFT specifically, but it can be used in other EFTs as well. In fact, it is a direct consequence of the systematic power counting utilized in an EFT approach, which makes NDA work in the first place [198]. However, it should be stressed that NDA is not a precise method to fix unknown LECs and can only be used to estimate their sizes.
Let us assume we have a given EFT Lagrangian, where the coupling constant g appears, which we want to estimate. The starting point of NDA is to calculate the so-called reduced coupling constant g^R of the coupling g, which is defined by [197]

$$g^R = g(4\pi)^{2-\mathcal{N}} \Lambda_{EFT}^{D-4} .$$

Here, $\mathcal{N}$ is the number of field operators in the Lagrangian term (operator) that includes g, D is the dimension of said operator and Λ_{EFT} is the scale, where the EFT breaks down. In the case of ChPT, this scale is the chiral symmetry breaking scale Λ_χ. After calculating g^R, one matches it to the respective reduced coupling of the Lagrangian from the fundamental theory. The concept is best understood by using an example. Let us estimate the order of magnitude of the axial-vector coupling g_A from the nucleon-pion Lagrangian (see Eq. (2.40) in chapter 2). The axial interaction term is given by

$$\mathcal{L}_{int} \propto -\frac{g_A}{F_\pi} \bar{\Psi} \gamma^\mu (\partial_\mu \phi) \gamma_5 \Psi .$$

We observe that there are three field operators (two nucleon fields and one pion field) and the dimension of the operator is $D = 5$ due to the derivative in front of the pion field. The reduced coupling $(g_A/F_\pi)^R$ then takes the form

$$\left(\frac{g_A}{F_\pi}\right)^R = \frac{g_A}{F_\pi}(4\pi)^{2-3}\Lambda_\chi^{5-4} = \frac{g_A}{F_\pi}\frac{1}{4\pi}\Lambda_\chi = g_A ,$$

where we used that $\Lambda_\chi \sim 4\pi F_\pi$ in the last step. We now need to match this reduced coupling constant to the fundamental theory QCD. The only coupling that appears in the QCD Lagrangian is the strong coupling constant g_s. The interaction term of the quarks with the gluon fields is (Eq. (2.17) in

chapter 2)

$$\mathcal{L}_{\text{QCD}} \propto -g_s \bar{q} \gamma^\mu A^a_\mu \lambda^a q \ .$$

The reduced coupling of g_s is then given by

$$(g_s)^R = \frac{g_s}{4\pi} \ ,$$

because we have three field operators in the interaction term and its dimension is $D = 4$. Naturally, we need to match the reduced couplings at a scale where QCD becomes non-perturbative and, therefore, we expect $(g_s)^R$ to be at least of order one, $(g_s)^R = O(1)$. Thus, it follows that

$$(g_s)^R = \left(\frac{g_A}{F_\pi}\right)^R = g_A \ ,$$

and hence we have $g_A \sim 1$, which agrees very well with the experimental value $g_A \simeq 1.27$ [13]. For more examples see also the appendix of Ref. [225]. We use NDA in chapter 5, when we estimate the sizes of the EDMs of the bottom baryons.

APPENDIX B

The Roper resonance in a finite volume

B.1 Passarino-Veltman Integrals

The Passarino-Veltman Integrals [226] (see also Ref. [227]) are a specific representation of loop integrals, which we use here. The infinities emerging from the evaluation of the loop integrals in dimensional regularization are contained in R, which is given by

$$R = \frac{2}{D-4} - \left[\log(4\pi) + \Gamma'(1) + 1\right] ,$$

where D denotes the space-time dimension and Γ is the Gamma function. This term will be cancelled in the $\widetilde{\text{MS}}$ renormalization scheme (see App. A.2), which is commonly used in ChPT calculations.

The following list contains the loop functions that appear in our calculations and gives their respective results in the infinite volume.

- Integral with one propagator:

$$\begin{aligned} A_0(m^2) &= -16\pi^2 i\mu^{4-D} \int \frac{d^D k}{(2\pi)^D} \frac{1}{k^2 - m^2 + i\epsilon} \\ &= -m^2 \left[R + \log\left(\frac{m^2}{\mu^2}\right)\right] . \end{aligned}$$

- Integral with two propagators:

$$\begin{aligned} B_0(p^2, m^2, M^2) &= -16\pi^2 i\mu^{4-D} \int \frac{d^D k}{(2\pi)^D} \frac{1}{[k^2 - m^2 + i\epsilon][(k-p)^2 - M^2 + i\epsilon]} \\ &= (-1) \left[R - 1 + \log\left(\frac{m^2}{\mu^2}\right) + \frac{p^2 - m^2 + M^2}{p^2} \log\left(\frac{M}{m}\right) \right. \\ &\quad \left. + \frac{2mM}{p^2} F(\Omega) \right] , \end{aligned}$$

where

$$F(\Omega) = \begin{cases} \sqrt{\Omega^2-1}\log(-\Omega-\sqrt{\Omega^2-1})\,, & \Omega \leq -1 \\ \sqrt{1-\Omega^2}\arccos(-\Omega)\,, & -1 \leq \Omega \leq 1 \\ \sqrt{\Omega^2-1}\log(\Omega+\sqrt{\Omega^2-1}) - i\pi\sqrt{\Omega^2-1}\,, & 1 \leq \Omega \end{cases},$$

and

$$\Omega = \frac{p^2 - m^2 - M^2}{2mM}\,.$$

- Tensor integrals with two propagators:

$$\begin{aligned} B^\mu(p^2,m^2,M^2) &= -16\pi^2 i\mu^{4-D}\int \frac{d^Dk}{(2\pi)^D}\frac{k^\mu}{[k^2-m^2+i\epsilon][(k-p)^2-M^2+i\epsilon]} \\ &:= p^\mu B_1(p^2,m^2,M^2)\,, \end{aligned}$$

where

$$B_1(p^2,m^2,M^2) = \frac{1}{2p^2}\left\{\left[p^2+m^2-M^2\right]B_0(p^2,m^2,M^2) - A_0(m^2) + A_0(M^2)\right\},$$

and

$$\begin{aligned} B^{\mu\nu}(p^2,m^2,M^2) &= -16\pi^2 i\mu^{4-D}\int \frac{d^Dk}{(2\pi)^D}\frac{k^\mu k^\nu}{[k^2-m^2+i\epsilon][(k-p)^2-M^2+i\epsilon]} \\ &:= g^{\mu\nu}B_{00}(p^2,m^2,M^2) + p^\mu p^\nu B_{11}(p^2,m^2,M^2) \end{aligned}$$

with

$$\begin{aligned} B_{00}(p^2,m^2,M^2) = \frac{1}{2(D-1)}\Big\{&2m^2B_0(p^2,m^2,M^2) + A_0(M^2) \\ &- \left[p^2+m^2-M^2\right]B_1(p^2,m^2,M^2)\Big\}\,, \end{aligned}$$

and

$$\begin{aligned} B_{11}(p^2,m^2,M^2) = \frac{1}{2p^2}\Big\{&\left[p^2+m^2-M^2\right]B_1(p^2,m^2,M^2) \\ &+ A_0(M^2) - 2B_{00}(p^2,m^2,M^2)\Big\}\,. \end{aligned}$$

- Integral with three propagators:

$$C_0(0,p^2,p^2,m^2,m^2,M^2) = i\mu^{4-D}\int\frac{d^Dk}{(2\pi)^D}\frac{-16\pi^2}{\left[k^2-m^2+i\epsilon\right]^2\left[(k-p)^2-M^2+i\epsilon\right]}$$
$$= \left(\frac{1}{2m}\right)\frac{\partial}{\partial m}B_0(p^2,m^2,M^2)\,,$$

  and

$$C_1(0,p^2,p^2,m^2,m^2,M^2) = \frac{1}{4p^2}\Big[B_0(p^2,m^2,M^2) - B_0(0,m^2,m^2)$$
$$+(m^2-p^2-M^2)C_0(0,p^2,p^2,m^2,m^2,M^2)\Big]\,.$$

There are also some special cases appearing, which are listed below

$$B_0(0,m^2,m^2) = (-1)\left[R+1+\log\left(\frac{m^2}{\mu^2}\right)\right]\,,$$

$$B_0(m^2,0,m^2) = (-1)\left[R-1+\log\left(\frac{m^2}{\mu^2}\right)\right]\,.$$

These relations can be shown with the explicit form of B_0 and it follows that

$$B_0(0,m^2,m^2)+2 = B_0(m^2,0,m^2)\,.$$

B.2 Useful Formulas

This section contains a handful of useful formulas that were used in our calculations.

- Feynman parameter:

$$\frac{1}{AB} = \int_0^1\frac{dy}{[yA+(1-y)B]^2}\,.$$

- Modified Bessel functions of the second kind (see, e.g., [228]):

$$K_\nu(z) := \int_0^\infty dt\cosh(\nu t)\,e^{-z\cosh(t)}\,,\quad \text{for } z>0\,.$$

  Special case:

$$K_0(z) = \int_0^\infty dt\frac{\cos(zt)}{\sqrt{t^2+1}}\,,\quad \text{for } z>0\,.$$

APPENDIX C

Electric dipole moments of baryons with bottom quarks

C.1 Form Factors

The full expression for the neutral and charged b-baryon form factors up to the order $O(\delta^2)$ with the tree-level results are

$$
\begin{aligned}
D^{\gamma}_{\Lambda_b^0}(q^2) &= 4c_1 - 4e\Big(b_{19} - \mu_{11}(\mu^{ub} - \mu^{db}) + \mu_{14}(\mu^{ub} + \mu^{db}) - 2\mu_{20}(\mu^{ub} - \mu^{db} - \mu^{sb}) \\
&\quad - \mathrm{Re}(V_{ub})(\nu_{11} - \nu_{14} + 2\nu_{20})\nu^{ub}\Big) \\
&\quad + \frac{eg_2}{4F_\pi^2}\Big(\mathrm{Re}(V_{ub})\nu_3\nu^{ub} + \mu_8(\mu^{ub} + \mu^{sb})\Big)\int_0^1 dx\,\frac{1}{\tilde{M}_K}\frac{\partial}{\partial\tilde{M}_K}J_1(-\Delta,\tilde{M}_K), \\
D^{\gamma}_{\Xi_b^0}(q^2) &= 4c_1 - 4e\Big(b_{19} - \mu_{11}(\mu^{ub} - \mu^{sb}) + \mu_{14}(\mu^{ub} + \mu^{sb}) - 2\mu_{20}(\mu^{ub} - \mu^{db} - \mu^{sb}) \\
&\quad - \mathrm{Re}(V_{ub})(\nu_{11} - \nu_{14} + 2\nu_{20})\nu^{ub}\Big) \\
&\quad + \frac{eg_2}{4F_\pi^2}\Big(\mathrm{Re}(V_{ub})\nu_3\nu^{ub} + \mu_8(\mu^{ub} + \mu^{db})\Big)\int_0^1 dx\,\frac{1}{\tilde{M}_\pi}\frac{\partial}{\partial\tilde{M}_\pi}J_1(-\Delta,\tilde{M}_\pi), \\
D^{\gamma}_{\Xi_b^-}(q^2) &= 4c_1 - 4e\Big(b_{16} + b_{19} + (\mu_{11} + \mu_{14})(\mu^{db} + \mu^{sb}) + 2\mu_{17}(\mu^{ub} + \mu^{db} + \mu^{sb}) \\
&\quad - 2\mu_{20}(\mu^{ub} - \mu^{db} - \mu^{sb}) + 2\mathrm{Re}(V_{ub})(\nu_{17} - \nu_{20})\nu^{ub}\Big) \\
&\quad - \frac{eg_2}{4\pi^2F_\pi^2}\Big(\mathrm{Re}(V_{ub})\nu_3\nu^{ub} + \mu_8(\mu^{ub} + \mu^{sb})\Big)\int_0^1 dx\,\frac{1}{\tilde{M}_K}\frac{\partial}{\partial\tilde{M}_K}J_1(-\Delta,\tilde{M}_K) \\
&\quad - \frac{eg_2}{4\pi^2F_\pi^2}\Big(\mathrm{Re}(V_{ub})\nu_3\nu^{ub} + \mu_8(\mu^{ub} + \mu^{db})\Big)\int_0^1 dx\,\frac{1}{\tilde{M}_\pi}\frac{\partial}{\partial\tilde{M}_\pi}J_1(-\Delta,\tilde{M}_\pi),
\end{aligned}
$$

$$
\begin{aligned}
D^{\gamma}_{\Sigma_b^+}(q^2) &= 2c_2 + 2e\Big(b_{17} - b_{20} + 2(\mu_{12} - \mu_{15})\mu^{ub} + 2\mu_{18}(\mu^{ub} + \mu^{db} + \mu^{sb}) \\
&\quad + 2\mu_{21}(\mu^{ub} - \mu^{db} - \mu^{sb}) + 2\mathrm{Re}(V_{ub})(\nu_{12} - \nu_{15} + \nu_{18} + \nu_{21})\nu^{ub}\Big) \\
&\quad + \frac{eg_1}{4\pi^2 F_\pi^2}\Big(\mathrm{Re}(V_{ub})\nu_2\nu^{ub} + \mu_7(\mu^{ub} + \mu^{sb})\Big)\int_0^1 dx\,\frac{1}{\tilde{M}_K}\frac{\partial}{\partial\tilde{M}_K}J_1(-\Delta, \tilde{M}_K) \\
&\quad + \frac{eg_1}{4\pi^2 F_\pi^2}\Big(\mathrm{Re}(V_{ub})\nu_2\nu^{ub} + \mu_7(\mu^{ub} + \mu^{db})\Big)\int_0^1 dx\,\frac{1}{\tilde{M}_\pi}\frac{\partial}{\partial\tilde{M}_\pi}J_1(-\Delta, \tilde{M}_\pi) \\
&\quad + \frac{eg_2}{2\pi^2 F_\pi^2}\Big(\mathrm{Re}(V_{ub})\nu_3\nu^{ub} + \mu_8(\mu^{ub} + \mu^{sb})\Big)\int_0^1 dx\,\frac{1}{\tilde{M}_K}\frac{\partial}{\partial\tilde{M}_K}J_1(0, \tilde{M}_K) \\
&\quad + \frac{eg_2}{2\pi^2 F_\pi^2}\Big(\mathrm{Re}(V_{ub})\nu_3\nu^{ub} + \mu_8(\mu^{ub} + \mu^{db})\Big)\int_0^1 dx\,\frac{1}{\tilde{M}_\pi}\frac{\partial}{\partial\tilde{M}_\pi}J_1(0, \tilde{M}_\pi), \\
D^{\gamma}_{\Sigma_b^0}(q^2) &= 2c_2 - 2e\Big(b_{20} - \mu_{12}(\mu^{ub} - \mu^{db}) + \mu_{15}(\mu^{ub} + \mu^{db}) - 2\mu_{21}(\mu^{ub} - \mu^{db} - \mu^{sb}) \\
&\quad - \mathrm{Re}(V_{ub})(\nu_{12} - \nu_{15} + 2\nu_{21})\nu^{ub}\Big) \\
&\quad + \frac{eg_1}{8F_\pi^2}\Big(\mathrm{Re}(V_{ub})\nu_2\nu^{ub} + \mu_7(\mu^{ub} + \mu^{sb})\Big)\int_0^1 dx\,\frac{1}{\tilde{M}_K}\frac{\partial}{\partial\tilde{M}_K}J_1(-\Delta, \tilde{M}_K) \\
&\quad + \frac{eg_2}{4F_\pi^2}\Big(\mathrm{Re}(V_{ub})\nu_3\nu^{ub} + \mu_8(\mu^{ub} + \mu^{sb})\Big)\int_0^1 dx\,\frac{1}{\tilde{M}_K}\frac{\partial}{\partial\tilde{M}_K}J_1(0, \tilde{M}_K), \\
D^{\gamma}_{\Sigma_b^-}(q^2) &= 2c_2 - 2e\Big(b_{17} + b_{20} + 2(\mu_{12} + \mu_{15})\mu^{db} + 2\mu_{18}(\mu^{ub} + \mu^{db} + \mu^{sb}) \\
&\quad - 2\mu_{21}(\mu^{ub} - \mu^{db} - \mu^{sb}) + 2\mathrm{Re}(V_{ub})(\nu_{18} - \nu_{21})\nu^{ub}\Big) \\
&\quad - \frac{eg_1}{4\pi^2 F_\pi^2}\Big(\mathrm{Re}(V_{ub})\nu_2\nu^{ub} + \mu_7(\mu^{ub} + \mu^{db})\Big)\int_0^1 dx\,\frac{1}{\tilde{M}_\pi}\frac{\partial}{\partial\tilde{M}_\pi}J_1(-\Delta, \tilde{M}_\pi) \\
&\quad - \frac{eg_2}{2\pi^2 F_\pi^2}\Big(\mathrm{Re}(V_{ub})\nu_3\nu^{ub} + \mu_8(\mu^{ub} + \mu^{db})\Big)\int_0^1 dx\,\frac{1}{\tilde{M}_\pi}\frac{\partial}{\partial\tilde{M}_\pi}J_1(0, \tilde{M}_\pi), \\
D^{\gamma}_{\Xi_b^{\prime 0}}(q^2) &= 2c_2 - 2e\Big(b_{20} - \mu_{12}(\mu^{ub} - \mu^{sb}) + \mu_{15}(\mu^{ub} + \mu^{sb}) - 2\mu_{21}(\mu^{ub} - \mu^{db} - \mu^{sb}) \\
&\quad - \mathrm{Re}(V_{ub})(\nu_{12} - \nu_{15} + 2\nu_{21})\nu^{ub}\Big) \\
&\quad + \frac{eg_1}{8F_\pi^2}\Big(\mathrm{Re}(V_{ub})\nu_2\nu^{ub} + \mu_7(\mu^{ub} + \mu^{db})\Big)\int_0^1 dx\,\frac{1}{\tilde{M}_\pi}\frac{\partial}{\partial\tilde{M}_\pi}J_1(-\Delta, \tilde{M}_\pi) \\
&\quad + \frac{eg_2}{4F_\pi^2}\Big(\mathrm{Re}(V_{ub})\nu_3\nu^{ub} + \mu_8(\mu^{ub} + \mu^{db})\Big)\int_0^1 dx\,\frac{1}{\tilde{M}_\pi}\frac{\partial}{\partial\tilde{M}_\pi}J_1(0, \tilde{M}_\pi),
\end{aligned}
$$

$$
\begin{aligned}
D^{\gamma}_{\Xi_b^{\prime -}}(q^2) = {} & 2c_2 - 2e\Big(b_{17} + b_{20} + (\mu_{12} + \mu_{15})(\mu^{db} + \mu^{sb}) + 2\mu_{18}(\mu^{ub} + \mu^{db} + \mu^{sb}) \\
& - 2\mu_{21}(\mu^{ub} - \mu^{db} - \mu^{sb}) + 2\mathrm{Re}(V_{ub})(\nu_{18} - \nu_{21})\nu^{ub}\Big) \\
& - \frac{eg_1}{8\pi^2 F_\pi^2}\Big(\mathrm{Re}(V_{ub})\nu_2\nu^{ub} + \mu_7(\mu^{ub} + \mu^{sb})\Big)\int_0^1 dx\, \frac{1}{\tilde{M}_K}\frac{\partial}{\partial \tilde{M}_K} J_1(-\Delta, \tilde{M}_K) \\
& - \frac{eg_1}{8\pi^2 F_\pi^2}\Big(\mathrm{Re}(V_{ub})\nu_2\nu^{ub} + \mu_7(\mu^{ub} + \mu^{db})\Big)\int_0^1 dx\, \frac{1}{\tilde{M}_\pi}\frac{\partial}{\partial \tilde{M}_\pi} J_1(-\Delta, \tilde{M}_\pi) \\
& - \frac{eg_2}{4\pi^2 F_\pi^2}\Big(\mathrm{Re}(V_{ub})\nu_3\nu^{ub} + \mu_8(\mu^{ub} + \mu^{sb})\Big)\int_0^1 dx\, \frac{1}{\tilde{M}_K}\frac{\partial}{\partial \tilde{M}_K} J_1(0, \tilde{M}_K) \\
& - \frac{eg_2}{4\pi^2 F_\pi^2}\Big(\mathrm{Re}(V_{ub})\nu_3\nu^{ub} + \mu_8(\mu^{ub} + \mu^{db})\Big)\int_0^1 dx\, \frac{1}{\tilde{M}_\pi}\frac{\partial}{\partial \tilde{M}_\pi} J_1(0, \tilde{M}_\pi), \\
D^{\gamma}_{\Omega_b^-}(q^2) = {} & 2c_2 - 2e\Big(b_{17} + b_{20} + 2(\mu_{12} + \mu_{15})\mu^{sb} + 2\mu_{18}(\mu^{ub} + \mu^{db} + \mu^{sb}) \\
& - 2\mu_{21}(\mu^{ub} - \mu^{db} - \mu^{sb}) + 2\mathrm{Re}(V_{ub})(\nu_{18} - \nu_{21})\nu^{ub}\Big) \\
& - \frac{eg_1}{4\pi^2 F_\pi^2}\Big(\mathrm{Re}(V_{ub})\nu_2\nu^{ub} + \mu_7(\mu^{ub} + \mu^{sb})\Big)\int_0^1 dx\, \frac{1}{\tilde{M}_K}\frac{\partial}{\partial \tilde{M}_K} J_1(-\Delta, \tilde{M}_K) \\
& - \frac{eg_2}{2\pi^2 F_\pi^2}\Big(\mathrm{Re}(V_{ub})\nu_3\nu^{ub} + \mu_8(\mu^{ub} + \mu^{sb})\Big)\int_0^1 dx\, \frac{1}{\tilde{M}_K}\frac{\partial}{\partial \tilde{M}_K} J_1(0, \tilde{M}_K).
\end{aligned}
$$

C.2 EDMs with NDA Estimates

Replacing the unknown LECs in the equations for the neutral and charged b-baryon EDMs with the NDA estimate leads to the following expressions

$$
\begin{aligned}
d^{\gamma}_{\Lambda_b^0} &= 4\left(\frac{m_b}{\Lambda^2}\right)\tilde{c}_1 - 4e\left(\frac{m_b}{4\pi\Lambda^2}\right)\tilde{b}_{19} + 4e\left(\frac{F_\pi}{4\pi\Lambda^2}\right)\left[\tilde{\mu}_{11} - \tilde{\mu}_{14} + 2\tilde{\mu}_{20} + \mathrm{Re}(V_{ub})(\tilde{\nu}_{11} - \tilde{\nu}_{14} + 2\tilde{\nu}_{20})\right] \\
&\quad + \frac{eg_2}{32\pi^2}\frac{\Lambda_\chi}{\Lambda^2}\left(\mathrm{Re}(V_{ub})\tilde{\nu}_3 + \tilde{\mu}_8\right)\left(1 + 2\ln\left[\frac{M_K}{\lambda}\right] + \frac{2\Delta\mathrm{Arccos}\left[\frac{\Delta}{M_K}\right]}{\sqrt{M_K^2 - \Delta^2}}\right), \\
d^{\gamma}_{\Xi_b^0} &= 4\left(\frac{m_b}{\Lambda^2}\right)\tilde{c}_1 - 4e\left(\frac{m_b}{4\pi\Lambda^2}\right)\tilde{b}_{19} + 4e\left(\frac{F_\pi}{4\pi\Lambda^2}\right)\left[\tilde{\mu}_{11} - \tilde{\mu}_{14} + 2\tilde{\mu}_{20} + \mathrm{Re}(V_{ub})(\tilde{\nu}_{11} - \tilde{\nu}_{14} + 2\tilde{\nu}_{20})\right] \\
&\quad + \frac{eg_2}{32\pi^2}\frac{\Lambda_\chi}{\Lambda^2}\left(\mathrm{Re}(V_{ub})\tilde{\nu}_3 + \tilde{\mu}_8\right)\left(1 + 2\ln\left[\frac{M_\pi}{\lambda}\right] + \frac{2\Delta}{\sqrt{\Delta^2 - M_\pi^2}}\ln\left[\frac{\Delta}{M_\pi} + \sqrt{\frac{\Delta^2}{M_\pi^2} - 1}\right]\right), \\
d^{\gamma}_{\Xi_b^-} &= 4\left(\frac{m_b}{\Lambda^2}\right)\tilde{c}_1 - 4e\left(\frac{m_b}{4\pi\Lambda^2}\right)(\tilde{b}_{16} + \tilde{b}_{19}) \\
&\quad - 4e\left(\frac{F_\pi}{4\pi\Lambda^2}\right)\left[\tilde{\mu}_{11} + \tilde{\mu}_{14} + 2\tilde{\mu}_{17} - 2\tilde{\mu}_{20} + 2\mathrm{Re}(V_{ub})(\tilde{\nu}_{17} - \tilde{\nu}_{20})\right] - \frac{eg_2}{32\pi^2}\frac{\Lambda_\chi}{\Lambda^2}\left(\mathrm{Re}(V_{ub})\tilde{\nu}_3 + \tilde{\mu}_8\right) \\
&\quad \times\left(2 + 2\ln\left[\frac{M_K}{\lambda}\right] + \frac{2\Delta\mathrm{Arccos}\left[\frac{\Delta}{M_K}\right]}{\sqrt{M_K^2 - \Delta^2}} + 2\ln\left[\frac{M_\pi}{\lambda}\right] + \frac{2\Delta}{\sqrt{\Delta^2 - M_\pi^2}}\ln\left[\frac{\Delta}{M_\pi} + \sqrt{\frac{\Delta^2}{M_\pi^2} - 1}\right]\right), \\
d^{\gamma}_{\Sigma_b^+} &= 2\left(\frac{m_b}{\Lambda^2}\right)\tilde{c}_2 + 2e\left(\frac{m_b}{4\pi\Lambda^2}\right)(\tilde{b}_{17} - \tilde{b}_{20}) \\
&\quad + 4e\left(\frac{F_\pi}{4\pi\Lambda^2}\right)\left[\tilde{\mu}_{12} - \tilde{\mu}_{15} + \tilde{\mu}_{18} + \tilde{\mu}_{21} + \mathrm{Re}(V_{ub})(\tilde{\nu}_{12} - \tilde{\nu}_{15} + \tilde{\nu}_{18} + \tilde{\nu}_{21})\right] \\
&\quad + \frac{eg_2}{16\pi^2}\frac{\Lambda_\chi}{\Lambda^2}\left(\mathrm{Re}(V_{ub})\tilde{\nu}_3 + \tilde{\mu}_8\right)\left(2 + 2\ln\left[\frac{M_K M_\pi}{\lambda^2}\right]\right) + \frac{eg_1}{32\pi^2}\frac{\Lambda_\chi}{\Lambda^2}\left(\mathrm{Re}(V_{ub})\tilde{\nu}_2 + \tilde{\mu}_7\right) \\
&\quad \times\left(2 + 2\ln\left[\frac{M_K}{\lambda}\right] + \frac{2\Delta\mathrm{Arccos}\left[\frac{\Delta}{M_K}\right]}{\sqrt{M_K^2 - \Delta^2}} + 2\ln\left[\frac{M_\pi}{\lambda}\right] + \frac{2\Delta}{\sqrt{\Delta^2 - M_\pi^2}}\ln\left[\frac{\Delta}{M_\pi} + \sqrt{\frac{\Delta^2}{M_\pi^2} - 1}\right]\right), \\
d^{\gamma}_{\Sigma_b^0} &= 2\left(\frac{m_b}{\Lambda^2}\right)\tilde{c}_2 - 2e\left(\frac{m_b}{4\pi\Lambda^2}\right)\tilde{b}_{20} + 2e\left(\frac{F_\pi}{4\pi\Lambda^2}\right)\left[\tilde{\mu}_{12} - \tilde{\mu}_{15} + 2\tilde{\mu}_{21} + \mathrm{Re}(V_{ub})(\tilde{\nu}_{12} - \tilde{\nu}_{15} + 2\tilde{\nu}_{21})\right] \\
&\quad + \frac{eg_1}{64\pi^2}\frac{\Lambda_\chi}{\Lambda^2}\left(\mathrm{Re}(V_{ub})\tilde{\nu}_2 + \tilde{\mu}_7\right)\left(1 + 2\ln\left[\frac{M_K}{\lambda}\right] + \frac{2\Delta\mathrm{Arccos}\left[\frac{\Delta}{M_K}\right]}{\sqrt{M_K^2 - \Delta^2}}\right) \\
&\quad + \frac{eg_2}{32\pi^2}\frac{\Lambda_\chi}{\Lambda^2}\left(\mathrm{Re}(V_{ub})\tilde{\nu}_3 + \tilde{\mu}_8\right)\left(1 + 2\ln\left[\frac{M_K}{\lambda}\right]\right),
\end{aligned}
$$

$$
\begin{aligned}
d^{\gamma}_{\Sigma_b^-} &= 2\left(\frac{m_b}{\Lambda^2}\right)\tilde{c}_2 - 2e\left(\frac{m_b}{4\pi\Lambda^2}\right)(\tilde{b}_{17}+\tilde{b}_{20}) - 4e\left(\frac{F_\pi}{4\pi\Lambda^2}\right)\left[\tilde{\mu}_{12}+\tilde{\mu}_{15}+\tilde{\mu}_{18}-\tilde{\mu}_{21}+\mathrm{Re}(V_{ub})(\tilde{\nu}_{18}-\tilde{\nu}_{21})\right] \\
&\quad - \frac{eg_1}{32\pi^2}\frac{\Lambda_\chi}{\Lambda^2}\left(\mathrm{Re}(V_{ub})\tilde{\nu}_2+\tilde{\mu}_7\right)\left(1+2\ln\left[\frac{M_\pi}{\lambda}\right]+\frac{2\Delta}{\sqrt{\Delta^2-M_\pi^2}}\ln\left[\frac{\Delta}{M_\pi}+\sqrt{\frac{\Delta^2}{M_\pi^2}-1}\right]\right) \\
&\quad - \frac{eg_2}{16\pi^2}\frac{\Lambda_\chi}{\Lambda^2}\left(\mathrm{Re}(V_{ub})\tilde{\nu}_3+\tilde{\mu}_8\right)\left(1+2\ln\left[\frac{M_\pi}{\lambda}\right]\right), \\
d^{\gamma}_{\Xi_b^{\prime 0}} &= 2\left(\frac{m_b}{\Lambda^2}\right)\tilde{c}_2 - 2e\left(\frac{m_b}{4\pi\Lambda^2}\right)\tilde{b}_{20} + 2e\left(\frac{F_\pi}{4\pi\Lambda^2}\right)\left[\tilde{\mu}_{12}-\tilde{\mu}_{15}+2\tilde{\mu}_{21}+\mathrm{Re}(V_{ub})(\tilde{\nu}_{12}-\tilde{\nu}_{15}+2\tilde{\nu}_{21})\right] \\
&\quad + \frac{eg_1}{64\pi^2}\frac{\Lambda_\chi}{\Lambda^2}\left(\mathrm{Re}(V_{ub})\tilde{\nu}_2+\tilde{\mu}_7\right)\left(1+2\ln\left[\frac{M_\pi}{\lambda}\right]+\frac{2\Delta}{\sqrt{\Delta^2-M_\pi^2}}\ln\left[\frac{\Delta}{M_\pi}+\sqrt{\frac{\Delta^2}{M_\pi^2}-1}\right]\right) \\
&\quad + \frac{eg_2}{32\pi^2}\frac{\Lambda_\chi}{\Lambda^2}\left(\mathrm{Re}(V_{ub})\tilde{\nu}_3+\tilde{\mu}_8\right)\left(1+2\ln\left[\frac{M_\pi}{\lambda}\right]\right), \\
d^{\gamma}_{\Xi_b^{\prime -}} &= 2\left(\frac{m_b}{\Lambda^2}\right)\tilde{c}_2 - 2e\left(\frac{m_b}{4\pi\Lambda^2}\right)(\tilde{b}_{17}+\tilde{b}_{20}) \\
&\quad - 2e\left(\frac{F_\pi}{4\pi\Lambda^2}\right)\left[\tilde{\mu}_{12}+\tilde{\mu}_{15}+2\tilde{\mu}_{18}-2\tilde{\mu}_{21}+2\mathrm{Re}(V_{ub})(\tilde{\nu}_{18}-\tilde{\nu}_{21})\right] \\
&\quad - \frac{eg_2}{32\pi^2}\frac{\Lambda_\chi}{\Lambda^2}\left(\mathrm{Re}(V_{ub})\tilde{\nu}_3+\tilde{\mu}_8\right)\left(2+2\ln\left[\frac{M_K M_\pi}{\lambda^2}\right]\right) - \frac{eg_1}{64\pi^2}\frac{\Lambda_\chi}{\Lambda^2}\left(\mathrm{Re}(V_{ub})\tilde{\nu}_2+\tilde{\mu}_7\right) \\
&\quad \times\left(2+2\ln\left[\frac{M_K}{\lambda}\right]+\frac{2\Delta\mathrm{Arccos}\left[\frac{\Delta}{M_K}\right]}{\sqrt{M_K^2-\Delta^2}}+2\ln\left[\frac{M_\pi}{\lambda}\right]+\frac{2\Delta}{\sqrt{\Delta^2-M_\pi^2}}\ln\left[\frac{\Delta}{M_\pi}+\sqrt{\frac{\Delta^2}{M_\pi^2}-1}\right]\right), \\
d^{\gamma}_{\Omega_b^-} &= 2\left(\frac{m_b}{\Lambda^2}\right)\tilde{c}_2 - 2e\left(\frac{m_b}{4\pi\Lambda^2}\right)(\tilde{b}_{17}+\tilde{b}_{20}) - 4e\left(\frac{F_\pi}{4\pi\Lambda^2}\right)\left[\tilde{\mu}_{12}+\tilde{\mu}_{15}+\tilde{\mu}_{18}-\tilde{\mu}_{21}+\mathrm{Re}(V_{ub})(\tilde{\nu}_{18}-\tilde{\nu}_{21})\right] \\
&\quad - \frac{eg_1}{32\pi^2}\frac{\Lambda_\chi}{\Lambda^2}\left(\mathrm{Re}(V_{ub})\tilde{\nu}_2+\tilde{\mu}_7\right)\left(1+2\ln\left[\frac{M_K}{\lambda}\right]+\frac{2\Delta\mathrm{Arccos}\left[\frac{\Delta}{M_K}\right]}{\sqrt{M_K^2-\Delta^2}}\right) \\
&\quad - \frac{eg_2}{16\pi^2}\frac{\Lambda_\chi}{\Lambda^2}\left(\mathrm{Re}(V_{ub})\tilde{\nu}_3+\tilde{\mu}_8\right)\left(1+2\ln\left[\frac{M_K}{\lambda}\right]\right),
\end{aligned}
$$

where $\tilde{c}_i$, $\tilde{b}_i$, $\tilde{\mu}_i$, and $\tilde{\nu}_i$ are dimensionless constants which are varied from -3 to $+3$ in the MC sampling. The estimation $4\pi F_\pi \sim \Lambda_\chi$ has been used at certain steps.

C.3 Loop Functions

In this appendix we give the loop functions in the heavy baryon formulation [62] which appear in the calculation of the diagrams in Fig. 5.1

$$\Delta_M = 2M^2\left[L + \frac{1}{16\pi^2}\ln\left(\frac{M}{\lambda}\right)\right] + O(n-4),$$

$$\frac{1}{i}\int\frac{d^nk}{(2\pi)^n}\frac{1}{M^2-k^2} = \Delta_M = M^{n-2}\,(4\pi)^{-n/2}\,\Gamma\Big(1-\frac{n}{2}\Big),$$

$$\frac{1}{i}\int\frac{d^nk}{(2\pi)^n}\frac{\{1,k_\mu,k_\mu k_\nu\}}{[v\cdot k-w][M^2-k^2]} = \Big\{J_0(w), v_\mu J_1(w), g_{\mu\nu}J_2(w)+v_\mu v_\nu J_3(w)\Big\},$$

$$\frac{1}{i}\int\frac{d^nk}{(2\pi)^n}\frac{\{1,k_\mu,k_\mu k_\nu\}}{[v\cdot k-w]^2[M^2-k^2]} = \Big\{G_0(w), v_\mu G_1(w), g_{\mu\nu}G_2(w)+v_\mu v_\nu G_3(w)\Big\},$$

$$\frac{1}{i}\int\frac{d^nk}{(2\pi)^n}\frac{1}{[v\cdot k-w)[M^2-k^2][(k+q)^2-M^2]} = \int_0^1 dx\,\frac{1}{2\widetilde{M}}\,\frac{\partial}{\partial\widetilde{M}}\,J_0\Big(\widetilde{w},\widetilde{M}\Big),$$

$$\frac{1}{i}\int\frac{d^nk}{(2\pi)^n}\frac{k_\mu}{[v\cdot k-w][M^2-k^2][(k+q)^2-M^2]} = \int_0^1 dx\left(\frac{v_\mu}{2\widetilde{M}}\,\frac{\partial}{\partial\widetilde{M}}\,J_1\Big(\widetilde{w},\widetilde{M}\Big) - \frac{x\,q_\mu}{2\widetilde{M}}\,\frac{\partial}{\partial\widetilde{M}}\,J_0\Big(\widetilde{w},\widetilde{M}\Big)\right),$$

$$\begin{aligned}\frac{1}{i}\int\frac{d^nk}{(2\pi)^n}\frac{k_\mu k_\nu}{[v\cdot k-w][M^2-k^2][(k+q)^2-M^2]} = \int_0^1 dx\Bigg(&\frac{g_{\mu\nu}}{2\widetilde{M}}\,\frac{\partial}{\partial\widetilde{M}}\,J_2\Big(\widetilde{w},\widetilde{M}\Big)\\ &+\frac{v_\mu v_\nu}{2\widetilde{M}}\,\frac{\partial}{\partial\widetilde{M}}\,J_3\Big(\widetilde{w},\widetilde{M}\Big)\\ &-\Big(q_\mu v_\nu+q_\nu v_\mu\Big)\,\frac{x}{2\widetilde{M}}\,\frac{\partial}{\partial\widetilde{M}}\,J_1\Big(\widetilde{w},\widetilde{M}\Big)\\ &+\frac{x^2\,q_\mu q_\nu}{2\widetilde{M}}\,\frac{\partial}{\partial\widetilde{M}}\,J_0\Big(\widetilde{w},\widetilde{M}\Big)\Bigg),\end{aligned}$$

where $\widetilde{w}(x) = w + xv\cdot q$, and $\widetilde{M}^2(x) = x(x-1)q^2 + M^2$. The analytical expressions for the loop functions in dimensional regularization are

$$J_0(w) = -4Lw + \frac{w}{8\pi^2}\left[1-2\ln\left(\frac{M}{\lambda}\right)\right] - \frac{1}{4\pi^2}\sqrt{M^2-w^2}\,\mathrm{ArcCos}\Big(\frac{-w}{M}\Big) + O(n-4),$$

for $M^2 > w^2$, and

$$J_0(w) = -4Lw + \frac{w}{8\pi^2}\left[1 - 2\ln\left(\frac{M}{\lambda}\right)\right] + \frac{1}{4\pi^2}\sqrt{w^2 - M^2}\ln\left(\frac{-w}{M} + \sqrt{\frac{w^2}{M^2} - 1}\right) + O(n-4),$$

for $w^2 > M^2$. Additionally, we used the definitions

$$J_1(w) = wJ_0(w) + \Delta_M, \quad J_2(w) = \frac{1}{n-1}\left[(M^2 - w^2)J_0(w) - w\Delta_M\right],$$

$$J_3(w) = wJ_1(w) - J_2(w),$$

$$G_i(w) = \frac{\partial}{\partial w}J_i(w), \quad i = 0, 1, 2, 3.$$

Acknowledgements

This thesis would not have been possible without the help of many colleagues, friends and family members. The following lines are dedicated to them.

First of all, I would like to thank my supervisor Prof. Dr. Dr. h.c. Ulf-G. Meißner for giving me the opportunity to write this doctoral thesis in his working group. He suggested me this interesting and challenging topic about the Roper resonance and also provided the necessary financial support. He was always curious about my work, gave me many useful remarks, and motivated me, especially when things got complicated. Unforgettable are also our numerous conversations about topics outside of physics, like the particularities of academic life, sports and the art of Swiss watchmaking. I really appreciate all the work he has done for me.
Next, I want to thank PD Dr. Akaki Rusetsky. He did not only agree to be the second assessor of this thesis, but was also always there when I needed his help. I am thankful for all the discussions we had and that he always checked my calculations for consistency.
Furthermore, I am deeply grateful to Maxim Mai who rejoined the *HISKP* in November 2021 and was from the beginning very interested in my work. I want to thank him for all his help and support over the last period of my doctoral studies. We had a lot of fruitful and funny discussions about the Roper resonance, theoretical physics in general and just everyday things.
Likewise, I want to thank my former office colleague Yasemin Ünal for all the interesting conversations we had and also for inviting me to join the EDM project. I felt very fortunate to be part of this project, where I really learned a lot. I am also thankful to Jordy de Vries and Christoph Hanhart for their help and support during the EDM collaboration.
Additionally, I am very grateful to Matthias Frink, Simon Holz, Helen Meyer, Fabian Müller, and Thomas Vonk who all supported me in numerous ways during my work on this thesis. I also greatly acknowledge my discussions with Liping He, Bastian Kubis, Bernard Metsch and Ferenc Pittler. Further, I want to thank Christa Börsch, Heike Frömbgen-Penkert and Barbara Kraus, the secretaries of the institute, for always helping me with bureaucratic issues. All in all, the whole theory working group at the *HISKP* ensured a pleasant work environment.
I also want to express my gratitude towards my long-term university friends Alexander Johnston, Steffen Pape, David Röser, Nils Stausberg, and Lina Zabawa who all managed to help me through the ups and downs of my undergraduate and graduate studies.
Finally, I want to thank my parents and my grandparents for their endless love and support, and for always believing in me. Last, but definitely not least, I want to thank my love Mia. I am so lucky that I have met you. You helped me in so many ways, which I can hardly put into words and I look forward to our future together.

Bibliography

[1] P. Ball, *The Elements: A very short introduction*, 1st ed., UOP Oxford, 2004 (cit. on p. 1).

[2] B. Pullman, *The Atom in the History of Human Thought*, 1st ed., Oxford University Press, 1998 (cit. on p. 1).

[3] L. H. Ryder, *QUANTUM FIELD THEORY*, Cambridge University Press, 1996, ISBN: 978-0-521-47814-4, 978-1-139-63239-3, 978-0-521-23764-2 (cit. on p. 1).

[4] M. E. Peskin and D. V. Schroeder, *An Introduction to quantum field theory*, Reading, USA: Addison-Wesley, 1995, ISBN: 978-0-201-50397-5 (cit. on pp. 1, 3, 8, 102–104).

[5] J. F. Donoghue, E. Golowich and B. R. Holstein, *Dynamics of the Standard Model*, vol. 2, Cambridge Monographs on Particle Physics, Nuclear Physics and Cosmology (35), Cambridge University Press, 2022, ISBN: 978-1-00-929103-3, 978-1-00-929100-2, 978-1-00-929101-9 (cit. on pp. 1, 3, 5, 8, 11).

[6] M. Gell-Mann, *A Schematic Model of Baryons and Mesons*, Phys. Lett. **8** (1964) 214 (cit. on p. 2).

[7] G. Zweig, *An SU(3) model for strong interaction symmetry and its breaking. Version 1*, (1964) (cit. on p. 2).

[8] V. E. Barnes et al., *Observation of a Hyperon with Strangeness Minus Three*, Phys. Rev. Lett. **12** (1964) 204 (cit. on p. 2).

[9] M. Y. Han and Y. Nambu, *Three Triplet Model with Double SU(3) Symmetry*, Phys. Rev. **139** (1965) B1006, ed. by T. Eguchi (cit. on p. 2).

[10] M. Mai, U.-G. Meißner and C. Urbach, *Towards a theory of hadron resonances*, Phys. Rept. **1001** (2023) 1, arXiv: 2206.01477 [hep-ph] (cit. on pp. 2, 8, 10, 44, 54).

[11] U.-G. Meißner, *Towards a theory of baryon resonances*, EPJ Web Conf. **241** (2020) 02003, ed. by R. Beck, A. Thiel, U. Thom and Y. Wunderlich, arXiv: 1908.06706 [nucl-th] (cit. on p. 2).

[12] L. D. Roper, *Evidence for a P-11 Pion-Nucleon Resonance at 556 MeV*, Phys. Rev. Lett. **12** (1964) 340 (cit. on pp. 2, 25).

[13] R. L. Workman et al., *Review of Particle Physics*, PTEP **2022** (2022) 083C01 (cit. on pp. 2, 7, 10, 13, 15, 63, 64, 106).

[14] C. Gattringer and C. B. Lang, *Quantum chromodynamics on the lattice*, vol. 788, Berlin: Springer, 2010, ISBN: 978-3-642-01849-7, 978-3-642-01850-3 (cit. on pp. 2, 8).

[15] C. B. Lang, L. Leskovec, M. Padmanath and S. Prelovsek, *Pion-nucleon scattering in the Roper channel from lattice QCD*, Phys. Rev. D **95** (2017) 014510, arXiv: 1610.01422 [hep-lat] (cit. on pp. 2, 25, 44, 45, 71–73, 98).

[16] Z.-W. Liu et al., *Hamiltonian effective field theory study of the* $\mathbf{N}^*(\mathbf{1440})$ *resonance in lattice QCD*, Phys. Rev. D **95** (2017) 034034, arXiv: 1607.04536 [nucl-th] (cit. on pp. 2, 25, 45).

[17] U.-G. Meißner and A. Rusetsky, *Effective Field Theories*, Cambridge University Press, 2022 (cit. on pp. 2, 3, 10–12, 15, 17, 19, 21, 46, 52).

[18] S. R. Beane and U. van Kolck, *The Role of the Roper in QCD*, J. Phys. G **31** (2005) 921, arXiv: nucl-th/0212039 (cit. on pp. 3, 26, 37).

[19] B. Borasoy, P. C. Bruns, U.-G. Meißner and R. Lewis, *Chiral corrections to the Roper mass*, Phys. Lett. B **641** (2006) 294, arXiv: hep-lat/0608001 (cit. on pp. 3, 26).

[20] D. Djukanovic, J. Gegelia and S. Scherer, *Chiral structure of the Roper resonance using complex-mass scheme*, Phys. Lett. B **690** (2010) 123, arXiv: 0903.0736 [hep-ph] (cit. on pp. 3, 26).

[21] B. Long and U. van Kolck, *The Role of the Roper in Chiral Perturbation Theory*, Nucl. Phys. A **870-871** (2011) 72, arXiv: 1105.2764 [nucl-th] (cit. on pp. 3, 26).

[22] J. Gegelia, U.-G. Meißner and D.-L. Yao, *The width of the Roper resonance in baryon chiral perturbation theory*, Phys. Lett. B **760** (2016) 736, arXiv: 1606.04873 [hep-ph] (cit. on pp. 3, 23, 26, 28, 37, 40, 63, 97).

[23] U. J. Wiese, *Identification of Resonance Parameters From the Finite Volume Energy Spectrum*, Nucl. Phys. B Proc. Suppl. **9** (1989) 609, ed. by A. S. Kronfeld and P. B. Mackenzie (cit. on pp. 3, 25).

[24] V. Bernard, U.-G. Meißner and A. Rusetsky, *The Delta-resonance in a finite volume*, Nucl. Phys. B **788** (2008) 1, arXiv: hep-lat/0702012 (cit. on pp. 3, 23–25, 32, 35–38).

[25] M. Lüscher, *Volume Dependence of the Energy Spectrum in Massive Quantum Field Theories. 2. Scattering States*, Commun. Math. Phys. **105** (1986) 153 (cit. on pp. 3, 65).

[26] M. Lüscher, *Two particle states on a torus and their relation to the scattering matrix*, Nucl. Phys. B **354** (1991) 531 (cit. on pp. 3, 31, 62, 65).

[27] M. Mai, M. Döring and A. Rusetsky, *Multi-particle systems on the lattice and chiral extrapolations: a brief review*, Eur. Phys. J. ST **230** (2021) 1623, arXiv: 2103.00577 [hep-lat] (cit. on pp. 3, 45).

[28] M. Mai and M. Döring, *Three-body Unitarity in the Finite Volume*, Eur. Phys. J. A **53** (2017) 240, arXiv: 1709.08222 [hep-lat] (cit. on pp. 3, 45, 61).

[29] R. A. Briceño, M. T. Hansen and S. R. Sharpe, *Relating the finite-volume spectrum and the two-and-three-particle S matrix for relativistic systems of identical scalar particles*, Phys. Rev. D **95** (2017) 074510, arXiv: 1701.07465 [hep-lat] (cit. on pp. 3, 45).

[30] M. Döring et al., *Three-body spectrum in a finite volume: the role of cubic symmetry*, Phys. Rev. D **97** (2018) 114508, arXiv: 1802.03362 [hep-lat] (cit. on pp. 3, 45).

[31] S. R. Sharpe, *Testing the threshold expansion for three-particle energies at fourth order in ϕ^4 theory*, Phys. Rev. D **96** (2017) 054515, [Erratum: Phys.Rev.D 98, 099901 (2018)], arXiv: 1707.04279 [hep-lat] (cit. on p. 3).

[32] P. Guo, *One spatial dimensional finite volume three-body interaction for a short-range potential*, Phys. Rev. D **95** (2017) 054508, arXiv: 1607.03184 [hep-lat] (cit. on pp. 3, 45).

[33] M. T. Hansen and S. R. Sharpe, *Applying the relativistic quantization condition to a three-particle bound state in a periodic box*, Phys. Rev. D **95** (2017) 034501, arXiv: 1609.04317 [hep-lat] (cit. on p. 3).

[34] M. T. Hansen and S. R. Sharpe, *Expressing the three-particle finite-volume spectrum in terms of the three-to-three scattering amplitude*, Phys. Rev. D **92** (2015) 114509, arXiv: 1504.04248 [hep-lat] (cit. on pp. 3, 45).

[35] U.-G. Meißner, G. Ríos and A. Rusetsky, *Spectrum of three-body bound states in a finite volume*, Phys. Rev. Lett. **114** (2015) 091602, [Erratum: Phys.Rev.Lett. 117, 069902 (2016)], arXiv: 1412.4969 [hep-lat] (cit. on pp. 3, 45).

[36] F. Müller and A. Rusetsky, *On the three-particle analog of the Lellouch-Lüscher formula*, JHEP **03** (2021) 152, arXiv: 2012.13957 [hep-lat] (cit. on pp. 3, 44–46).

[37] D. B. Kaplan, *More effective field theory for nonrelativistic scattering*, Nucl. Phys. B **494** (1997) 471, arXiv: nucl-th/9610052 (cit. on pp. 3, 43, 45).

[38] P. F. Bedaque, H. W. Hammer and U. van Kolck, *Renormalization of the three-body system with short range interactions*, Phys. Rev. Lett. **82** (1999) 463, arXiv: nucl-th/9809025 (cit. on pp. 3, 20, 43, 45, 54).

[39] P. F. Bedaque, H. W. Hammer and U. van Kolck, *The Three boson system with short range interactions*, Nucl. Phys. A **646** (1999) 444, arXiv: nucl-th/9811046 (cit. on pp. 3, 20, 43, 45).

[40] E. Braaten and H.-W. Hammer, *Universality in few-body systems with large scattering length*, Phys. Rept. **428** (2006) 259, arXiv: cond-mat/0410417 (cit. on pp. 3, 20, 43, 45, 46).

[41] H.-W. Hammer, J.-Y. Pang and A. Rusetsky, *Three-particle quantization condition in a finite volume: 1. The role of the three-particle force*, JHEP **09** (2017) 109, arXiv: 1706.07700 [hep-lat] (cit. on pp. 3, 19, 20, 43, 45, 46).

[42] H.-W. Hammer, J.-Y. Pang and A. Rusetsky, *Three particle quantization condition in a finite volume: 2. general formalism and the analysis of data*, JHEP **10** (2017) 115, arXiv: 1707.02176 [hep-lat] (cit. on pp. 3, 20, 43, 45, 46, 61).

[43] D. Severt, *Towards the finite-volume spectrum of the Roper resonance*, PoS **LATTICE2022** (2023) 085, arXiv: 2210.09423 [hep-lat] (cit. on pp. 3, 67).

[44] A. D. Sakharov, *Violation of CP invariance, C asymmetry, and baryon asymmetry of the universe*, Pisma Zh. Eksp. Teor. Fiz. **5** (1967) 32 (cit. on p. 3).

[45] B. Grzadkowski, M. Iskrzynski, M. Misiak and J. Rosiek, *Dimension-Six Terms in the Standard Model Lagrangian*, JHEP **10** (2010) 085, arXiv: 1008.4884 [hep-ph] (cit. on pp. 3, 12, 76, 78).

[46] C. Abel et al., *Measurement of the permanent electric dipole moment of the neutron*, Phys. Rev. Lett. **124** (2020) 081803, arXiv: 2001.11966 [hep-ex] (cit. on pp. 4, 9, 76).

[47] A. S. Fomin et al., *Feasibility of measuring the magnetic dipole moments of the charm baryons at the LHC using bent crystals*, JHEP **08** (2017) 120, arXiv: 1705.03382 [hep-ph] (cit. on pp. 4, 77, 91, 95).

[48] S. Aiola et al., *Progress towards the first measurement of charm baryon dipole moments*, Phys. Rev. D **103** (2021) 072003, arXiv: 2010.11902 [hep-ex] (cit. on pp. 4, 77, 91, 95).

[49] E. Bagli et al., *Electromagnetic dipole moments of charged baryons with bent crystals at the LHC*, Eur. Phys. J. C **77** (2017) 828, [Erratum: Eur.Phys.J.C 80, 680 (2020)], arXiv: 1708.08483 [hep-ex] (cit. on pp. 4, 77, 91, 95).

[50] V. M. Biryukov and J. Ruiz Vidal, *Improved experimental layout for dipole moment measurements at the LHC*, Eur. Phys. J. C **82** (2022) 149, arXiv: 2110.00845 [hep-ex] (cit. on p. 4).

[51] S. L. Glashow, *Partial Symmetries of Weak Interactions*, Nucl. Phys. **22** (1961) 579 (cit. on p. 5).

[52] S. Weinberg, *A Model of Leptons*, Phys. Rev. Lett. **19** (1967) 1264 (cit. on p. 5).

[53] A. Salam, *Weak and Electromagnetic Interactions*, Conf. Proc. C **680519** (1968) 367 (cit. on p. 5).

[54] P. W. Higgs, *Broken Symmetries and the Masses of Gauge Bosons*, Phys. Rev. Lett. **13** (1964) 508, ed. by J. C. Taylor (cit. on p. 5).

[55] N. Cabibbo, *Unitary Symmetry and Leptonic Decays*, Phys. Rev. Lett. **10** (1963) 531 (cit. on p. 8).

[56] M. Kobayashi and T. Maskawa, *CP Violation in the Renormalizable Theory of Weak Interaction*, Prog. Theor. Phys. **49** (1973) 652 (cit. on p. 8).

[57] H. Fritzsch and M. Gell-Mann, *Current algebra: Quarks and what else?*, eConf **C720906V2** (1972) 135, ed. by J. D. Jackson and A. Roberts, arXiv: hep-ph/0208010 (cit. on p. 8).

[58] C.-N. Yang and R. L. Mills, *Conservation of Isotopic Spin and Isotopic Gauge Invariance*, Phys. Rev. **96** (1954) 191, ed. by J.-P. Hsu and D. Fine (cit. on p. 8).

[59] D. J. Gross and F. Wilczek, *Ultraviolet Behavior of Nonabelian Gauge Theories*, Phys. Rev. Lett. **30** (1973) 1343, ed. by J. C. Taylor (cit. on p. 8).

[60] F.-K. Guo et al., *The electric dipole moment of the neutron from 2+1 flavor lattice QCD*, Phys. Rev. Lett. **115** (2015) 062001, arXiv: 1502.02295 [hep-lat] (cit. on p. 9).

[61] T. Vonk, *Phenomenology of the QCD Θ-angle and axions in nuclear and particle physics*, PhD thesis: Rheinische Friedrich-Wilhelms-Universität Bonn, Bonn U., 2022 (cit. on p. 10).

[62] V. Bernard, N. Kaiser and U.-G. Meißner, *Chiral dynamics in nucleons and nuclei*, Int. J. Mod. Phys. E **4** (1995) 193, arXiv: hep-ph/9501384 (cit. on pp. 11, 13, 16, 117).

[63] S. Weinberg, *Phenomenological Lagrangians*, Physica A **96** (1979) 327, ed. by S. Deser (cit. on p. 11).

[64] J. C. Collins, *Renormalization: An Introduction to Renormalization, the Renormalization Group and the Operator-Product Expansion*, Cambridge Monographs on Mathematical Physics, Cambridge University Press, 1984 (cit. on pp. 12, 103).

[65] H. Akdag, B. Kubis and A. Wirzba, *C and CP violation in effective field theories*, (2022), arXiv: 2212.07794 [hep-ph] (cit. on p. 12).

[66] C. Vafa and E. Witten, *Restrictions on Symmetry Breaking in Vector-Like Gauge Theories*, Nucl. Phys. B **234** (1984) 173 (cit. on p. 13).

[67] J. Goldstone, *Field Theories with Superconductor Solutions*, Nuovo Cim. **19** (1961) 154 (cit. on p. 13).

[68] J. Goldstone, A. Salam and S. Weinberg, *Broken Symmetries*, Phys. Rev. **127** (1962) 965 (cit. on p. 13).

[69] J. Gasser and H. Leutwyler, *Chiral Perturbation Theory to One Loop*, Annals Phys. **158** (1984) 142 (cit. on pp. 14, 85).

[70] J. Gasser and H. Leutwyler, *Chiral Perturbation Theory: Expansions in the Mass of the Strange Quark*, Nucl. Phys. B **250** (1985) 465 (cit. on pp. 14, 15).

[71] M. Gell-Mann, R. J. Oakes and B. Renner, *Behavior of current divergences under SU(3) x SU(3)*, Phys. Rev. **175** (1968) 2195 (cit. on p. 14).

[72] S. Scherer and M. R. Schindler, *A Primer for Chiral Perturbation Theory*, vol. 830, 2012, ISBN: 978-3-642-19253-1 (cit. on p. 16).

[73] J. Gasser, M. E. Sainio and A. Svarc, *Nucleons with Chiral Loops*, Nucl. Phys. B **307** (1988) 779 (cit. on pp. 16, 17).

[74] A. Krause, *Baryon Matrix Elements of the Vector Current in Chiral Perturbation Theory*, Helv. Phys. Acta **63** (1990) 3 (cit. on p. 17).

[75] T. Fuchs, J. Gegelia, G. Japaridze and S. Scherer, *Renormalization of relativistic baryon chiral perturbation theory and power counting*, Phys. Rev. D **68** (2003) 056005, arXiv: hep-ph/0302117 (cit. on pp. 17, 31).

[76] D. Severt, U.-G. Meißner and J. Gegelia, *Flavor decomposition of the pion-nucleon σ-term*, JHEP **03** (2019) 202, arXiv: 1902.10508 [hep-ph] (cit. on pp. 17, 31).

[77] T. Becher and H. Leutwyler, *Baryon chiral perturbation theory in manifestly Lorentz invariant form*, Eur. Phys. J. C **9** (1999) 643, arXiv: hep-ph/9901384 (cit. on p. 17).

[78] E. E. Jenkins and A. V. Manohar, *Baryon chiral perturbation theory using a heavy fermion Lagrangian*, Phys. Lett. B **255** (1991) 558 (cit. on pp. 17, 76, 84).

[79] V. Bernard, N. Kaiser, J. Kambor and U.-G. Meißner, *Chiral structure of the nucleon*, Nucl. Phys. B **388** (1992) 315 (cit. on pp. 18, 76, 84).

[80] H. Georgi, *An Effective Field Theory for Heavy Quarks at Low-energies*, Phys. Lett. B **240** (1990) 447 (cit. on p. 18).

[81] H.-Y. Cheng et al., *Corrections to chiral dynamics of heavy hadrons: SU(3) symmetry breaking*, Phys. Rev. D **49** (1994) 5857, [Erratum: Phys.Rev.D 55, 5851–5852 (1997)], arXiv: hep-ph/9312304 (cit. on pp. 18, 79).

[82] T.-M. Yan et al., *Heavy quark symmetry and chiral dynamics*, Phys. Rev. D **46** (1992) 1148, [Erratum: Phys.Rev.D 55, 5851 (1997)] (cit. on pp. 18, 79, 80).

[83] L. L. Foldy and S. A. Wouthuysen, *On the Dirac theory of spin 1/2 particle and its nonrelativistic limit*, Phys. Rev. **78** (1950) 29 (cit. on p. 19).

[84] G. Colangelo, J. Gasser, B. Kubis and A. Rusetsky, *Cusps in K —> 3 pi decays*, Phys. Lett. B **638** (2006) 187, arXiv: hep-ph/0604084 (cit. on pp. 19, 46).

[85] V. Bernard, M. Lage, U.-G. Meißner and A. Rusetsky, *Resonance properties from the finite-volume energy spectrum*, JHEP **08** (2008) 024, arXiv: 0806.4495 [hep-lat] (cit. on pp. 19, 44, 46, 48).

[86] D. Severt and U.-G. Meißner, *The Roper Resonance in a finite volume*, Commun. Theor. Phys. **72** (2020) 075201, arXiv: 2003.05745 [hep-lat] (cit. on pp. 23, 43, 45, 62, 67, 71, 73).

[87] V. Bernard, D. Hoja, U.-G. Meißner and A. Rusetsky, *The Mass of the Delta resonance in a finite volume: fourth-order calculation*, JHEP **06** (2009) 061, arXiv: 0902.2346 [hep-lat] (cit. on pp. 24, 37).

[88] V. Bernard, *Chiral Perturbation Theory and Baryon Properties*, Prog. Part. Nucl. Phys. **60** (2008) 82, arXiv: 0706.0312 [hep-ph] (cit. on p. 24).

[89] R. G. Edwards, *Hadron Spectroscopy*, PoS **LATTICE2019** (2020) 253 (cit. on p. 24).

[90] M. Tanabashi et al., *Review of Particle Physics*, Phys. Rev. D **98** (2018) 030001 (cit. on pp. 25, 37).

[91] A. Rusetsky, *Three particles on the lattice*, PoS **LATTICE2019** (2019) 281, arXiv: 1911.01253 [hep-lat] (cit. on pp. 25, 45).

[92] T. Bauer, S. Scherer and L. Tiator,
Electromagnetic transition form factors of the Roper resonance in effective field theory,
Phys. Rev. C **90** (2014) 015201, arXiv: 1402.0741 [nucl-th] (cit. on p. 25).

[93] M. Gelenava, *Electromagnetic transition form factors of the Roper resonance in baryon chiral perturbation theory*, Eur. Phys. J. A **54** (2018) 88, arXiv: 1711.03494 [nucl-th] (cit. on p. 25).

[94] B. Golli, H. Osmanović, S. Širca and A. Švarc,
Genuine quark state versus dynamically generated structure for the Roper resonance,
Phys. Rev. C **97** (2018) 035204, arXiv: 1709.09025 [hep-ph] (cit. on p. 25).

[95] J.-j. Wu, D. B. Leinweber, Z.-w. Liu and A. W. Thomas,
Structure of the Roper Resonance from Lattice QCD Constraints,
Phys. Rev. D **97** (2018) 094509, arXiv: 1703.10715 [nucl-th] (cit. on p. 25).

[96] W. Rarita and J. Schwinger, *On a theory of particles with half integral spin*,
Phys. Rev. **60** (1941) 61 (cit. on p. 27).

[97] C. Hacker, N. Wies, J. Gegelia and S. Scherer,
Including the Delta(1232) resonance in baryon chiral perturbation theory,
Phys. Rev. C **72** (2005) 055203, arXiv: hep-ph/0505043 (cit. on p. 27).

[98] H.-B. Tang and P. J. Ellis, *Redundance of Delta isobar parameters in effective field theories*,
Phys. Lett. B **387** (1996) 9, arXiv: hep-ph/9606432 (cit. on p. 28).

[99] H. Krebs, E. Epelbaum and U.-G. Meißner, *Redundancy of the off-shell parameters in chiral effective field theory with explicit spin-3/2 degrees of freedom*, Phys. Lett. B **683** (2010) 222, arXiv: 0905.2744 [hep-th] (cit. on p. 28).

[100] R. Mertig, M. Bohm and A. Denner,
FEYN CALC: Computer algebraic calculation of Feynman amplitudes,
Comput. Phys. Commun. **64** (1991) 345 (cit. on p. 29).

[101] V. Shtabovenko, R. Mertig and F. Orellana, *New Developments in FeynCalc 9.0*,
Comput. Phys. Commun. **207** (2016) 432, arXiv: 1601.01167 [hep-ph] (cit. on p. 29).

[102] J. Gasser and H. Leutwyler,
Spontaneously Broken Symmetries: Effective Lagrangians at Finite Volume,
Nucl. Phys. B **307** (1988) 763 (cit. on p. 31).

[103] A. Ali Khan et al.,
The Nucleon mass in N(f) = 2 lattice QCD: Finite size effects from chiral perturbation theory,
Nucl. Phys. B **689** (2004) 175, arXiv: hep-lat/0312030 (cit. on p. 31).

[104] S. R. Beane and M. J. Savage, *Baryon axial charge in a finite volume*,
Phys. Rev. D **70** (2004) 074029, arXiv: hep-ph/0404131 (cit. on p. 31).

[105] D. Severt, M. Mai and U.-G. Meißner,
Particle-dimer approach for the Roper resonance in a finite volume, JHEP **04** (2023) 100,
arXiv: 2212.02171 [hep-lat] (cit. on p. 43).

[106] M. Mai, C. Culver, A. Alexandru, M. Döring and F. X. Lee,
Cross-channel study of pion scattering from lattice QCD, Phys. Rev. D **100** (2019) 114514,
arXiv: 1908.01847 [hep-lat] (cit. on pp. 44, 65, 66).

[107] V. Crede and W. Roberts, *Progress towards understanding baryon resonances*, Rept. Prog. Phys. **76** (2013) 076301, arXiv: 1302.7299 [nucl-ex] (cit. on p. 44).

[108] A. Thiel, F. Afzal and Y. Wunderlich, *Light Baryon Spectroscopy*, Prog. Part. Nucl. Phys. **125** (2022) 103949, arXiv: 2202.05055 [nucl-ex] (cit. on p. 44).

[109] Y.-R. Liu, H.-X. Chen, W. Chen, X. Liu and S.-L. Zhu, *Pentaquark and Tetraquark states*, Prog. Part. Nucl. Phys. **107** (2019) 237, arXiv: 1903.11976 [hep-ph] (cit. on p. 44).

[110] F.-K. Guo et al., *Hadronic molecules*, Rev. Mod. Phys. **90** (2018) 015004, [Erratum: Rev.Mod.Phys. 94, 029901 (2022)], arXiv: 1705.00141 [hep-ph] (cit. on p. 44).

[111] N. Brambilla et al., *The XYZ states: experimental and theoretical status and perspectives*, Phys. Rept. **873** (2020) 1, arXiv: 1907.07583 [hep-ex] (cit. on p. 44).

[112] A. Ali, L. Maiani and A. D. Polosa, *Multiquark Hadrons*, Cambridge University Press, 2019, ISBN: 978-1-316-76146-5, 978-1-107-17158-9, 978-1-316-77419-9 (cit. on p. 44).

[113] R. F. Lebed, R. E. Mitchell and E. S. Swanson, *Heavy-Quark QCD Exotica*, Prog. Part. Nucl. Phys. **93** (2017) 143, arXiv: 1610.04528 [hep-ph] (cit. on p. 44).

[114] U. Löring, B. C. Metsch and H. R. Petry, *The Light baryon spectrum in a relativistic quark model with instanton induced quark forces: The Nonstrange baryon spectrum and ground states*, Eur. Phys. J. A **10** (2001) 395, arXiv: hep-ph/0103289 (cit. on p. 44).

[115] S. Capstick and N. Isgur, *Baryons in a Relativized Quark Model with Chromodynamics*, AIP Conf. Proc. **132** (1985) 267, ed. by S. Oneda (cit. on p. 44).

[116] S. Capstick and W. Roberts, *Quasi two-body decays of nonstrange baryons*, Phys. Rev. D **49** (1994) 4570, arXiv: nucl-th/9310030 (cit. on p. 44).

[117] S.-x. Qin, L. Chang, Y.-x. Liu, C. D. Roberts and D. J. Wilson, *Interaction model for the gap equation*, Phys. Rev. C **84** (2011) 042202, arXiv: 1108.0603 [nucl-th] (cit. on p. 44).

[118] C. D. Roberts and A. G. Williams, *Dyson-Schwinger equations and their application to hadronic physics*, Prog. Part. Nucl. Phys. **33** (1994) 477, arXiv: hep-ph/9403224 (cit. on p. 44).

[119] G. Eichmann, H. Sanchis-Alepuz, R. Williams, R. Alkofer and C. S. Fischer, *Baryons as relativistic three-quark bound states*, Prog. Part. Nucl. Phys. **91** (2016) 1, arXiv: 1606.09602 [hep-ph] (cit. on p. 44).

[120] S. Durr et al., *Ab-Initio Determination of Light Hadron Masses*, Science **322** (2008) 1224, arXiv: 0906.3599 [hep-lat] (cit. on p. 44).

[121] G. P. Engel, C. B. Lang, D. Mohler and A. Schäfer, *QCD with Two Light Dynamical Chirally Improved Quarks: Baryons*, Phys. Rev. D **87** (2013) 074504, arXiv: 1301.4318 [hep-lat] (cit. on p. 44).

[122] C. Alexandrou, T. Leontiou, C. N. Papanicolas and E. Stiliaris, *Novel analysis method for excited states in lattice QCD: The nucleon case*, Phys. Rev. D **91** (2015) 014506, arXiv: 1411.6765 [hep-lat] (cit. on p. 44).

[123] A. Walker-Loud et al.,
Light hadron spectroscopy using domain wall valence quarks on an Asqtad sea,
Phys. Rev. D **79** (2009) 054502, arXiv: 0806.4549 [hep-lat] (cit. on p. 44).

[124] J. Bulava et al., *Nucleon, Δ and Ω excited states in $N_f = 2 + 1$ lattice QCD*,
Phys. Rev. D **82** (2010) 014507, arXiv: 1004.5072 [hep-lat] (cit. on p. 44).

[125] J. J. Dudek, R. G. Edwards, M. J. Peardon, D. G. Richards and C. E. Thomas,
Toward the excited meson spectrum of dynamical QCD, Phys. Rev. D **82** (2010) 034508,
arXiv: 1004.4930 [hep-ph] (cit. on p. 44).

[126] C. Alexandrou et al.,
Lattice investigation of the scalar mesons $a_0(980)$ and κ using four-quark operators,
JHEP **04** (2013) 137, arXiv: 1212.1418 [hep-lat] (cit. on p. 44).

[127] C. Alexandrou, T. Korzec, G. Koutsou and T. Leontiou,
Nucleon Excited States in N_f=2 lattice QCD, Phys. Rev. D **89** (2014) 034502,
arXiv: 1302.4410 [hep-lat] (cit. on p. 44).

[128] M. Fischer et al., *The ρ-resonance from $N_f = 2$ lattice QCD including the physical pion mass*,
Phys. Lett. B **819** (2021) 136449, arXiv: 2006.13805 [hep-lat] (cit. on p. 44).

[129] D. J. Wilson, R. A. Briceno, J. J. Dudek, R. G. Edwards and C. E. Thomas,
Coupled $\pi\pi$, $K\bar{K}$ scattering in P-wave and the ρ resonance from lattice QCD,
Phys. Rev. D **92** (2015) 094502, arXiv: 1507.02599 [hep-ph] (cit. on p. 44).

[130] M. Mai, *Review of the $\Lambda(1405)$ A curious case of a strangeness resonance*,
Eur. Phys. J. ST **230** (2021) 1593, arXiv: 2010.00056 [nucl-th] (cit. on p. 44).

[131] T. Hyodo and M. Niiyama, *QCD and the strange baryon spectrum*,
Prog. Part. Nucl. Phys. **120** (2021) 103868, arXiv: 2010.07592 [hep-ph] (cit. on p. 44).

[132] U.-G. Meißner, *Two-pole structures in QCD: Facts, not fantasy!*, Symmetry **12** (2020) 981,
arXiv: 2005.06909 [hep-ph] (cit. on p. 44).

[133] N. Isgur and G. Karl, *Hyperfine Interactions in Negative Parity Baryons*,
Phys. Lett. B **72** (1977) 109 (cit. on p. 45).

[134] N. Isgur and G. Karl,
Positive Parity Excited Baryons in a Quark Model with Hyperfine Interactions,
Phys. Rev. D **19** (1979) 2653, [Erratum: Phys.Rev.D 23, 817 (1981)] (cit. on p. 45).

[135] O. Krehl, C. Hanhart, S. Krewald and J. Speth, *What is the structure of the Roper resonance?*,
Phys. Rev. C **62** (2000) 025207, arXiv: nucl-th/9911080 (cit. on p. 45).

[136] R. A. Arndt, W. J. Briscoe, I. I. Strakovsky and R. L. Workman,
Extended partial-wave analysis of piN scattering data, Phys. Rev. C **74** (2006) 045205,
arXiv: nucl-th/0605082 (cit. on p. 45).

[137] M. Döring, C. Hanhart, F. Huang, S. Krewald and U.-G. Meißner, *Analytic properties of the scattering amplitude and resonances parameters in a meson exchange model*,
Nucl. Phys. A **829** (2009) 170, arXiv: 0903.4337 [nucl-th] (cit. on p. 45).

[138] L. Alvarez-Ruso, "On the nature of the Roper resonance",
Mini-Workshop Bled 2010: Dressing Hadrons, 2010 1, arXiv: 1011.0609 [nucl-th]
(cit. on p. 45).

[139] M. T. Hansen and S. R. Sharpe, *Lattice QCD and Three-particle Decays of Resonances*, Ann. Rev. Nucl. Part. Sci. **69** (2019) 65, arXiv: 1901.00483 [hep-lat] (cit. on p. 45).

[140] A. L. Kiratidis et al., *Search for low-lying lattice QCD eigenstates in the Roper regime*, Phys. Rev. D **95** (2017) 074507, arXiv: 1608.03051 [hep-lat] (cit. on p. 45).

[141] B. Hörz and A. Hanlon, *Two- and three-pion finite-volume spectra at maximal isospin from lattice QCD*, Phys. Rev. Lett. **123** (2019) 142002, arXiv: 1905.04277 [hep-lat] (cit. on p. 45).

[142] T. D. Blanton, F. Romero-López and S. R. Sharpe, *$I = 3$ Three-Pion Scattering Amplitude from Lattice QCD*, Phys. Rev. Lett. **124** (2020) 032001, arXiv: 1909.02973 [hep-lat] (cit. on p. 45).

[143] C. Culver, M. Mai, R. Brett, A. Alexandru and M. Döring, *Three pion spectrum in the $I = 3$ channel from lattice QCD*, Phys. Rev. D **101** (2020) 114507, arXiv: 1911.09047 [hep-lat] (cit. on p. 45).

[144] M. Fischer et al., *Scattering of two and three physical pions at maximal isospin from lattice QCD*, Eur. Phys. J. C **81** (2021) 436, arXiv: 2008.03035 [hep-lat] (cit. on p. 45).

[145] M. T. Hansen, R. A. Briceño, R. G. Edwards, C. E. Thomas and D. J. Wilson, *Energy-Dependent $\pi^+\pi^+\pi^+$ Scattering Amplitude from QCD*, Phys. Rev. Lett. **126** (2021) 012001, arXiv: 2009.04931 [hep-lat] (cit. on p. 45).

[146] A. Alexandru et al., *Finite-volume energy spectrum of the $K^-K^-K^-$ system*, Phys. Rev. D **102** (2020) 114523, arXiv: 2009.12358 [hep-lat] (cit. on p. 45).

[147] T. D. Blanton et al., *Interactions of two and three mesons including higher partial waves from lattice QCD*, JHEP **10** (2021) 023, arXiv: 2106.05590 [hep-lat] (cit. on p. 45).

[148] S. R. Beane et al., *Charged multihadron systems in lattice QCD+QED*, Phys. Rev. D **103** (2021) 054504, arXiv: 2003.12130 [hep-lat] (cit. on p. 45).

[149] P. Bühlmann and U. Wenger, *Finite-volume effects and meson scattering in the 2-flavour Schwinger model*, PoS **LATTICE2021** (2022) 463, arXiv: 2112.15228 [hep-lat] (cit. on p. 45).

[150] M. Mai et al., *Three-Body Dynamics of the a1(1260) Resonance from Lattice QCD*, Phys. Rev. Lett. **127** (2021) 222001, arXiv: 2107.03973 [hep-lat] (cit. on p. 45).

[151] M. Garofalo, M. Mai, F. Romero-López, A. Rusetsky and C. Urbach, *Three-body resonances in the φ^4 theory*, (2022), arXiv: 2211.05605 [hep-lat] (cit. on p. 45).

[152] K. Polejaeva and A. Rusetsky, *Three particles in a finite volume*, Eur. Phys. J. A **48** (2012) 67, arXiv: 1203.1241 [hep-lat] (cit. on p. 45).

[153] R. A. Briceno and Z. Davoudi, *Three-particle scattering amplitudes from a finite volume formalism*, Phys. Rev. D **87** (2013) 094507, arXiv: 1212.3398 [hep-lat] (cit. on p. 45).

[154] M. T. Hansen and S. R. Sharpe,
Relativistic, model-independent, three-particle quantization condition,
Phys. Rev. D **90** (2014) 116003, arXiv: 1408.5933 [hep-lat] (cit. on pp. 45, 61).

[155] P. Guo and V. Gasparian, *A solvable three-body model in finite volume*,
Phys. Lett. B **774** (2017) 441, arXiv: 1701.00438 [hep-lat] (cit. on p. 45).

[156] Y. Meng, C. Liu, U.-G. Meißner and A. Rusetsky,
Three-particle bound states in a finite volume: unequal masses and higher partial waves,
Phys. Rev. D **98** (2018) 014508, arXiv: 1712.08464 [hep-lat] (cit. on p. 45).

[157] P. Guo and T. Morris, *Multiple-particle interaction in (1+1)-dimensional lattice model*,
Phys. Rev. D **99** (2019) 014501, arXiv: 1808.07397 [hep-lat] (cit. on p. 45).

[158] M. Mai and M. Döring, *Finite-Volume Spectrum of $\pi^+\pi^+$ and $\pi^+\pi^+\pi^+$ Systems*,
Phys. Rev. Lett. **122** (2019) 062503, arXiv: 1807.04746 [hep-lat] (cit. on p. 45).

[159] M. Mai, M. Döring, C. Culver and A. Alexandru,
Three-body unitarity versus finite-volume $\pi^+\pi^+\pi^+$ spectrum from lattice QCD,
Phys. Rev. D **101** (2020) 054510, arXiv: 1909.05749 [hep-lat] (cit. on p. 45).

[160] P. Guo, *Propagation of particles on a torus*, Phys. Lett. B **804** (2020) 135370,
arXiv: 1908.08081 [hep-lat] (cit. on p. 45).

[161] T. D. Blanton, F. Romero-López and S. R. Sharpe,
Implementing the three-particle quantization condition including higher partial waves,
JHEP **03** (2019) 106, arXiv: 1901.07095 [hep-lat] (cit. on p. 45).

[162] M. T. Hansen, F. Romero-López and S. R. Sharpe,
Generalizing the relativistic quantization condition to include all three-pion isospin channels,
JHEP **07** (2020) 047, [Erratum: JHEP 02, 014 (2021)], arXiv: 2003.10974 [hep-lat]
(cit. on p. 45).

[163] P. Guo and B. Long, *Multi- π^+ systems in a finite volume*, Phys. Rev. D **101** (2020) 094510,
arXiv: 2002.09266 [hep-lat] (cit. on p. 45).

[164] T. D. Blanton and S. R. Sharpe,
Relativistic three-particle quantization condition for nondegenerate scalars,
Phys. Rev. D **103** (2021) 054503, arXiv: 2011.05520 [hep-lat] (cit. on p. 45).

[165] J.-Y. Pang et al., *Spurious poles in a finite volume*, JHEP **07** (2022) 019,
arXiv: 2204.04807 [hep-lat] (cit. on p. 45).

[166] R. Brett et al., *Three-body interactions from the finite-volume QCD spectrum*,
Phys. Rev. D **104** (2021) 014501, arXiv: 2101.06144 [hep-lat] (cit. on p. 45).

[167] F. Müller, J.-Y. Pang, A. Rusetsky and J.-J. Wu,
Relativistic-invariant formulation of the NREFT three-particle quantization condition,
JHEP **02** (2022) 158, arXiv: 2110.09351 [hep-lat] (cit. on p. 45).

[168] M. T. Hansen, F. Romero-López and S. R. Sharpe,
Decay amplitudes to three hadrons from finite-volume matrix elements, JHEP **04** (2021) 113,
arXiv: 2101.10246 [hep-lat] (cit. on p. 45).

[169] T. D. Blanton and S. R. Sharpe,
Three-particle finite-volume formalism for $\pi+\pi+K+$ and related systems,
Phys. Rev. D **104** (2021) 034509, arXiv: 2105.12094 [hep-lat] (cit. on p. 45).

[170] A. W. Jackura, *Three-body scattering and quantization conditions from S matrix unitarity*,
(2022), arXiv: 2208.10587 [hep-lat] (cit. on p. 45).

[171] F. Müller, J.-Y. Pang, A. Rusetsky and J.-J. Wu,
Three-particle Lellouch-Lüscher formalism in moving frames, (2022),
arXiv: 2211.10126 [hep-lat] (cit. on p. 45).

[172] D. Guo, A. Alexandru, R. Molina, M. Mai and M. Döring,
Extraction of isoscalar $\pi\pi$ phase-shifts from lattice QCD, Phys. Rev. D **98** (2018) 014507,
arXiv: 1803.02897 [hep-lat] (cit. on pp. 45, 65).

[173] M. Mai, B. Hu, M. Döring, A. Pilloni and A. Szczepaniak,
Three-body Unitarity with Isobars Revisited, Eur. Phys. J. A **53** (2017) 177,
arXiv: 1706.06118 [nucl-th] (cit. on p. 46).

[174] F. Müller, T. Yu and A. Rusetsky, *Finite-volume energy shift of the three-pion ground state*,
Phys. Rev. D **103** (2021) 054506, arXiv: 2011.14178 [hep-lat] (cit. on p. 46).

[175] L. Barca, G. Bali and S. Collins, *Towards N to Nπ matrix elements from Lattice QCD*, (2022),
arXiv: 2211.12278 [hep-lat] (cit. on p. 47).

[176] J.-Y. Pang, J.-J. Wu and L.-S. Geng, *DDK system in finite volume*,
Phys. Rev. D **102** (2020) 114515, arXiv: 2008.13014 [hep-lat] (cit. on p. 48).

[177] J. Gasser, B. Kubis and A. Rusetsky, *Cusps in K –> 3pi decays: a theoretical framework*,
Nucl. Phys. B **850** (2011) 96, arXiv: 1103.4273 [hep-ph] (cit. on pp. 50, 52).

[178] J. R. Batley et al., *Precise tests of low energy QCD from K(e4)decay properties*,
Eur. Phys. J. C **70** (2010) 635 (cit. on p. 55).

[179] M. Hoferichter, J. Ruiz de Elvira, B. Kubis and U.-G. Meißner,
Roy–Steiner-equation analysis of pion–nucleon scattering, Phys. Rept. **625** (2016) 1,
arXiv: 1510.06039 [hep-ph] (cit. on p. 56).

[180] Z. Fu, *Lattice QCD study of the s-wave $\pi\pi$ scattering lengths in the I=0 and 2 channels*,
Phys. Rev. D **87** (2013) 074501, arXiv: 1303.0517 [hep-lat] (cit. on p. 65).

[181] R. A. Briceno, J. J. Dudek, R. G. Edwards and D. J. Wilson,
Isoscalar $\pi\pi$ scattering and the σ meson resonance from QCD,
Phys. Rev. Lett. **118** (2017) 022002, arXiv: 1607.05900 [hep-ph] (cit. on p. 65).

[182] R. A. Briceno, J. J. Dudek, R. G. Edwards and D. J. Wilson,
Isoscalar $\pi\pi$, $K\overline{K}$, $\eta\eta$ scattering and the σ, f_0, f_2 mesons from QCD,
Phys. Rev. D **97** (2018) 054513, arXiv: 1708.06667 [hep-lat] (cit. on p. 65).

[183] L. Liu et al., *Isospin-0 $\pi\pi$ s-wave scattering length from twisted mass lattice QCD*,
Phys. Rev. D **96** (2017) 054516, arXiv: 1612.02061 [hep-lat] (cit. on p. 65).

[184] C. Culver, M. Mai, A. Alexandru, M. Döring and F. X. Lee,
Pion scattering in the isospin $I = 2$ channel from elongated lattices,
Phys. Rev. D **100** (2019) 034509, arXiv: 1905.10202 [hep-lat] (cit. on p. 65).

[185] D. Guo, A. Alexandru, R. Molina and M. Döring,
Rho resonance parameters from lattice QCD, Phys. Rev. D **94** (2016) 034501,
arXiv: 1605.03993 [hep-lat] (cit. on p. 65).

[186] U.-G. Meißner, *The Beauty of Spin*,
J. Phys. Conf. Ser. **295** (2011) 012001, ed. by H. Stroher and F. Rathmann,
arXiv: 1012.0924 [hep-ph] (cit. on p. 66).

[187] C. Alexandrou, J. W. Negele, M. Petschlies, A. Strelchenko and A. Tsapalis,
Determination of Δ Resonance Parameters from Lattice QCD,
Phys. Rev. D **88** (2013) 031501, arXiv: 1305.6081 [hep-lat] (cit. on p. 66).

[188] C. Alexandrou, J. W. Negele, M. Petschlies, A. V. Pochinsky and S. N. Syritsyn,
Study of decuplet baryon resonances from lattice QCD, Phys. Rev. D **93** (2016) 114515,
arXiv: 1507.02724 [hep-lat] (cit. on p. 66).

[189] C. W. Andersen, J. Bulava, B. Hörz and C. Morningstar, *Elastic $I = 3/2p$-wave nucleon-pion scattering amplitude and the Δ(1232) resonance from N_f=2+1 lattice QCD*,
Phys. Rev. D **97** (2018) 014506, arXiv: 1710.01557 [hep-lat] (cit. on p. 66).

[190] F. Pittler et al., *Elastic $\pi - N$ scattering in the $I = 3/2$ channel*,
PoS **LATTICE2021** (2022) 226, arXiv: 2112.04146 [hep-lat] (cit. on p. 66).

[191] G. Silvi et al.,
P-wave nucleon-pion scattering amplitude in the Δ(1232) channel from lattice QCD,
Phys. Rev. D **103** (2021) 094508, arXiv: 2101.00689 [hep-lat] (cit. on p. 66).

[192] P. Jordan, J. von Neumann and E. P. Wigner,
On an Algebraic generalization of the quantum mechanical formalism,
Annals Math. **35** (1934) 29 (cit. on p. 70).

[193] Y. Ünal, D. Severt, J. de Vries, C. Hanhart and U.-G. Meißner,
Electric dipole moments of baryons with bottom quarks, Phys. Rev. D **105** (2022) 055026,
arXiv: 2111.13000 [hep-ph] (cit. on p. 75).

[194] Y. Ünal and U.-G. Meißner, *Strong CP violation in spin-1/2 singly charmed baryons*,
JHEP **01** (2021) 115, arXiv: 2008.01371 [hep-ph] (cit. on pp. 75, 77).

[195] J. Bsaisou, U.-G. Meißner, A. Nogga and A. Wirzba, *P- and T-Violating Lagrangians in Chiral Effective Field Theory and Nuclear Electric Dipole Moments*,
Annals Phys. **359** (2015) 317, arXiv: 1412.5471 [hep-ph] (cit. on pp. 75, 76, 81).

[196] J. Bsaisou, *Electric Dipole Moments of Light Nuclei in Chiral Effective Field Theory*,
PhD thesis: Bonn U., 2014 (cit. on pp. 76, 78, 81).

[197] S. Weinberg, *Larger Higgs Exchange Terms in the Neutron Electric Dipole Moment*,
Phys. Rev. Lett. **63** (1989) 2333 (cit. on pp. 76, 92, 105).

[198] A. Manohar and H. Georgi, *Chiral Quarks and the Nonrelativistic Quark Model*,
Nucl. Phys. B **234** (1984) 189 (cit. on pp. 76, 92, 105).

[199] W. C. Griffith et al., *Improved Limit on the Permanent Electric Dipole Moment of Hg-199*,
Phys. Rev. Lett. **102** (2009) 101601, arXiv: 0901.2328 [physics.atom-ph] (cit. on p. 76).

[200] J. de Vries, R. G. E. Timmermans, E. Mereghetti and U. van Kolck,
The Nucleon Electric Dipole Form Factor From Dimension-Six Time-Reversal Violation,
Phys. Lett. B **695** (2011) 268, arXiv: 1006.2304 [hep-ph] (cit. on pp. 76, 92).

[201] J. de Vries, E. Mereghetti, R. G. E. Timmermans and U. van Kolck,
The Effective Chiral Lagrangian From Dimension-Six Parity and Time-Reversal Violation,
Annals Phys. **338** (2013) 50, arXiv: 1212.0990 [hep-ph] (cit. on pp. 76, 78).

[202] N. Yamanaka and E. Hiyama,
Weinberg operator contribution to the nucleon electric dipole moment in the quark model,
Phys. Rev. D **103** (2021) 035023, arXiv: 2011.02531 [hep-ph] (cit. on p. 76).

[203] J. Kley, T. Theil, E. Venturini and A. Weiler,
Electric dipole moments at one-loop in the dimension-6 SMEFT, (2021),
arXiv: 2109.15085 [hep-ph] (cit. on p. 76).

[204] W. Dekens et al.,
Unraveling models of CP violation through electric dipole moments of light nuclei,
JHEP **07** (2014) 069, arXiv: 1404.6082 [hep-ph] (cit. on pp. 76, 79).

[205] E. Braaten, C. S. Li and T. C. Yuan,
The Gluon Color - Electric Dipole Moment and Its Anomalous Dimension,
Phys. Rev. D **42** (1990) 276 (cit. on pp. 77, 93, 94).

[206] Y. T. Chien, V. Cirigliano, W. Dekens, J. de Vries and E. Mereghetti,
Direct and indirect constraints on CP-violating Higgs-quark and Higgs-gluon interactions,
JHEP **02** (2016) 011, arXiv: 1510.00725 [hep-ph] (cit. on pp. 77, 93, 94).

[207] H. Gisbert and J. Ruiz Vidal, *Improved bounds on heavy quark electric dipole moments*,
Phys. Rev. D **101** (2020) 115010, arXiv: 1905.02513 [hep-ph] (cit. on pp. 77, 93, 94).

[208] U. Haisch and G. Koole, *Beautiful and charming chromodipole moments*,
JHEP **09** (2021) 133, arXiv: 2106.01289 [hep-ph] (cit. on pp. 77, 93, 94).

[209] Y. Nakai and M. Reece, *Electric Dipole Moments in Natural Supersymmetry*,
JHEP **08** (2017) 031, arXiv: 1612.08090 [hep-ph] (cit. on p. 78).

[210] M. Jung and A. Pich, *Electric Dipole Moments in Two-Higgs-Doublet Models*,
JHEP **04** (2014) 076, arXiv: 1308.6283 [hep-ph] (cit. on p. 78).

[211] W. Dekens, J. de Vries, M. Jung and K. K. Vos,
The phenomenology of electric dipole moments in models of scalar leptoquarks,
JHEP **01** (2019) 069, arXiv: 1809.09114 [hep-ph] (cit. on pp. 78, 79).

[212] R.-X. Shi, Y. Xiao and L.-S. Geng, *Magnetic moments of the spin-1/2 singly charmed baryons in covariant baryon chiral perturbation theory*, Phys. Rev. D **100** (2019) 054019,
arXiv: 1812.07833 [hep-ph] (cit. on p. 79).

[213] N. Jiang, X.-L. Chen and S.-L. Zhu, *Mass and axial charge of heavy baryons*,
Phys. Rev. D **90** (2014) 074011, arXiv: 1403.5404 [hep-ph] (cit. on pp. 79, 80).

[214] B. Borasoy, *The Electric dipole moment of the neutron in chiral perturbation theory*,
Phys. Rev. D **61** (2000) 114017, arXiv: hep-ph/0004011 (cit. on pp. 79, 86).

[215] F.-K. Guo, C. Hanhart and U.-G. Meißner,
Mass splittings within heavy baryon isospin multiplets in chiral perturbation theory,
JHEP **09** (2008) 136, arXiv: 0809.2359 [hep-ph] (cit. on p. 80).

[216] N. Jiang, X.-L. Chen and S.-L. Zhu,
Electromagnetic decays of the charmed and bottom baryons in chiral perturbation theory,
Phys. Rev. D **92** (2015) 054017, arXiv: 1505.02999 [hep-ph] (cit. on p. 80).

[217] U.-G. Meißner and S. Steininger, *Baryon magnetic moments in chiral perturbation theory*,
Nucl. Phys. B **499** (1997) 349, arXiv: hep-ph/9701260 (cit. on p. 80).

[218] B. Kubis and U.-G. Meißner, *Baryon form-factors in chiral perturbation theory*,
Eur. Phys. J. C **18** (2001) 747, arXiv: hep-ph/0010283 (cit. on p. 80).

[219] G. 't Hooft, *Dimensional regularization and the renormalization group*,
Nucl. Phys. B **61** (1973) 455 (cit. on p. 85).

[220] S. Weinberg, *New approach to the renormalization group*, Phys. Rev. D **8** (1973) 3497
(cit. on p. 85).

[221] S. Scherer and M. R. Schindler, *Quantum chromodynamics and chiral symmetry*,
Lect. Notes Phys. **830** (2012) 1 (cit. on p. 85).

[222] A. Shindler, *Flavor-diagonal CP violation: the electric dipole moment*,
Eur. Phys. J. A **57** (2021) 128 (cit. on p. 92).

[223] T. Bhattacharya, V. Cirigliano, R. Gupta, H.-W. Lin and B. Yoon,
Neutron Electric Dipole Moment and Tensor Charges from Lattice QCD,
Phys. Rev. Lett. **115** (2015) 212002, arXiv: 1506.04196 [hep-lat] (cit. on p. 92).

[224] D. Severt, *Sigma-Term Physics*, Master Thesis: University of Bonn, 2018
(cit. on pp. 101, 103).

[225] J. de Vries, *Hadronic time-reversal violation in effective field theory*,
PhD thesis: U. Groningen (main), 2012 (cit. on p. 106).

[226] G. Passarino and M. J. G. Veltman,
One Loop Corrections for e+ e- Annihilation Into mu+ mu- in the Weinberg Model,
Nucl. Phys. B **160** (1979) 151 (cit. on p. 107).

[227] R. K. Ellis, Z. Kunszt, K. Melnikov and G. Zanderighi,
One-loop calculations in quantum field theory: from Feynman diagrams to unitarity cuts,
Phys. Rept. **518** (2012) 141, arXiv: 1105.4319 [hep-ph] (cit. on p. 107).

[228] M. Abramowitz and I. A. Stegun, *Handbook of Mathematical Functions*,
Dover Publications, Inc., 1972 (cit. on p. 109).